Role of GPR84 in Kidney Injury in a Surrogate COVID-19 Mouse Model

Amélie Blais

A thesis submitted in partial fulfilment of the requirements for the

Master's degree in Cellular and Molecular Medicine

Department of Cellular and Molecular Medicine

Faculty of Medicine

University of Ottawa


uOttawa
L'Université canadienne
Canada's university

ABSTRACT

40% of severe acute respiratory syndrome coronavirus two (SARS-CoV-2) severe cases develop acute kidney injury (AKI). Current treatment for renal complications limits financial and material resources available. To explore alternative treatments and accelerate research in case of future coronavirus outbreaks, a mouse model of coronavirus disease 2019-associated AKI (C19-AKI) would represent a critical biomedical research tool. The surrogate model of C19-AKI (SMC) developed consisted of angiotensin-converting enzyme two (ACE2) knockout (KO) mice receiving 400 ng/kg/min of angiotensin (Ang) II by osmotic minipump for eight days with a single injection of lipopolysaccharide (LPS; 10 mg/kg) on the seventh day of Ang II and euthanasia 24 hours after LPS. Similarly, to C19-AKI, the SMC exhibited albuminuria, elevated blood urea nitrogen, electrolyte imbalance, neutrophil infiltration, and upregulation of the G-coupled protein receptor (GPR)84 and pro-inflammatory and injury markers. GPR84 was found in bronchoalveolar lavage fluid neutrophils of coronavirus disease 2019 (COVID-19) patients, suggesting a potential implication of GPR84 in the disease. We hypothesised that GPR84 deletion or antagonism with GLPG-1205 could attenuate SMC's indices of renal injury and inflammation. GLPG-1205 and GPR84 KO had no effects in the SMC model, as suggested by unchanged albuminuria, electrolytes, and markers expression. Interestingly, neutrophil infiltration was attenuated by GLPG-1205 only. The SMC is an interesting tool for therapeutic development for infections associated with renal injury, such as SARS-CoV-2. GPR84 role in the SMC needs to be further assessed.

RÉSUMÉ (FRENCH ABSTRACT)

40 % des cas graves de coronavirus du syndrome respiratoire aigu sévère deux (SARS-CoV-2) développent une insuffisance rénale aiguë (IRA). Les traitements actuels pour les complications rénales limitent les ressources financières et matérielles disponibles. Afin d'explorer des traitements alternatifs et accélérer la recherche en cas d'éventuelles épidémies de coronavirus, un modèle d'IRA induit par la maladie à coronavirus 2019 (C19-IRA) serait un outil de recherche essentiel. Le modèle substitut de C19-IRA (MSC) développé était composé de souris dépourvue de l'enzyme de conversion de l'angiotensine deux (ACE2) recevant 400 ng/kg/min d'angiotensine (Ang) II par mini-pompe osmotique pendant huit jours et une injection de lipopolysaccharide (LPS; 10 mg/kg) le septième jour d'Ang II, soit 24 heures avant l'euthanasie. Comme le C19-IRA, le MSC a démontré de l'albuminurie, une élévation de l'azote uréique sanguin, un débalancement électrolytique, de l'infiltration de neutrophiles ainsi qu'une expression élevée du récepteur couplé à la protéine G (GPR)84 et des marqueurs inflammatoires et de dommage rénal. L'expression de GPR84 a été décelé dans les fluides de lavage bronchoalvéolaire des patients de maladie à coronavirus 2019 (COVID-19), indiquant une implication potentielle de GPR84 dans la maladie. La délétion génétique ou l'antagonisme de GPR84 avec GLPG-1205 pourrait possiblement atténuer l'inflammation et les lésions rénale dans le MSC. GLPG-1205 et la délétion de GPR84 n'ont eu aucun effet dans le MSC, tel que suggéré par l'albuminurie, les niveaux d'électrolytes et l'expression des marqueurs inchangés. Curieusement, l'infiltration des neutrophiles a atténué par GLPG-1205 seulement. Le MSC est un outil intéressant pour le développement thérapeutique pour les atteintes rénales liées à des infections, tel que SARS-CoV-2. Le rôle de GPR84 dans le MSC demande une évaluation plus approfondie.

GRAPHICAL ABSTRACT

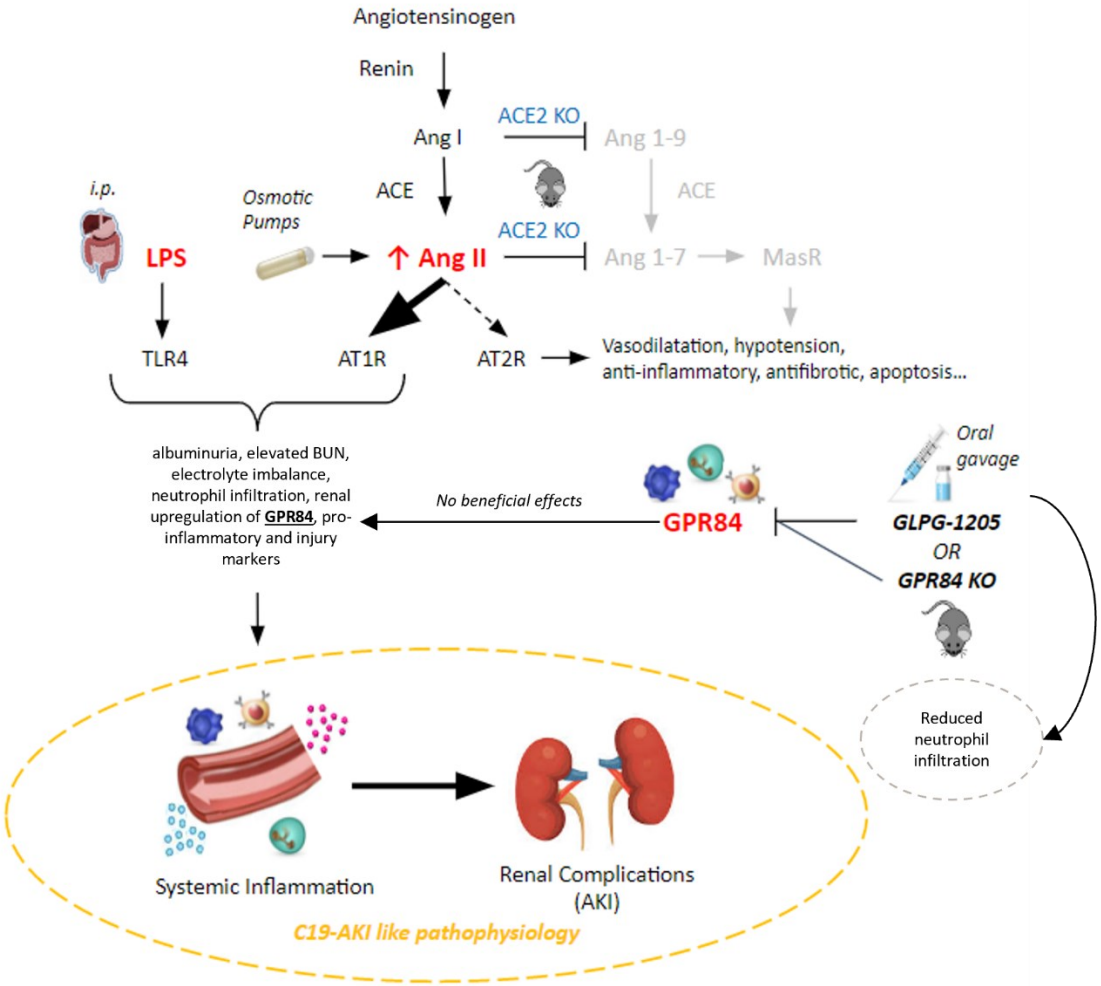

Figure 1. **Graphical abstract.** The surrogate mouse model of coronavirus disease 2019-associated acute kidney injury (C19-AKI), abbreviated SMC, consists of an angiotensin-converting enzyme (ACE)2 knockout (KO) mice administered a low pressor dose of Angiotensin (Ang) II (400 ng/kg/min by osmotic pump) with a single administration of lipopolysaccharide (LPS; 10mg/kg i.p.). ACE2 KO and Ang II administration leads to a renin-angiotensin system (RAS) imbalance favouring the RAS pro-inflammatory arm. The RAS anti-inflammatory arm is presented on the figure in light gray. The combination of Ang II, LPS, and ACE2 KO leads to a pro-inflammatory climate with fibrosis and vasoconstriction through the Toll-like receptor 4 (TLR4) and the angiotensin type 1 receptor (AT1R) signaling. Similarly, to the C19-AKI, the SMC led to albuminuria, elevated blood urea nitrogen (BUN), electrolyte imbalance, neutrophil infiltration, renal upregulation of the G-coupled protein receptor 84 (GPR84), as well as renal upregulation of pro-inflammatory, injury and immune cell markers. GPR84 is present in immune cells and is involved in the pro-inflammatory response. It is hypothesized that GPR84 antagonists (e.g., GLPG-1205) and GPR84 KO mice could reduce indices of C19-AKI by inhibiting GPR84 function. In the SMC, GLPG-1205 and GPR84 KO had no beneficial effects on renal inflammation, injury, and function. Interestingly, GLPG-1205 exclusively led to a significant reduction in neutrophil. AT2R: Angiotensin type 2 receptor. i.p.: intraperitoneal injection. MasR: Mas receptor.

LIST OF JOURNAL ARTICLES

1. Cheff V, Trentin-Sonoda M, Blais A, Thibodeau JF, Holterman CE, Gutsol A, Kennedy CRJ, Hebert R. High fat diet is protective against kidney injury in hypertensive-diabetic mice, but leads to liver injury. PLOS ONE. *(Submitted August 2022)*

2. Simard JC, Thibodeau JF, Leduc M, Tremblay M, Laverdure A, Sarra-Bournet F, Gagnon W, Ouboudinar J, Richard J, Gervais L, Felton A, Letourneau S, Geerts L, Cloutier MP, Hince K, Corpuz R, Blais A, Marques-Quintela V, Duceppe JF, Abbott SD, Zacharie B, **Blais A**, Cheff V, Laurin P, Laplante SR, Kennedy CRJ, Hébert RL, Leblond FA, Grouix B, Gagnon L. Fatty acid mimetic PBI-4547 restores metabolic homeostasis via GPR84 in mice with non-alcoholic fatty liver disease. Scientific Reports. 2020 Jul 29;10(1): 12778

3. Thibodeau JF, Simard JC, Holterman CE, **Blais A**, Cloutier MP, Medeiros T, Leduc M, Grouix B, Leblond FA, Burger D, Hébert RL, Kennedy CRJ, Gagnon L. PBI-4050 via GPR40 activation improves adenine-induced kidney injury in mice. Clin Sci (Lond). 2019 Jul 2;133(14):1587-1602

LIST OF CONFERENCE ABSTRACTS

1. **A Blais**, CE Holterman, FA Leblond, RL Hébert, CRJ Kennedy. Targeting GPR84 to prevent Acute Kidney Injury. M3K 2021.

2. V Cheff, **A Blais**, CE Holterman, JF Thibodeau, RL Hébert. Characterization of a Novel Mouse Model of Metabolic Syndrome Induced-Chronic Kidney Disease. WCN-ISN 2021.

3. V Cheff, **A Blais**, CE Holterman, RL Hébert, CRJ Kennedy, JF Thibodeau. Dual GPR40/GPR84 Fatty Acid Receptor Deletion Improves Adenine-Induced Renal Injury in Mice. ERA-EDTA, 2020.

4. JF Thibodeau, **A Blais**, F Sarra-Bournet, B Groulx, A Gutsol, RL Hébert, L Gagnon, CRJ Kennedy. PBI-4050 Reduces Renal Injury in a Mouse Model of Aristolochic Acid Induced Nephropathy. Am. Soc. Of Neph. Kidney week, Washington, DC, 2019

5. JF Thibodeau, K Hince, **A Blais**, R Corpuz, M Leduc, F Leblond, B Groulx, RL Hébert, CRJ Kennedy, L Gagnon. PBI-4610 Improves Renal Function, Anemia and Histopathological Abnormalities in Adenine Induced CKD. Am. Soc. Of Neph. Kidney week, Washington, DC, 2019

6. T Medeiros, JF Thibodeau, **A Blais**, C Holterman, V Tang, MA Langlois, C Kennedy, L Gagnon, D Burger. Assessment of Urine Microparticles Levels in Aristolochic Acid Induced Nephropathy in WT and GPR40 Receptor Knockout Mice. Am. Soc. Of Neph. Kidney week, Washington, DC, 2019

7. T Medeiros, **A Blais**, JF Thibodeau, D Burger. Profile of Urinary Glomerular-And Tubular-Derived Microparticles in Kidney Disease. Can. Soc. Of Neph. Annual Meeting, Montreal, QC, 2019.

8. JF Thibodeau, CE Holterman, **A Blais**, MP Cloutier, JC Simard, A Blais, A Laverdure, L Gagnon, B Grouix, M Leduc, P Laurin, RL Hébert, F Leblond, CRJ Kennedy. PBI-4050 Reduces Systemic Inflammation, Electrolyte Disturbances and Renal Injury in Mice with Sepsis-Induced Acute Kidney Injury; Role of GPR84. Am. Soc. Of Neph. Kidney Week, San Diego, CA, 2018

TABLE OF CONTENTS

LIST OF TABLES

LIST OF FIGURES

LIST OF ACRONYMS

(1 or 2) W Post-LPS: (One or two)-week post-lipopolysaccharide injection
1W Pump: One week of Angiotensin II osmotic minipump
ACE (2): Angiotensin-converting enzyme (two)
ACR: Albumin to creatinine ratio
AKI: Acute kidney injury
Ang (I or II): Angiotensin (I or II)
ARG-1: Arginase-one
AT (1 or 2) R: Angiotensin type (one or two) receptor
BUN: Blood urea nitrogen
C19-AKI: Coronavirus disease 2019-associated acute kidney injury
CKD: Chronic kidney disease
COVID-19: Coronavirus diseases 2019
cps: Centipoise
CTGF: Connective tissue growth factor
(e)GFR: (Estimated) glomerular filtration rate
ESRD: End-stage renal disease
EV(s): Extracellular vesicle(s)
F4-80: EGF-like module-containing mucin-like hormone receptor-like one
GAPDH: Glyceraldehyde three-phosphate dehydrogenase
GPR (40 or 84): G-coupled protein receptor (40 or 84)
H&E: Hematoxylin and eosin
HET: Heterozygous
i.p.: Intraperitoneal
IL: Interleukin
KIM-1: Kidney injury molecule one
KO: Knockout
LPS: Lipopolysaccharide
MIP-2: Macrophage inflammatory protein two
NGAL: Neutrophil gelatinase-associated lipocalin
(q or RT) PCR: (Quantitative or reverse transcriptase) polymerase chain reaction
RAS: Renin-angiotensin system

SARS-CoV (-2): Severe acute respiratory syndrome coronavirus (two)

SBP: Systolic blood pressure

SMC: Surrogate model of coronavirus disease 2019-associated acute kidney injury

TNF- α: Tumor necrosis factor-alpha

WT: Wild type

ACKNOWLEDGEMENTS

First, I would like to thank my supervisor, Dr. Christopher Kennedy, for giving me the opportunity to do my master's degree in his laboratory. I deeply appreciated all the knowledge and advice you shared with me. I want to thank my colleagues, Dr. Chet Holterman and Véronique Cheff for their support throughout the thesis and valuable advice. I would like to thank my thesis advisory committee members, Dr. Richard Hébert and Dr. Dylan Burger for their time, feedback, and encouragement. Big thank you to our collaborators, Liminal Biosciences, and more particularly François Leblond, for his precious suggestions. We would also like to thank Liminal Bioscienes for providing us the pharmaceutical antagonist used in this thesis. I also want to thank my former mentor, Dr. Jean-Francois Thibodeau for believe in me years ago. Thank you for opening this world of opportunities to me. Thank you all for teaching me what great research is and being exceptional mentors! Thanks to Dr. Fengxia Xiao and Dr. Alexey Gutsol for teaching me new laboratory techniques. I also want to thank Dr. Gutsol for all the histological analysis and immunohistochemistry. Thank you to Lihua (Julie) Zhu for taking care of my animal weaning. Thank you to our 2021 summer student, Amanda Richardson, for her help on urinary extracellular vesicle analysis. I want to thank my laboratory manager, Gabriele Cherton-Horvat, for her help on samples shipment. I would also like to thank anyone from the University of Ottawa's animal care and veterinary service (ACVS), Louise Pelletier histology core and the Kidney Research Centre that participated in this project. Lastly, I want to give a special thank you to my family, close friends, and my partner for their unconditional support throughout my studies. Je vous remercie de m'avoir encouragé pendant tout ce temps. Je vous adore.

Statement of contributions:

Amélie Blais performed all the animal breeding, project management, *in vivo* experiments, and data analysis.

Chet Holterman performed osmotic minipump implantation, spot urine collection, and euthanasia sample collection while also reviewing data analysis.

Véronique Cheff helped with euthanasia sample collection and reviewing data analysis.

Alexey Gutsol performed general histological analyses and the immunohistochemistry.

Amanda Richardson helped with urinary extracellular vesicles analysis.

François Leblond, from Liminal Biosciences, provided advice on experiments and pharmaceutical antagonist use. Liminal Biosciences provided the pharmaceutical antagonist used in this project.

Christopher Kennedy was the principal investigator who conceived the project and supervised all experiments and data analysis.

COPYRIGHTED CONTENTS

No copyrighted content was used or need to be declared in the document.

CHAPTER 1: GENERAL INTRODUCTION

1.1. Kidney

The urinary system is an essential part of an organism's functioning. The urinary system is responsible for urine production and evacuation from the organism[1]. The urinary system is composed of the kidneys, the ureters, the bladder, and the urethra[1,2]. Kidneys are two bean-shaped, fist-sized organs located on each side of the spine below the rib cage[2]. The kidneys remove wastes and extra fluids from the bloodstream leading to the production of urine[2,3]. The urine is brought from the kidneys to the bladder (by two ureters), where urine is stored[1,2]. At urination, urine is evacuated from the bladder through the urethra[1]. The kidneys are involved in blood pressure regulation through the production of renin, an important member of the renin-angiotensin system (RAS; further discussed below)[2,3,4]. The kidney also plays a role in red blood cell production, maintenance of bone health, and vitamin D metabolism[2,3,5].

The blood containing metabolic waste enters the kidneys through the renal artery. Inside each human kidney, an average of one million functional units, called nephrons, are responsible to remove waste and excess fluid from the bloodstream and regulate electrolyte levels[2,6]. The nephrons are composed of the blood filtering component, called the glomerulus, and the tubule that allows the excretion and reabsorption of electrolytes and metabolites[2]. The elements discussed in this paragraph are also presented in Figure 2. At the kidney, the renal artery separates into smaller arterioles which connect to each nephron through a knot of leaky capillaries called the glomerulus (glomerular capillaries)[6]. The glomerulus is in the renal corpuscle region of the nephron[6]. The glomerulus is surrounded by a layer of cells and proteins called the glomerular filtration barrier, which allows the passage of small molecules (e.g. water, salts, and low molecular weight organic molecules) in the

Bowman's capsule (Bowman's space) while large molecules over 15 kilodaltons such as proteins stay in the bloodstream[6,7]. The first layer of the glomerular filtration barrier is the endothelial cells lining the glomerular capillaries[7]. Along with glycocalyx (negatively charged proteoglycans, glycoproteins, and glycolipids), the fenestrated glomerular endothelial cells keep negatively charged molecules and plasma proteins in the bloodstream[7]. The second layer of the glomerular filtration barrier is the glomerular basement membrane (labelled as the shared basement membrane in Figure 2), which is the physical bridge between the glomerular endothelial cells and the podocytes that maintain the glomerular filtration barrier together[6,7,8]. The glomerular basement membrane is composed of collagen IV, laminin, fibronectin, nitrogen, and negatively charged sulphate proteoglycans, which adds another sieving layer[6,7,8]. The third and final layer of the glomerular filtration barrier is the podocytes[6,7]. Podocytes are octopus-shaped cells that regulates the flow from the glomerulus through the slit diaphragm[6,7]. The slit diaphragm is a molecular arrangement found between the 40 nm opening of the podocytes' foot processes[6,7]. The slit diaphragm is composed of various proteins (e.g. nephrin, podocin, Neph 1/2, cadherins, and CD2-associated protein) and connects neighbouring foot processes while also anchoring the podocytes to the glomerular basement membrane[7]. Podocytes are also responsible for glomerular basement membrane and glomerular endothelial cell regeneration[6,7]. Indeed, many stated a reciprocal relationship between the endothelial cells, glomerular basement membrane, and podocytes[6-16]. It was shown that podocyte play a role in the function, structure, growth, survival, differentiation, and permeability of endothelial cell through paracrine signaling of diverse cytokines, including the vascular growth factor A [8-16]. Podocyte's vascular growth factor A overexpression was also shown to lead to the glomerular basement membrane thickening, hinting at a

relation between the glomerular basement membrane and the podocytes[9]. Additionally, both the endothelial cells and the podocytes highly express components (e.g., fibronectin and thrombospondin) and key molecules involved in the extracellular matrix regulation, such as plasminogen activator inhibitor 1[10].

After the renal corpuscle, the filtrate goes through the different sections of the tubule, the proximal tubule, the loop of Henle, and the distal tubule[6]. On all its length, the tubule is wrapped in arterioles and venules (peritubular capillaries), allowing reabsorbed molecules from the tubule to go back into the bloodstream. It also allows further excretion of certain molecules from the bloodstream to the tubule after the glomerulus[6]. In the proximal tubule, various small molecules such as glucose, amino acids, and mineral are reabsorbed[6]. 70% of the sodium in the filtrate is reabsorbed at the proximal tubule[6]. In the loop of Henle water is reabsorbed, thereby concentrating the urine filtrate. In the last segment of the tubule, the distal tubule, various minerals concentrations, such as calcium, sodium, potassium and magnesium and water content are being adjusted[6,17]. The fine tuning occurring in the distal tubule is regulated by aldosterone, a hormone produced by the adrenal gland in situations of low blood volume and hyperkalemia (high level of blood potassium)[6,17]. The macula densa cells located in the distal tubule area and nearby the glomerulus and arteriole control the filtration rate by monitoring the salt concentration in the distal tubule and secreting vasoconstrictor locally. The vasoconstrictor restricts the afferent arteriole leading to a reduction in the blood flow going to the glomerulus thereby reducing the filtration rate[6]. This process is described as tubular glomerular feedback[18]. The macula densa is also involved in blood pressure regulation as it can control renin secretion by the juxtaglomerular cells, and smooth muscle cells around the arteriole[6]. Once the urine enters the last section of the nephron, the distal tubule, the urine goes into the

collecting duct[6]. The collecting duct is an arborized network that collects urine from multiple nephrons[6]. Not only does the collecting duct bring the urine from the nephrons to the ureter, but it is also able to further reabsorb water and salts when the organism's hydration levels are low[6,19]. Indeed, parts of the collecting tubule can reabsorb water under the action of vasopressin, a hormone that increases the collecting duct permeability, allowing water to be reabsorbed from the urine[19,20]. Urea reabsorption (urea recycling) in the collecting duct is also regulated by vasopressin[19]. Urea is a product of protein and nitrogen breakdown and an important element for the urine concentrating process in the kidneys[19,21]. Like the distal tubule, the collecting duct can also reabsorb sodium and excrete potassium under the influence of aldosterone. Additionally, some cells in the collecting duct participate in pH homeostasis[6]. Overall, blood filtration and urine production by the kidneys is an elegant process that is constantly adjusting to the organism's needs.

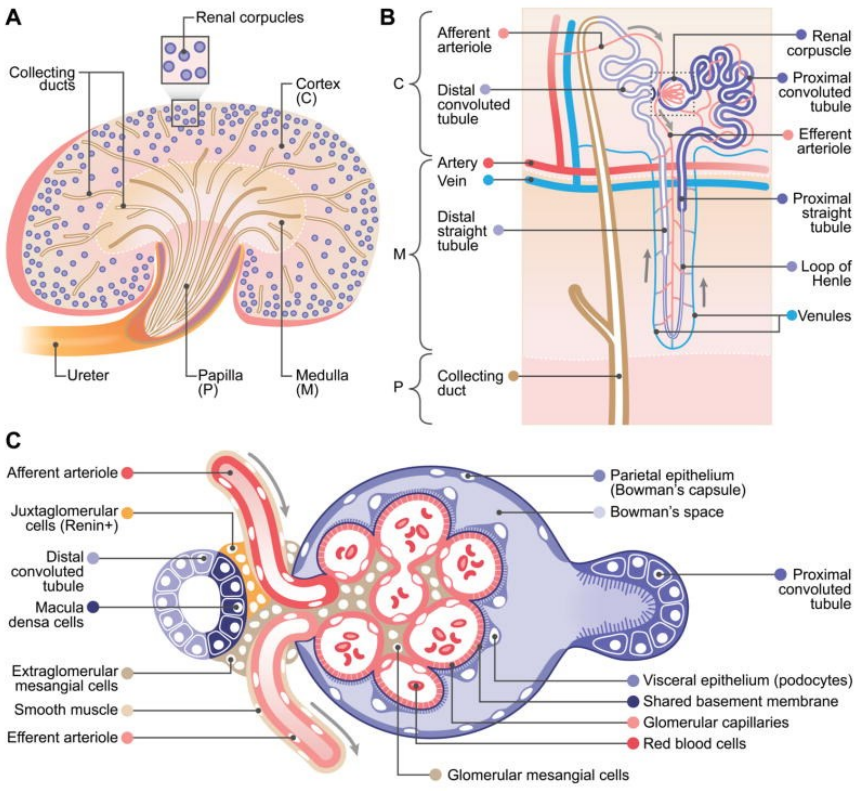

Figure 2. **Kidney and nephron anatomy. A.** General kidney anatomy. **B.** General nephron anatomy. **C.** Detailed glomerulus anatomy. Figure retrieved from *McMahon, A.P.*, 2016[6].

In healthy individuals, approximately 180 to 225 liters of blood, 20% of the cardiac output, is filtered by the kidneys daily[3,6]. Around two litres of urine are produced daily[3]. Renal function and glomerular health are assessed by two main measures, the glomerular filtration rate (GFR) and albumin to creatinine ratio (ACR)[22]. As the name says, GFR is a measure of the speed at which the blood is filtered by the glomerulus. GFR is assessed by measuring the blood and urine concentration of a non-reabsorbed substance (completely excreted by the tubule)[23,24]. For GFR urine flow (urine volume per time unit) is also needed[24]. GFR is calculated as the urine concentration of the substance of interest multiplied by the urine flow and divided by the plasma concentration of the substance of interest[24]. The non-reabsorbed substance can either be endogenous (e.g. creatinine) or injected into the individual (e.g. inulin)[23,24]. More often, creatinine is used to estimate GFR as it is more accessible and cheaper to perform[23]. Creatinine is a waste product from dietary protein breakdown and muscle metabolism[24]. It is said that GFR calculated from creatinine is the estimated glomerular filtration rate (eGFR) since peritubular capillaries secrete further some creatinine in the tubule, leading to a 10-20% overestimation of GFR[24]. In healthy individuals, eGFR is usually between 100 to 150 mL/min (or 90 to 120 mL/min/1.73m^2)[23,24]. A reduction in eGFR or an elevation in plasma creatinine is commonly indicative of abnormal renal function[23,24]. However, different factors can affect eGFR values such as age, sex, race, diet (meat/protein intake), lifestyle, muscle mass, and chronic conditions, among many[23,24]. Another measure evaluated in renal function is ACR (also known as albuminuria)[25,26]. ACR is the concentration of urine albumin divided by urine creatinine concentration[25]. Albumin is the most abundant plasma protein that modulates oncotic pressure and allows the transport of various substances such as ions, fatty acids and drugs[26]. In healthy kidneys, the glomerular filtration barrier is normally impermeable to

albumin and very little protein gets in the urine[6,7,25]. As mentioned earlier, the glomerular filtration barrier restricts passage of large molecules such as albumin and other large protein in the blood[6,7]. Normal ACR values lie below 30 mg/g (A1 category)[25]. An increase in ACR hints at renal damage and early kidney disease[25,27]. ACR between 30 and 300 mg/g (microalbuminuria; A2 category) for over three months hints at the possibility of chronic kidney disease (CKD) whereas ACR above 300 mg/g (macroalbuminuria; A3 category) is often accompanied by a reduction in GFR[25]. Table 1 presents the risk of progression, morbidity and mortality associated with the GFR and ACR values[28]. Finally, Blood urea nitrogen (BUN) is another measure that can provide indices on kidney function[29]. BUN is the concentration of urea nitrogen in the blood[29]. Urea nitrogen is a product of dietary protein breakdown filtered and excreted by the kidneys[29]. In individuals with healthy kidneys, BUN is between 7 and 20 mg/dL (2.5 to 7.1 mM)[29]. When kidneys are not functioning properly and GFR is reduced, BUN can increase[29]. Note that certain medications (e.g., prednisone and some antibiotics), as well as intestine and stomach bleeding, can increase BUN concentration without affecting kidney health[29].

Table 1. **Risk of kidney disease progression, morbidity, and mortality according to GFR and ACR (albuminuria) level.** Acronyms are defined below. Table reproduced from the National kidney foundation with modifications[20].

				ACR Categories (mg urine albumin/ g urine creatinine)		
				A1 (Normal to mildly increased)	A2 Moderately increased	A3 Severely increased
				< 30	30-299	≥ 300
GFR Stages (mL/min/1.73m²)	G1	Normal or high	≥ 90	Low Risk	Moderately Increased Risk	High Risk
	G2	Mildly decreased	60-90	Low Risk	Moderately Increased Risk	High Risk
	G3a	Mildly to moderately decreased	45-59	Moderately Increased Risk	High Risk	Very High Risk
	G3b	Moderately to severely decreased	30-44	High Risk	Very High Risk	Very High Risk
	G4	Severely decreased	15-29	Very High Risk	Very High Risk	Highest Risk
	G5	Kidney failure	< 15	Highest Risk	Highest Risk	Highest Risk

ACR: Albumin to creatinine ratio; GFR: Glomerular filtration rate

1.2. Renal Diseases

In 2017, kidney disease was the twelfth leading cause of death worldwide[30]. In 2019, 41 thousand Canadians had end-stage renal disease (ESRD)[31]. In Canada, the number of dialysis patients doubled from 1999 to 2019[31]. The United States spends approximately 48 billion dollars annually on kidney disease treatment. Less than 10% of CKD patients across the globe are receiving dialysis treatment or kidney transplants[32]. Most of the patients treated for kidney diseases are in the United States, Japan, Germany, Brazil, and Italy[33]. These statistics highlight the growing impact of kidney disease and the urgent need for early detection methods and alternative treatment.

Kidney disease (or nephropathy) is a group of various diseases that impact renal function directly or indirectly[34]. Ultimately, nephropathy leads to inefficiency or inability of blood filtration causing an accumulation of waste and toxins in the bloodstream[34,35]. During nephropathy, if the glomeruli and, or the tubules are damaged there can also be a loss of important protein, electrolytes, and red blood cells through urine[35]. Uremic wastes and toxins accumulation along with proteins and electrolytes lost lead to various side effects such as tiredness, weakness, difficulty concentrating, trouble sleeping, itchy skin, consistent eye puffiness, feet and ankles swelling, low appetite, and muscle cramping[35]. Frequent urination, foamy and, or bloody urine are important signs of kidney disease[35]. Not only does nephropathy lead to filtration problems but also gives rise to systemic complications such as high blood pressure, anemia, bone fragility and nerve damage while also increasing the risk of cardiovascular disease development[34]. Symptoms linked to nephropathy are also associated with other conditions, which can lead to a delayed diagnosis[35]. Additionally, severe symptoms of nephropathy are often noticed in the late stages of kidney disease

when kidneys are failing[35]. Because of this, 90% of patients with kidney disease are not diagnosted[35]. This demonstrates the need for better prognostic tests to diagnose patients in the early stages of the disease and increase their chance of recovery. There are various causes for the development of kidney disease going from glomerulonephritis (glomeruli inflammation) to genetic disorders (e.g. polycystic kidney disease), renal birth defect, autoimmune diseases, drugs and toxins, sepsis (systemic inflammation), and urinary system obstruction[34,36]. Kidney disease can also be developed indirectly by other conditions such as diabetes and high blood pressure[34]. Additionally, chances of developing kidney disease increase with age and are more frequent in certain ethnic populations such as African Americans, Hispanic Americans, Native Americans, Asians, and Pacific Islanders[34].

Kidney diseases are separated into two large categories, acute kidney injury (AKI) and CKD. AKI is described as a sudden episode of kidney failure or kidney damage with a quick reduction in GFR over 24 to 48 hours[37,38]. AKI is discussed in further detail in the following section. CKD is defined as a reduction in GFR that persists over three months and progresses to include persistent parenchymal (functional parts of the kidney) inflammation and fibrosis along with glomerular filtration barrier injury[38,39,40,41]. In addition to glomerulonephritis, genetic disorders, congenital disability, autoimmune diseases, diabetes and high blood pressure, CKD can also be caused by AKI[34,36,42]. Indeed, 64% of AKI patients progress toward CKD[43]. Non-resolving immune response and inflammation from AKI can lead to CKD and ESRD[42]. Persistent immune response and inflammation complicate tissue repair, thereby leading to maladaptive repair and dysfunction[42]. It was shown that individuals with an apparent recovery from an AKI episode can also be at risk for progression to CKD[42]. It's also interesting to note that CKD can promote AKI as well[36]. In the end, both AKI

and CKD can lead to ESRD (also known as kidney failure), where the kidney function is reduced by 85 to 90% (GFR < 15 mL/min/1.73m^2)[28,44]. Patients with ESRD require dialysis or kidney transplant as their kidneys cannot sustain the organism's needs[44]. The relationship between AKI, CKD and ESRD are summarized in Figure 3. Currently, kidney disease treatments are limited to dialysis and kidney transplant. Unfortunately, to this day no drug treatment has shown preventive AKI effects or has reduced mortality rate and AKI to CKD progression in clinical trials[42]. However, medications can be given during kidney disease (AKI and CKD) to help with symptoms and complications such as high blood pressure, diabetes, anemia, and swelling medication[37]. This medication also helps to slow CKD progression[34].

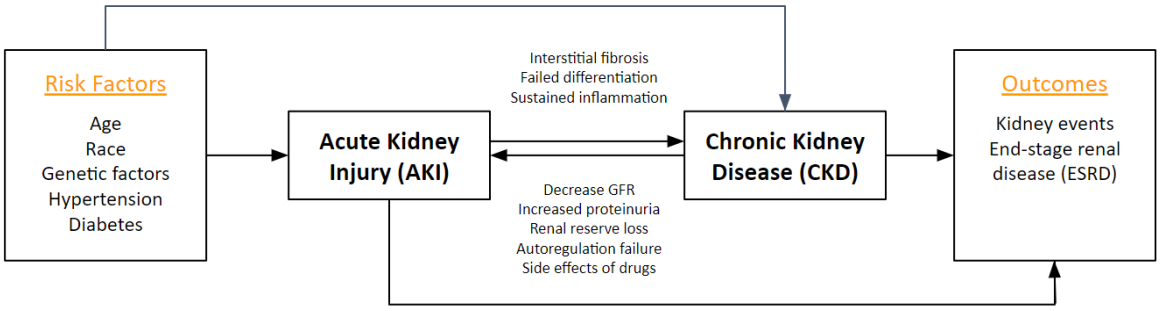

Figure 3. **Relationship between acute kidney injury (AKI), chronic kidney disease (CKD) and end-stage renal disease (ESRD).** Risk factors of AKI and CKD are not limited to the one presented in the figure. AKI can lead to CKD through interstitial fibrosis, failed differentiation and sustained inflammation. CKD can promote AKI events via decreased glomerular filtration rate (GFR), increased proteinuria, renal reserve loss, autoregulation failure and drug side effects. Both AKI and CKD can lead to kidney events such as ESRD. Figured reproduced and modified from *Bao, Y.-W. et al.*, 2018[36].

1.3. Acute Kidney Injury

As mentioned earlier, AKI, previously known as acute renal failure, is described as a sudden and often reversible episode of kidney failure or kidney damage with a quick reduction in GFR over 24 to 48 hours[37,38,45]. The kidney Disease: Improving Global Outcomes (KDIGO) has three different criteria to define AKI[45]. Not all criteria

need to be met to diagnose AKI[45]. KDIGO defines AKI as an increase in serum creatinine of 26.5 μM or more within 48 hours but also as a one-and-a-half-time increase of serum creatinine from baseline within seven days of AKI[36,45]. A urine volume lower than 0.5 mL/kg/hour for a minimum of six hours is another criterion that applies to AKI according to KDIGO[36,45]. It's important to note that BUN and creatinine levels may be in the normal range immediately after the insult[45]. It can take a certain period before seeing an increase in those measures[45]. AKI leads to the accumulation of various products such as waste, toxins, water, and sodium while possibly creating an electrolyte imbalance[37,45]. Seven percent of hospital and 30% of intensive care unit admissions are related to AKI[45]. The AKI in-hospital mortality rate is between 40 and 50%, while in the intensive care unit the mortality rate is over 50%[45]. AKI causes can be separated into three categories, prerenal, renal, and post-renal. Prerenal AKI is linked to reduced blood flow to the kidneys[45]. For example, important fluid loss, severe allergic reactions, burns, heart attacks, major surgeries, and sepsis are causes of prerenal AKI[37,45]. Intrinsic renal AKIs are caused by insults targeting the kidneys, leading to inflammation and glomerular or tubular damage[37,45]. Direct damage to the kidney can happen through prolonged sepsis and ischemia, multiple myeloma cancer, drugs, toxins, and inflammatory or autoimmune renal conditions[37,45]. Post-renal AKI is related to any obstruction that blocks the urinary system such as bladder, prostate or cervical cancer, enlarged prostate, kidney stones, and blood clots in the urinary tract[37,45]. Symptoms of AKI include low urine volume, swelling of the lower body and eye area, fatigue, shortness of breath, nausea, and chest pain or pressure[37]. In severe cases, AKI leads to seizures and coma[37]. However, for some, AKI presents itself without symptoms and is only detected with medical tests such as GFR, blood or urine analysis, imaging, and biopsy[37].

Many AKI insults have a similar pathophysiology[36,42]. After the initial injury, tubular cell death leads to the release of their content, damage-associated molecular patterns[42]. Damage-associated molecular patterns lead to an innate immune response through their recognition by Toll-like receptors on tissue-resident cells (e.g., dendritic cells, fibroblast, and neighbouring tubular cells) and recruited leukocytes[42]. The cells recognizing the damage-associated molecular patterns will then secrete pro-inflammatory molecules (cytokines and chemokines) in order to attract diverse inflammatory cells on-site, which further leads to more cell death, more damage-associated molecular patterns and more cell recruitment[42]. Those cytokines and chemokines also promote the activation of the adaptive immune response, adding to the maintenance of the inflammatory response[42]. Both immune responses also promote extracellular matrix production by myofibroblast, leading to fibrosis[42]. Fibrosis is a typical outcome of renal disease[42]. The quantity of cell death dictates the severity of AKI[42]. Therefore, removing the cause of the injury and introducing interventions to reduce inflammation is essential to avoid severe AKI[42]. In parallel, some immune cells, lymphocytes and macrophages have anti-inflammatory effects that counteract the inflammation and promote repair[42]. Kidney repair involves tubular cells, epithelial cells, immune cells (e.g., macrophages) and stromal cells[42]. During the early AKI, where inflammation is higher, macrophages have the M1 pro-inflammatory phenotype and as time goes on, macrophages transit into the reparative M2 phenotype where they promote tubule regeneration[42]. Furthermore, fibroblasts participate in renal repair by enclosing and stabilizing the damaged area prior to tubular cell proliferation and tubule regeneration[42]. In brief, AKI recovery and chances of CKD development are dependent on a delicate balance and transition macrophages from inflammatory to reparative (anti-inflammatory) phenotype[34,36,42]. As explained in the previous section,

persistent inflammation during AKI leads to maladaptive repair and dysfunction, which increases the risk of CKD development[34,36,42].

In cases of AKI, hospitalization is often required[37]. The root cause of AKI needs to be diagnosed and treated[37]. Treatment is also provided for AKI symptoms and complications[37,45]. Fluids and in certain cases diuretics are given to AKI patients to help with urine output[45]. Nephrotoxic drugs are avoided, and the doses of other medications are reviewed[45]. Levels of sodium, extracellular fluids and blood pH are monitored to avoid further complications[45]. Often patients are placed on renal replacement therapies (RRT) such as dialysis and extracorporeal blood purification (e.g. hemofiltration and hemodialysis), which replaces the kidneys' blood filtering function and alleviate stress on the kidneys until they recover from the injury[37,45]. Recovery can take a few days or weeks up to months in some cases[45]. A recovery analysis showed that 41% of AKI patients have not fully recovered their renal function at discharge[46]. The one year-mortality rate in patients that haven't fully recovered renal function upon hospital leave was of 60%, while in those that did fully recover, the mortality rate is at 30%[46].

While most cases of AKI arise from well known and described causes, new causes of AKI continuously appear. An example of this is the emergence of AKI cases linked with SAR-CoV-2 infection, a virus discovered in 2019-2020.

1.4. Coronavirus Disease 2019

At the end of 2019, the severe acute respiratory syndrome coronavirus two (SARS-CoV-2) emerged in Wuhan, China, and led to a global pandemic[47,48]. As of September 26, 2022, SARS-CoV-2 infected more than 612 million people and caused 6.5 million deaths[49]. SARS-CoV-2 is classified as a β-coronavirus along with the 2002

severe acute respiratory syndrome coronavirus (SARS-CoV) and the 2012 Middle East respiratory syndrome coronavirus (MERS-CoV)[50]. Different studies suggest that the bat is SARS-CoV-2's reservoir, but the intermediate host remains unknown[50,51]. SARS-CoV-2 is transmitted between humans through droplet inhalation as well as direct and indirect contact[50]. Coronaviruses use their trans-membrane spike glycoprotein (also called S protein) to enter the host cells (Figure 4)[51]. The S protein is composed of two subunits, an S1 subunit that binds to the host cells and an S2 subunit that fuses the viral and cellular membrane[51]. The cleavage of the S protein between its two subunits by a cell surface's protein, the transmembrane serine protease two in the case of SARS-CoV-2, allows the activation of the S2 fusion machinery and the entry of the virus into the host cells[51]. After entering the cells, the virus uses the cellular machinery to replicate itself and spread to neighbouring cells[50].

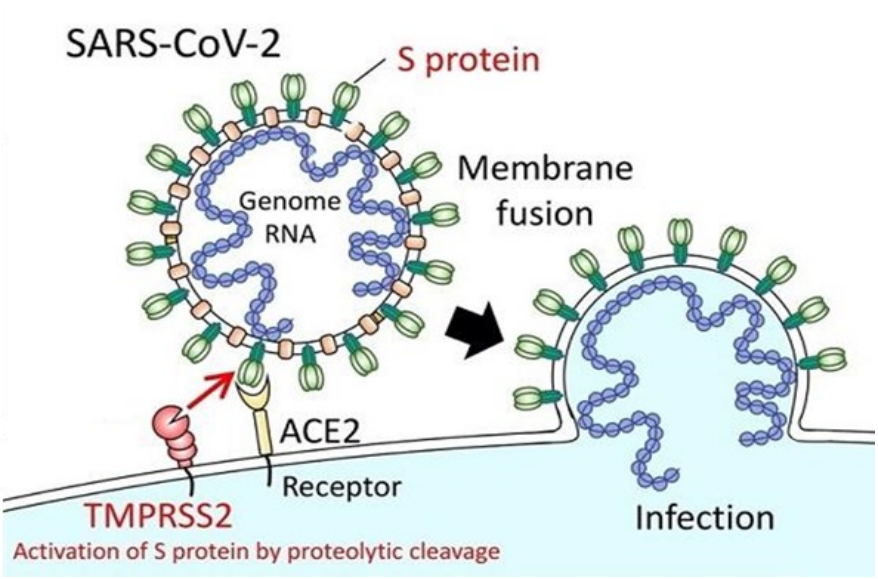

Figure 4. **Severe acute respiratory syndrome coronavirus 2 (SARS-CoV-2) entry in host cells.** SARS-CoV-2 enters host cells using its trans-membrane spike (S) glycoprotein, composed of an S1 and S2 subunit. The S1 subunit binds to the angiotensin-converting enzyme 2 (ACE2) located on the host cells. The cleavage of the S protein by the transmembrane serine protease 2 (TMPRSS2) activates the S2 subunit, which allows the fusion of SARS-CoV-2 with the host cells, leading to the infection of the host. Figure retrieved and modified from *Ishfaq, R. et al*., 2020[52].

The disease caused by SARS-CoV-2 called the coronavirus diseases 2019 (COVID-19), has an incubation period of one to 14 days[53]. Individuals over 60 and individuals with chronic medical conditions (e.g., diabetes, hypertension, lung, and kidney diseases) or that are immunocompromised seem to be at greater risk for more severe symptoms[53]. COVID-19 is generally characterized by symptoms similar to the seasonal flu and cold, such as dry cough, fever, fatigue, and nasal congestion[50]. Dyspnoea (shortness of breath), nausea, diarrhea, anosmia (loss of smell) and ageusia (loss of taste) are other less frequent symptoms seen in COVID-19 patients[50,54]. Some are also experiencing an asymptomatic infection[55]. In the most severe cases, COVID-19 is mostly a respiratory illness characterized by pneumonia and hypoxemic respiratory failure that can be accompanied by different complications, including multiple organ failure and AKI[48,55]. COVID-19 has a one percent mortality rate in the general population but increases to 50% in intensive care unit patients[55].

1.5. Coronavirus Disease 2019-Associated Acute Kidney Injury

As mentioned earlier, AKI is a complication seen in COVID-19[48]. A retrospective study found that the incidence of AKI in COVID-19 patients was 57% compared to 25% in the historical cohort[55]. Early reports from Wuhan demonstrate that 3 to 7% of hospitalized patients develop AKI[56]. Data from Italy showed that COVID-19 patients in the intensive care unit are four times more likely to develop an AKI than patients outside of the intensive care unit[56]. In the United States, the incidence of AKI in COVID-19 patients is between 28 and 46%, with a mortality of 35 to 41%[57]. In certain countries such as China, the coronavirus disease 2019-associated acute kidney injury (C19-AKI) incidence is as low as 5.5% because of the higher numbers of hospital admissions that allow early detection and medical support[55]. Additionally, it seems that

C19-AKI is an independent risk factor of mortality in hospitalized patients with a hazard ratio of 3.5 to 4.7[48,55,56]. Factors contributing to C19-AKI are similar to those of other AKI such as obesity, CKD history, renal transplant recipient, and certain medication (e.g., vasopressor and nephrotoxic drugs)[55]. Severe COVID-19 symptoms and the use of mechanical ventilation during SARS-CoV-2 infection are other risk factors for C19-AKI[55]. Additionally, individuals of advanced age, African descent, male sex, diabetic, and, or living in a nursing home are at increased risk of developing C19-AKI[55]. Like other forms of AKI, C19-AKI has various causes including hypotension, hypovolemia, thrombosis, endotheliitis, acute tubular necrosis, viral infection of renal parenchyma, collapsing glomerulopathy, glomerulonephritis, and acute interstitial nephritis[55].

Numerous medical groups shared their description of C19-AKI. *Hilton et al*. published a review in 2022 summarizing the information currently available on C19-AKI[55]. From their review, mild acute tubular injury is the most common finding in C19-AKI, which is further supported by low molecular weight proteinuria often seen in C19-AKI[55]. AKI is also characterized by hematuria, albuminuria, increased serum creatinine, inflammatory dysregulation, cytokine storm, acute tubular necrosis and various glomerulopathies (e.g. global/segmental glomerulosclerosis and collapsing glomerulopathy)[47,48,58,59]. In some cases, there's also coagulopathy, vasculitis, myoglobin casts, thrombotic microangiopathy and membranous glomerulopathy[47,48,55,58,59]. The glomerular collapsing and the glomerulosclerosis described in C19-AKI share similarities with the one caused by apolipoprotein L-one gene variants[55]. Indeed, in both scenarios, glomerular collapsing and glomerulosclerosis are characterized by glomerular segmental collapse, parietal cell hypertrophy or capillary and podocyte effacement[55]. Apolipoprotein L-one gene encodes for a high-density lipoprotein produced by the liver and involved in the

trypanosome lytic factor from the innate immune system[55,60]. Apolipoprotein L-one possesses a secretary signal that allows its excretion in the bloodstream[60]. However, some apolipoprotein L-one variants (risk alleles; G1 and G2) lack this signal which inhibits protein excretion and can lead to renal injury[60]. As apolipoprotein L-one G1 and G2 variants are common among individuals of African descent, their risk of developing focal segmental glomerulosclerosis is increased by 17 times[55]. Additionally, apolipoprotein L-one risk alleles could increase the risk of collapsing glomerulopathy during SARS-CoV-2 infection[61]. A 2015 study showed that interferons upregulate apolipoprotein L-one expression through antiviral pathways[62]. *In vivo*, interferon administration in patients with apolipoprotein L-one risk alleles lead to the development of collapsing focal segmental glomerulosclerosis[61,62]. It was demonstrated that SARS-CoV-2 infection leads to type one interferon production, which potentially could upregulate apolipoprotein L-one during COVID-19[63]. Other viruses, such as the human immunodeficiency virus (HIV), have been described as a strong risk factor for apolipoprotein L-one-associated renal disease through a strong interferon production and anti-viral response[62].

AKI in COVID-19 can be caused by various other direct and indirect insults[55]. C19-AKI causes include potential viral tropism, immune and inflammatory response (e.g. cytokine storm), coagulopathy and pulmonary COVID-19 complications (Figure 5)[47,48,50,55,58,59]. SARS-CoV-2 S protein has been found beyond the glomerulus suggesting that the virus infects tubular cells and, or the glomerular filtration barrier is damaged[55]. As explained earlier, SARS-CoV-2 enters host cells by binding to the angiotensin-converting enzyme two (ACE2), which is expressed in various locations including the proximal tubules[55]. Therefore, the possibility of SARS-CoV-2 entering the kidneys and causing tubular damage can not be ignored[55]. Alternatively, it is

hypothesized that the virus could be endocytosed by the kidney injury molecule one (KIM-1), an injury molecule expressed by pulmonary and renal epithelial cells[55]. However, SARS-CoV-2 renal tropism is still a subject of debate as other studies have shown no sign of viral infection in the kidneys[47,48,50,55,58,59]. Note that the timing of the renal biopsy could play a role in the diverse response to viral tropism in the kidneys[55]. The immune and inflammatory response, more specifically the complement activation and cytokine storm, occurring during SARS-CoV-2 infection can also lead to C19-AKI[55]. The complement is an assembly of serum and cell surface proteins that interact with each other and are involved in the innate immune response[64]. In the kidneys, the complement activation leads to the deposition and targeting of the tubular basement membrane by the complement, leading to chronic renal inflammation and tubulointerstitial fibrosis[55]. On the other hand, a cytokine storm is a life-threatening inflammatory response causing elevated levels of cytokines (e.g. interleukin (IL)-1, IL-6, and tumor necrosis factor-alpha (TNF-α)) and hyperactivated immune cells[55]. Events such as sepsis can lead to cytokine storms[55]. In COVID-19, the high levels of monocytes and macrophages, as well as pre-existing conditions, could be responsible for the increase in cytokines such as IL-1, IL-6, and TNF-α[55]. IL-6 is known for being involved in AKI development through induction of pro-inflammatory cytokines and chemokines secretion by the renal endothelium, leading to microvascular dysfunction[55]. A 100-fold increase in IL-6 has been linked with increased rates of AKI[55]. Moreover, coagulopathy can be involved in the development of C19-AKI[55]. COVID-19 infection is presented with pulmonary and systemic endotheliitis[55]. The SARS-CoV-2 infection has prothrombotic and sepsis characteristics[55]. Thrombosis has been noted in the heart, brain, and kidney microvasculature, potentially leading to organ damage and injuries such as AKI[55]. Indeed, in severe COVID-19 thrombotic microangiopathy,

characterized by thrombocytopenia and microthrombi causes ischemic injury in pulmonary vascular and kidneys[55]. In addition to direct renal damage giving rise to C19-AKI, AKI during SARS-CoV-2 infection can also originate from indirect insults such as therapeutics interventions for other complications and systemic effects of COVID-19[55]. For example, increased breathing work, fever, gastrointestinal infection, and use of nephrotoxic drugs (e.g., certain antibiotics) during COVID-19 can lead to hypovolemia and AKI development[55]. Since the organism is an assembly of interconnected tissues and organs, pulmonary complications can impact renal health during COVID-19 disease[55]. Hemodynamic instability and fluid restriction strategies in ARDS patients, as well as respiratory failure, can worsen renal injury through renal hypoxemia, renovascular resistance, hypercapnia and reduced GFR[55].

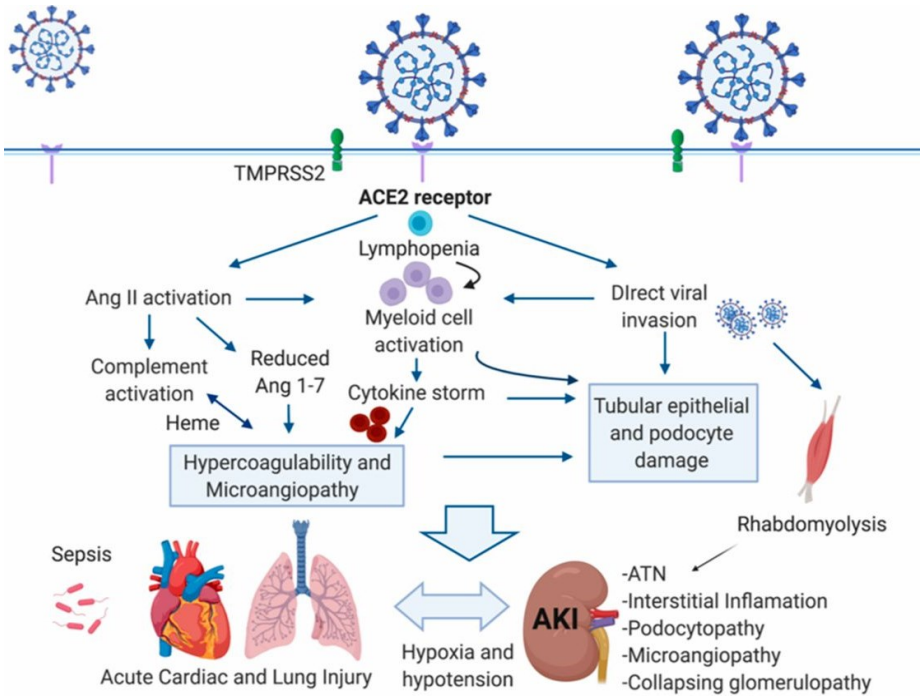

Figure legend on the following page (Figure 5).

Figure 5. **Biology of coronavirus disease 2019 (COVID-19) associated acute kidney injury (AKI; C19-AKI).** C19-AKI has different potential causes, including viral tropism, immune and inflammatory response, coagulopathy, multi-organ complications and therapeutic interventions. Severe acute respiratory syndrome coronavirus two (SARS-CoV-2) tropism could lead to C19-AKI development as the angiotensin converting enzyme two (ACE2) is expressed on proximal tubule cells and the kidney injury molecule one (KIM-1) may cause viral endocytosis in renal epithelial cells. Complement deposition and immune cell infiltration in the kidneys during COVID-19 could promote C19-AKI development. Complement deposition in the tubular basement membrane can lead to chronic renal inflammation and tubulointerstitial fibrosis while increased number of immune cells (e.g., monocytes and macrophages) increase cytokines levels. Hypercoagulation and thrombosis can lead to ischemic injuries in various tissue, including the lungs and kidneys. Multiple organ complications occurring during SARS-CoV-2 infection can promote or worsen renal complications. Therapeutics interventions used during COVID-19, such as fluids restriction in acute respiratory distress syndrome, can exacerbate renal complications as well. This goes without including the renin-angiotensin system (RAS) imbalance caused by the reduced presence of ACE2 due to SARS-CoV-2 entry in host cells, thereby leading to an increase in angiotensin (Ang) II concentration and reduction in Ang 1-7 production. ATN: Acute tubular necrosis. TMPRSS2: Transmembrane serine protease 2. Figure retrieved from *Batlle, D. et al*., 2020[65].

Assessment and treatment of AKI during COVID-19 are performed in the same manner as other AKIs[55]. Diagnosis of C19-AKI is done through examination of the patient medical history, volume status, hemodynamic and urinalysis[55]. Interestingly, in a COVID-19 study where urinalysis was performed, proteinuria was found in 65.8% of patients, and hematuria was seen in 41.7% of patients while only 4.7% of patients were diagnosed with AKI according to the KIDGO criteria[55]. In addition to the traditional assessment of AKI, other biomarkers start being used for early detection[55]. Indeed, neutrophil gelatinase-associated lipocalin (NGAL) and KIM-1 are two well-known markers of renal injury[55]. NGAL and KIM-1 are produced by the distal tubule and proximal tubule respectively during renal injury[55]. In COVID-19, those two markers are linked with AKI development and could predict mortality and renal replacement therapies (RRT) needs[55]. Tissue inhibitor of metalloproteinases two and the insulin-like growth factor-binding protein seven are two other biomarkers being tested to assess early AKI[55]. As explained in one of the previous sections, other than RRT, there are no treatment available for AKI, instead, the underlying causes, symptoms emerging from, and complications of AKI must be addressed[37,45,55]. Volume

resuscitation can reduce the risk of AKI and respiratory failure[55]. Salts levels (e.g., hypochloremia, hypernatremia) and blood pH are monitored[55]. Drug doses are adjusted to avoid further renal damage as well. Like other causes of AKI, C19-AKI can require dialysis and other RRT[55]. During the pandemic, as more patients required RRT and due to other factors, resources were limited and certain supplies were in shortage, which added additional stress to the healthcare system[37,55]. This situation asked for strategic and patient-adjusted use of RRT devices[55]. It was noted that no benefits came from performing early RRT compared to the patient-adjusted timing of RRT[55]. Extracorporeal blood purification has been used as well in COVID-19 to remove inflammatory mediators from blood circulation and reduce organ damage like AKI[55]. Studies using extracorporeal blood purification on COVID-19 patients gave mixed results[55]. Some state that extracorporeal blood purification reduced cytokine levels, improved hemodynamics, and reduced mortality while others present reduced survival during extracorporeal blood purification therapy and no difference in cytokine levels[55]. Experimental treatments are also being evaluated in COVID-19 patients such as complement and IL-6 cytokine inhibitors, prophylactic administration of heparin, inhibitors of the viral ribonucleic acid (RNA)-dependent RNA polymerase, and corticosteroids. Most therapies show potential benefits, but more studies are required[55].

As the pandemic is ongoing, its progression and extent remain unknown. The long-term consequences of SARS-CoV-2 infection on overall and renal health (e.g., AKI to CKD progression) remain to be assessed. Statistics show that at discharge, 50% of C19-AKI patients have not recovered their baseline values. In an American study, from 20% of patients on RRT, 63% died during hospitalization[55]. Of the survivors, 33% were on dialysis at discharge and 16% stayed on dialysis for 2 months

after intensive care unit administration[55]. In a German study, 90% of patients that required RRT were dialysis independent after 151 days[55]. This all goes without mentioning the possibility of other coronaviruses' emerging in the future to potentially affect kidney health. Hence, understanding C19-AKI etiology and progression is necessary to reduce its incidence and find potential therapeutic options to alleviate the disease. Furthermore, findings made on C19-AKI could be transferred to treat and better understand other types of AKI.

1.6. Renin-Angiotensin System

As previously discussed, SARS-CoV-2 makes its entry into the host cells using its S protein, which binds to a cell surface protein from the host cells. Similar to SARS-CoV, SARS-CoV-2 uses the ACE2 protein to bind to the host cells, which promotes the clathrin-dependent endocytosis of the virus-ACE2 complex[50,66]. ACE2 is an important member of the RAS, a hormonal system that regulates blood pressure, body fluids, electrolytes, and vascular resistance[67].

The RAS is composed of two counter-regulatory arms called the classical (or RAS) arm and the alternative anti-inflammatory (or anti-RAS) arm (Figure 6)[4,68]. The classical arm is composed of angiotensin-converting enzyme (ACE), angiotensin two (Ang II) and angiotensin type one receptor (AT1R), while the alternative arm includes ACE2, angiotensin (Ang) 1-7 and the Mas receptor[68]. In the classical arm, the angiotensinogen produced by the liver and adipose tissue is cleaved by renin, a protease released by the kidneys, to produce angiotensin one (Ang I), which is then hydrolyzed by ACE to produce Ang II[4]. Ang II has vasoconstrictive and hypertensive effects while also promoting inflammation and cell proliferation[69]. Ang II can bind to AT1R and Angiotensin type two receptor (AT2R). Ang II binding to AT1R promotes

vasoconstriction and aldosterone secretion, which increases sodium reabsorption and blood pressure[4,69]. Ang II binding to AT2R has effects that are opposed to the ones generated by AT1R, such as vasodilatation, hypotension, and apoptosis, and can inhibit AT1R functions[69]. In the alternative arm, ACE2 converts Ang II into Ang 1-7, which binds to the Mas receptor[4]. Ang 1-7 binding to Mas receptor has vasodilating, anti-inflammatory, anti-proliferative and antifibrotic effects[4]. Ang 1-7/Mas receptor effects oppose the actions of Ang II/AT1R[4].

ACE2 plays an essential role in SARS-CoV-2 cell entry. ACE2 is a cell membrane enzyme that cleaves one Ang I and Ang II residue to produce Ang 1-9 and Ang 1-7, respectively[50,70]. ACE2 is expressed along the surface of epithelial cells of the mouth and tongue as well as on type I and II alveolar epithelial cells, enterocytes, and various cardiac cells[50]. In the kidney, ACE2 is highly expressed in proximal tubule cells and is present in podocytes to a lower extent[50]. SARS-CoV-2 binds to ACE2, which leads to its internalization and reduced presence on the cell surface resulting in an imbalance in RAS (Figure 6)[4,68]. It is thought that the reduced activity of ACE2 leads to an over-activation of the classical ACE/Ang II/AT1R arm that has pro-inflammatory features, worsening respiratory, cardiovascular and renal complications[4,68]. Reducing the imbalance in the RAS could help with the inflammation seen in COVID-19.

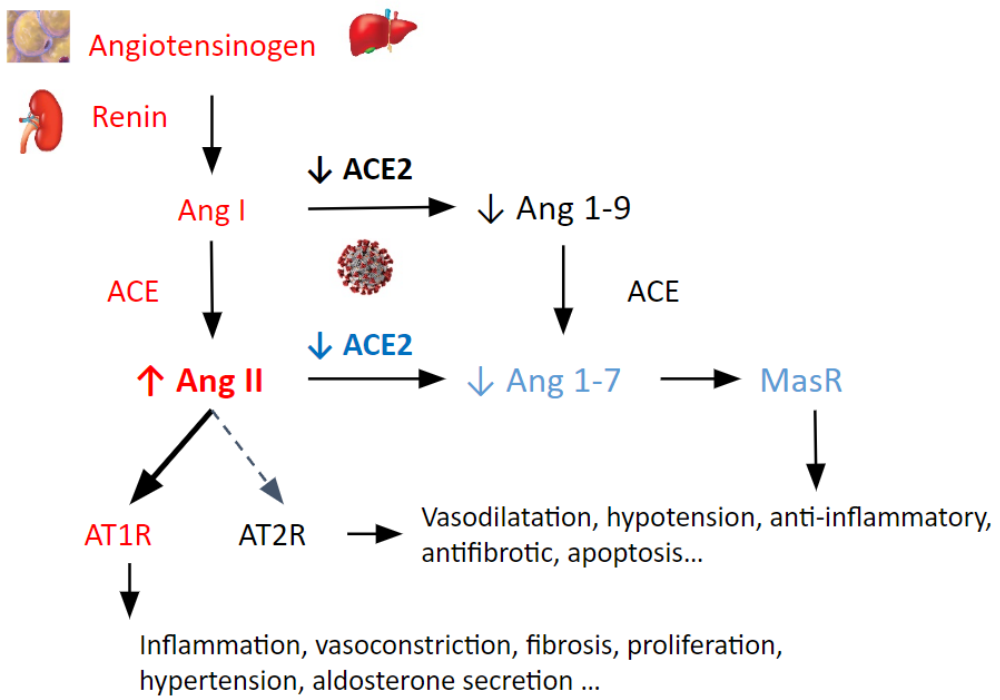

Figure 6. **The renin-angiotensin system (RAS)**. The RAS is composed of the classical arm (in red) and the alternative arm (in blue). In the classical arm, the angiotensinogen produced by the liver and adipose tissue is cleaved by renin, a protease released by the kidneys, to produce angiotensin (Ang) I, which is then hydrolyzed by angiotensin-converting enzyme (ACE) to produce Ang II. Ang II binding to angiotensin type I receptor (AT1R) promotes inflammation, vasoconstriction, fibrosis, proliferation, and aldosterone secretion, which increases sodium reabsorption and blood pressure. Ang II binding to angiotensin type II receptor (AT2R) leads to vasodilatation, hypotension, and apoptosis while also having anti-inflammatory and anti-fibrotic effects. Ang II has a higher infinity for AT1R compared to AT2R. In the alternative arm, ACE2 converts Ang II into Ang 1-7, which binds to the mass receptor (MasR). MasR binding leads have similar effects to AT2R binding. Entry of severe acute respiratory syndrome coronavirus 2 (SARS-CoV-2) leads to an internalization of ACE2 on host cells, thereby causing a RAS imbalance.

1.7. Animal Model of Coronavirus Disease 2019

Since the beginning of the pandemic, many groups have been developing and testing COVID-19 therapies and SARS-CoV-2 vaccines. To evaluate those treatments, animal models of COVID-19 disease are needed. Mice are the prominent animal model used in human disease and drug research due to their inexpensive housing, simplicity in breeding and their 85% similarities with the human genome[71,72]. Although the ACE2 protein has an 82% similarity between human and mice, SARS-CoV-2 doesn't bind to ACE2 and lead to infection in mice[73,74]. To work around this

limitation, two principal types of COVID-19 mouse model were developed[74]. One COVID-19 mouse model consists of the adaptation of mouse ACE2 and SARS-CoV-2 to increase their affinity, leading to viral entry and infection[73,74]. There are two main methods to increase SARS-CoV-2 and mouse ACE2 binding[74]. The first method consists of the incubation of a pool of SARS-CoV-2 variants in mouse lung, a tissue with a high ACE2 expression[74]. Certain variants will have a S protein with a higher affinity for the mouse ACE2 binding site, which will lead to viral entry and replication in the mouse cell. The variant with high affinity to the mouse ACE2 can then be isolated from the mouse tissue and further characterized[74]. This method produced mice that were sensitive to the virus but only developed mild COVID-19 symptoms[74]. The second method uses reverse genetics to adapt the ACE2 receptor binding domain to increase virus binding and infection[74]. This method can also be applied to transmembrane serine protease two to obtain a model for transmembrane serine protease two inhibitor testing[73]. *Dinnon et al* developed a mouse adapted model of SARS-CoV-2 where they reverse engineered the SAR-CoV-2 S protein to increase the S protein and mouse ACE2 affinity[75]. Their recombinant virus led to viral entry and replication in the airways[75]. It's important to note that ACE2 and SARS-CoV-2 adaptation methods could lead to an outgrowth of new viruses with unknown symptoms and disease severity[74]. The second method to have SARS-CoV-2 infection in mice is the use of humanized mice[74]. In other words, instead of modifying the mouse ACE2 or the virus, the mouse ACE2 gene would be replaced by the human version of ACE2[74]. Several transgenic human ACE2 mice have been developed to study SARS-CoV infection and potential treatments[73,74]. Since both SARS-CoV and SARS-CoV-2 use ACE2 for cell entry, human ACE2 mice previously developed for SARS-CoV can be used to study SARS-CoV-2[73,74]. The human ACE2 in those mice can be placed

under the same regulation as the endogenous mouse ACE2 or it can be placed under a promoter that allows expression of human ACE2 to be modulated[74]. Indeed, human ACE2 can be placed under the control of a universal promoter, which allows the researcher to modulate the ACE2 expression in the organism[74]. Human ACE2 expression can also be regulated by a tissue specific promoter, meaning that human ACE2 can be modulated and expressed in specific tissues exclusively[74]. Transgenic ACE2 mice can be infected by SARS-CoV-2, leading to different intensity of disease depending on the expression pattern of ACE2[74]. Instead of a permanent genetic modification, it is also possible to temporarily express human ACE2 in mice using viruses such as adenovirus that express human ACE2[74]. The adenovirus with human ACE2 enters and uses the host cell machinery to replicate its genome, including the human ACE2 gene[74]. This allows for SARS-CoV-2 entry and infection in the host[74]. Usually, the adenovirus (and human ACE2 in this scenario) is cleared from the organism by one week[74]. This system has the advantage of being easily applied to various murine strain[74]. Transgenic ACE2 mice offer an interesting platform to further understand SARS-CoV-2 pathophysiology and evaluate vaccines and treatments against COVID-19[74]. However, ACE2 expression in transgenic ACE2 mice can be ectopic and potentially lead to modification in tissue and cellular viral tropism[74].

Although many publications present the clinical description of COVID-19 and its AKI complication, the mechanism underlying C19-AKI remains unclear[56]. Currently, there is no mouse model of COVID-19 that presents all the characteristics seen in humans[74]. There are also no publications about a model of C19-AKI so far. Furthermore, the use of SARS-CoV-2 in animal research requires a containment level three facilities thereby limiting the scale of COVID-19 research[76]. Unfortunately, not all research institutes have access to those establishments, which limits the amount of

research on the subject. In this thesis, a model presenting similarities with C19-AKI and requiring no viral entities is proposed. This surrogate model of C19-AKI is accessible (no containment level three facilities needed) and simple to use.

1.8. G-Coupled Protein Receptor 84

Inflammation is an important contributor to the progression of many forms of AKI[77]. The recovery from an AKI episode depends on the level of tubular lesions and on the ability to overcome renal inflammation[42]. Many studies suggest that infiltrating immune cells (e.g. neutrophils and macrophages) and resident immune cells have a key role in the injury and recovery seen in AKI[42,78,79]. In the early phase of AKI, macrophages are driven towards a pro-inflammatory M1 phenotype that later shifts into a reparative and pro-fibrotic M2 phenotype[42]. Macrophage failure to switch from a pro-inflammatory to a reparative phenotype leads to chronic inflammation and progressive renal function decline[42,78]. Therefore, macrophage polarization is an important aspect of AKI recovery and could be a viable treatment avenue for C19-AKI and AKI in general.

In recent years, our group has investigated the involvement of the pro-inflammatory G-coupled protein receptor 84 (GPR84) in renal disease. G-coupled protein receptors (GPRs) are cell surface receptors composed of seven transmembrane domains[80]. GPRs are one of the largest families of protein, with more than 50% of drugs targeting these receptors[80]. They are involved in various pathways and are activated by various compounds, including light, ions, amino acids, nucleotides, lipids and peptides[80]. GPR84 acts through the pertussis toxin sensitive $G_{i/o}$ pathway but can also act through the $G_{q/i}$ pathway[81,82]. GPR84 is said to respond to medium-chain (9-14 carbons) free fatty acids. However, a recent review on the

receptor points out that medium-chain free fatty acids have a modest potency in activating GPR84[81,83]. In this review, *Marsango et al*. suggest that medium-chain free fatty acids are orthosteric agonists[83]. An orthosteric binding site is usually an extracellular pocket on the receptor where endogenous ligands bind, and that can be modified by the binding of a modulator to an allosteric site[83]. GPR84 is highly expressed in various immune cells, including splenic T and B cells, monocytes, macrophages, neutrophils and peripheral leukocytes and is also expressed in adipocytes, epithelial cells, fibroblast, and podocytes[80,83,84,85]. GPR84 was de-orphaned in 2006 (member of FFA-sensing GPRs now) and is said to have a role in linking fatty acid metabolism to immunological regulation[80,81]. In different immune cells, GPR84 is related to cytokine production, reactive oxygen species generation, and calcium influx[86]. It has been shown that GPR84 activation in macrophage-like cells (RAW264.7) and adipocytes increase the production of pro-inflammatory factors such as IL-12, TNF-α, IL-1β and IL-33[81,84]. Additionally, GPRs coupled to Gi proteins, like GPR84, inhibit cyclic adenosine monophosphate (cAMP)-dependent pathways, such as the M2 macrophage polarization by IL-4 inhibition, suggesting that GPR84 could block macrophage transition from a pro-inflammatory to an anti-inflammatory and reparative phenotype (Figure 7)[87,88]. Indeed, GPR84 knockout (KO) mice have increased type 2 T helper cytokines production (e.g. IL-4, IL-5 and IL-13) and reduced kidney fibrosis[81,85,89]. Interestingly, GPR84 was found in bronchoalveolar lavage fluid neutrophils from COVID-19 patients in the intensive care unit[90]. Our group showed that GPR84 plays an important role in renal fibrosis in various CKD mouse models, including 5/6 nephrectomy, doxorubicin-induced nephropathy, and adenine-induced CKD[85]. In these models, GPR84 expression increased in macrophages, podocytes and proximal tubule cells and was accompanied by increased cytokine production[85].

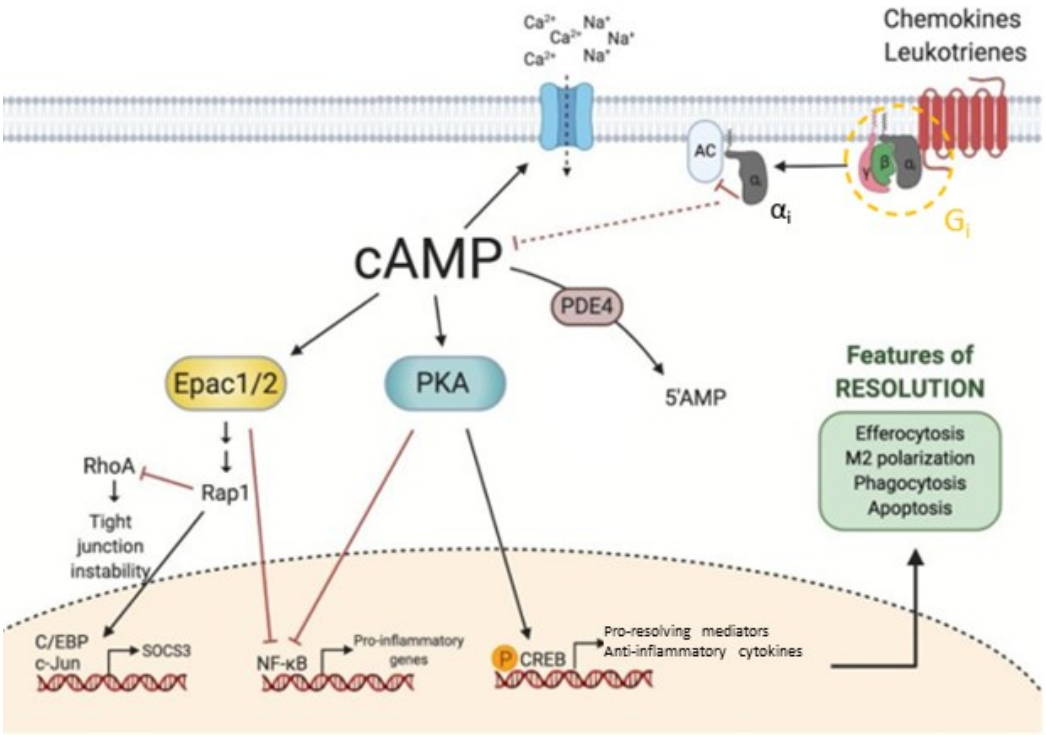

Figure 7. **Cyclic adenosine monophosphate (cAMP) inhibition by G-coupled protein receptors (GPR) coupled to G_i protein.** cAMP is produced by converting adenosine triphosphate (ATP) to cAMP by adenylyl cyclase (AC). Phosphodiesterase-4 (PDE4) converts cAMP to adenosine monophosphate (AMP), thereby reducing cAMP levels. Activation of GPR coupled to a Gi protein leads to AC inhibition by the $G_{\alpha/i}$ subunit, thereby affecting cAMP-dependent pathways. cAMP activates cAMP gated ion channels, protein kinase A (PKA) and the exchange protein 1/2 activated by cAMP (Epac1/2). Cyclic adenosine monophosphate-responsive element binding protein (CREB) phosphorylation by PKA promotes the expression of pro-resolving mediators and anti-inflammatory cytokines, leading to resolution of inflammation through reparative M2 macrophage polarization, apoptosis, phagocytosis, and efferocytosis. PKA also inhibits inflammatory gene expression by nuclear factor kappa-light-chain-enhancer of activated B cells (NF-κB). cAMP activation of Epac1/2 inhibits pro-inflammatory cytokines, which helps with the resolution of inflammation as well. Figure retrieved and modified from *Tavares L.P., et a*l, 2020[91].

1.9. G-Coupled Protein Receptor 84 Antagonists

Several pharmaceutical companies are currently developing GPR84 antagonists. These compounds exhibit antifibrotic and anti-inflammatory effects in various tissues, suggesting again that GPR84 participates in fibrosis and inflammation[85]. PBI-4050 (3-pentylbenzeneacetic acid sodium salt) is a fatty acid derivative GPR84 antagonist or inverse agonist developed by Liminal Biosciences (formerly Prometic Biosciences)[83,85]. PBI-4050 is also an agonist for free fatty acid one

and free fatty acid two, also known as GPR40 and GPR43, respectively[83]. PBI-4050 was tested in phase II clinical trials related to type II diabetes and metabolic syndrome Alström syndrome, and idiopathic pulmonary fibrosis[92,93,94]. A preclinical study in a mouse model of type 2 diabetes showed that PBI-4050 improved glycemic levels and had antifibrotic effects in the kidney[95]. In a preclinical model of nonalcoholic steatohepatitis, PBI-4050 reduced neutrophil migration, monocyte-derived macrophage activation and levels of fibrosis seen in the liver[96]. Our group also demonstrated that PBI-4050 has anti-inflammatory and antifibrotic effects in different preclinical mouse models of kidney diseases[85]. Indeed, in these models, PBI-4050 reduced macrophage activation as well as pro-inflammatory and pro-fibrotic markers[85]. Additionally, in a lipopolysaccharide (LPS) sepsis-induced model, PBI-4050 reduced the level of several circulating pro-inflammatory cytokines (e.g., IL-6, TNF-α, monocyte chemoattractant protein-one, and interferon gamma)[97].

GLPG-1205 ($C_{22}H_{22}N_2O_4$) is another GPR84 antagonist developed by Galapagos NV[98]. In idiopathic pulmonary fibrosis preclinical animal studies, GLPG-1205 showed a reduction in signs and symptoms of idiopathic pulmonary fibrosis[98]. In a mouse dextran sodium sulphate-induced chronic inflammatory bowel disease model, GLPG-1205 reduced disease activity index score and neutrophil infiltration[82,99]. In two preclinical lung fibrosis models (bleomycin and irradiation), GLPG-1205 improved lung function decreased collagen deposit and reduced manganese superoxide dismutase (which degrades reactive oxygen species) in bronchial epithelial cells and parenchymal macrophages[100]. Additionally, GLPG-1205 recently completed phase II clinical trials for idiopathic pulmonary fibrosis and ulcerative colitis[98,101,102]. In the literature, GLPG-1205 has not yet been evaluated in renal disease. However, other GPR84 antagonists, such as PBI-4050 have shown interesting results in various

kidney models[85,92,93,95,96]. Overall, studies conducted on GPR84, and its antagonists demonstrate a potential therapy for C19-AKI.

1.10. Rationale

At the end of 2019, the SARS-CoV-2 emerged in Wuhan, China, and led to a global pandemic[47,48]. In 40% of SARS-CoV-2 severe cases admitted to the hospital, pulmonary complications are accompanied by AKI[3,48]. Current treatment for renal complications includes dialysis, which limits financial and material resources available for non-COVID-19 patients and applies additional stress on the healthcare system[37]. Adjuvant therapies are needed to prevent C19-AKI and improve patient outcomes. Additionally, the progression and the extent of the pandemic remain unknown, as it is ongoing. The long-term consequences of SARS-CoV-2 infection on overall and renal health (e.g., AKI to CKD progression) remain to be assessed. This all goes without mentioning the possibility of other coronaviruses' emergence in the future potentially affecting kidney health. To explore such treatments and accelerate research in case of a future coronavirus outbreak, a mouse model of C19-AKI would represent a critical biomedical research tool.

GPR84 is highly expressed in various immune cells, including monocytes, macrophages, neutrophils and peripheral leukocytes[80,84,85]. GPR84 is involved in fatty acid metabolism, immunological regulation, cytokine production, reactive oxygen species generation, and calcium influx[80,81,86]. In COVID-19 patients, GPR84 has been found in bronchoalveolar lavage fluid neutrophils, pointing toward a possible implication of GPR84 in the disease[90]. In various CKD mouse models, an increased expression of GPR84 in macrophages, podocytes, and proximal tubule cells along with increased cytokine production was seen, suggesting that GPR84 contributes to

inflammation-associated injuries[85]. In preclinical models of renal injury, genetic deletion and pharmaceutical antagonists of GPR84 with PBI-4050 showed anti-inflammatory and antifibrotic effects[81,85,89]. Additionally, PBI-4050 completed phase II clinical trials in, idiopathic pulmonary fibrosis, type II diabetes, and Alström syndrome[92,93,94]. GLPG-1205, another GPR84 antagonist, also completed phase II clinical trials in idiopathic pulmonary fibrosis as well as in ulcerative colitis[98,101,102]. Therefore, GPR84 deletion or pharmacological antagonism with PBI-4050 or GLPG-1205 could attenuate indices of renal injury in a surrogate C19-AKI mouse model.

1.11. Purpose

The purpose of the work described in this thesis is to develop a surrogate mouse model presenting similarities with C19-AKI without the use of viral particles and assess the role of GPR84 in the model.

1.12. Objectives and Hypotheses

The objectives and hypotheses of this thesis are the following. Hypotheses are presented graphically in Figure 8.

Objective 1: Develop a new surrogate mouse model of C19-AKI disease that mimics the pro-inflammatory context of this condition, consisting of an ACE2 KO mouse administered a low pressor dose of Ang II and LPS.

Hypothesis 1: Mice with genetic deletion of ACE2 administered Ang II and LPS will develop AKI with similarities to C19-AKI.

Objective 2: Determine the role of GPR84 in our surrogate model of C19-AKI through genetic deletion and the use of the GPR84 antagonist, GLPG-1205.

Hypothesis 2: Genetic and pharmacological inhibition of GPR84 will reduce indices of AKI seen in our surrogate mouse model of C19-AKI.

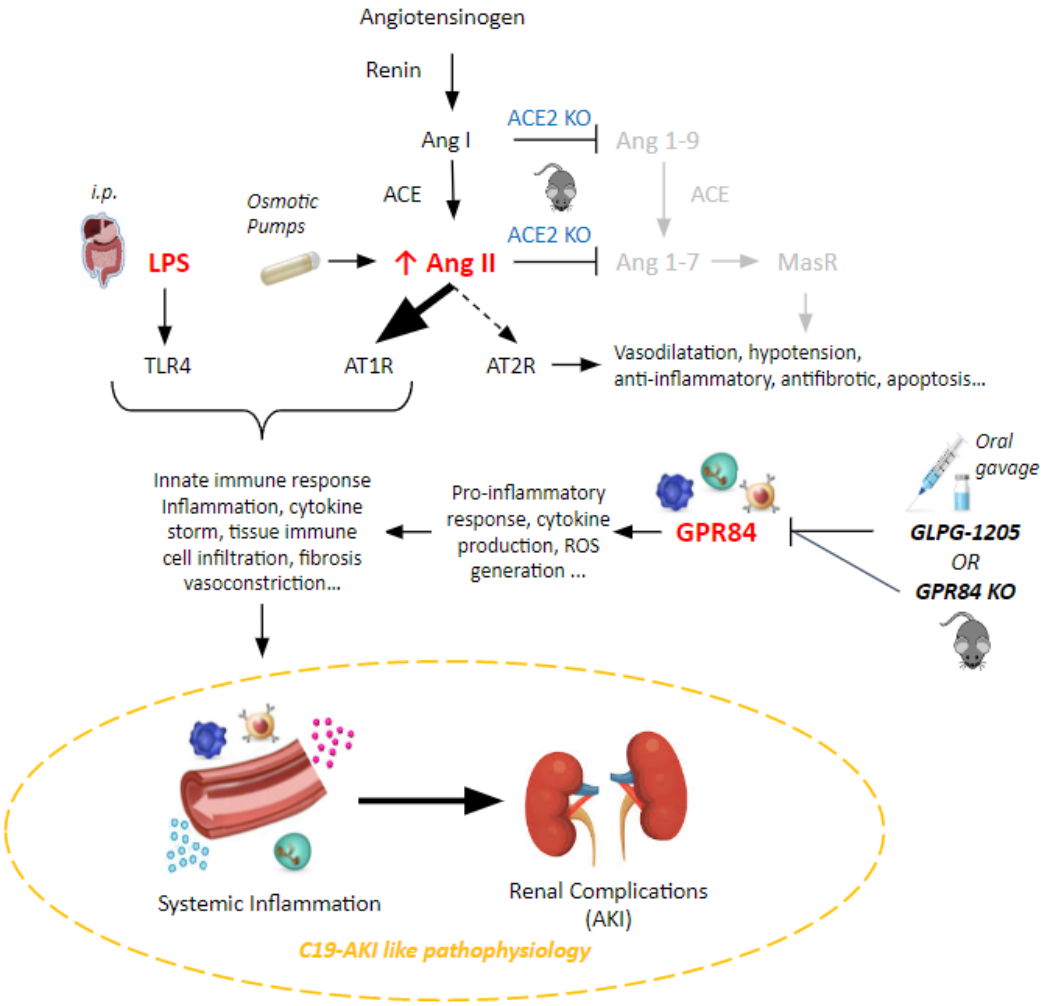

Figure 8. **Graphical hypotheses.** The surrogate mouse model of coronavirus disease 2019-associated acute kidney injury (C19-AKI) mouse model consists of an angiotensin-converting enzyme (ACE)2 knockout (KO) mice administered a low pressor dose of Angiotensin (Ang) II (400 ng/kg/min by osmotic pump) with a single administration of lipopolysaccharide (LPS; 10mg/kg i.p.). ACE2 KO and Ang II administration leads to a renin-angiotensin system (RAS) imbalance favouring the RAS pro-inflammatory arm. The RAS anti-inflammatory arm is presented on the figure in light gray. The combination of Ang II, LPS, and ACE2 KO leads to a pro-inflammatory climate with fibrosis and vasoconstriction through the Toll-like receptor 4 (TLR4) and the angiotensin type 1 receptor (AT1R) signaling. This climate causes systemic inflammation and renal complications, similarly to COVID-19-associated acute kidney injury (C19-AKI). G protein-coupled receptor 84 (GPR84) is present in immune cells and is involved in the pro-inflammatory response. It is hypothesized that GPR84 antagonists (e.g., GLPG-1205) and GPR84 KO mice reduces indices of C19-AKI by inhibiting GPR84 function. GPR84 antagonists could be used as adjuvant therapy in COVID-19 and improve patients' outcomes. AT2R: Angiotensin type 2 receptor. i.p.: intraperitoneal injection. MasR: Mas receptor. ROS: Reactive oxygen species.

CHAPTER 2: MATERIALS AND METHODS

2.1. Animals

ACE2 constitutive KO mice developed by Taconic Biosciences Inc. (Rensselaer, NY; model TF3738) were utilized. This line is a mixed strain composed of C57BL/6NTac, 129S5 and C57BL/6J (B6;129S5), with C57BL/6NTac being the main background[103,104]. The KO was achieved by inserting a β-Galactosidase/ Neomycin (LacZ/Neo) cassette within the second exon, leading to the inactivity of ACE2 full-length isoform[103,104]. Mice produce three ACE2 splice variants of 3566, 3422, and 1714 base pairs[104]. Both the 3566 and 3422 base pairs transcripts produce an 805 amino acids (full-length) isoform whereas the 1714 base pairs transcript results in a 521 amino acids isoform[103,104]. Taconic has not stated if the 521 amino acids ACE2 isoform is produced and functional in its ACE2 KO mice[103,104]. *Crackower et al.* described ACE2 KO as healthy and fertile animals presenting no alteration in renal structure or function compared to wild type (WT) littermates[105]. Additionally, as presented in the results section of this thesis, no differences in renal function were noted between male ACE2 KO and their WT littermate at baseline (2 months old). However, *Crackower et al.* noted impairment in the heart's contractility in absence of ACE2[105]. ACE2 KO animals presented thinner left ventricular walls and increased chamber dimensions, leading to a reduction in left ventricular pressure[105]. A gradual reduction in systemic blood pressure between three and six months of age was also noticed in ACE2 KO[105]. Ang I and Ang II levels were increased in kidneys, heart, and plasma of ACE2 KO since Ang I and Ang II are both substrates of ACE2[105]. Hypoxia-induced genes were also upregulated in ACE2 KO's heart[105].

ACE2 genotype was determined by polymerase chain reaction (PCR) with the following primers (Table 2) on a 2% agarose electrophoresis gel. Genotyping consisted of two PCR reactions, a targeted reaction that contained the targeted primers and an endogenous reaction with endogenous primers. An internal control gene (immunoglobulin-associated beta) was included in both reactions. The Thermocycling program started with 5 minutes at 94°C, followed by 30 cycles of 45 seconds at 94°C, 30 seconds at 58°C and 40 seconds at 72°C and finished with 5 minutes at 72°C (one cycle).

Table 2. **Primers sequences and concentrations for ACE2 genotyping.** Acronyms used in the table are defined below.

Primer	Sequence (5' - 3')	Concentration in reaction (µM)
Targeted_Neo3A	GCAGCGCATCGCCTTCTATC	0.30 (T)
Endogenous, Targeted_37	GCTCAATAACGACTTAGAACAT	0.30 (E, T)
Endogenous_3	GATGTCCAGCTCCTCCTGG	0.30 (E)
Internal Control_F	GTGGCACGGAACTTCTAGTC	0.25 (E, T)
Internal Control_R	CTTGTCAAGTAGCAGGAAGA	0.25 (E, T)

ACE2: Angiotensin converting enzyme 2; E: Endogenous reaction; F: Forward; R: Reverse; T: Targeted reaction

C57BL6 GPR84 constitutive KO mice developed by Deltagen (San Mateo, CA; Number T1285) were also utilized. In these mice, 257 base pairs of the GPR84 coding region were replaced by a Lac0-SA-IRES-lacZ-WT Neo/Kan cassette, leading to non-translation of the first three transmembrane domains[85,98]. No phenotypic differences were noted between GPR84 KO and WT littermates in the literature[85,98]. GPR84 genotype was assessed by PCR on a 1.4% electrophoresis agarose gel. The primers used are described below (Table 3). Genotyping required a multiplex reaction that included all primers and an endogenous reaction that contained endogenous primers only. REDExtract-N-Amp Ready Mix (Sigma, St. Louis, MO) was used for ACE2 and

GPR84 PCR reactions. The Thermocycling program started with 7 minutes at 95°C followed by 30 cycles of 10 seconds at 96°C, 30 seconds at 60°C and 45 seconds at 72°C and finished with 7 minutes at 68°C (one cycle).

Table 3. **Primers sequences and concentrations for GPR84 genotyping.** Acronyms used in the table are defined below.

Primer	Sequence (5' - 3')	Concentration in reaction (µM)
Endogenous_GPR84	ACAGCTCAGATGCCAACTTCTCCTG	0.125 (M); 0.50 (E)
Endogenous, Targeted_GPR84	TCCTAGAGCAATGAGACAGAGGGTG	0.25 (M); 0.50 (E)
Targeted_GPR84	GACGAGTTCTTCTGAGGGGATCGATC	0.25 (M)

GPR84: G-coupled protein receptor 84; E: Endogenous reaction; M: Multiplex reaction

Both ACE2 KO mice and GPR84 mice were bred and housed at the University of Ottawa Animal Care Facility. The Animal Care Veterinary Services at the University of Ottawa monitored experimental animals. Animals had free access to food and water. WT (and heterozygous, HET, for GPR84) littermates were used as controls. Experimental and breeding procedures were approved by the University of Ottawa Animal Care Committee and performed under the ME-2033 protocol. All work was performed in accordance with the guidelines of the Canadian Council on Animal Care.

2.2. Model

In this project, the model developed involved ACE2 KO and GPR84 KO mice on Ang II and LPS. The Ang II and LPS combination was applied to GPR84 KO mice to assess GPR84 role in the model. ACE2 KO on Ang II and LPS will be referred to as the surrogate model of C19-AKI (SMC) from here on. Note that the combination of ACE2 deletion, Ang II and LPS was considered the model. However, due to time limitations, ACE2 and GPR84 animals were not intercrossed. Therefore, the study

performed on GPR84 animals was labelled as “GPR84 Ang II + LPS” as GPR84 mice possess WT ACE2 alleles.

In brief, the SMC model consisted of an ACE2 KO mouse receiving a low pressor dose of Ang II and LPS. Eight to ten-week-old males were administered Ang II (Bachem, Bubendorf, Switzerland; dissolved in 0.9% saline) at a dose of 400ng/kg/min (subcutaneous) by osmotic minipumps (Alzet Osmotic Pumps, Cupertino, CA; model 1004) for eight days. Seven days following the Ang II osmotic minipump implantation, ACE2 KO mice were administered 10 mg/kg of LPS (Sigma, Oakville, ON; *Escherichia coli* (0127:B8 strain); dissolved in 0.9% saline) by intraperitoneal (i.p.) injection. Control animals (ACE2 WT) received a sham surgery and i.p. saline injection instead of LPS. All animals were placed on heat pads and received saline subcutaneous injections five to six hours after LPS and one hour before euthanasia to avoid animal loss and dehydration. GLPG-1205 treatment (provided by Liminal Biosciences Inc., Laval, QC) was evaluated at two different doses (30 mg/kg and 90 mg/kg) in 0.5% 400 centipoise (cps) methylcellulose (Spectrum Chemical, New Brunswick, NJ) or 0.5% 4000 cps methylcellulose (MP Biomedicals, Solon, OH). Treatment was given daily by oral gavage either from 24 hours post-pump surgery up to LPS injection (7 days; prophylaxis treatment) or at the time of LPS injection. Vehicle animals received 0.5% 400 or 4000 cps methylcellulose by daily oral gavage for the same period as treated groups. No treatment or vehicle was given on the day of euthanasia. Mice were euthanized 24 hours after LPS injection by cervical dislocation under isoflurane. A summary of the model is presented in Figure 43 of the appendices.

As explained in the introduction, the (e)GFR and ACR are the two main parameters measured to assess renal function[22]. However, eGFR could not be

measured in this study as the instrument our group routinely use to measure plasma creatinine (high-performance liquid chromatography; HPLC) was out of service and alternative methods gave inconclusive results (consult the discussion for further details). Moreover, urine flow, which our group typically measure by metabolic cage, could not be measured in this study due to animal wellness in the last 24 hours prior to euthanasia. With this in mind, the ACR was the main parameter used to detect AKI. In healthy kidneys, ACR values lie below 30 mg/g[25]. An ACR between 30 and 300 mg/g (microalbuminuria) or above 300 mg/g (macroalbuminuria) hints at renal damage and early kidney disease[25,27]. In addition to ACR, BUN and electrolyte concentration were also measured to assess renal function, although they are not gold-standard for AKI diagnosis. In healthy kidneys, BUN is between 7 and 20 mg/dL (2.5 to 7.1 mM)[29]. AKI can also lead to electrolyte imbalance, which is why that parameter was assessed[37,45].

2.3. Biological Sample Collection

As explained in Figure 43 of the appendices, a variety of relevant biological samples were collected throughout the timeline. Before Ang II and LPS (baseline), body weight, plasma, urine, and systolic blood pressure (SBP) were collected. After the pump surgery up to LPS injection (1W pump), body weight, urine and SBP were collected. At endpoint (AKI; 24 hours post-LPS), body weight, plasma, urine, tibia length, kidneys (weight, paraformaldehyde (PFA) fixation, sucrose dehydration, and snap-freezing), and liver weight were collected. Body weight was taken on the first day of baseline, the last day of 1W pump, and at AKI. Relative body weight was obtained by dividing the value of each biological replicate by the mean of their respective group at baseline and multiplying by 100 to make it a percentage. Note that bodyweight at

1W pump included the weight of the Ang II pump. Baseline blood was collected by saphenous vein bleed in heparinized capillaries (Pittsburgh, PA; one per animal). Capillaries were centrifuged at 5000 RCF (5000 g) for 10 minutes at 4°C. Plasma was then isolated and stored at -80°C. At AKI, blood was collected by cardiac puncture with a heparinized needle. Blood was kept on ice until centrifugation at 16278 RCF (13000 rpm) for 5 minutes at 4°C. The supernatant (plasma) was collected and stored at -80°C. Baseline and 1W pump urine were collected by spot urine and spun at 595 RCF (2500 rpm) for 20 minutes at 4°C to remove debris and cells. The supernatant was collected and stored at -80°C. AKI urine collection was collected by bladder puncture but processed in the same fashion afterwards. At AKI, both kidneys were collected, unencapsulated, and weighted individually. The left kidney was cut in half (sagittal cut). One half was fixed with 4% PFA (Sigma-Aldrich, St. Louis, MO) in 1X phosphate buffered saline (PBS) for 24 hours at 4ºC and transferred in 70% ethanol before paraffin embedding. Note that for a few studies, fixation was performed at room temperature with agitation as under fixation was noticed at 4ºC. The other left kidney half was dehydrated in 30% sucrose (Sigma, St. Louis, MO) for 24 hours at 4ºC before being embedded in the optimal cutting compound. The right kidney was cut into small pieces and snap-frozen in liquid nitrogen for messenger ribonucleic acid (mRNA) gene expression.

2.4. Systolic Blood Pressure

Systolic blood pressure (SBP) was acquired at baseline (before Ang II + LPS) and 1W pump (before LPS) by tail-cuff photoplethysmography (BP 2000, Visitech systems, Apex, NC) to verify the increase of systemic Ang II by the osmotic pumps. At baseline, mice were trained for five days. The last three days of training, where the

mice were acclimated to the procedure, were used as baseline measurements. SBP was also measured daily from the fifth to the seventh day after pump surgery (1W pump measurements). On the seventh day after pump surgery, the SBP was measured prior to LPS injection. Five preliminary and ten recorded measures were taken. Three days of SBP measures for each timepoint were combined. Recorded measures where no reading could be taken, were automatically removed beforehand. Outliers were calculated using the ten recorded measured of the three days composing a timepoint. Outliers were defined as values over or under the average ± (2 x standard error). Once outliers were removed a new average and standard error of the mean (SEM) were calculated. Note that for some pilot studies, SBP was taken for a longer period. However, each time point consisted of at least three measurement days. Relative SBP was obtained by dividing the value of each biological replicate by the mean of their respective group at baseline and multiplying by 100 to make it a percentage.

2.5. Plasma and Urine Biochemistry Analysis

Biochemistry from plasma and urine collected at AKI was analyzed by IDEXX Laboratories (Markham, ON) or IDEXX Bioanalytics (North Grafton, MA), depending on the study. The change from IDEXX Laboratories to IDEXX Bioanalytics was done during this project as IDEXX Bioanalytics are specialized in small animal sample analysis and required smaller volumes of samples. Details of the biochemistry panels performed, and the sample volume sent are presented in Table 4. All analyses by IDEXX were done blindly.

Table 4. **Plasma and urine biochemistry.** IDEXX location and details on panel performed. Acronyms used are defined below.

Location	IDEXX Laboratories	IDEXX Bioanalytics	
Panel Name	BUNC	63076	63077
Sample Type	Plasma	Plasma	Urine
Volume (µL)	120	180	50-140
Panel Component	Creatinine, urea (BUN), BUN: creatinine ratio	Albumin, bicarbonate (total CO_2), BUN, calcium, chloride, cholesterol, creatinine, glucose, magnesium, phosphorus, potassium, sodium, total protein, triglyceride	Calcium, chloride, creatinine, glucose, magnesium, phosphorous, potassium, sodium, urea nitrogen

BUN: Blood urea nitrogen; CO_2: Carbon dioxide

2.6. Urine Albumin to Creatinine Ratio

Urine albumin was measured with the Bethyl laboratories' mouse albumin enzyme-linked immunosorbent assay (ELISA) kit (Montgomery, TX.) according to the manufacturer's instructions. Urine creatinine was determined with Exocell's creatinine companion kit (Philadelphia, PA) according to the manufacturer's instructions with modification on data acquisition wavelength. Absorbance was measured at 492 nm as the 500 nm wavelength was not available on the spectrophotometer used. The FLUOstar Galaxy spectrophotometer was used for the two assays (BMG LABTECH, Cary, NC). Samples and standards for both assays were prepared up to 24 hours before performing the assays (stored at 4°C once diluted). Urine albumin was normalized to urine creatinine to obtain ACR.

2.7. Renal Gene Expression

Quantification of various inflammatory, fibrotic, injury, and immune cell markers, as well as GPR84, was performed in kidneys by quantitative polymerase chain reaction (qPCR). Genes evaluated are presented in Table 5. The gene selection was based on the literature assessing renal gene expression in LPS-induced sepsis AKI

as the SMC is closely related to this model[55,141,142,160,164-172]. The role of the gene selected in inflammation, fibrosis, injury, as well as their role as immune cell markers is presented in Table 7 of the appendices.

At euthanasia, the right kidneys were cut into small pieces, snap-frozen in liquid nitrogen and stored at -80°C. Kidneys were brought into powder using the COE Capmixer (GC America, Alsip, IL). ribonucleic acid (RNA) was isolated using the QIAGEN RNEasy Minikit (QIAGEN, Toronto, ON) according to the manufacturer's instructions. The optional deoxyribonucleic acid (DNA) digestion was performed with the QIAGEN RNase-free DNase Set (QIAGEN, Toronto, ON). RNA was quantified with 2 µL of sample on the Epoch Microplate Spectrophotometer (BioTek, Winooski, VT) and the Gen5 software (Version 2.09; BioTek, Winooski, VT). 2000 ng of RNA per reaction per sample were used for reverse transcriptase polymerase chain reaction (RT-PCR) with the Applied Biosystems' High-Capacity complementary deoxyribonucleic acid (cDNA) Reverse Transcription kit (Foster City, CA). qPCR was performed with 2 µL of cDNA, 0.4 µM of primers, and the PowerUp SYBR Master Mix (Applied Biosystems; Foster City, CA) according to manufacturer's instruction. Cycling for melting temperature over or equal to 60°C was utilized for all primers. Applied Biosystems ABI Prism 7000 Fast Sequence Detection System or ABI 7300 Real-Time PCR System (Foster City, CA) were used for qPCR, depending on the study. Gene expression was determined using the two^-(delta delta cycle threshold) (2^-(ddCt)) analysis method[107]. Gene expression was normalized to glyceraldehyde three-phosphate dehydrogenase (GAPDH). Water and no reverse transcriptase control were also performed to confirm that the expression noted was not background noise.

Table 5. **Primer sequences used for renal qPCR.**

Gene	Animal	Orientation	Sequence (5' - 3')
Arginase-1 (ARG-1)	Mouse	Forward	GACCACAGTCTGGCAGTTGG
		Reverse	TACGTCTCGCAAGCCAATGT
Connective tissue growth factor (CTGF)	Mouse	Forward	CCAGACCCAACTATGATGC
		Reverse	ACTTAGCCCTGTATGTCTTCA
EGF-like module-containing mucin-like hormone receptor-like 1 (F4-80)	Mouse	Forward	CCAGCACATCCAGCCAAAG
		Reverse	ACATCAGTCTTCCAGGAGACACA
Glyceraldehyde 3-phosphate dehydrogenase (GAPDH)	Mouse	Forward	TGCACCACCAACTGCTTAGC
		Reverse	GGCATGGACTGTGGTCATGAG
G-coupled protein receptor 84 (GPR84)	Mouse	Forward	TGTGAAAACTGGGAACCTC
		Reverse	GCCCAACACAGACTCATGG
Interleukin (IL)-1β	Mouse	Forward	ATGGCA ACTGTTCCTGAACTCAACT
		Reverse	CAGGACAGGTATAGATTCTTTCCTTT
IL-6	Mouse	Forward	AGGATACCACTCCCAACAGACCT
		Reverse	CAAGTGCATCATCGTTGTTCATAC
IL-10	Mouse	Forward	TAGAAGTGATGCCCCAGGCAG
		Reverse	TCACTCTTCACCTGCTCCACTGC
Kidney injury molecule 1 (KIM-1)	Mouse	Forward	AAACCAGAGATTCCCACACG
		Reverse	GTCGTGGGTCTTCCTGTAGC
Macrophage inflammatory protein 2 (MIP-2)	Mouse	Forward	CCAAGGGTTGACTTCAAGAAC
		Reverse	AGCGAGGCACATCAGGTACG
Neutrophil gelatinase-associated lipocalin (NGAL)	Mouse	Forward	CAAGCAATACTTCAAAATTACCCTGTA
		Reverse	GCAAAGCGGGTGAAACGTT
Tumor necrosis factor alpha (TNF-α)	Mouse	Forward	AGGGTCTGGGCCATAGAACT
		Reverse	CCACCACGCTCTTCTGTCTAC

qPCR: Quantitative polymerase chain reaction

2.8. Histology

As mentioned previously, both kidneys were collected and unencapsulated at euthanasia. The left kidney was cut in half (sagittal cut). One half was fixed with 4% Paraformaldehyde (PFA; Sigma-Aldrich, St. Louis, MO) in 1X PBS for 24 hours at 4°C and transferred in 70% ethanol before paraffin embedding. Note that for a few studies, fixation was performed at room temperature with agitation as under fixation was noticed at 4°C. The other left kidney half was dehydrated in 30% sucrose (Sigma, St. Louis, MO) for 24 hours at 4°C before being embedded in optimal cutting compound and stored at -80°C. PFA fixed kidney halves were embedded in paraffin, 4 µm sectioned and stained with hematoxylin and eosin (H&E) by the University of Ottawa's

Louise Pelletier Histology Core. General renal structure assessment was performed with H&E slide under a light microscope with 400X or 1000X magnification. Images were acquired with a microscope Zeiss Imager A1 (Carl Zeiss, Oberkochen, Germany) equipped with Olympus camera DP73 (Olympus Canada, Richmond Hill, ON, Canada).

Kidney myeloperoxidase immunohistochemistry was performed on paraffin-embedded sections mounted on glass slides. Slides were deparaffinized and rehydrated with xylene (two washes of five to ten minutes), 100% ethanol (two washes of ten minutes), 90% ethanol (one wash of five minutes), 70% ethanol (one wash of five minutes) and distilled water (one wash of five to ten minutes). Antigen retrieval was done in boiling Tris-ethylenediaminetetraacetic acid (EDTA) buffer (10mM Tris Base, 1mM EDTA, 0.05% Tween 20, pH 9.0) for 20 minutes. Slides were rinsed with water for ten minutes and blocked with BLOXALL® Endogenous Blocking Solution (Vector Labs, Burlingame, CA) for ten minutes and then with normal horse serum from the ImmPRESS® HRP Horse Anti-rabbit IgG Polymer Detection Kit (Vector Labs, Brockville, ON). Between blocking steps, the slides were washed in PBS for ten minutes. The primary antibody (anti-Myeloperoxidase antibody; Abcam, Toronto, ON) was diluted at 1:500 in 1% bovine serum albumin in 1X PBS and was incubated on slides overnight at 4°C. Slides were washed three times in PBS for ten minutes and secondary antibody incubation with the ready to use (no dilution) ImmPRESS polymer (horse anti-rabbit) reagent from the ImmPRESS® HRP Horse Anti-rabbit IgG Polymer Detection Kit (Vector Labs, Brockville, ON) for 30 minutes at room temperature. Slides were washed three times in PBS for ten minutes. Slide were then stained with 3,3′-Diaminobenzidine (DAB) staining solution for ten minutes (0.067% DAB, 0.024% hydrogen peroxide) and washed two times with PBS for ten minutes. Slides were

counterstained for one minute in Mayer's Hematoxylin Solution (Electron Microscopy Sciences, Hatfield, PA) and rinsed with water for ten minutes. Slides were cleared with 70% ethanol (one wash of five minutes), 90% ethanol (one wash of five minutes), 100% ethanol (two washes of ten minutes) and xylene (two washes of ten minutes). Slides were mounted in Acrytol mounting medium (Electron Microscopy Sciences, Hatfield, PA). Images were acquired with a microscope Zeiss Imager A1 (Carl Zeiss, Oberkochen, Germany) equipped with Olympus camera DP73 (Olympus Canada, Richmond Hill, ON, Canada). Number of neutrophils (myeloperoxidase positive cells) were counted per field view at 200X magnification (four to 20 fields per animal, two to eight animals per group). All histological analyses were performed blindly.

2.9. Urine Extracellular Vesicles Quantification

Extracellular vesicles (EVs) from baseline, 1W pump and AKI urine were quantified with the Zetaview Particle Tracking Analyzer (Particle Metrix, Ammersee, Germany). As mentioned earlier, urine samples were spun at 595 RCF (2500 rpm) for 20 minutes at 4°C to remove debris and cells. On each day of acquisition, the instrument was washed with 0.2 µm filtered nanopure water, the cell quality was verified, and the camera was focused. Additionally, the camera's sensitivity/exposure was adjusted on every acquisition day based on one sample. Sensitivity was set between 70 and 85. Urine samples were 50 to 200-fold diluted in sterile 0.1 µm filtered 1X PBS. The dilution that gave 80-200 particles per frame (3-4 x 10^7 particles/mL) was selected for each sample individually. The instrument was rinsed with nanopure water between each sample. Particles' concentration and size were collected on 11 different camera positions. Outlying values were removed by the instrument's algorithm. Samples' particle concentrations were normalized to urine creatinine and then

averaged (per group per study). Particles of 0 to 1020 nm were analyzed. Relative frequency of exosome- (30-90 nm) and microparticle-sized particles (90-990 nm) was calculated as the particle count in a specific diameter range (30-90 nm or 90-990 nm) divided by the total particle count in the whole diameter range (0-1020 nm).

2.10. Statistics

Figures and statistical analysis were conducted on GraphPad Prism 5.0 (San Diego, CA). Values over or under the average ± (2 x standard error), also known as outliers, were removed before statistical analysis. Data are presented as mean ± standard error of the mean (SEM). Normal distribution of the data was confirmed in the SMC + GLPG-1205 (Prophylaxis, 400 cps methylcellulose) and the GPR84 Ang II + LPS study were tested for normality (data not shown) using the D'Agostino-Pearson normality test and the Shapiro-Wilk normality test. Statistical analysis for studies with one group variable (control vs model) was performed by unpaired t-test with Welch's correction. Statistical analyses for studies with the GPR84 antagonist were done by one-way analysis of variance (ANOVA) with a Dunnett post-test. Untreated group on the model (SMC Vehicle) was selected as the "control" group. Note that the control treated group (Control GLPG-1205) was not included in the statistical analysis to simplify the analyses. Statistical analyses for the GPR84 KO Ang II + LPS studies were done by one-way ANOVA with a Bonferroni post-test comparing HET/WT control with HET/WT Ang II + LPS, KO control with KO Ang II + LPS, and HET/WT Ang II + LPS with KO Ang II + LPS. Statistical significance was defined as follow: *$p \leq 0.05$, **$p \leq 0.01$, and ***$p \leq 0.001$.

CHAPTER 3: RESULTS

3.1. Development of a new surrogate mouse model of coronavirus disease 2019-associated acute kidney injury

In 40% of SARS-CoV-2 severe cases admitted to the hospital, pulmonary complications are accompanied by AKI[48]. Current treatment for renal complications limits financial and material resources while also applying additional stress on the healthcare system[37]. Indeed, during the pandemic, a surge in COVID-19 patients in addition to regular dialysis patients challenged the management and allocation of RRT to the patients[37,55]. Additionally, supply chain shortages made the acquisition of new RRT instruments difficult and lengthy, thereby adding stress on the healthcare system[37,55]. The unknown progression of the current pandemic, the assessment of long-term consequences of SARS-CoV-2 infection on overall and renal health as well as potential new coronavirus outbreaks in the following years further drives the need for a complete understanding of C19-AKI pathophysiology and adjuvant therapies development. To explore such treatments and accelerate research in case of future coronavirus outbreaks, a mouse model of C19-AKI (SMC) would represent a critical biomedical research tool.

Here a surrogate model of C-19 AKI (abbreviated SMC) is proposed (Figure 43 of the appendices). The model consists of ACE2 KO mice receiving a low pressor dose of Ang II (400 ng/kg/min) by osmotic minipump for eight days with a single i.p. injection of LPS (10 mg/kg) on the seventh-day post-minipump implantation. Mice are euthanized 24 hours after the LPS challenge. Long-term pilots were also performed to assess the model's potential for CKD development. In the long-term pilots, mice were euthanized 19 to 21 days following the LPS challenge (Ang II for 28 to 29 days). In

both timelines, control (WT) littermates received a sham surgery and a saline injection instead of Ang II minipump implantation and LPS i.p. injection, respectively. Table 6 of the appendices presents details on animals' age, sex, genotype, and group size of all studies performed. In the Ang II + LPS pilot, where euthanasia was performed 24 hours post-LPS, only WT mice were utilized. The long-term pilots were performed on WT (Ang II + LPS long-term pilot) and ACE2 KO (SMC long-term pilot) animals.

3.1.1. Wild type mice on angiotensin II for seven days and lipopolysaccharide for 24 hours (Ang II + LPS pilot)

The first pilot performed had for objective to assess the effects of Ang II and LPS combination on renal function, injury, and inflammation. This pilot was executed on WT mice (male and female of eight to 25 weeks old). The animals (Ang II + LPS group) received 400 ng/kg/min of Ang II for eight to eleven days by osmotic minipump and were injected with 10 mg/kg of LPS 24 hours prior to euthanasia. Control animals had a sham surgery and a saline i.p. injection instead of an Ang II minipump implantation and an LPS injection. To monitor animals' wellness, body weight was measured at baseline (before Ang II and LPS administration), 1W Pump (one week of Ang II administration, before LPS), and AKI (at euthanasia, 24 hours post-LPS; Figure 9. A and B). Septic models such as LPS present a reduction in water and food intake, thus leading to dehydration and a decrease in body weight[108,109]. Therefore, body weight was also measured to determine that the septic model was working. At baseline, the control and Ang II + LPS body weights were 24.7 g and 23.9 g while 1W Pump body weights were 24.1 g and 23.7 g, respectively. 24 hours after LPS (AKI), the body weights were 24.0 g and 21.1 g for the control and Ang II + LPS groups, respectively. Body weight reported in grams and relative body weight showed no

significant differences between groups at any timepoint. To verify successful Ang II delivery, SBP was assessed at 1W Pump and baseline (Figure 9. C and D). Low pressor doses of Ang II such as the one utilized in this project lead to a delayed and gradual increase in SBP[110]. Both control and Ang II + LPS mice had a baseline SBP of 112 mm Hg. One week after Ang II minipump implantation (1W Pump), control and Ang II + LPS SBP were 113 mm Hg and 125 mm Hg, respectively. SBP reported in mm Hg and relative SBP showed no significant differences between groups at any timepoint. In this study, two pilots were combined. In the first pilot, Ang II was administered for seven days whereas in the second pilot Ang II was given for ten days prior to LPS. The difference in time of Ang II administration was to investigate whether SBP stabilizes or increases beyond seven days. Prolonged administration of Ang II (ten days) was not statistically different from the seven-day administration (128 mm Hg vs 122 mm Hg; Figure 9.E). Therefore, administration of LPS seven days after Ang II osmotic minipump implantation was selected for subsequent studies. In kidney disease, a reduction in renal blood flow or the number of nephrons can occur and lead to kidney atrophy[111]. Therefore, renal atrophy was assessed through the normalization of kidney weight to tibia length at euthanasia. Ang II + LPS had no significant effect on normalized kidney weight (Figure 9.F).

Renal function was assessed through ACR and BUN. ACR is the concentration of urine albumin divided by urine creatinine concentration[25]. In healthy kidneys, the glomerular filtration barrier keeps large proteins, such as albumin, in the blood and therefore very little protein gets in the urine[6,7,25]. An increase in ACR is suggestive of renal damage and early kidney disease[25,27]. When healthy, ACR values lie below 30 mg/g (30 µg/mg)[25]. An ACR between 30 and 300 mg/g is described as microalbuminuria, whereas an ACR above 300 is macroalbuminuria[25]. At baseline, the

control and Ang II + LPS ACR were not significantly different (13 µg/mg vs 16 µg/mg; Figure 10.A). At AKI, the Ang II + LPS mice ACR significantly increased (912 µg/mg) in comparison to the control mice at the same timepoint (8 µg/mg; ***p≤ 0.001). BUN can also provide indices on kidney health[29]. Urea nitrogen is a product of dietary protein breakdown filtered and excreted by the kidneys[29]. In healthy kidneys, BUN is between 7 mg/dL and 20 mg/dL (2.5 mM and 7.1 mM)[29]. When kidneys are not functioning properly and GFR is reduced, BUN can increase[29]. BUN was measured in plasma collected at euthanasia (AKI; Figure 10.B). A significant increase in BUN at AKI was observed in Ang II + LPS mice (25.6 mM) compared to control mice (6.8 mM; ***p≤ 0.001).

To evaluate renal inflammation and fibrosis and immune cell infiltration, qPCR was performed on whole kidneys. Various pro-inflammatory, pro-fibrotic and immune cell markers as well as GPR84 were assessed. The genes measured and their role in inflammation and fibrosis or as immune cell markers are presented in Table 7 of appendices[80,81,84-86,112-129]. All genes evaluated were significantly upregulated in the Ang II + LPS group (vs control; *p≤ 0.05, **p≤ 0.01, or ***p≤ 0.001) except for the EGF-like module-containing mucin-like hormone receptor-like one (F4-80) and IL-10, where the expression was not significantly different (1.7- and 1.5-fold vs control, respectively; Figure 11). Ang II + LPS significantly increased connective tissue growth factor (CTGF), IL-1β, and TNF-α expression between 2.7 and 10.4-fold (vs control; *p≤ 0.05 or **p≤ 0.01; Figure 11.B, E, and K). arginase-one (ARG-1), IL-6, KIM-1, macrophage inflammatory protein two (MIP-2), and NGAL expression was significantly increased in Ang II + LPS mice by 43, 331, 82, 126 and 527-fold, respectively (vs control; **p≤ 0.01, or ***p≤ 0.001; Figure 11.A, F, and H-J). GPR84, a protein of interest for the second part of this thesis, was significantly upregulated by 73-fold in the Ang II + LPS

group compared to the control group (**p≤ 0.01; Figure 11.D).

The general renal structure was evaluated with H&E-stained kidney slides (Figures 12 and 13). Staining showed that Ang II + LPS combination led to proximal tubule lesions characterized by nuclear loss, vacuolization of cytoplasm and protein casts (Figure 12.B-C). Furthermore, glomerulopathy was seen in Ang II + LPS mice, as shown by the focal disappearance of endothelial and mesangial cells (Figure 13.B). Increased cellularity in the interstitial space was also noted (Figure 12.C). To identify the infiltrated cells, immunohistochemistry with various immune markers was performed, starting with myeloperoxidase, a neutrophil marker (Figure 14)[130]. The myeloperoxidase immunohistochemistry demonstrated a significant increase of neutrophils in the kidney of Ang II + LPS mice (Figure 14.B) compared to control mice (Figure 14.A; 27 vs 0 neutrophils per field; **p≤ 0.01).

Urinary EVs were measured by nanoparticle tracking analysis (Figure 15). Note that the following graph describes particle concentration, median size and relative frequency as the Zetaview Particle Tracking Analyzer quantifies all particles within a liquid, which includes EVs. EVs are bilipid layered vesicles of 40 to over 1000 nm in diameter that contain proteins, peptides, lipids, and nucleic acids[131,132]. EVs are found in various biological fluids, including urine and plasma[131]. EVs play a key role in autocrine and paracrine cell communication in physiological and stress conditions[132]. Interest in EVs has increased in the last years due to their potential as biomarkers of renal injury and possible use for therapeutics delivery[131]. The particle concentration and median size between groups were compared at baseline and AKI timepoint (Figure 15.A-B). The urinary particle concentration (normalized to urine creatinine) was not significantly different between control and Ang II + LPS mice at baseline and AKI (Figure 15.A). Median particle size was also not significantly different between

control and Ang II + LPS at both timepoints (Figure 15.B). EVs can be classified into three categories, exosomes, microparticles and apoptotic bodies[132]. Exosomes are small intracellular vesicles (40 to 100 nm in diameter) secreted by exocytosis through multivesicular bodies[132]. Microparticles are mid-size EVs (100 to 1000 nm in diameter) formed by membrane blebbing[132]. Apoptotic bodies are the biggest EVs (over 1000 nm in diameter) and are produced during cell death through apoptosis-specific pathways[132]. In the model, the relative frequency of exosomes and microparticle-sized particles was assessed (Figure 15.C-D). Relative frequency of urinary exosome and microparticle-sized particles was not significantly different between control and Ang II + LPS animals at both timepoints evaluated.

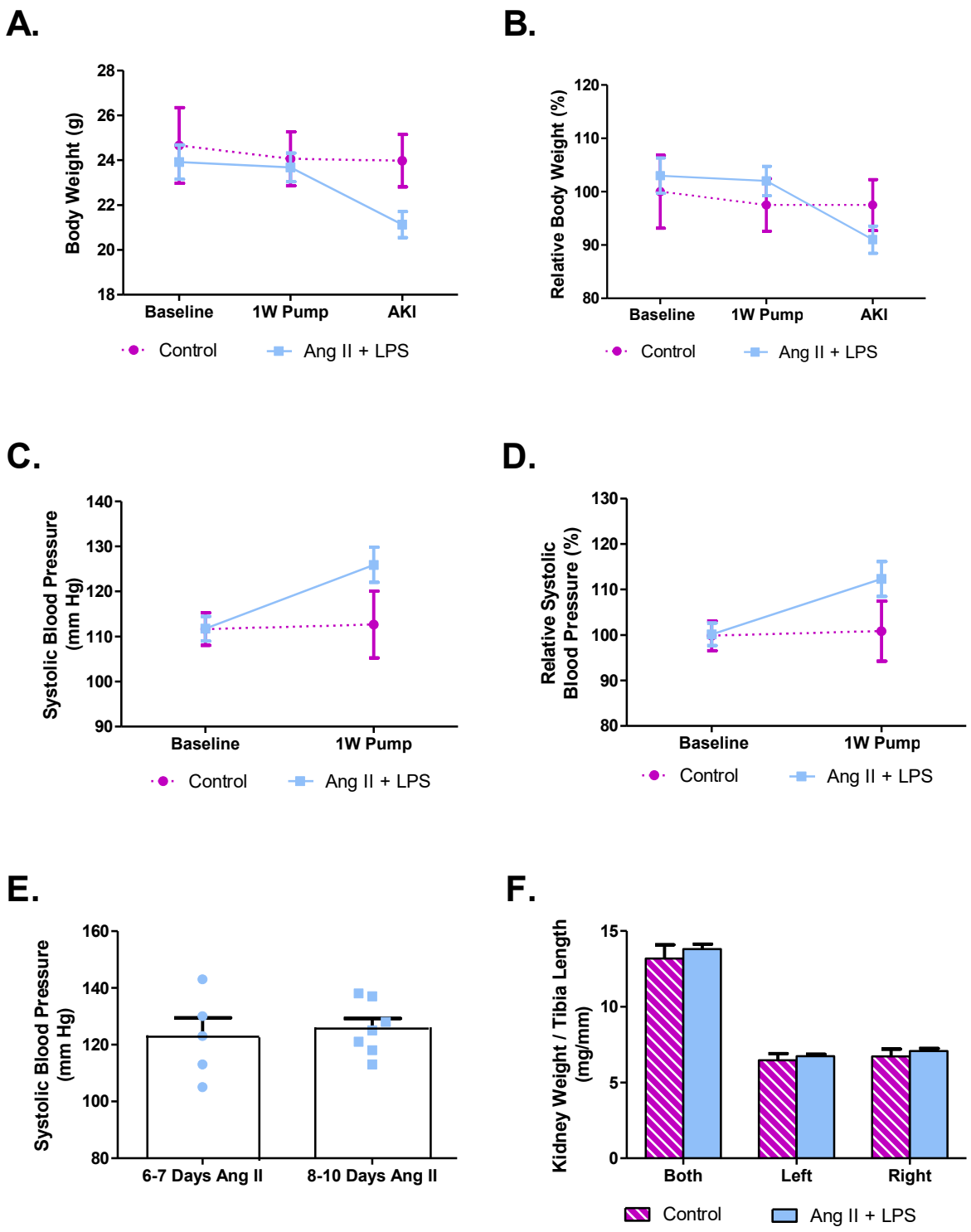

Figure legend on the following page (Figure 9).

Figure 9. **Ang II + LPS pilot body weight, systolic blood pressure and normalized kidney weight.** **A-B.** Body weight reported in grams (**A.**) and relative (**B.**) to baseline (before angiotensin II and lipopolysaccharide; Ang II and LPS), 1W Pump (1 week with Ang II minipump, before LPS), and AKI (24 hours post-LPS injection). 1W Pump body weight (in gram and relative) included the Ang II osmotic minipump weight. **C-D.** Systolic blood pressure (SBP) reported in mm Hg (**C.**) and relative (**D.**) to baseline and 1W Pump. SBP was obtained by tail-cuff photoplethysmography. The last three measurement days of each timepoint were combined. Five preliminary measures and at least seven actual measures were recorded each day. Normalizations (**B.** and **D.**) were obtained by dividing the value of each biological replicate by the mean of their respective group at baseline and multiplying by 100. **E.** SBP comparison of five to seven days and eight to ten days of Ang II minipumps. **F.** Both (combined), left and right kidney weight normalized to tibia length at AKI. Control: n=6; Ang II + LPS: n=12. Outlying values were removed from the analysis. Data presented as mean ± standard error of the mean (SEM). An unpaired t-test with Welch's correction for all figures comparing groups at each time point or category was performed (no significant differences detected; $p > 0.05$). 1W Pump: One-week minipump; AKI: Acute kidney injury.

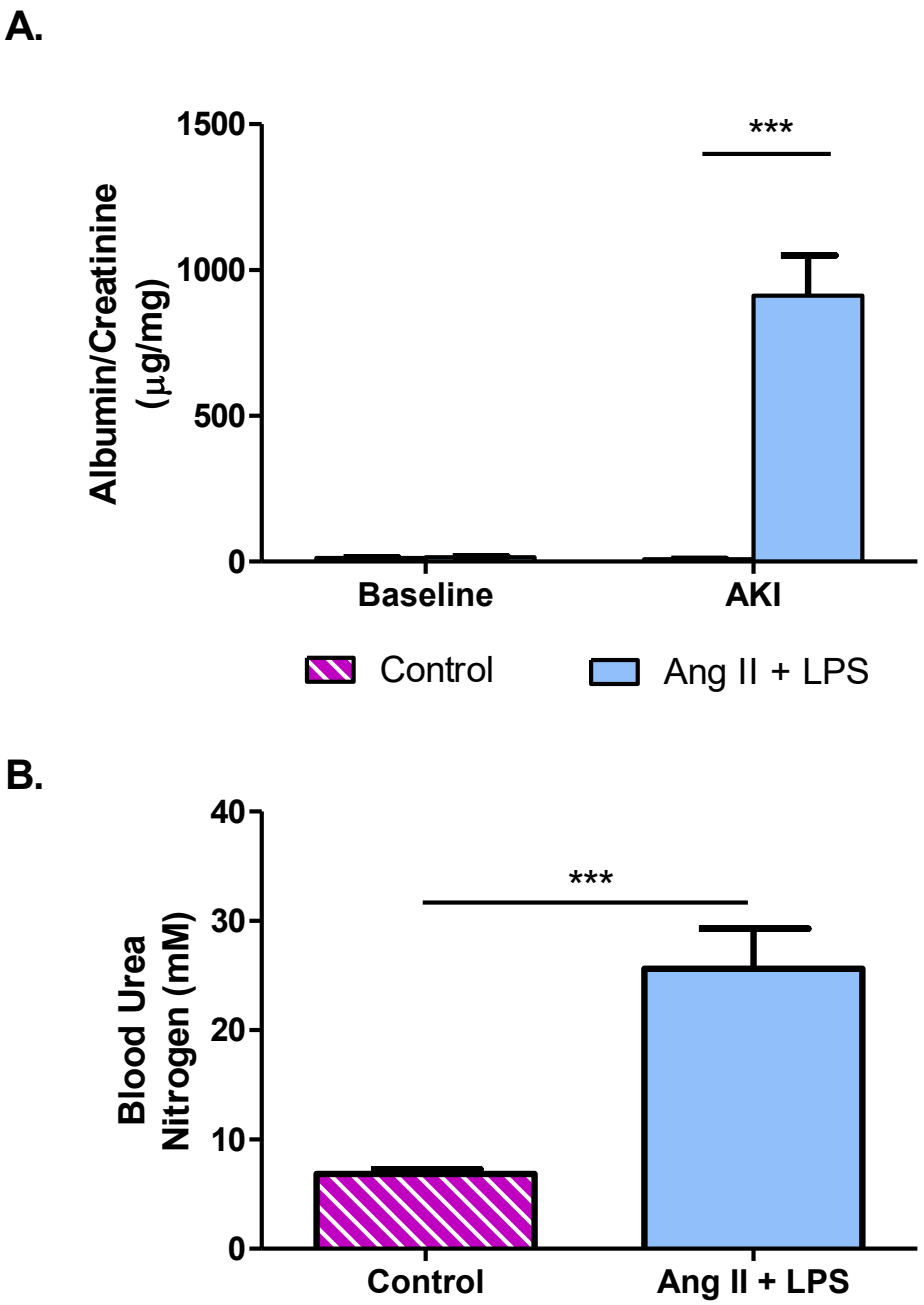

Figure 10. **Ang II + LPS pilot albumin to creatinine ratio and blood urea nitrogen. A.** Albumin to creatinine ratio (ACR) at baseline (before angiotensin II and lipopolysaccharide; Ang II and LPS), and AKI (24 hours post-LPS injection). Albuminuria and urine creatinine were obtained by enzyme-linked immunosorbent assay (ELISA) and Jaffe reaction assay, respectively. **B.** Blood urea nitrogen (BUN) at AKI. Analysis blindly performed by IDEXX Laboratories. Control: n=6; Ang II + LPS: n=12. Outlying values were removed from the analysis. Data presented as mean ± standard error of the mean (SEM). An unpaired t-test with Welch's correction for all figures comparing groups at each time point was performed (***p≤ 0.001). AKI: Acute kidney injury.

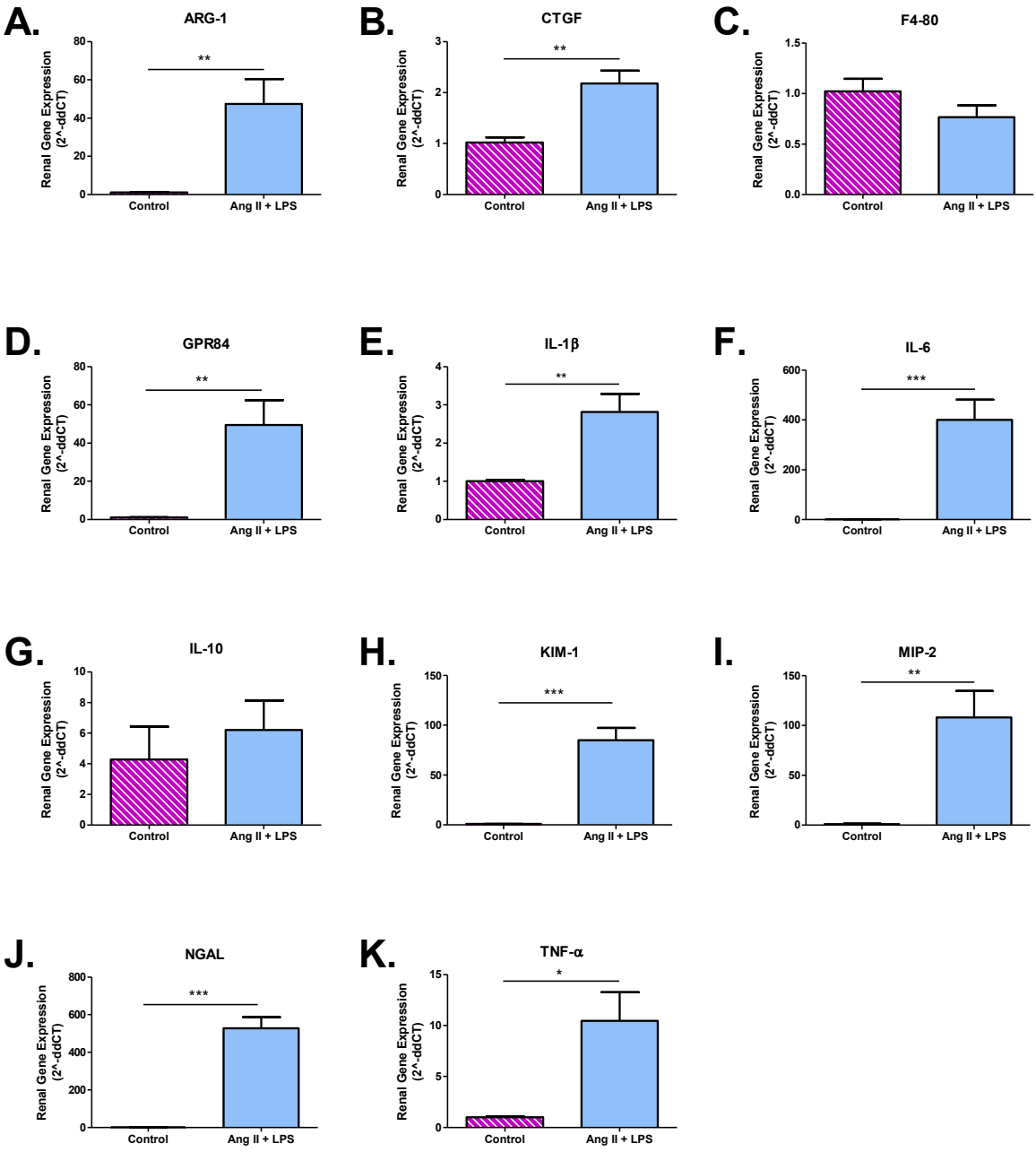

Figure 11. **Ang II + LPS pilot renal expression of GPR84, and inflammatory, fibrotic, injury, and immune cell markers.** Messenger ribonucleic acid (mRNA) expression of arginase 1 (ARG-1; **A.**), connective tissue growth factor (CTGF; **B.**), EGF-like module-containing mucin-like hormone receptor-like 1 (F4-80; **C.**), G-coupled protein receptor 84 (GPR84; **D.**), interleukin (IL)-1 beta (**E.**), IL-6 (**F.**), IL-10 (**G.**), kidney injury molecule 1 (KIM-1; **H.**), macrophage inflammatory protein 2 (MIP-2; **I.**), neutrophil gelatinase-associated lipocalin (NGAL; **J.**), and tumour necrosis factor-alpha (TNF-α; **K.**) normalized to glyceraldehyde three-phosphate dehydrogenase (GAPDH) at AKI (24 hours post-lipopolysaccharide injection). Gene expression was assessed by quantitative polymerase chain reaction (qPCR). Control: n=6; Ang II + LPS: n=12. Outlying values were removed from the analysis. Data presented as mean ± standard error of the mean (SEM). An unpaired t-test with Welch's correction for all figures comparing groups for each gene was performed (*p≤ 0.05; **p≤ 0.01; ***p≤ 0.001). Ang II + LPS: Angiotensin II + lipopolysaccharide; AKI: Acute kidney injury.

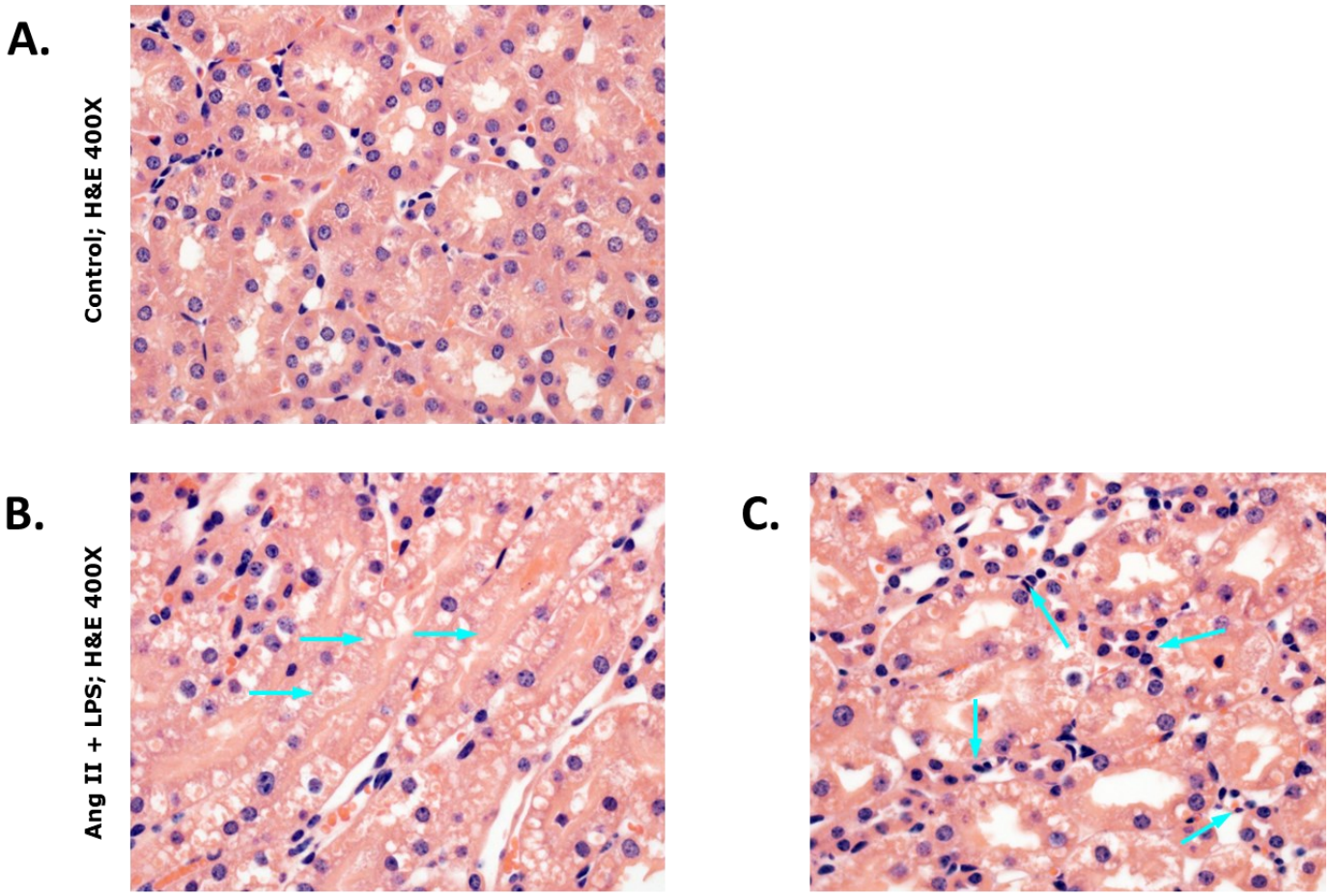

Figure 12. **Ang II + LPS pilot general tubular structure. A.** Control proximal tubules. **B.** Lesions of proximal tubules in Ang II + LPS kidneys characterized by nuclear loss, vacuolization of cytoplasm, and protein casts (arrows; →). **C.** Increased cellularity in the interstitial space (arrows; →) of Ang II + LPS kidneys. Kidneys collected at euthanasia (AKI; 24 hours post-lipopolysaccharide) were fixed in paraformaldehyde (PFA) for 24 hours at 4°C, embedded in paraffin, sliced at 4 µm and stained with hematoxylin and eosin (H&E). Pictures were taken at x400 magnification. AKI: Acute kidney injury; Ang II + LPS: Angiotensin II + lipopolysaccharide.

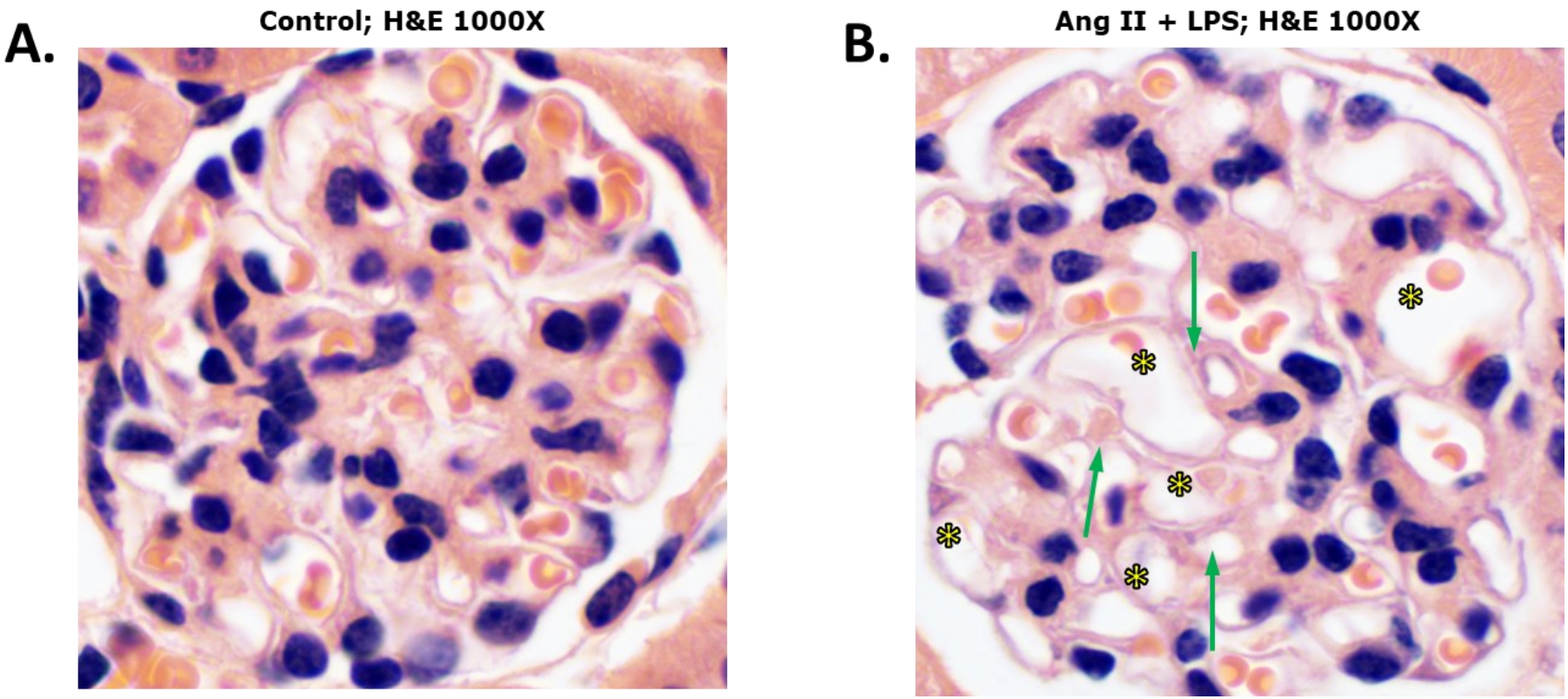

Figure 13. **Ang II + LPS pilot general glomerular structure. A.** Control glomerulus. **B.** Glomerulopathy in Ang II + LPS kidneys appeared as focal disappearance of endothelial (asterisks; *) and mesangial (arrows, →) cells. Kidneys collected at euthanasia (AKI; 24 hours post-lipopolysaccharide) were fixed in paraformaldehyde (PFA) for 24 hours at 4°C, embedded in paraffin, sliced at 4 µm and stained with hematoxylin and eosin (H&E). Pictures were taken at x1000 magnification. AKI: Acute kidney injury; Ang II + LPS: Angiotensin II + lipopolysaccharide.

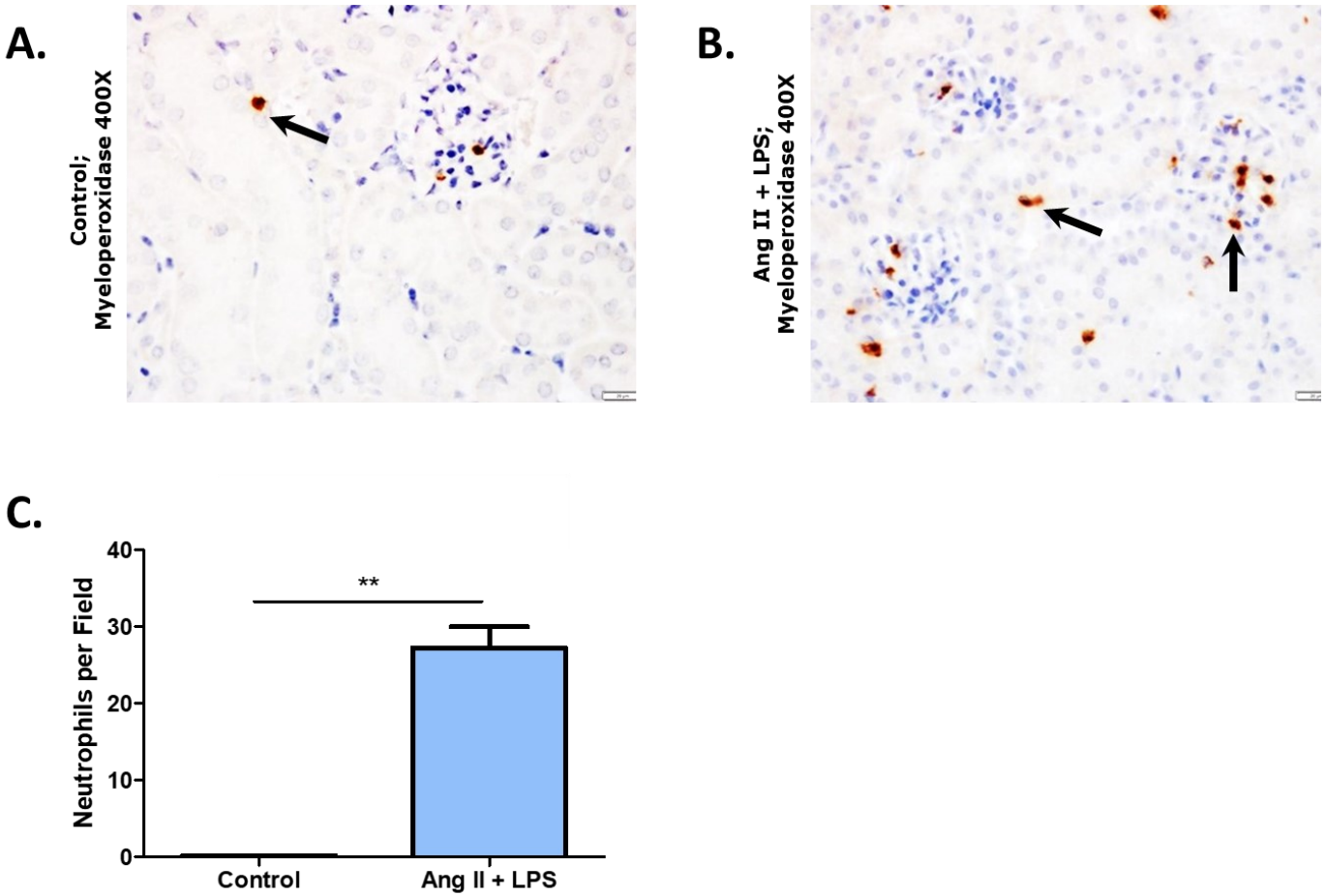

Figure 14. **Ang II + LPS pilot renal neutrophil infiltration.** Representative immunohistochemistry images of myeloperoxidase expression (arrows, →) in control (**A.**) and Ang II + LPS (**B.**) in kidneys at AKI (24 hours post-LPS). Mayer's Hematoxylin counterstain, 400X magnification. **C.** Quantification of neutrophils (Myeloperoxidase positive events) per field. Four to seven fields were averaged per biological replicate. Control: n=3; Ang II + LPS: n=4. Outlying values were removed from the analysis. Data presented as mean ± standard error of the mean (SEM). An unpaired t-test with Welch's correction was performed (**p≤ 0.01). AKI: Acute kidney injury.

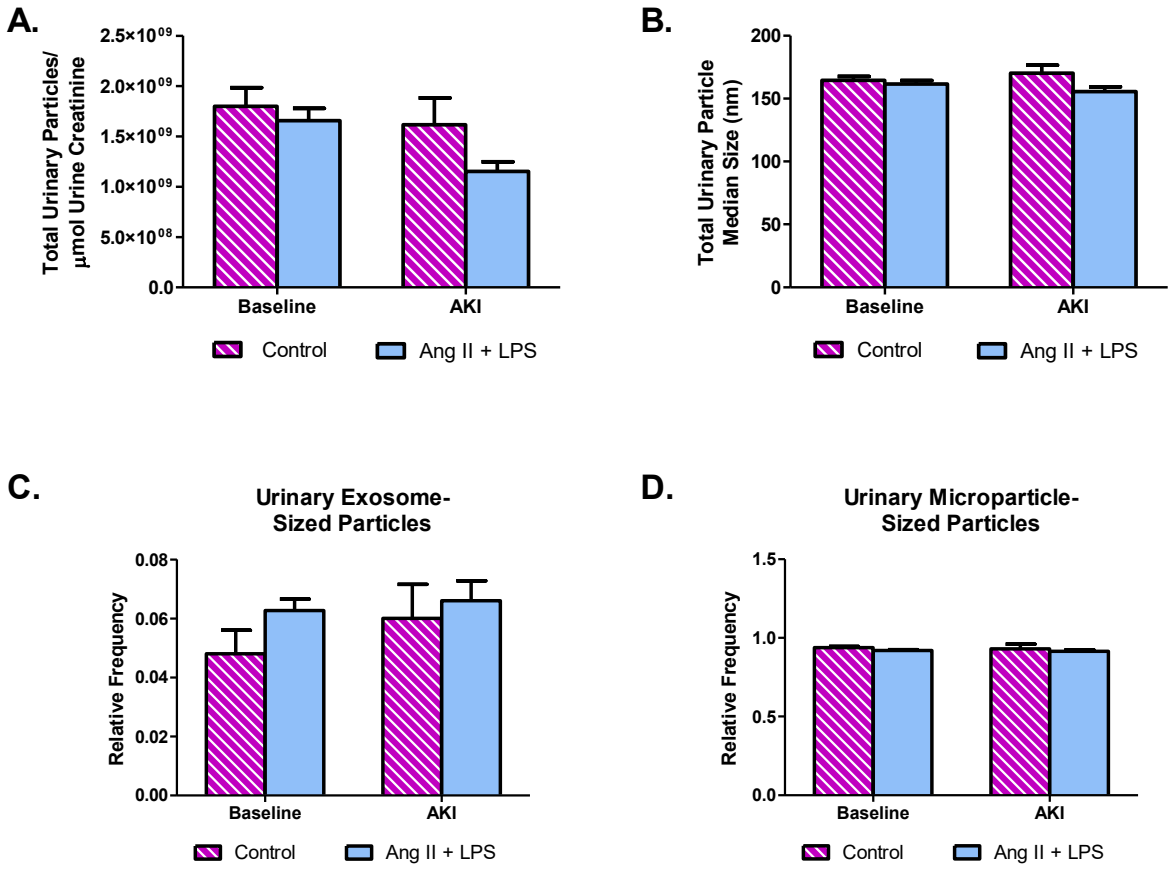

Figure 15. **Ang II + LPS pilot urinary particles (extracellular vesicles). A.** Total urinary particles concentration normalized to urine creatinine concentration at baseline (before angiotensin II and lipopolysaccharide; Ang II and LPS), and AKI (24 hours post-LPS injection). Urine creatinine concentration was obtained by Jaffe reaction assay. **B.** Total urinary particle median size at baseline and AKI. **C.-D.** Urinary exosome (30-90 nm diameter; **C.**) and microparticle (90-990 nm diameter; **D.**) sized particles expressed as relative frequency at baseline and AKI. Relative frequency was calculated as the particle count in a specific diameter range (30-90 nm or 90-990 nm) divided by the total particle count in the whole diameter range (0-1020 nm). Particle concentrations, median sizes, and counts were obtained by nanoparticle tracking analysis. Particle counts were given from 0-1020 nm in 30 nm bins. Control: n=6; Ang II + LPS: n=12. Outlying values were removed from the analysis. Data presented as mean ± standard error of the mean (SEM). An unpaired t-test with Welch's correction for all figures comparing groups at each time was performed (no significant differences detected; $p > 0.05$). AKI: Acute kidney injury.

3.1.2. Wild type mice administered angiotensin II for 29 days and injected once with lipopolysaccharide 19 days before euthanasia (Ang II + LPS long-term pilot)

The second pilot was performed to assess the potential of AKI to CKD transition with the Ang II and LPS combination. Six to eight weeks-old WT male and female mice were utilized in this pilot. Here, animals (Ang II + LPS group) received 400 ng/kg/min of Ang II for 29 days by osmotic minipumps and were injected once with 10 mg/kg of LPS ten days after minipump implantation. Control animals had a sham surgery and a saline i.p. injection instead of an Ang II minipump implantation and an LPS injection. Euthanasia was performed 19 days after the LPS (or saline) injection. Body weight and SBP were measured at baseline (before Ang II and LPS), 1W Pump (one week with Ang II minipump, before LPS), AKI (24 hours post LPS), and weekly after (post) LPS until euthanasia (endpoint; three weeks post-LPS). Body weight and SBP data are presented in Figure 16. A-D. At baseline, the control and Ang II + LPS body weights were 20.3 g and 22.2 g, respectively (Figure 16.A-B). After one week of Ang II (1W Pump), body weight in control was 20.3 g while in Ang II + LPS body weight was 22.6 g. At AKI, the body weights were 20.7 g and 20.6 g for the control and Ang II + LPS groups, respectively. From one to two weeks after LPS (1W and 2W post-LPS) control body weight went from 21.6 g to 22.1 g while Ang II + LPS body weight went from 22.5 g to 24.6 g. At endpoint, control, and Ang II + LPS body weights were 23.0 g and 24.7 g, respectively. Body weight reported in grams and relative body weight to baseline showed no significant differences between groups at any timepoint. As for SBP, control and Ang II + LPS had SBP of 109 mm Hg and 114 mm Hg at baseline, respectively (Figure 16.C-D). One week following Ang II minipump implantation (1W Pump), control SBP was 112 mm Hg, while Ang II + LPS SBP was 120 mm Hg. From 1W post-LPS to 2W post-LPS, control SBP went from 112 mm Hg to 117 mm Hg and

Ang II + LPS SBP went from 128 to 127 mm Hg. A significant difference between control and Ang II + LPS SBP (in mm Hg) was seen at 1W Pump (*p≤ 0.05) exclusively. In relative (to baseline) SBP, no significant differences are observed. When it comes to normalized kidney weight at endpoint, no significant differences were seen (Figure 16.E).

In this pilot, kidney function was assessed by ACR and BUN (Figure 17). ACR has been measured at baseline, AKI, and endpoint. At baseline, the control and Ang II + LPS body weights were 31 µg/mg and 9 µg/mg, respectively (not significant; Figure 17.A-B). 24 hours after LPS (AKI), ACR significantly increased in Ang II + LPS mice (85 µg/mg; *p≤ 0.05) compared to control mice (16 µg/mg). At endpoint, control, and Ang II + LPS ACRs were 189 µg/mg and 5 µg/mg, respectively (not significant). When looking at individual control biological replicates' ACR values at endpoint, it was noted that one of five control replicates had an ACR of 921 µg/mg while the other four replicates had ACRs between 3 µg/mg and 15 µg/mg (Figure 17.B). Endpoint BUN was also analyzed at endpoint and presented no significant differences between control and Ang II + LPS (7.3 mM for both groups; Figure 17.C). Renal inflammation, fibrosis and immune cell infiltration were evaluated through whole kidney qPCR using the genes presented in Table 7 of the appendices. Three weeks post-LPS (endpoint), no significant differences in expression were seen in Ang II + LPS mice for all the genes measured (0.03-to-1.71-fold expression vs control; Figure 18.A-K).

Moreover, kidney health was also assessed by urinary EVs (Figure 19). As mentioned previously, the following data describes urinary particles since the Zetaview Particle Tracking Analyzer counts all particles found within a liquid, including EVs. Urine Evs were evaluated at baseline, AKI, and endpoint. When looking at the concentration of urinary particles normalized to urine creatinine, no significant

differences were observed between control and Ang II + LPS at baseline, AKI and endpoint (Figure 19.A). Throughout the study, the urinary particle median size remained consistent between groups and timepoints (no significant differences; Figure 19.B). Both urinary exosome and microparticle-sized particles also presented no significant differences in relative frequency between groups and timepoint (Figure 19.C-D).

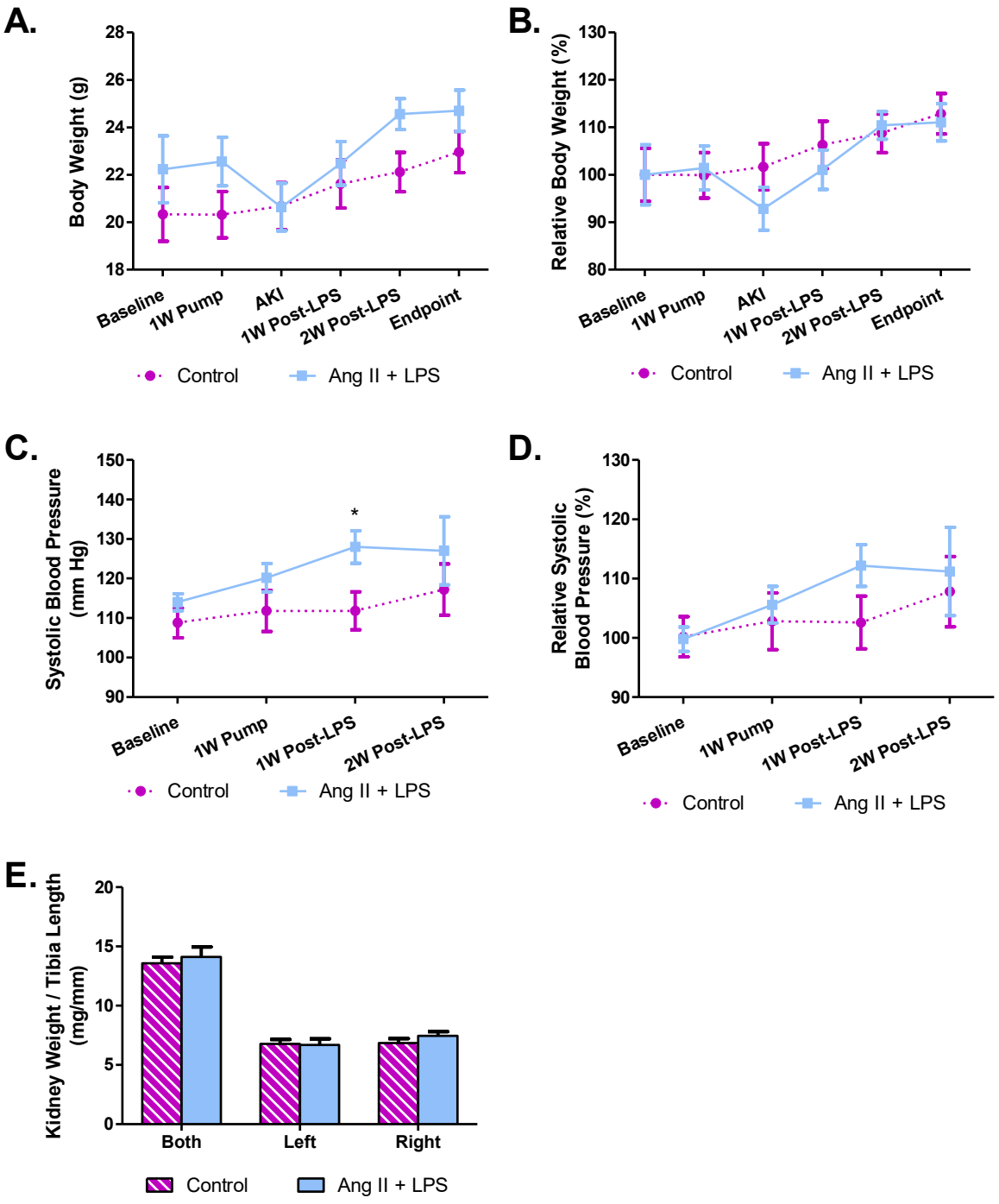

Figure legend on the following page (Figure 16).

Figure 16. **Ang II + LPS long-term pilot body weight, systolic blood pressure and normalized kidney weight. A-B.** Body weight reported in grams (**A.**) and relative (**B.**) to baseline (before angiotensin II and lipopolysaccharide; Ang II and LPS), 1W Pump (1 week with Ang II minipump, before LPS), AKI (24 hours post-LPS injection), 1W post-LPS (one-week post-LPS injection), 2W post-LPS (two weeks post-LPS injection) and endpoint (at euthanasia; 3 weeks post-LPS injection). From 1W Pump to 2W post-LPS, body weight (in gram and relative) included the Ang II osmotic minipump weight. **C-D.** Systolic blood pressure (SBP) reported in mm Hg (**C.**) and relative (**D.**) to baseline, 1W Pump, 1W post-LPS, and 2W post-LPS. SBP was obtained by tail-cuff photoplethysmography. The last three measurement days of each timepoint were combined. Five preliminary measures and at least seven actual measures were recorded each day. Normalizations (**B.** and **D.**) were obtained by dividing the value of each biological replicate by the mean of their respective group at baseline and multiplying by 100. **E.** Both (combined), left and right kidney weight normalized to tibia length at endpoint. Control: n=5; Ang II + LPS: n=5. Outlying values were removed from the analysis. Data presented as mean ± standard error of the mean (SEM). An unpaired t-test with Welch's correction for all figures comparing groups at each time point or category was performed (*p≤ 0.05). 1W: One-week; 2W: Two-week AKI: Acute kidney injury.

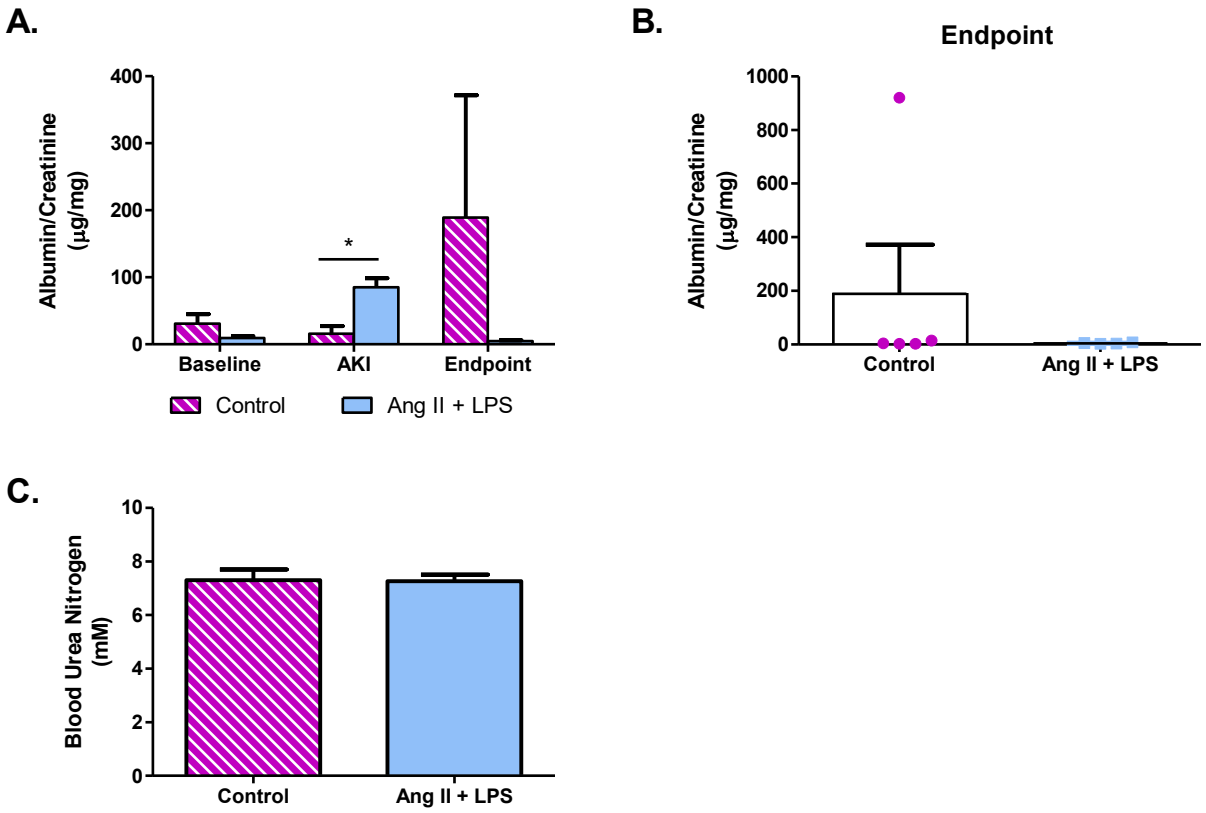

Figure 17. **Ang II + LPS long-term pilot albumin to creatinine ratio and blood urea nitrogen. A.** Albumin to creatinine ratio (ACR) at baseline (before angiotensin II and lipopolysaccharide; Ang II and LPS), AKI (24 hours post-LPS injection) and endpoint (at euthanasia; 3 weeks post-LPS injection). Albuminuria and urine creatinine were obtained by enzyme-linked immunosorbent assay (ELISA) and Jaffe reaction assay, respectively. **B.** Individual biological replicates ACR at endpoint. **C.** Blood urea nitrogen (BUN) at endpoint. Analysis blindly performed by IDEXX Laboratories. Control: n=5; Ang II + LPS: n=5. Outlying values were removed from the analysis. Data presented as mean ± standard error of the mean (SEM). An unpaired t-test with Welch's correction for all figures comparing groups at each time point was performed (*p≤ 0.05). AKI: Acute kidney injury.

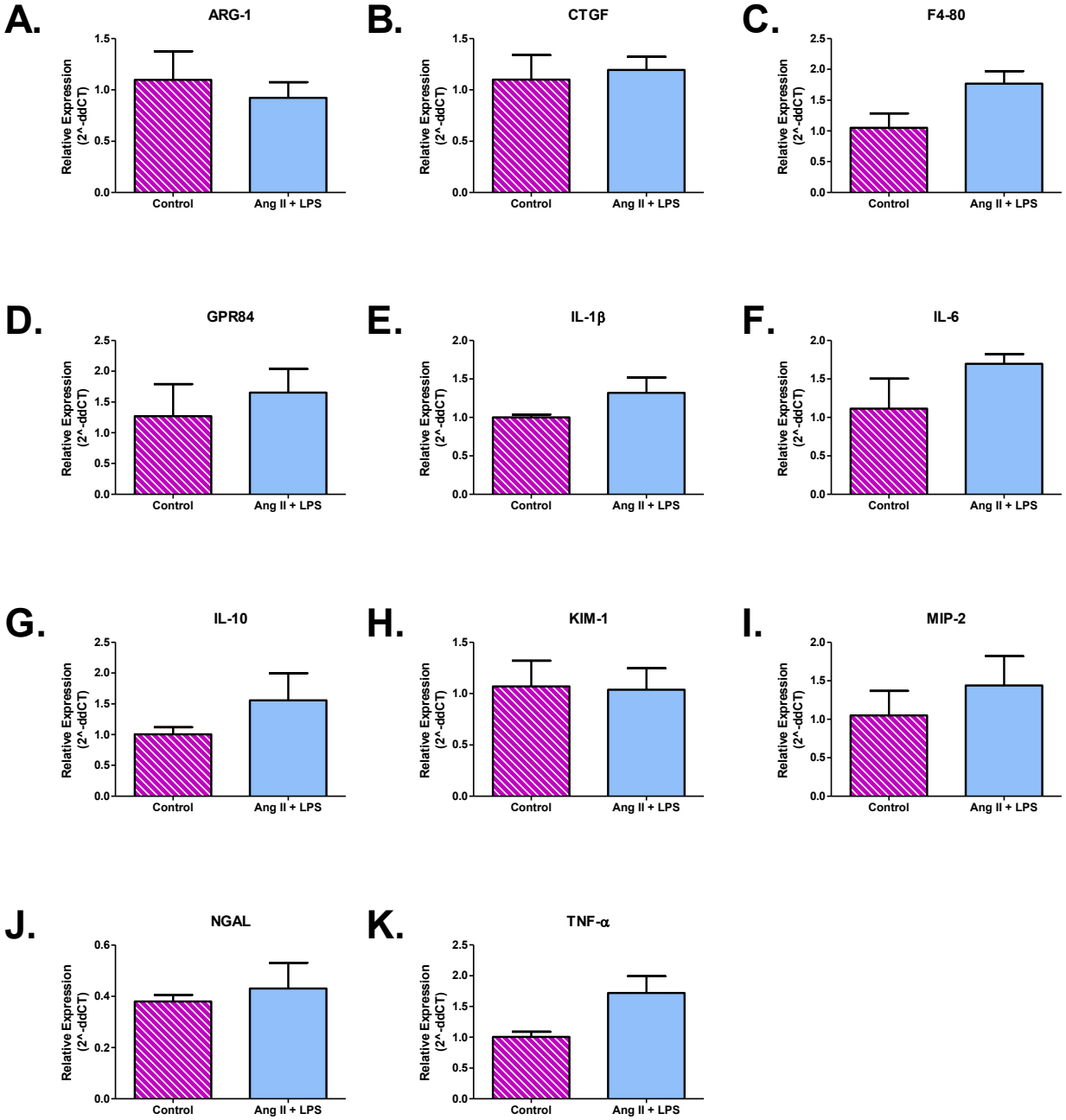

Figure 18. **Ang II + LPS long-term pilot renal expression of GPR84, and inflammatory, fibrotic, injury, and immune cell markers.** Messenger ribonucleic acid (mRNA) expression of arginase 1 (ARG-1; **A.**), connective tissue growth factor (CTGF; **B.**), EGF-like module-containing mucin-like hormone receptor-like 1 (F4-80; **C.**), G-coupled protein receptor 84 (GPR84; **D.**), interleukin (IL)-1 beta (**E.**), IL-6 (**F.**), IL-10 (**G.**), kidney injury molecule 1 (KIM-1; **H.**), macrophage inflammatory protein 2 (MIP-2; **I.**), neutrophil gelatinase-associated lipocalin (NGAL; **J.**), and tumour necrosis factor-alpha (TNF-α; **K.**) normalized to glyceraldehyde three-phosphate dehydrogenase (GAPDH) at endpoint (at euthanasia; 3 weeks post-LPS injection). Gene expression was assessed by quantitative polymerase chain reaction (qPCR). Control: n=5; Ang II + LPS: n=5. Outlying values were removed from the analysis. Data presented as mean ± standard error of the mean (SEM). An unpaired t-test with Welch's correction for all figures comparing groups for each gene was performed (no significant differences detected). Ang II + LPS: Angiotensin II + lipopolysaccharide.

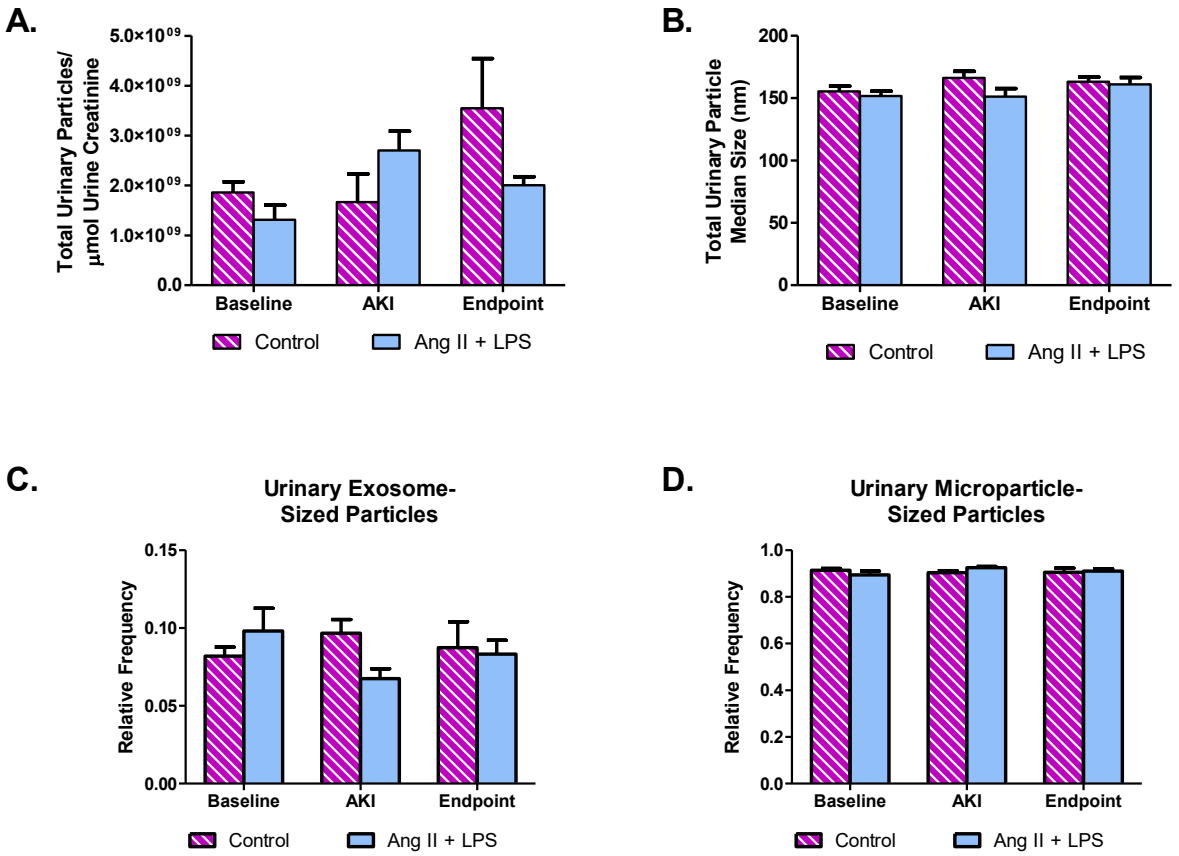

Figure 19. **Ang II + LPS long-term pilot urinary particles (extracellular vesicles). A.** Total urinary particles concentration normalized to urine creatinine concentration at baseline (before angiotensin II and lipopolysaccharide; Ang II and LPS), AKI (24 hours post-LPS injection), and endpoint (at euthanasia; 3 weeks post-LPS injection). Urine creatinine concentration was obtained by Jaffe reaction assay. **B.** Total urinary particle median size at baseline, AKI, and endpoint. **C.-D.** Urinary exosome (30-90 nm diameter; **C.**) and microparticle (90-990 nm diameter; **D.**) sized particles expressed as relative frequency at baseline, AKI, and endpoint. Relative frequency was calculated as the particle count in a specific diameter range (30-90 nm or 90-990 nm) divided by the total particle count in the whole diameter range (0-1020 nm). Particle concentrations, median sizes, and counts were obtained by nanoparticle tracking analysis. Particle counts were given from 0-1020 nm in 30 nm bins. Control: n=5; Ang II + LPS: n=5. Outlying values were removed from the analysis. Data presented as mean ± standard error of the mean (SEM). An unpaired t-test with Welch's correction for all figures comparing groups at each time was performed (no significant differences detected; $p > 0.05$). AKI: Acute kidney injury.

3.1.3. Angiotensin-converting enzyme 2 knockout mice on angiotensin II for seven days and injected once with lipopolysaccharide 21 days before euthanasia (SMC long-term pilot)

This pilot followed a similar timeline to the Ang II + LPS long-term pilot presented earlier. The breeding scheme now allowed the use of ACE2 mice (eight to nine-week-old males). Therefore, ACE2 KO mice received 400 ng/kg/min of Ang II for 28 days by osmotic minipumps and were injected with 10 mg/kg of LPS seven days after minipump implantation. Euthanasia was done 21 days after the LPS injection. The control group was ACE2 WT mice receiving a sham surgery and a saline injection. This pilot allowed the assessment of ACE2 KO, Ang II and LPS combination on kidney function, inflammation, and injury. As explained previously, the combination of ACE2 KO, Ang II and LPS is considered the SMC model and will be named so in subsequent sections of the thesis. Body weight and SBP were measured regularly throughout the study (Figure 20.A-D). At baseline, the control and SMC body weights were 26.9 g and 22.3 g, respectively (Figure 20.A-B). After one week of Ang II (1W Pump), body weight in control was 26.6 g while in SMC body weight was 22.9 g. At AKI, the body weights were 26.6 g and 20.8 g for the control and SMC groups, respectively. From one to two weeks after LPS (1W and 2W post-LPS) control body weight went from 27.1 g to 29.6 g while SMC body weight went from 21.4 g to 23.1 g. At endpoint, control and SMC body weights were 31.8 g and 24.4 g, respectively. Significant differences were noted in gram body weight between control and SMC at each timepoint (**p≤ 0.01 or ***p≤ 0.001) but not in relative (to baseline) body weight. As for SBP, control and SMC had SBP of 118 mm Hg and 125 mm Hg at baseline, respectively (Figure 20.C-D). One week following Ang II minipump implantation (1W Pump), control SBP was 111 mm Hg, while Ang II + LPS SBP was 133 mm Hg. From 1W post-LPS to 2W post-LPS,

control SBP went from 110 mm Hg to 113 mm Hg and Ang II + LPS SBP went from 125 to 123 mm Hg. SBP reported in mm Hg and relative SBP to baseline showed no significant differences between groups at any timepoint. When it comes to normalized kidney weight, significant differences were seen between control and SMC mice (*p≤ 0.05 or **p≤ 0.01; Figure 20.E). Control group combined (both), left and right normalized kidney weight was 16.6 mg/mm, 8.1 mg/mm, and 8.6 mg/m, respectively. In SMC, both, left and right normalized kidney weights were significantly smaller with normalized weights of 12.2 mg/mm (**p≤ 0.01), 5.7 mg/mm (*p≤ 0.05) and 6.5 mg/mm (**p≤ 0.01), respectively.

In this pilot, kidney function was assessed through ACR exclusively while renal inflammation and injury were analyzed with IL-6 and KIM-1 by qPCR (Figure 21.A-D). GPR84 expression was also evaluated at endpoint by qPCR (Figure 21.E). ACR was measured at baseline, AKI, and endpoint. At baseline, the control and SMC ACRs were 22 µg/mg and 10 µg/mg, respectively (Figure 21.A). 24 hours after LPS (AKI), the ACRs were 331 µg/mg and 384 µg/mg for the control and SMC groups, respectively. When looking at the control group's individual biological replicates' ACR, it was noticed that one of five replicates had an ACR of 1013 µg/mg, another replicate had an ACR of 26 µg/mg, and two other replicates had ACRs between 126 and 156 µg/mg (Figure 21.B). One control biological replicate was not measured at AKI as no urine was available. At endpoint, control and SMC ACRs were 6 µg/mg and 26 µg/mg, respectively (Figure 21.A). No significant differences in ACR between groups at any timepoint were reported. Renal expression of IL-6 and KIM-1 and GPR84 showed no significant differences three weeks following LPS insult (0.5-to-1.28-fold expression vs control; Figure 21.C-E). Indeed, a significant decrease in IL-6 expression in SMC was noted (0.5-fold vs control; **p≤ 0.01).

Urinary EVs were quantified using the Zetaview Particle Tracking Analyzer, which analyzes all particles contained in a liquid including EVs. Only baseline and AKI EVs were quantified in this pilot (Figure 22). The total urinary particle concentration and median size were not significantly different between control and SMC at baseline and AKI (Figure 22.A-B). Urinary exosome and microparticle-sized particles also showed no significant differences over time between control and SMC (Figure 22.C-D).

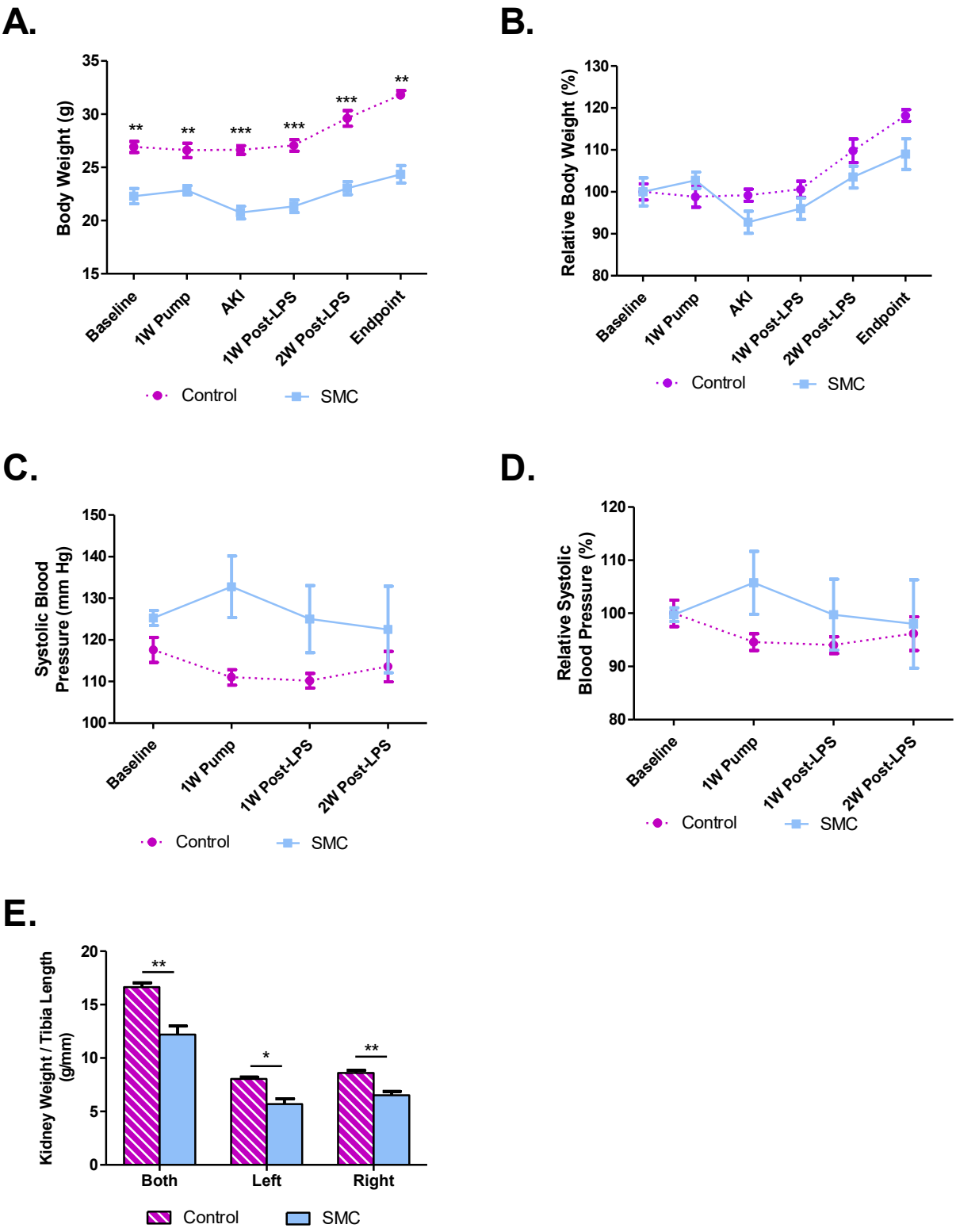

Figure legend on the following page (Figure 20).

Figure 20. **SMC long-term pilot body weight, systolic blood pressure and normalized kidney weight. A-B.** Body weight reported in grams (**A.**) and relative (**B.**) to baseline (before angiotensin II and lipopolysaccharide; Ang II and LPS), 1W Pump (1 week with Ang II minipump, before LPS), AKI (24 hours post-LPS injection), 1W post-LPS (one-week post-LPS injection), 2W post-LPS (two weeks post-LPS injection) and endpoint (at euthanasia; 3 weeks post-LPS injection). From 1W Pump to 2W post-LPS, body weight (in gram and relative) included the Ang II osmotic minipump weight. **C-D.** Systolic blood pressure (SBP) reported in mm Hg (**C.**) and relative (**D.**) to baseline, 1W Pump, 1W post-LPS, and 2W post-LPS. SBP was obtained by tail-cuff photoplethysmography. The last three measurement days of each timepoint were combined. Five preliminary measures and at least seven actual measures were recorded each day. Normalizations (**B.** and **D.**) were obtained by dividing the value of each biological replicate by the mean of their respective group at baseline and multiplying by 100. **E.** Both (combined), left and right kidney weight normalized to tibia length at endpoint. Control: n=5; SMC: n=4. Outlying values were removed from the analysis. Data presented as mean ± standard error of the mean (SEM). An unpaired t-test with Welch's correction for all figures comparing groups at each time point or category was performed (*p≤ 0.05; **p≤ 0.01; ***p≤ 0.001). 1W: One-week; 2W: Two-week AKI: Acute kidney injury; SMC: Surrogate model of coronavirus disease 2019-associated acute kidney injury.

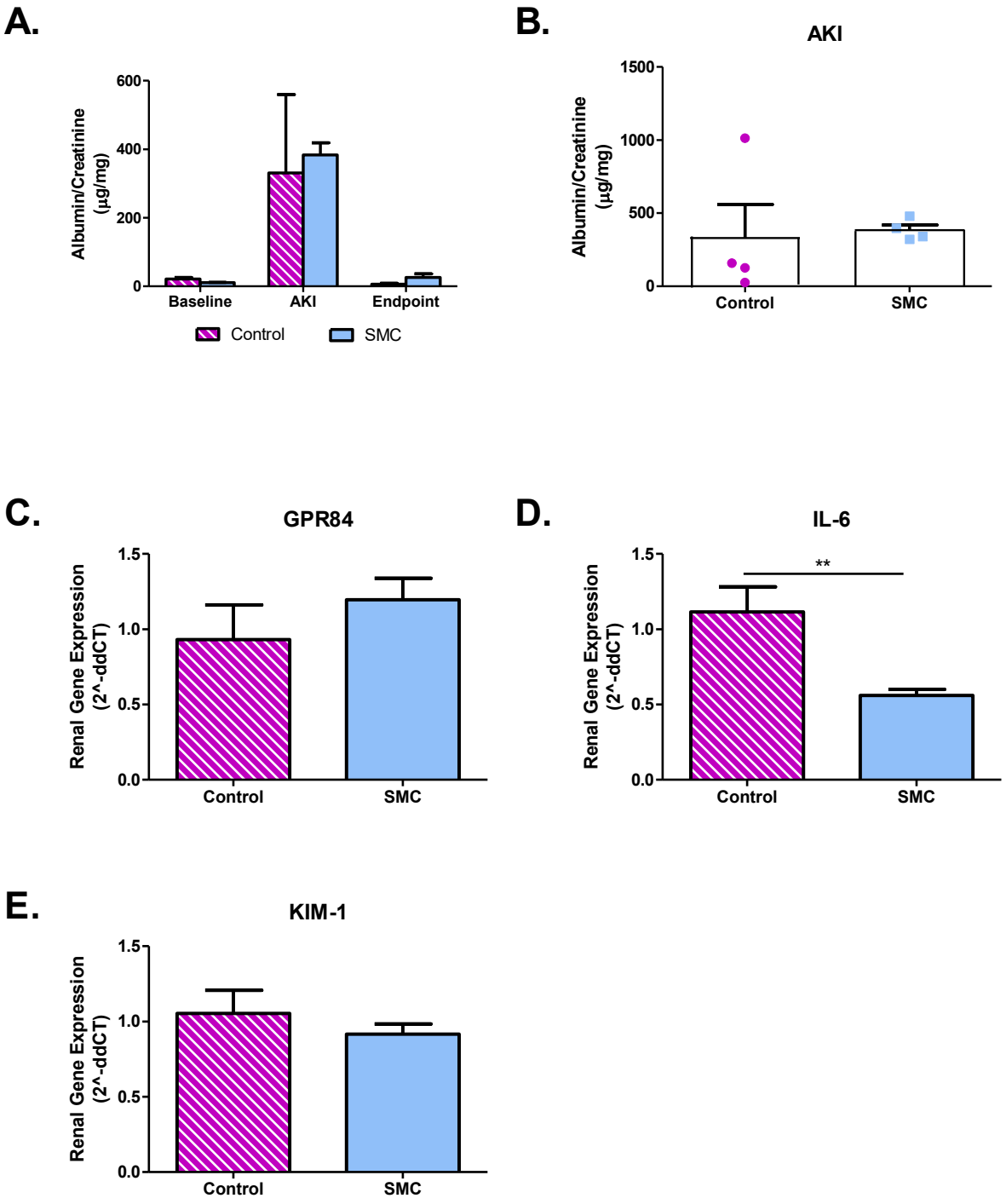

Figure legend on the following page (Figure 21).

Figure 21. **SMC long-term pilot albumin to creatinine ratio and renal gene expression. A.** Albumin to creatinine ratio (ACR) at baseline (before angiotensin II and lipopolysaccharide; Ang II and LPS), AKI (24 hours post-LPS injection) and endpoint (at euthanasia; 3 weeks post-LPS injection). Albuminuria and urine creatinine were obtained by enzyme-linked immunosorbent assay (ELISA) and Jaffe reaction assay, respectively. **B.** Individual biological replicates ACR at AKI. **C-E.** Messenger ribonucleic acid (mRNA) expression of G-coupled protein receptor 84 (GPR84; **C.**), interleukin-6 (IL-6; **D.**), and kidney injury molecule 1 (KIM-1; **E**) normalized to glyceraldehyde three-phosphate dehydrogenase (GAPDH) at endpoint (at euthanasia; 3 weeks post-LPS injection). Gene expression was assessed by quantitative polymerase chain reaction (qPCR). Control: n=5; SMC: n=4. Outlying values were removed from the analysis. Data presented as mean ± standard error of the mean (SEM). An unpaired t-test with Welch's correction for all figures comparing groups at each timepoint and gene was performed (**p≤ 0.01). SMC: Surrogate model of coronavirus disease 2019-associated acute kidney injury.

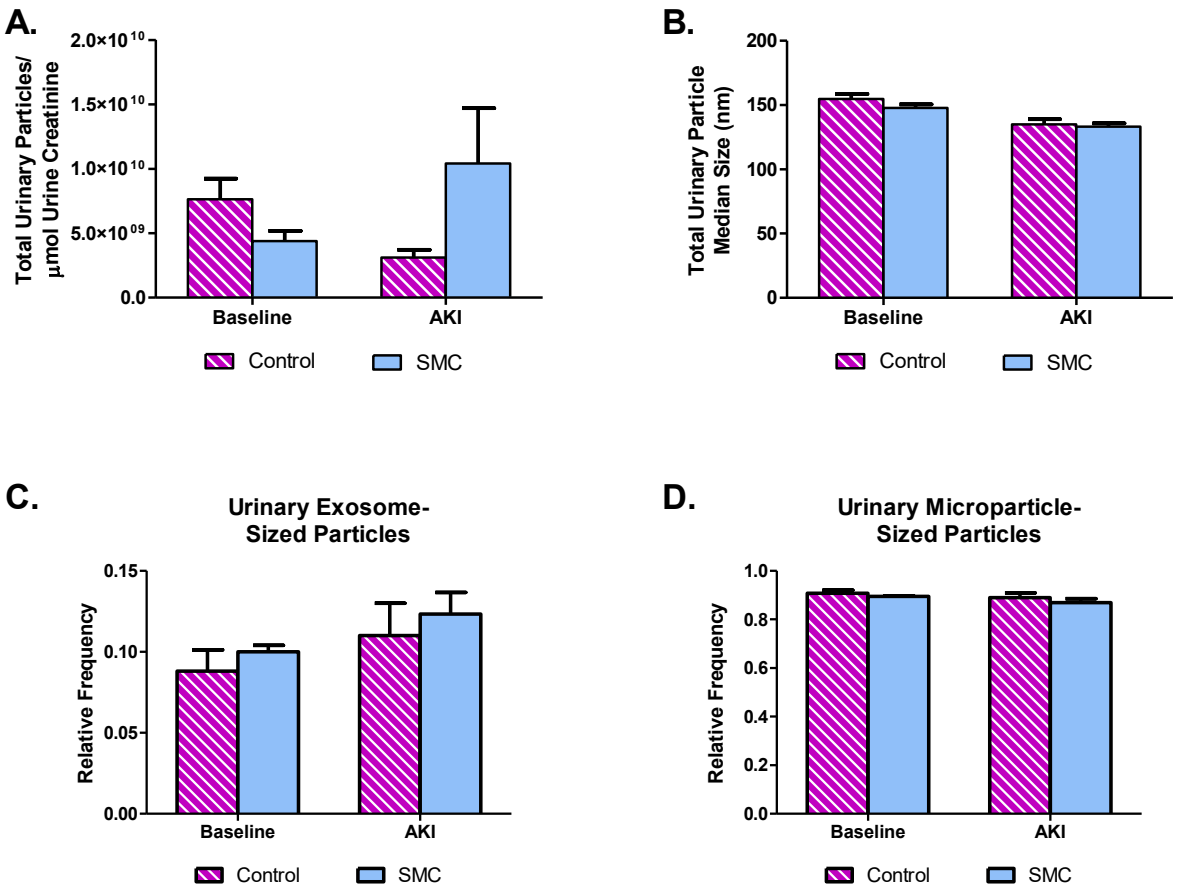

Figure 22. **SMC long-term pilot urinary particles (extracellular vesicles). A.** Total urinary particles concentration normalized to urine creatinine concentration at baseline (before angiotensin II and lipopolysaccharide; Ang II and LPS), and AKI (24 hours post-LPS injection). Urine creatinine concentration was obtained by Jaffe reaction assay. **B.** Total urinary particle median size at baseline and AKI. **C.-D.** Urinary exosome (30-90 nm diameter; **C.**) and microparticle (90-990 nm diameter; **D.**) sized particles expressed as relative frequency at baseline and AKI. Relative frequency was calculated as the particle count in a specific diameter range (30-90 nm or 90-990 nm) divided by the total particle count in the whole diameter range (0-1020 nm). Particle concentrations, median sizes, and counts were obtained by nanoparticle tracking analysis. Particle counts were given from 0-1020 nm in 30 nm bins. Control: n=5; SMC: n=4. Outlying values were removed from the analysis. Data presented as mean ± standard error of the mean (SEM). An unpaired t-test with Welch's correction for all figures comparing groups at each time was performed (no significant differences detected; $p > 0.05$). AKI: Acute kidney injury; SMC: Surrogate model of coronavirus disease 2019-associated acute kidney injury.

3.2. Assessment of GPR84 role in the new surrogate mouse model of coronavirus disease 2019-associated acute kidney injury using a GPR84 antagonist (GLPG-1205)

The second objective of this thesis was to determine the role of GPR84 in the SMC model by GPR84 antagonism and GPR84 global genetic deletion. In this section, the studies performed with the GPR84 antagonist GLPG-1205 are presented. As explained in the introduction, GPR84 is highly expressed in various immune cells, including monocytes, macrophages, neutrophils and peripheral leukocytes[80,84,85]. GPR84 is involved in fatty acid metabolism, immunological regulation, cytokine production, reactive oxygen species generation, and calcium influx[80,81,86]. In COVID-19 patients, GPR84 has been found in bronchoalveolar lavage fluid neutrophils, pointing toward a possible implication of GPR84 in the disease[90]. In CKD models, GPR84 was increased in macrophages, podocytes, and proximal tubule cells along with cytokine production, suggesting that GPR84 contributes to inflammation-associated injuries[85]. In preclinical models of renal injury, genetic deletion and pharmaceutical antagonists of GPR84 (e.g. PBI-4050) showed anti-inflammatory and antifibrotic effects[81,85,89]. Additionally, GLPG-1205, a GPR84 antagonist, recently completed phase II clinical trials for idiopathic pulmonary fibrosis and ulcerative colitis[98,101,102]. GPR84 pharmacological antagonism with GLPG-1205 could attenuate indices of renal injury in a SMC.

Three studies using GLPG-1205 are presented. Different drug dose, administration period and vehicle viscosity were evaluated. In the first study utilizing the GPR84 antagonist (section 3.2.1.), a dose of 30 mg/kg of GLPG-1205 in 4000 cps 0.5% methylcellulose vehicle was given once at the time of LPS injection (co-administered with LPS). In the second study (section 3.2.2.), GLPG-1205 was administered at a dose of 90 mg/kg in 4000 cps 0.5% methylcellulose as a prophylaxis

treatment. The prophylaxis treatment was administered daily from the day following minipump implantation until LPS injection, making seven days of treatment. The last study performed (section 3.2.3.) with GLPG-1205 resembles the second study with the exception that the vehicle used (methylcellulose) had a lower viscosity (400 cps). Studies have demonstrated that mucosal drug absorption reduces with increasing viscosity[133,134]. Therefore, using a lower viscosity vehicle (400 cps methylcellulose) could increase drug absorption and thereby potentially increase its effects. A lower viscosity vehicle was used to see if it would increase GLPG-1205 effects on renal function, injury, and inflammation.

All studies evaluating GLPG-1205 were performed on the SMC model where eight to ten-week-old ACE2 KO male mice were implanted with an Ang II osmotic minipump (400 ng/kg/min) for eight days. Seven days following minipump implantation, mice were given 10 mg/kg of LPS by i.p. injection. Mice were euthanized 24 hours post-LPS injection. As stated earlier, control animals (eight to ten-week-old ACE2 WT males) received a sham surgery and an i.p. injection of saline instead of an Ang II minipump and LPS injection. For all studies, GLPG-1205 treatment was given by oral gavage. Vehicle animals were administered 0.5% methylcellulose (same viscosity used for the treated groups) by oral gavage as well. Table 6 of the appendices presents details on animals' age, genotype, and group size as well as treatment type, dose and vehicle used in all studies.

3.2.1. GLPG-1205 co-administration with LPS treatment in the surrogate mouse model of coronavirus disease 2019-associated acute kidney injury

In this study, where GLPG-1205 was tested for the first time on the SMC model, 30 mg/kg of GLPG-1205 in 4000 cps 0.5% methylcellulose vehicle was administered once at the same time as LPS injection (24 hours before euthanasia). Body weight, SBP, normalized kidney weight, ACR, BUN, and renal expression of pro-inflammatory, pro-fibrotic, injury and immune cell markers were evaluated. Additionally, liver weight normalized to tibia length was measured. For most drugs, metabolism and biotransformation mostly occur in the liver[135,136]. Certain medications (e.g., acetaminophen and cholesterol-lowering medications) can lead to liver damage and hepatic cell death[136]. To assess general liver health following GLPG-1205 administration, normalized liver weight was analyzed. Figure 23 presents body weight, SBP as well as normalized kidney and liver weight. Baseline body weights in the control vehicle-treated, control GLGP-1205-treated, SMC vehicle-treated, and SMC GLPG-1205-treated mice were 24.7 g, 26.1 g, 25.3 g, and 23.3 g, respectively (Figure 23.A-B). After one week of Ang II (1W Pump), body weights in the control vehicle and control GLGP-1205 groups were 24.5 g and 25.3 g, while in SMC vehicle and SMC GLPG-1205 groups body weights were 26.1 g and 23.5 g, respectively. At AKI, the body weights were 24.5 g, 25.4 g, 23.8 g, and 21.9 g for the control vehicle, control GLGP-1205, SMC vehicle and SMC GLPG-1205 groups, respectively. Significant differences in (gram) body weight was seen exclusively between the SMC vehicle and SMC GLGP-1205 groups at baseline (*p≤ 0.05), 1W Pump (**p≤ 0.01) and AKI (**p≤ 0.01). However, relative (to baseline) body weight showed no significant differences between SMC vehicle-treated and SMC GLPG-1205-treated mice at any timepoint. As for SBP, baseline values were 122 mm Hg for the control vehicle group, 117 mm Hg

for the control GLPG-1205 group, 119 mm Hg for the SMC vehicle group, and 127 mm Hg for the SMC GLGP-1205 group (Figure 23.C-D). At 1W Pump SBP were 122 mm Hg, 116 mm Hg, 121 mm Hg, and 126 mm Hg for control vehicle-treated mice, control GLPG-1205-treated mice, SMC vehicle-treated mice, and SMC GLPG-1205-treated mice, respectively. SBP reported in mm Hg and relative to baseline showed no significant differences between SMC vehicle and SMC GLPG-1205 or control vehicle groups at any timepoint. When it comes to normalized kidney (Figure 23.E) and liver (Figure 23.F), no significant differences were seen between groups.

ACR and BUN were measured to assess renal function. At Baseline, ACR was 16 µg/mg in control vehicle-treated and control GLPG-1205-treated mice, while ACRs in SMC vehicle-treated and SMC GLPG-1205-treated mice were 20 µg/mg and 76 µg/mg, respectively (no significant differences; Figure 24.A). When looking SMC GLPG-1205 biological replicates ACR at baseline, it was noted that one of the 12 replicates had an ACR of 514 µg/mg while ten other replicates had ACRs between 9 and 87 µg/mg (Figure 24.B). One of SMC GLPG-1205 biological replicates (baseline) was removed from the analysis as it was an outlier. After one week of Ang II (1W Pump), ACRs in the control vehicle and control GLGP-1205, SMC vehicle and SMC GLPG-1205 groups were 14 µg/mg, 16 µg/mg, 19 µg/mg, and 18 µg/mg respectively (no significant differences; Figure 24.A). At AKI, a significant increase in the SMC vehicle group ACR (551 µg/mg) was observed compared to the control vehicle group (10 µg/mg; **$p \leq 0.01$). GLPG-1205 treatment failed to significantly reduce ACR in the SMC GLPG-1205 group (338 µg/mg vs 551 µg/mg in SMC vehicle). Control GLGP-1205 ACR was 14 µg/mg. When it comes to BUN, no significant differences were seen between the SMC vehicle (5.5 mM) and the SMC GLPG-1205 (6.6 mM), as well as between the SMC vehicle and the control vehicle group (2.7 mM; Figure 24.C). Control

GLPG-1205 BUN was also 2.7 mM.

Various pro-inflammatory, pro-fibrotic, injury and immune cell markers were measured by qPCR (Figure 25). SMC vehicle animals presented a significant upregulation in all genes evaluated (**p≤ 0.01 or ***p≤ 0.001 vs control vehicle) except for MIP-2 (non-significant 217-fold expression vs control vehicle; Figure 25.I). Indeed, ARG-1, IL-6, IL-10, KIM-1, and NGAL presented a 28, 330, 55, 711, and 792-fold increase from the control vehicles (**p≤ 0.01 or ***p≤ 0.001; Figure 25.A, F-H, J). Other genes evaluated (CTFG, F4-80, IL-1β, and TNF-α) had a lower but significant upregulation between 3 and 9-fold (**p≤ 0.01 or ***p≤ 0.001 vs control vehicle; Figure 25.B-C, E, and K). GLPG-1205 treatment in SMC (SMC GLPG-1205) had no significant effect on the expression of any of the genes assessed. In SMC vehicle, GPR84 renal expression significantly increased by 202-fold (vs control vehicle; ***p≤ 0.001) while SMC GLPG-1205-treated mice had no significant effect on GPR84 expression (131-fold vs control vehicle; Figure 25.D). Similar gene expression was noted between the control vehicle and control GLPG-1205 groups (Figure 25.).

Similarly, to the Ang II + LPS pilot, increased cellularity was noted in all the SMC + GLPG-1205 studies (data not shown; section 3.2.). Therefore, immunohistochemistry was done to identify the infiltrating cells, starting with myeloperoxidase. Neutrophil staining (Figure 26) presented an average of 0 neutrophils in both control vehicle-treated mice and control GLGP-1205-treated mice. In the SMC vehicle group, the number of neutrophils was significantly increased to 31 neutrophils per field (vs control vehicle; ***p≤ 0.001). In the SMC GLGP-1205 the number of neutrophils in the kidneys was significantly reduced to 20 neutrophils per field (vs SMC vehicle; ***p≤ 0.001). A visual representation of the myeloperoxidase staining in SMC + GLPG-1205 is presented in section 3.2.3. (Figure 26).

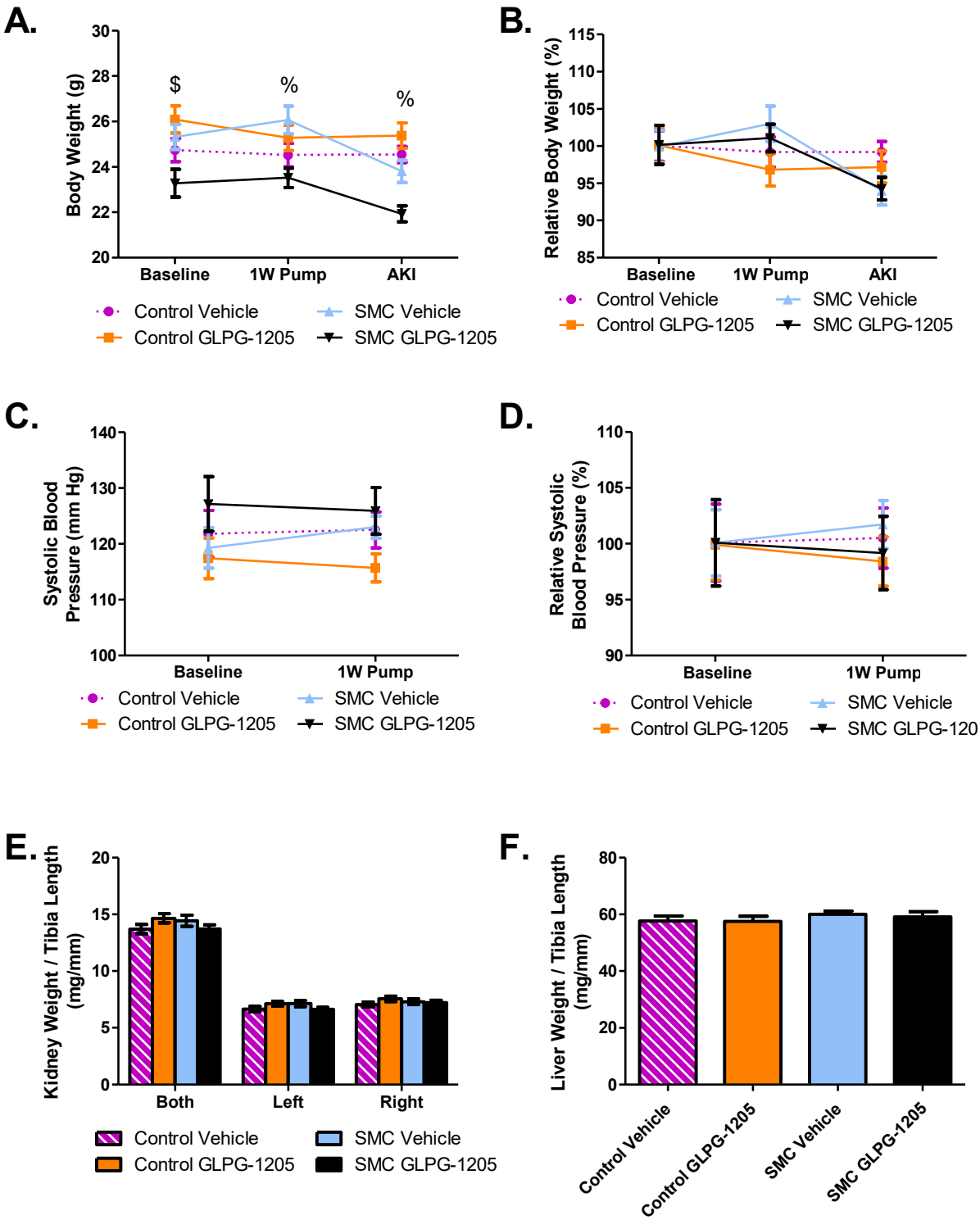

Figure legend on the following page (Figure 23).

Figure 23. **SMC + GLPG-1205 (co-administered with LPS) body weight, systolic blood pressure, normalized kidney weight, and normalized liver weight. A-B.** Body weight reported in grams (**A.**) and relative (**B.**) to baseline (before angiotensin II and lipopolysaccharide; Ang II and LPS), 1W Pump (1 week with Ang II minipump, before LPS), and AKI (24 hours post-LPS injection). 1W Pump body weight (in gram and relative) included the Ang II osmotic minipump weight. **C-D.** Systolic blood pressure (SBP) reported in mm Hg (**C.**) and relative (**D.**) to baseline and 1W Pump. SBP was obtained by tail-cuff photoplethysmography. The last three measurement days of each timepoint were combined. Five preliminary measures and at least seven actual measures were recorded each day. Normalizations (**B.** and **D.**) were obtained by dividing the value of each biological replicate by the mean of their respective group at baseline and multiplying by 100. **E.** Both (combined), left and right kidney weight normalized to tibia length at AKI. **F.** Liver weight normalized to tibia length at AKI. Control vehicle: n=10; Control GLPG-1205: n=10; SMC vehicle: n=11; SMC GLGP-1205: n=12. Outlying values were removed from the analysis. Data presented as mean ± standard error of the mean (SEM). One-way analysis of variance (ANOVA) with a Dunnett post-test comparing SMC vehicle to control vehicle and SMC GLPG-1205 was performed at each timepoint or category ($: *p≤ 0.05 SMC vehicle vs SMC GLGP-1205; %: **p≤ 0.01 SMC vehicle vs SMC GLGP-1205). 1W Pump: One-week minipump; AKI: Acute kidney injury; SMC: Surrogate model of coronavirus disease 2019-associated acute kidney injury.

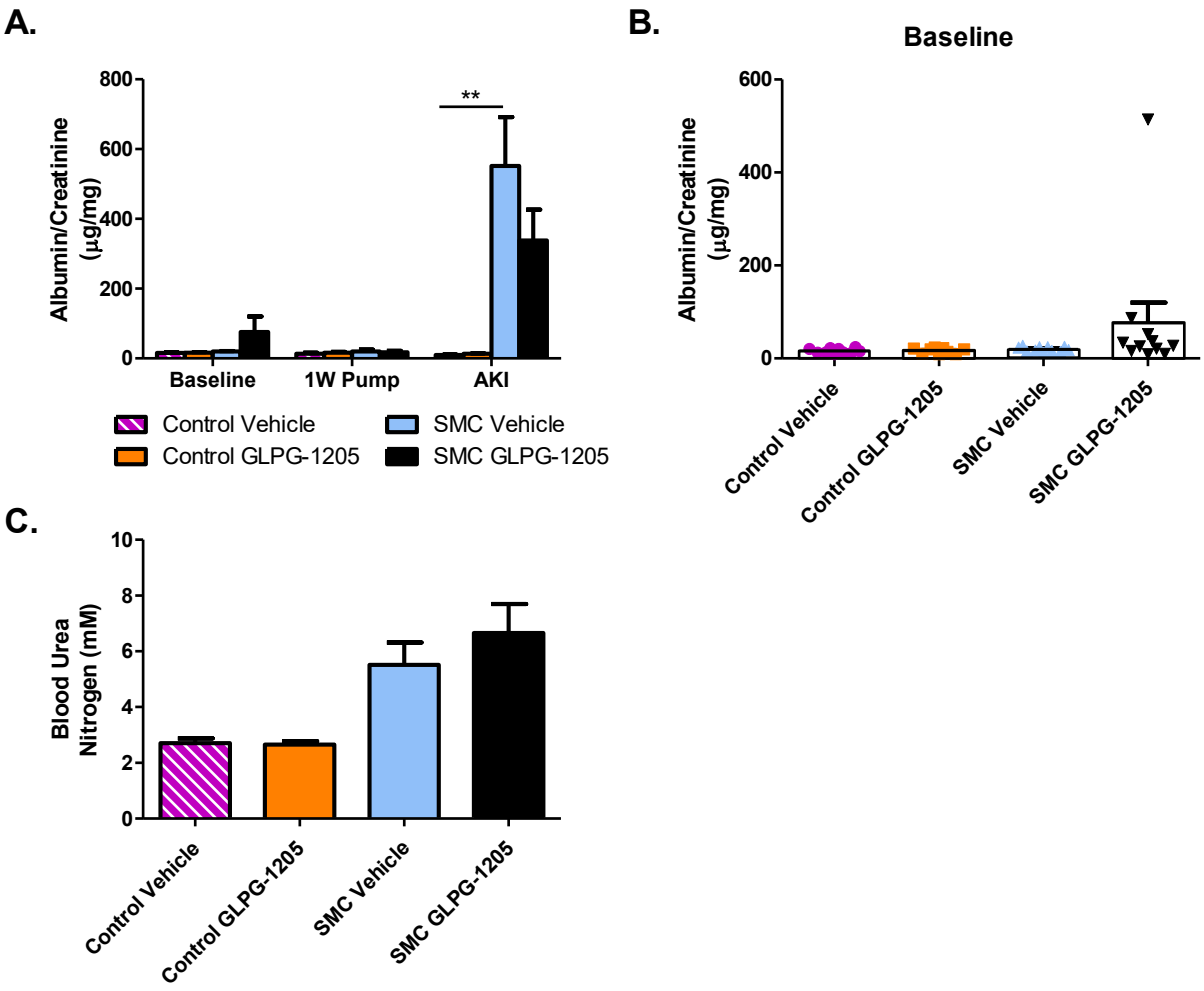

Figure 24. **SMC + GLPG-1205 (co-administered with LPS) albumin to creatinine ratio and blood urea nitrogen. A.** Albumin to creatinine ratio (ACR) at baseline (before angiotensin II and lipopolysaccharide; Ang II and LPS), and AKI (24 hours post-LPS injection). Albuminuria and urine creatinine were obtained by enzyme-linked immunosorbent assay (ELISA) and Jaffe reaction assay, respectively. **B.** Individual biological replicates ACR at baseline. **C.** Blood urea nitrogen (BUN) at AKI. Analysis blindly performed by IDEXX Laboratories. Control vehicle: n=10; Control GLPG-1205: n=10; SMC vehicle: n=11; SMC GLGP-1205: n=12. Outlying values were removed from the analysis. Data presented as mean ± standard error of the mean (SEM). One-way analysis of variance (ANOVA) with a Dunnett post-test comparing SMC vehicle to control vehicle and SMC GLPG-1205 was performed at each timepoint (**p≤ 0.01). 1W Pump: One-week minipump; AKI: Acute kidney injury; SMC: Surrogate model of coronavirus disease 2019-associated acute kidney injury.

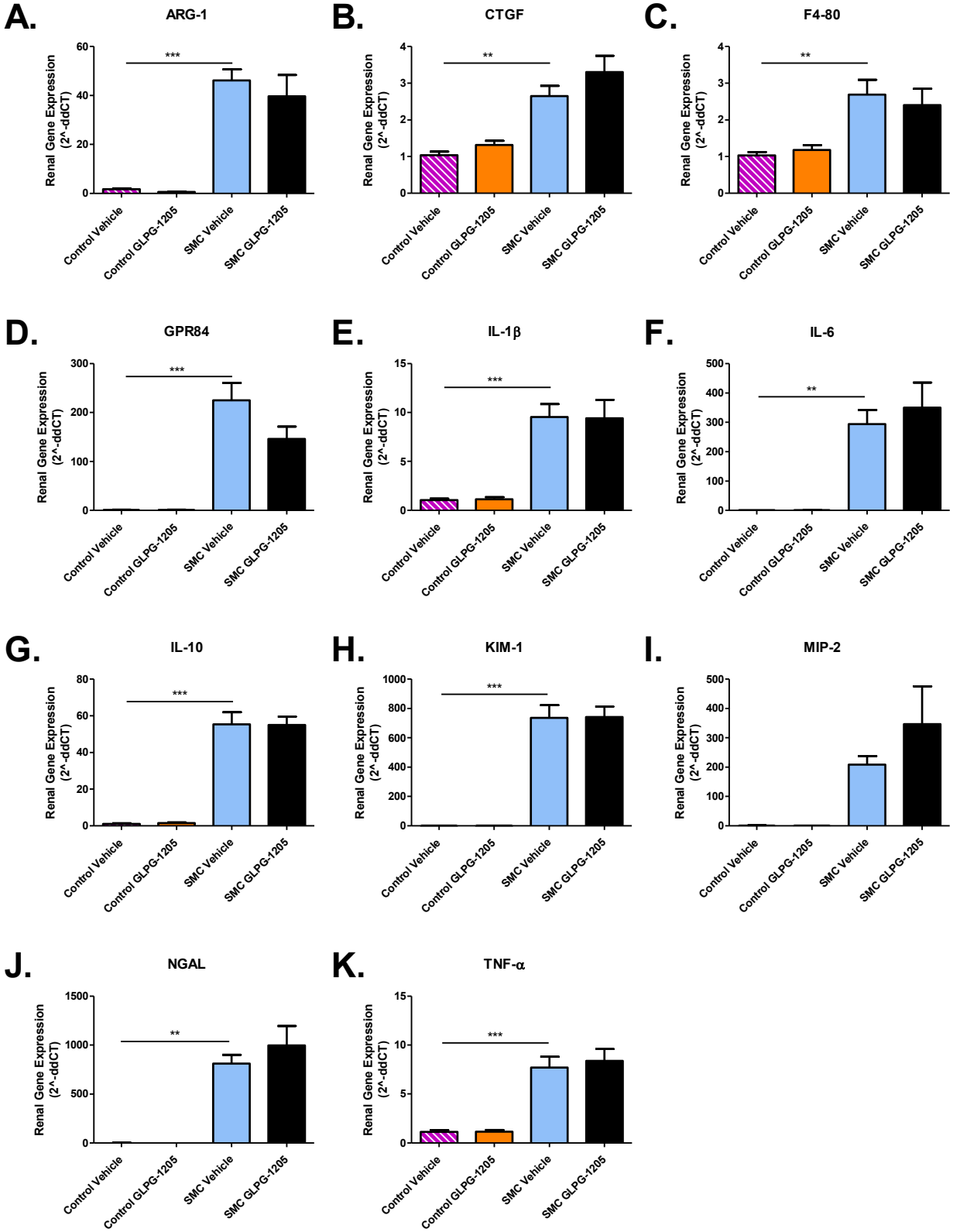

Figure legend on the following page (Figure 25).

Figure 25 **SMC + GLPG-1205 (co-administered with LPS) renal expression of GPR84, and inflammatory, fibrotic, injury, and immune cell markers.** Messenger ribonucleic acid (mRNA) expression of arginase 1 (ARG-1; **A.**), connective tissue growth factor (CTGF; **B.**), EGF-like module-containing mucin-like hormone receptor-like 1 (F4-80; **C.**), G-coupled protein receptor 84 (GPR84; **D.**), interleukin (IL)-1 beta (**E.**), IL-6 (**F.**), IL-10 (**G.**), kidney injury molecule 1 (KIM-1; **H.**), macrophage inflammatory protein 2 (MIP-2; **I.**), neutrophil gelatinase-associated lipocalin (NGAL; **J.**), and tumour necrosis factor-alpha (TNF-α; **K.**) normalized to glyceraldehyde three-phosphate dehydrogenase (GAPDH) at AKI (24 hours post-lipopolysaccharide injection). Gene expression was assessed by quantitative polymerase chain reaction (qPCR). Control vehicle: n=10; Control GLPG-1205: n=10; SMC vehicle: n=11; SMC GLGP-1205: n=12. Outlying values were removed from the analysis. Data presented as mean ± standard error of the mean (SEM). One-way analysis of variance (ANOVA) with a Dunnett post-test comparing SMC vehicle to control vehicle and SMC GLPG-1205 was performed at each timepoint (**p≤ 0.01; ***p≤ 0.001). AKI: Acute kidney injury; SMC: Surrogate model of coronavirus disease 2019-associated acute kidney injury.

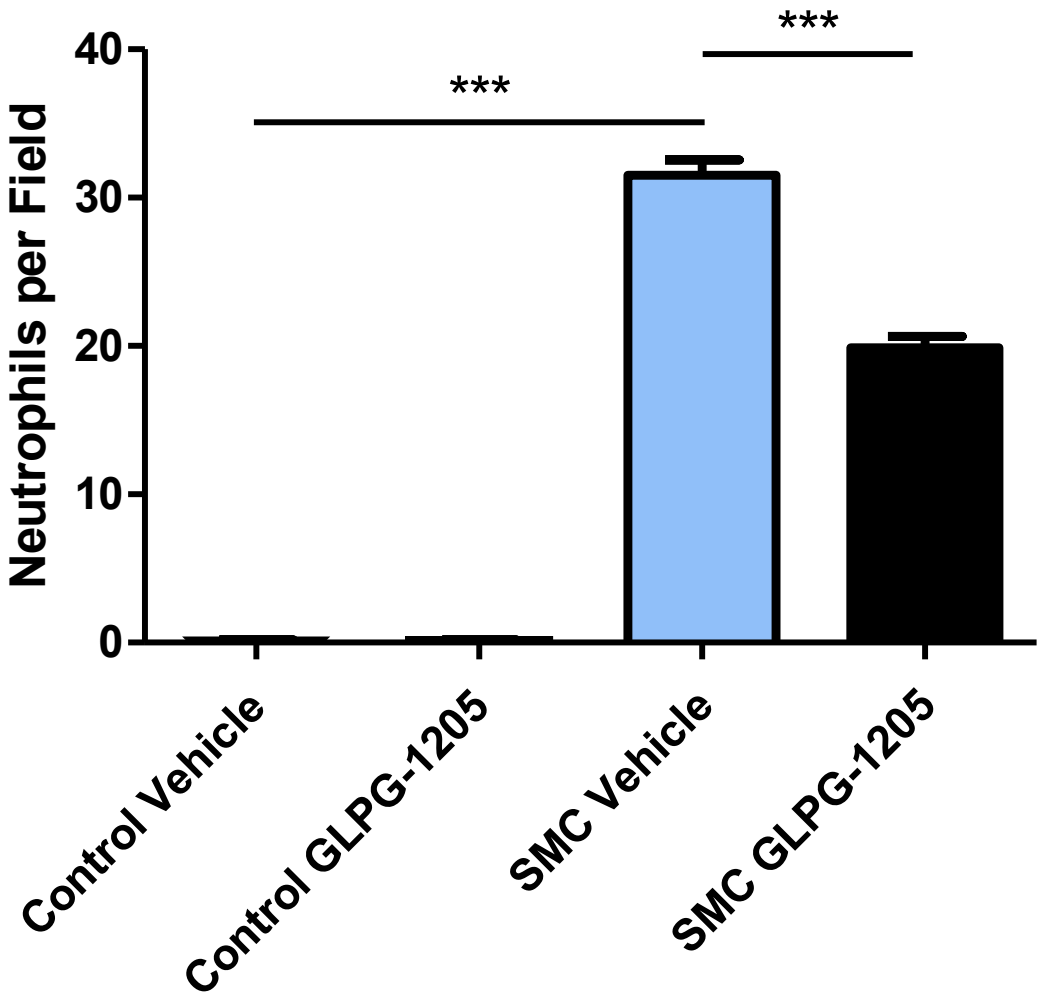

Figure 26. **SMC + GLPG-1205 (co-administered with LPS) renal neutrophil infiltration.** Quantification of neutrophils (Myeloperoxidase positive events) per field from myeloperoxidase immunohistochemistry on AKI (24 hours post-LPS) kidneys. Four to ten fields were averaged per biological replicate. Control vehicle: n=5; Control GLPG-1205: n=5; SMC vehicle: n=7; SMC GLGP-1205: n=8. Outlying values were removed from the analysis. Data presented as mean ± standard error of the mean (SEM). One-way analysis of variance (ANOVA) with a Dunnett post-test comparing SMC vehicle to control vehicle and SMC GLPG-1205 was performed (***p≤ 0.001). AKI: Acute kidney injury.

3.2.2. GLPG-1205 prophylaxis treatment in the surrogate mouse model of coronavirus disease 2019-associated acute kidney injury using 4000 cps methylcellulose

In this second study evaluating GLPG-1205 on the SMC model, a prophylaxis treatment was selected. Mice were administered 90 mg/kg of GLPG-1205 in 0.5% 4000 cps methylcellulose daily from the day following Ang II minipump implantation until LPS injection (seven days of treatment). Animal wellness, renal function and injury were assessed using the same method as prior studies. Baseline body weights in the control vehicle-treated, control GLGP-1205-treated, SMC vehicle-treated, and SMC GLPG-1205-treated mice were 25.6 g, 25.4 g, 23.0 g, and 18.9 g, respectively (Figure 27.A-B). After one week of Ang II (1W Pump), body weights in the control vehicle and control GLGP-1205 groups were 25.2 g and 25.7 g, while in the SMC vehicle and SMC GLPG-1205 groups body weights were 22.1 g and 18.4 g, respectively. At AKI, the body weights were 25.0 g, 25.7 g, 22.1 g, and 19.1 g for the control vehicle, control GLGP-1205, SMC vehicle and SMC GLPG-1205 groups, respectively. Significant differences in body weight between SMC vehicle and control vehicle groups were noted at all timepoint (*p≤ 0.05). Additionally, significant differences in body weight were observed between SMC vehicle and SMC GLPG-1205 groups at baseline (***p≤ 0.001), 1W Pump (**p≤ 0.01), and AKI (*p≤ 0.05). However, when normalizing groups' body weight to their respective baseline, no significant differences between groups were seen at any timepoint. As for SBP, baseline values were 119 mm Hg for the control vehicle group, 112 mm Hg for the control GLPG-1205 group, 114 mm Hg for the SMC vehicle group, and 113 mm Hg for the SMC GLGP-1205 group (Figure 27.C-D). At 1W Pump SBP was 114 mm Hg for control vehicle-treated and control GLPG-1205-treated mice while SBPs were 119 mm Hg, and 129 mm Hg for SMC vehicle-treated and SMC GLPG-1205-treated mice,

respectively. SBP reported in mm Hg and relative to baseline showed no significant differences between groups at any timepoint. When it comes to normalized kidney and liver weight, no significant differences in were observed between groups (Figure 27.E-F).

ACR and BUN were measured to assess kidney function (Figure 28). At Baseline, ACR in control vehicle-treated, control GLPG-1205-treated, SMC vehicle-treated and SMC GLPG-1205-treated mice were 36 µg/mg, 27 µg/mg, 29 µg/mg, and 23 µg/mg respectively (no significant differences; Figure 28.A). After one week of Ang II (1W Pump), ACRs in the control vehicle and control GLGP-1205, SMC vehicle and SMC GLPG-1205 groups were 53 µg/mg, 42 µg/mg, 289 µg/mg, and 274 µg/mg respectively (no significant differences). When assessing individual biological replicates' ACR at 1W Pump, four of the six SMC vehicle biological replicates had an ACR between 46 and 196 µg/mg while the other two replicates had ACRs of 512 µg/mg and 778 µg/mg (Figure 28.B). In SMC GLPG-1205, two of the five biological replicates had ACRs between 55 and 78 µg/mg while the other three replicates had ACRs between 297 and 421 µg/mg. At AKI, a significant increase in the SMC vehicle group ACR (316 µg/mg) was observed compared to the control vehicle group (28 µg/mg; ***p≤ 0.001; Figure 28.A). GLPG-1205 treatment did not significantly affect on ACR in the SMC GLPG-1205 group (309 µg/mg vs 316 µg/mg in SMC vehicle). When assessing individual biological replicates' ACR at AKI, one of the five SMC GLP-1205 biological replicates had an ACR of 97 µg/mg while three other replicates had ACRs between 255 and 361 µg/mg (Figure 28.C). No urine was available for analysis for one of the SMC GLP-1205 replicates. Control GLGP-1205 ACR was 24 µg/mg at AKI. Differences in BUN at AKI between groups were not statistically significant (Figure 28.D). Indeed, the control vehicle BUN was at 2.9 mM, while the SMC vehicle and

SMC GLPG-1205 BUN were at 3.7 mM and 3.2 mM, respectively. Control animals treated with GLPG-1205 had a BUN of 2.1 mM.

AKI can lead to electrolyte imbalance[37,45]. Therefore, plasma concentrations of chloride, potassium, and sodium, as well as urine sodium concentrations, were measured. A significant increase in plasma chloride was seen in SMC vehicle-treated mice (123 mM vs 109 mM control vehicle; ***p≤ 0.001) while GLPG-1205 treatment in SMC had no significant difference in plasma chloride (122 mM in SMC GLGP-1205; Figure 29.A). Plasma potassium was not significantly different in the SMC vehicle (5.7 mM) in comparison to control vehicle (6.5 mM; Figure 29.B). SMC GLPG-1205-treated animals, on the other hand, had a significantly increased plasma potassium concentration compared to SMC vehicle-treated animals (6.8 mM vs 5.7 mM; *p≤ 0.05). Control GLPG-1205 plasma potassium was 6.1 mM. Plasma sodium was significantly increased in the SMC vehicle group (157 mM) compared to the control vehicle group (147 mM; **p≤ 0.01) while no significant difference was observed in the SMC GLPG-1205 group (155 mM; Figure 29.C). Control GLPG-1205 plasma sodium concentration was of 149 mM. As for urine sodium, concentrations were 188 mM vs 49 mM in the control vehicle and SMC vehicle, respectively (no significant differences; Figure 29.D). GLPG-1205 Treatment in SMC also had no significant effect on urine sodium concentration (57 mM SMC GLPG-1205) when compared with SMC vehicle. Control GLPG-1205 urine sodium concentration was of 158 mM.

Renal expression of GPR84, as well as pro-inflammatory, pro-fibrotic, injury and immune cell markers, were quantified by qPCR (Figure 30). For all genes, except for CTGF (1.7-fold expression vs control vehicle; Figure 30.B), significant upregulation was seen in the SMC vehicle (**p≤ 0.01 or ***p≤ 0.001 vs control vehicle; Figure 30.A, C-K). For F4-80, IL-1β, and TNF-α, a 3 to 10-fold increase was observed in SMC

vehicle mice (**p≤ 0.01 or ***p≤ 0.001 vs control vehicle; Figure 30.C, E, K). For ARG-1, IL-6, IL-10, KIM-1, MIP-2, and NGAL, a fold increase of 23, 224, 69, 860, 320, and 909, respectively, were noted (**p≤ 0.01 or ***p≤ 0.001 vs control vehicle; Figure 30.A, F-J). No significant differences in gene expression occurred in SMC GLPG-1205-treated mice in comparison to SMC vehicle-treated mice (Figure 30). In SMC vehicle, GPR84 expression was significantly upregulated compared to the control vehicle group (161-fold increase; ***p≤ 0.001; Figure 30.D). However, SMC GLPG-1205-treated mice had no significant effect on GPR84 expression (150-fold expression vs control vehicle). The expression of all genes was similar in the control vehicle and control GLPG-1205 groups (Figure 30).

Like in previous studies, immunohistochemistry with myeloperoxidase antibody was performed on the kidneys. The quantification of neutrophils (Figure 31) in control vehicle-treated mice and control GLGP-1205-treated mice presented an average of 0 neutrophils per field. In the SMC vehicle group, the number of neutrophils was significantly increased to 25 neutrophils per field (vs control vehicle; ***p≤ 0.001). The number of neutrophils was not significantly different in SMC GLGP-1205 compared to SMC vehicles with 21 neutrophils per field. A visual representation of the myeloperoxidase staining in SMC + GLPG-1205 is presented in section 3.2.3. (Figure 31).

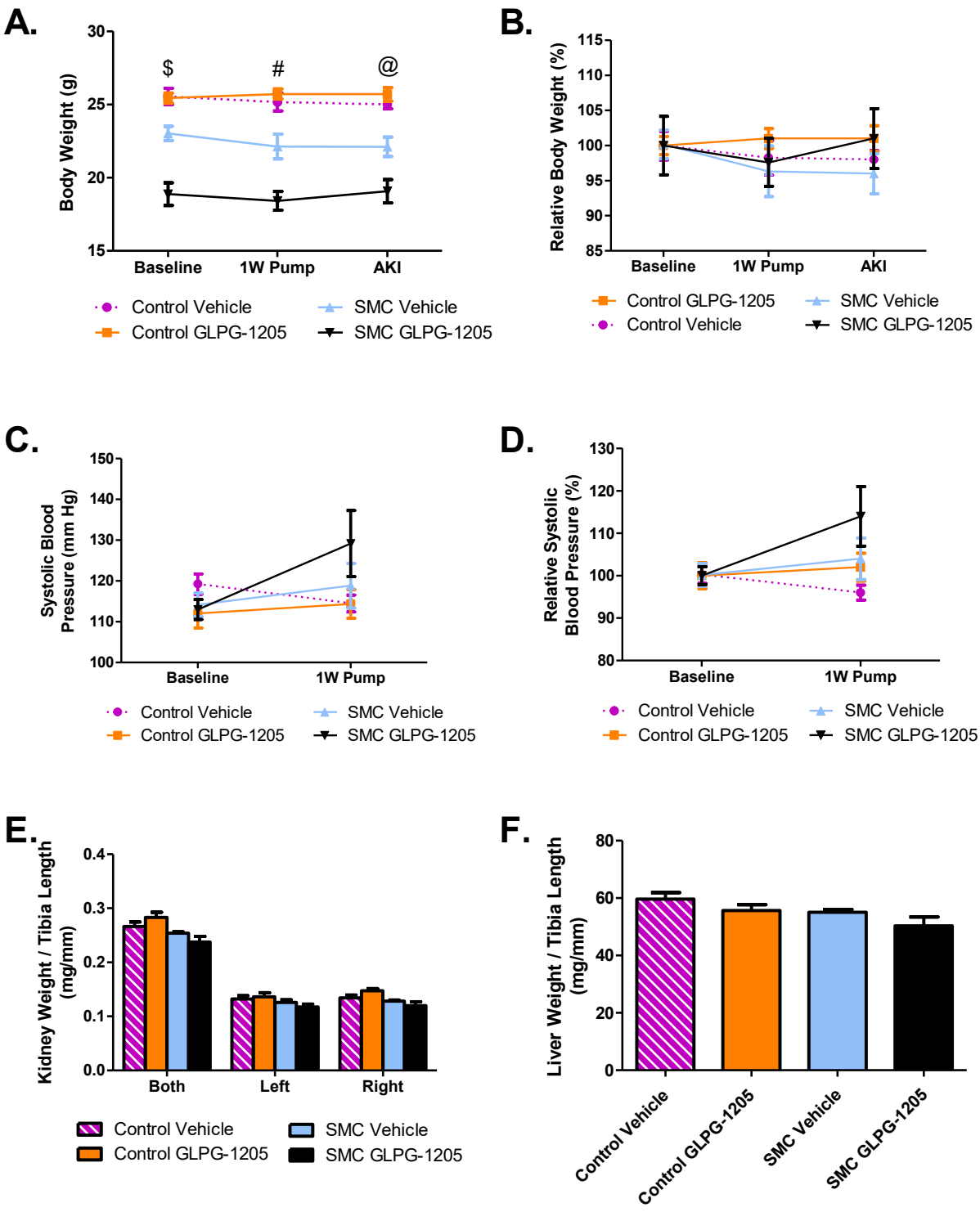

Figure legend on the following page (Figure 27).

Figure 27. **SMC + GLPG-1205 (prophylaxis treatment, 4000 cps methylcellulose) body weight, systolic blood pressure, normalized kidney weight, and normalized liver weight. A-B.** Body weight reported in grams (**A.**) and relative (**B.**) to baseline (before angiotensin II and lipopolysaccharide; Ang II and LPS), 1W Pump (1 week with Ang II minipump, before LPS), and AKI (24 hours post-LPS injection). 1W Pump body weight (in gram and relative) included the Ang II osmotic minipump weight. **C-D.** Systolic blood pressure (SBP) reported in mm Hg (**C.**) and relative (**D.**) to baseline and 1W Pump. SBP was obtained by tail-cuff photoplethysmography. The last three measurement days of each timepoint were combined. Five preliminary measures and at least seven actual measures were recorded each day. Normalizations (**B.** and **D.**) were obtained by dividing the value of each biological replicate by the mean of their respective group at baseline and multiplying by 100. **E.** Both (combined), left and right kidney weight normalized to tibia length at AKI. **F.** Liver weight normalized to tibia length at AKI. Control vehicle: n=4; Control GLPG-1205: n=5; SMC vehicle: n=6; SMC GLGP-1205: n=5. Outlying values were removed from the analysis. Data presented as mean ± standard error of the mean (SEM). One-way analysis of variance (ANOVA) with a Dunnett post-test comparing SMC vehicle to control vehicle and SMC GLPG-1205 was performed at each timepoint or category ($: *p≤ 0.05 SMC vehicle vs control vehicle and ***p≤ 0.001 SMC vehicle vs SMC GLGP-1205; #: *p≤ 0.05 SMC vehicle vs control vehicle and **p≤ 0.01 SMC vehicle vs SMC GLGP-1205; @: *p≤ 0.05 SMC vehicle vs control vehicle and SMC GLGP-1205). 1W Pump: One-week minipump; AKI: Acute kidney injury; SMC: Surrogate model of coronavirus disease 2019-associated acute kidney injury.

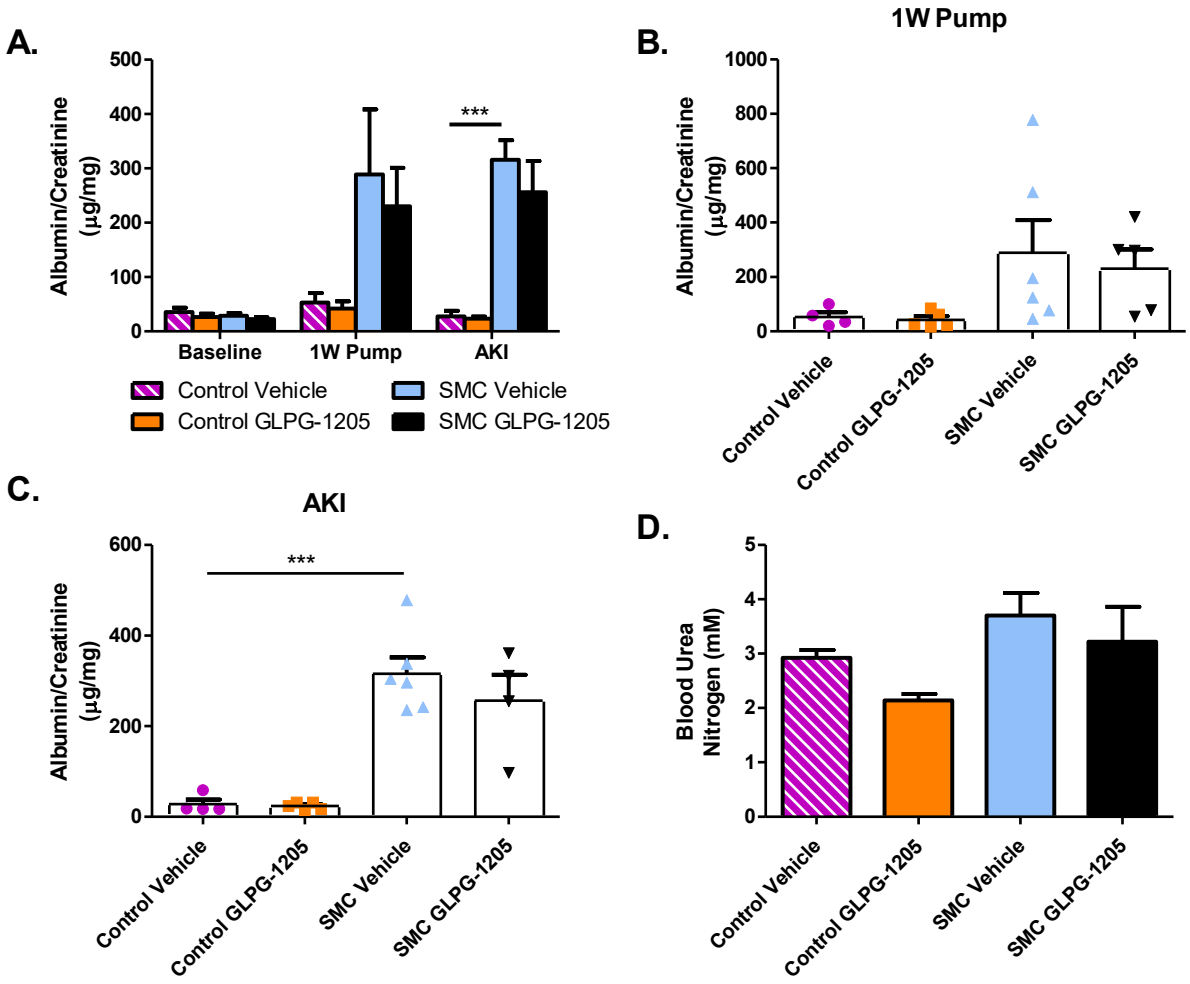

Figure 28. **SMC + GLPG-1205 (prophylaxis treatment, 4000 cps methylcellulose) albumin to creatinine ratio and blood urea nitrogen. A.** Albumin to creatinine ratio (ACR) at baseline (before angiotensin II and lipopolysaccharide; Ang II and LPS), and AKI (24 hours post-LPS injection). Albuminuria and urine creatinine were obtained by enzyme-linked immunosorbent assay (ELISA) and Jaffe reaction assay, respectively. **B.** Individual biological replicates ACR at 1W Pump. **C.** Individual biological replicates ACR at AKI. **D.** Blood urea nitrogen (BUN) at AKI. Analysis blindly performed by IDEXX Bioanalytics. Control vehicle: n=4; Control GLPG-1205: n=5; SMC vehicle: n=6; SMC GLGP-1205: n=5. Outlying values were removed from the analysis. Data presented as mean ± standard error of the mean (SEM). One-way analysis of variance (ANOVA) with a Dunnett post-test comparing SMC vehicle to control vehicle and SMC GLPG-1205 was performed at each timepoint (***p≤ 0.001). 1W Pump: One-week minipump; AKI: Acute kidney injury; SMC: Surrogate model of coronavirus disease 2019-associated acute kidney injury.

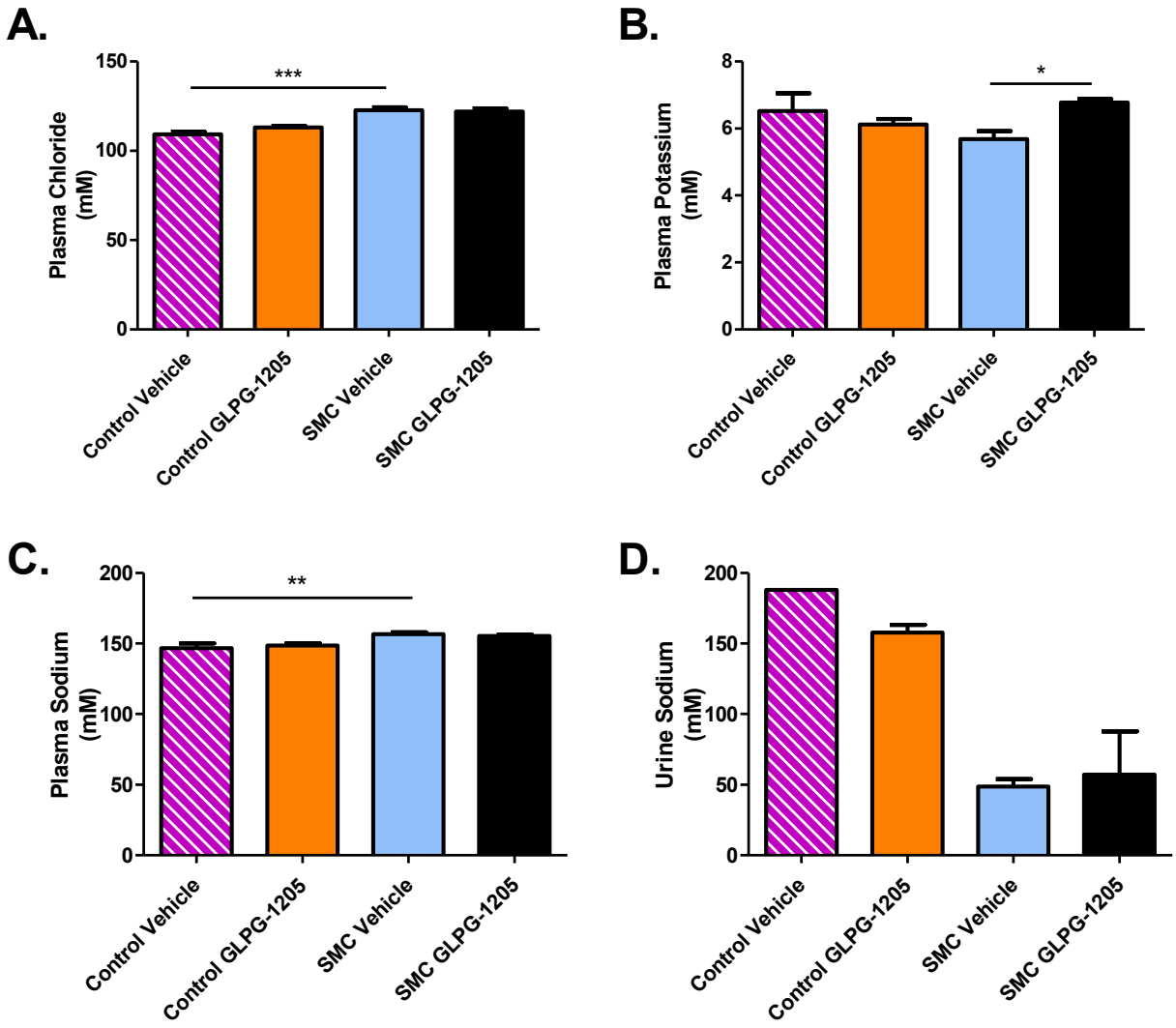

Figure 29. **SMC + GLPG-1205 (prophylaxis treatment, 4000 cps methylcellulose) plasma chloride, plasma potassium, plasma sodium and urine sodium.** plasma chloride (**A.**), plasma potassium (**B.**), plasma sodium (**C.**), and urine sodium (**D.**) concentrations at AKI (at euthanasia, 24 hours post-lipopolysaccharide). Analysis performed blindly by IDEXX Bioanalytics. Control vehicle: n=4; Control GLPG-1205: n=5; SMC vehicle: n=6; SMC GLGP-1205: n=5. Outlying values were removed from the analysis. Data presented as mean ± standard error of the mean (SEM). One-way analysis of variance (ANOVA) with a Dunnett post-test comparing SMC vehicle to control vehicle and SMC GLPG-1205 was performed (*p≤ 0.05; **p≤ 0.01; ***p≤ 0.001). AKI: Acute kidney injury; SMC: Surrogate model of coronavirus disease 2019-associated acute kidney injury.

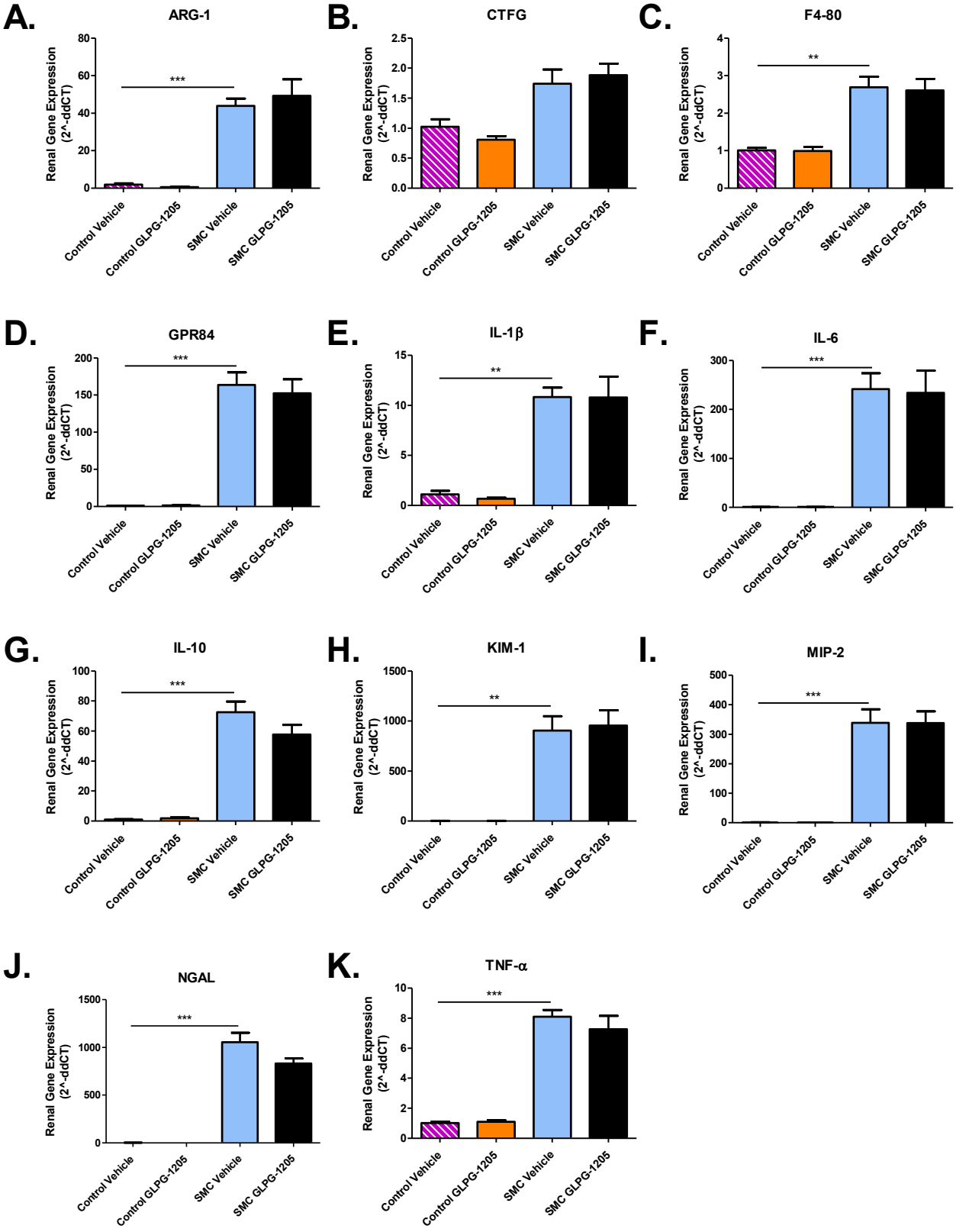

Figure legend on the following page (Figure 30).

Figure 30. **SMC + GLPG-1205 (prophylaxis treatment, 4000 cps methylcellulose) renal expression of GPR84, and inflammatory, fibrotic, injury, and immune cell markers.** Messenger ribonucleic acid (mRNA) expression of arginase 1 (ARG-1; **A.**), connective tissue growth factor (CTGF; **B.**), EGF-like module-containing mucin-like hormone receptor-like 1 (F4-80; **C.**), G-coupled protein receptor 84 (GPR84; **D.**), interleukin (IL)-1 beta (**E.**), IL-6 (**F.**), IL-10 (**G.**), kidney injury molecule 1 (KIM-1; **H.**), macrophage inflammatory protein 2 (MIP-2; **I.**), neutrophil gelatinase-associated lipocalin (NGAL; **J.**), and tumour necrosis factor-alpha (TNF-α; **K.**) normalized to glyceraldehyde three-phosphate dehydrogenase (GAPDH) at AKI (24 hours post-lipopolysaccharide injection). Gene expression was assessed by quantitative polymerase chain reaction (qPCR). Control vehicle: n=4; Control GLPG-1205: n=5; SMC vehicle: n=6; SMC GLGP-1205: n=5. Outlying values were removed from the analysis. Data presented as mean ± standard error of the mean (SEM). One-way analysis of variance (ANOVA) with a Dunnett post-test comparing SMC vehicle to control vehicle and SMC GLPG-1205 was performed at each timepoint (**p≤ 0.01; ***p≤ 0.001). AKI: Acute kidney injury; SMC: Surrogate model of coronavirus disease 2019-associated acute kidney injury.

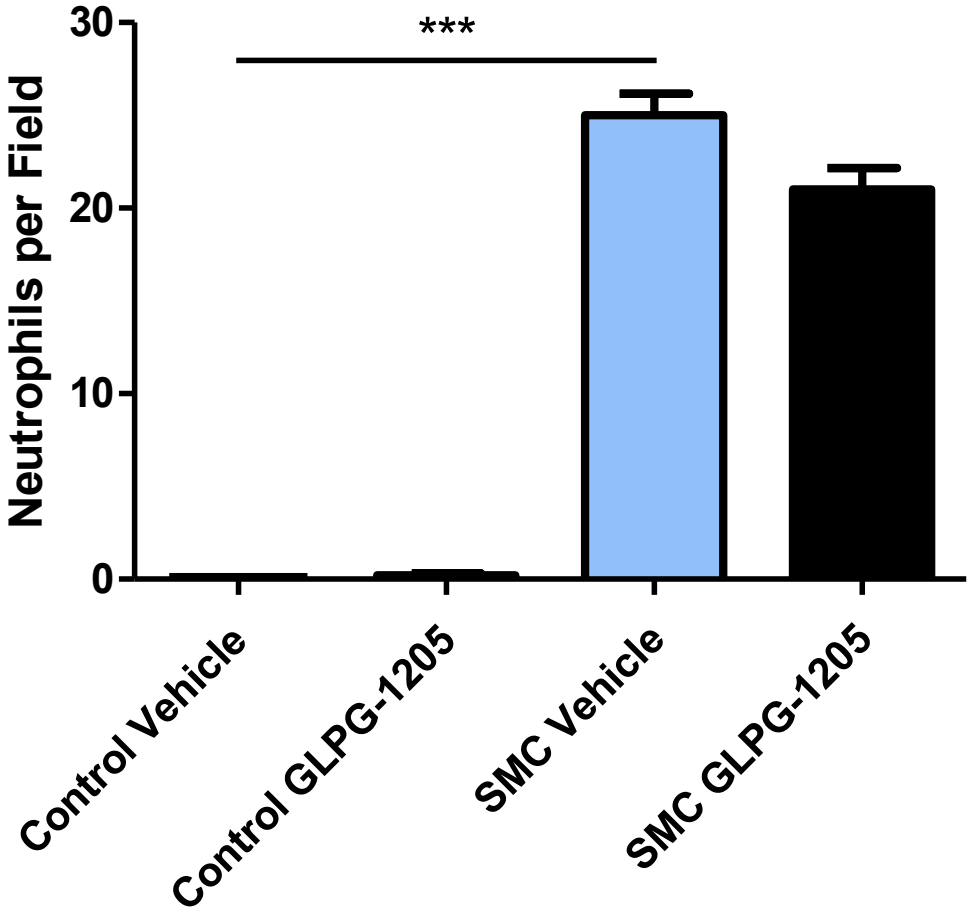

Figure 31. **SMC + GLPG-1205 (prophylaxis treatment, 4000 cps methylcellulose) renal neutrophil infiltration.** Quantification of neutrophils (Myeloperoxidase positive events) per field from myeloperoxidase immunohistochemistry on AKI (24 hours post-LPS) kidneys. Five to 12 fields were averaged per biological replicate. Control vehicle: n=2; Control GLPG-1205: n=2; SMC vehicle: n=3; SMC GLGP-1205: n=3. Outlying values were removed from the analysis. Data presented as mean ± standard error of the mean (SEM). One-way analysis of variance (ANOVA) with a Dunnett post-test comparing SMC vehicle to control vehicle and SMC GLPG-1205 was performed (***p≤ 0.001). AKI: Acute kidney injury.

3.2.3. GLPG-1205 prophylaxis treatment in the surrogate mouse model of coronavirus disease 2019-associated acute kidney injury using 400 cps methylcellulose

In this third and last study with GLPG-1205 on the SMC model, a prophylaxis treatment was performed, similar to the previous study. The vehicle used in this study was 400 cps methylcellulose instead of 4000 cps methylcellulose. Studies have demonstrated that mucosal drug absorption reduces with increasing viscosity[133,134]. Therefore, using a lower viscosity vehicle (400 cps methylcellulose) could increase drug absorption and thereby potentially increase its effects. Figure 32 presents body weight, SBP, as well as normalized kidney and liver weight. Baseline body weights in the control vehicle-treated, control GLGP-1205-treated, SMC vehicle-treated, and SMC GLPG-1205-treated mice were 26.1 g, 27.2 g, 23.3 g, and 25.2 g, respectively (Figure 32.A-B). After one week of Ang II (1W Pump), body weights in the control vehicle and control GLGP-1205 groups were 24.0 g and 25.4 g, while in the SMC vehicle and SMC GLPG-1205 groups body weights were 23.3 g and 24.9 g, respectively. At AKI, the body weights were 24.6 g, 25.6 g, 21.9 g, and 23.4 g for the control vehicle, control GLGP-1205, SMC vehicle and SMC GLPG-1205 groups, respectively. Significant differences in gram body weight were noted between the control vehicle and SMC vehicle at baseline (*p≤ 0.05) and AKI (**p≤ 0.01) as well as between the SMC vehicle and SMC GLPG-1205 at 1W Pump (*p≤ 0.05). However, when normalizing groups' body weight to their respective baseline, no significant differences were seen between the group and timepoints stated above. In fact, only a significant difference in relative body weight was observed between the SMC vehicle and control vehicle group at 1W Pump (*p≤ 0.05). As for SBP, baseline values were 117 mm Hg for the control vehicle and control GLPG-1205 groups, while in SMC vehicle and SMC GLPG-1205 groups SBPs were 118 mm Hg and 116 mm Hg,

respectively (Figure 32.C-D). At 1W Pump SBP was 113 mm Hg in control vehicle-treated mice, 116 mm Hg in control GLPG-1205-treated mice, 125 mm Hg in SMC vehicle-treated mice, and 123 mm Hg in SMC GLPG-1205-treated mice. SBP reported in mm Hg and relative to baseline showed no significant differences between groups at any timepoint. When it comes to normalized kidney weight (Figure 32.E), SMC GLPG-1205 combined (both) kidney weight was significantly different compared to SMC vehicle (*p≤ 0.05). Individual kidney weight, on the other hand, showed no significant differences between groups. Normalized liver weight was also not significantly different between groups (Figure 32.F).

As in the previous prophylaxis study, ACR, and BUN were analyzed along with plasma chloride, potassium, and sodium as well as urine sodium (Figures 33 and 34). At Baseline, ACR in control vehicle-treated, control GLPG-1205-treated, SMC vehicle-treated and SMC GLPG-1205-treated mice were 29 µg/mg, 38 µg/mg, 24 µg/mg, and 22 µg/mg respectively (no significant differences; Figure 33.A). After one week of Ang II (1W Pump), ACRs in the control vehicle and control GLGP-1205, SMC vehicle and SMC GLPG-1205 groups were 31 µg/mg, 33 µg/mg, 24 µg/mg, and 198 µg/mg respectively (no significant differences). When assessing individual biological replicates' ACR at 1W Pump, two of the nine SMC GLPG-1205 replicates had ACRs of 622 and 744 µg/mg while the other six replicates had ACRs between 17 and 98 µg/mg (Figure 33.B). The ACR value of one SMC GLPG-1205 replicate was removed from the analysis as it was an outlier. At AKI, a significant increase in the SMC vehicle group ACR (435 µg/mg) was observed compared to the control vehicle group (25 µg/mg; **p≤ 0.01; Figure 33.A). GLPG-1205 treatment did not significantly affect on ACR in the SMC GLPG-1205 group (385 µg/mg vs 435 µg/mg in SMC vehicle). Control GLGP-1205 ACR was 21 µg/mg at AKI. BUN at AKI was 5.5 mM in SMC vehicle while

BUN in control vehicle was at 3.1 mM (no significant difference; Figure 33.C). GLPG-1205 treatment in SMC (SMC GLPG-1205) had no significant effect on BUN concentration (5.4 mM). Plasma chloride, potassium and sodium were significantly increased at AKI in SMC vehicles with respective concentration of 122 mM, 5.4 mM, and 157 mM, respectively (**p≤ 0.01 or ***p≤ 0.001 vs control vehicle; Figure 34.A-C). In control vehicle- treated mice plasma chloride, potassium and sodium concentration were 112 mM, 4.4 mM, and 151 mM, while in control GLPG-1205-treated mice, concentrations were 112 mM, 3.9 mM, and 150 mM, respectively. GLPG-1205 had no significant effects on plasma chloride, potassium, and sodium concentrations (121 mM, 5.2 mM, and 157 mM, respectively). A significant decrease in urine sodium concentration in the SMC vehicle-treated mice (67 mM) was observed at AKI compared to control vehicle-treated mice (204 mM; *p≤ 0.05; Figure 34.D). GLPG-1205 had no significant affect on urine sodium in SMC (44 mM in SMC GLPG-1205-treated mice). Control GLPG-1205-treated mice had a urine sodium concentration of 114 mM.

Figure 35 presents the renal expression of pro-inflammatory, pro-fibrotic, injury and immune cell markers as well as GPR84 at AKI. For all genes evaluated, except for IL-1β (6.2-fold vs control vehicle; Figure 35.C), expression was significantly increased in SMC vehicle-treated mice (*p≤ 0.05, **p≤ 0.01, or ***p≤ 0.001). In SMC vehicle-treated mice, ARG-1, and TNF-α had a 16 and 10-fold increase in expression (*p≤ 0.05, or **p≤ 0.01 vs control vehicle; Figure 35.A, C, I). IL-6, IL-10, KIM-1, MIP-2, and NGAL expression also increased by 274, 57, 1060, 203, and 1407-fold, respectively in the SMC vehicle (*p≤ 0.05 or ***p≤ 0.001 vs control vehicle; Figure 35.D-H). The addition of the GLPG-1205 in SMC (SMC GLPG-1205) led to a significant upregulation of 1.77, and 1.98-fold of ARG-1 and IL-1β, respectively (*p≤

0.05 or **p≤ 0.01 vs control vehicle; Figure 35. A, C). The other genes evaluated in SMC GLPG-1205 (except GPR84) did not present significant differences in expression compared to the SMC vehicle (Figure 35.D-I). A significant GPR84 upregulation was observed in SMC vehicle-treated mice (114-fold vs control vehicle; *p≤ 0.05), which was further significantly increased in the SMC GLPG-1205 group (204-fold vs control vehicle, *p≤ 0.05; Figure 35.B). For all genes, control vehicle-treated mice and control GLPG-1205-treated mice showed similar expression (Figure 35).

Neutrophil infiltration was also quantified in this study by myeloperoxidase immunohistochemistry (Figure 36). The myeloperoxidase staining (Figure 36.A-D) demonstrated little to no neutrophils in the control vehicle and control GLPG-1205 groups while the SMC vehicle and SMC GLPG-1205 groups presented increased neutrophils presence. Quantification of neutrophils per field (Figure 36.E) showed a significant increase of neutrophil in SMC vehicle compared to control vehicle with respective counts of 32 and 0 neutrophils per filed on average (***p≤ 0.001). The GLPG-1205 treatment in the SMC (SMC GLPG-1205) significantly reduced the number of neutrophils per field to 29 (vs SMC vehicle; *p≤ 0.05). As seen in previous studies the number of neutrophils per field in control GLPG-1205-treated mice was of 0 on average.

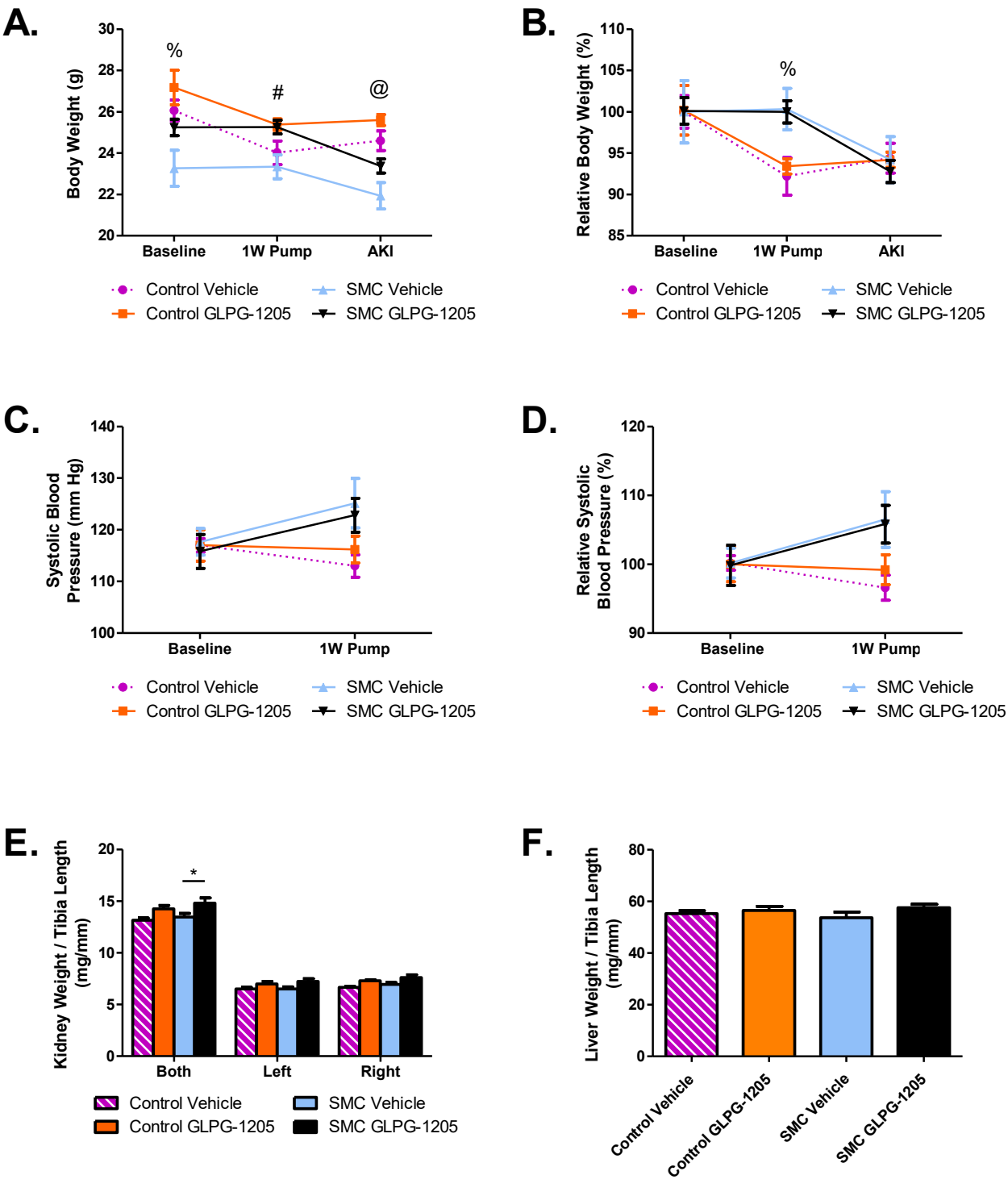

Figure legend on the following page (Figure 32).

Figure 32. **SMC + GLPG-1205 (prophylaxis treatment, 400 cps methylcellulose) body weight, systolic blood pressure, normalized kidney weight, and normalized liver weight. A-B.** Body weight reported in grams (**A.**) and relative (**B.**) to baseline (before angiotensin II and lipopolysaccharide; Ang II and LPS), 1W Pump (1 week with Ang II minipump, before LPS), and AKI (24 hours post-LPS injection). 1W Pump body weight (in gram and relative) included the Ang II osmotic minipump weight. **C-D.** Systolic blood pressure (SBP) reported in mm Hg (**C.**) and relative (**D.**) to baseline and 1W Pump. SBP was obtained by tail-cuff photoplethysmography. The last three measurement days of each timepoint were combined. Five preliminary measures and at least seven actual measures were recorded each day. Normalizations (**B.** and **D.**) were obtained by dividing the value of each biological replicate by the mean of their respective group at baseline and multiplying by 100. **E.** Both (combined), left and right kidney weight normalized to tibia length at AKI. **F.** Liver weight normalized to tibia length at AKI. Control vehicle: n=5; Control GLPG-1205: n=5; SMC vehicle: n=9; SMC GLGP-1205: n=9. Outlying values were removed from the analysis. Data presented as mean ± standard error of the mean (SEM). One-way analysis of variance (ANOVA) with a Dunnett post-test comparing SMC vehicle to control vehicle and SMC GLPG-1205 was performed at each timepoint or category (%: *p≤ 0.05 SMC vehicle vs control vehicle; #: *p≤ 0.05 SMC vehicle vs SMC GLGP-1205; @: **p≤ 0.01 SMC vehicle vs control vehicle; *p≤ 0.05). 1W Pump: One-week minipump; AKI: Acute kidney injury; SMC: Surrogate model of coronavirus disease 2019-associated acute kidney injury.

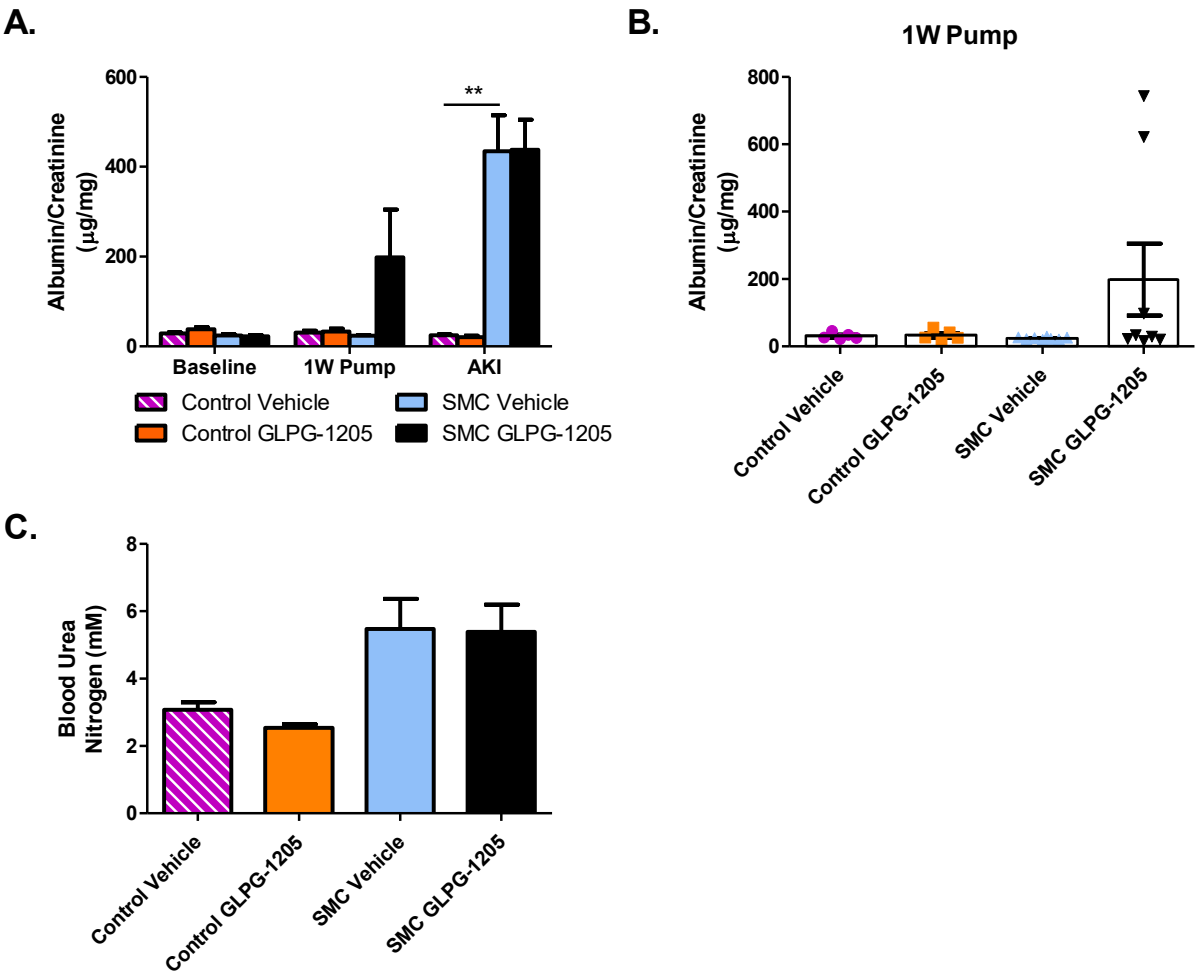

Figure 33. **SMC + GLPG-1205 (prophylaxis treatment, 400 cps methylcellulose) albumin to creatinine ratio and blood urea nitrogen. A.** Albumin to creatinine ratio (ACR) at baseline (before angiotensin II and lipopolysaccharide; Ang II and LPS), and AKI (24 hours post-LPS injection). Albuminuria and urine creatinine were obtained by enzyme-linked immunosorbent assay (ELISA) and Jaffe reaction assay, respectively. **B.** Individual biological replicates ACR at 1W Pump. **C.** Blood urea nitrogen (BUN) at AKI. Analysis blindly performed by IDEXX Bioanalytics. Control vehicle: n=5; Control GLPG-1205: n=5; SMC vehicle: n=9; SMC GLGP-1205: n=9. Outlying values were removed from the analysis. Data presented as mean ± standard error of the mean (SEM). One-way analysis of variance (ANOVA) with a Dunnett post-test comparing SMC vehicle to control vehicle and SMC GLPG-1205 was performed at each timepoint (**p≤ 0.01). 1W Pump: One-week minipump; AKI: Acute kidney injury; SMC: Surrogate model of coronavirus disease 2019-associated acute kidney injury.

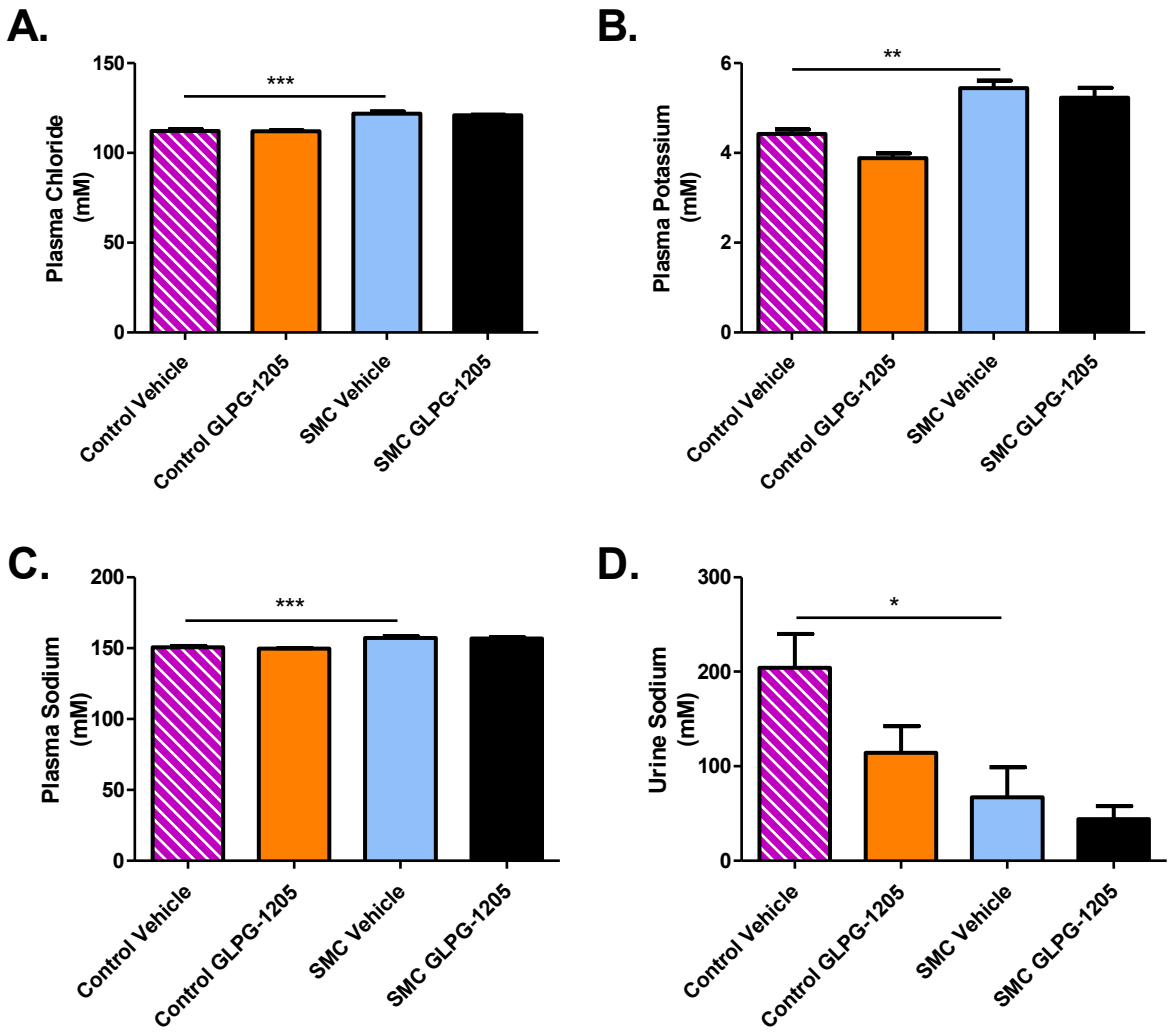

Figure 34. **SMC + GLPG-1205 (prophylaxis treatment, 400 cps methylcellulose) plasma chloride, plasma potassium, plasma sodium and urine sodium.** plasma chloride (**A.**), plasma potassium (**B.**), plasma sodium (**C.**), and urine sodium (**D.**) concentrations at AKI (at euthanasia, 24 hours post-lipopolysaccharide). Analysis performed blindly by IDEXX Bioanalytics. Control vehicle: n=5; Control GLPG-1205: n=5; SMC vehicle: n=9; SMC GLGP-1205: n=9. Outlying values were removed from the analysis. Data presented as mean ± standard error of the mean (SEM). One-way analysis of variance (ANOVA) with a Dunnett post-test comparing SMC vehicle to control vehicle and SMC GLPG-1205 was performed (*p≤ 0.05; **p≤ 0.01; ***p≤ 0.001). AKI: Acute kidney injury; SMC: Surrogate model of coronavirus disease 2019-associated acute kidney injury.

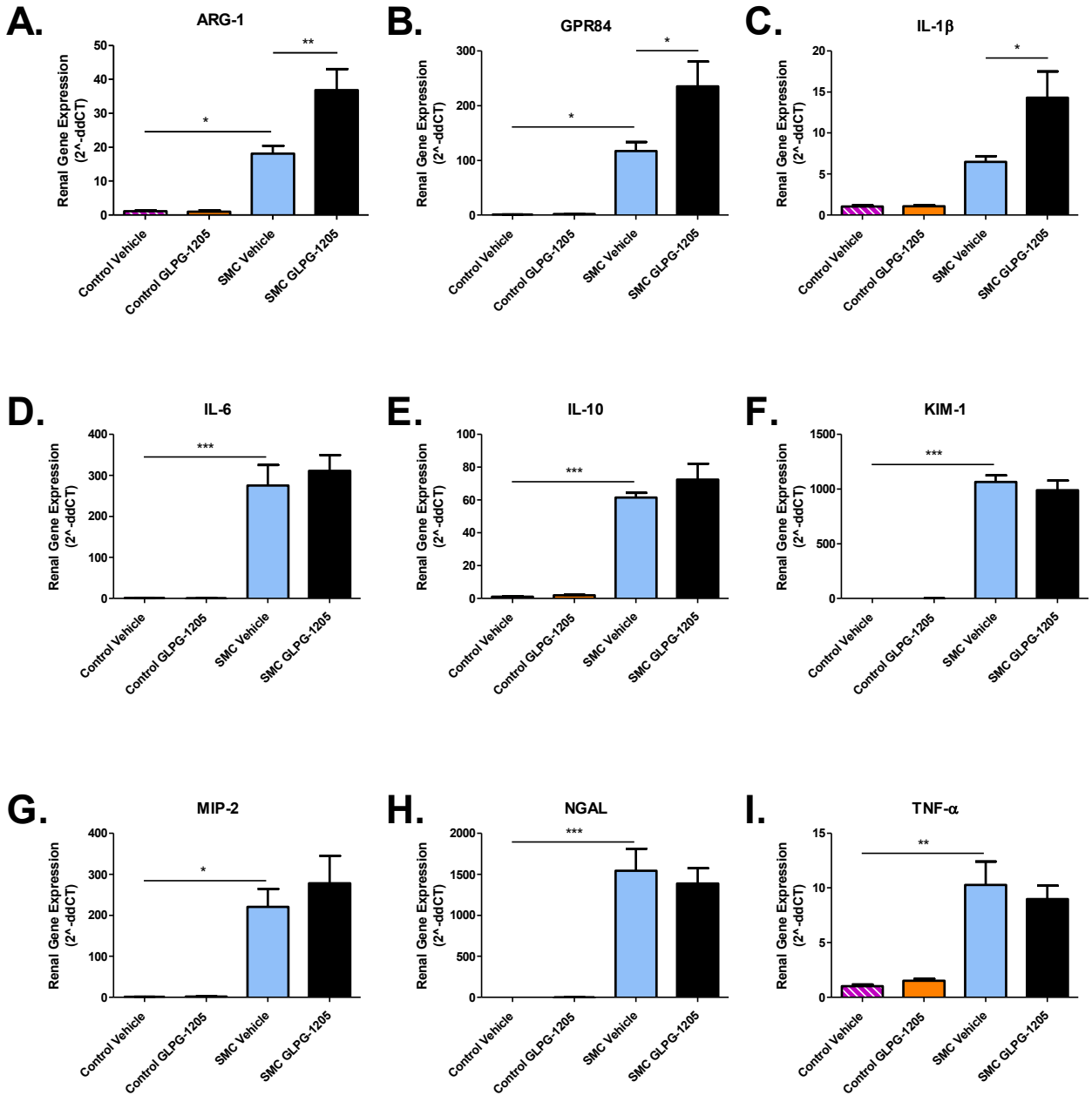

Figure 35. **SMC + GLPG-1205 (prophylaxis treatment, 400 cps methylcellulose) renal expression of GPR84, and inflammatory, fibrotic, injury, and immune cell markers.** Messenger ribonucleic acid (mRNA) expression of arginase 1 (ARG-1; **A.**), G-coupled protein receptor 84 (GPR84; **B.**), interleukin (IL)-1 beta (**C.**), IL-6 (**D.**), IL-10 (**E.**), kidney injury molecule 1 (KIM-1; **F.**), macrophage inflammatory protein 2 (MIP-2; **G.**), neutrophil gelatinase-associated lipocalin (NGAL; **H.**), and tumour necrosis factor-alpha (TNF-α; **I.**) normalized to glyceraldehyde three-phosphate dehydrogenase (GAPDH) at AKI (24 hours post-lipopolysaccharide injection). Gene expression was assessed by quantitative polymerase chain reaction (qPCR). Control vehicle: n=5; Control GLPG-1205: n=5; SMC vehicle: n=9; SMC GLGP-1205: n=9. Outlying values were removed from the analysis. Data presented as mean ± standard error of the mean (SEM). One-way analysis of variance (ANOVA) with a Dunnett post-test comparing SMC vehicle to control vehicle and SMC GLPG-1205 was performed at each timepoint (*p≤ 0.05; **p≤ 0.01; ***p≤ 0.001). AKI: Acute kidney injury; SMC: Surrogate model of coronavirus disease 2019-associated acute kidney injury.

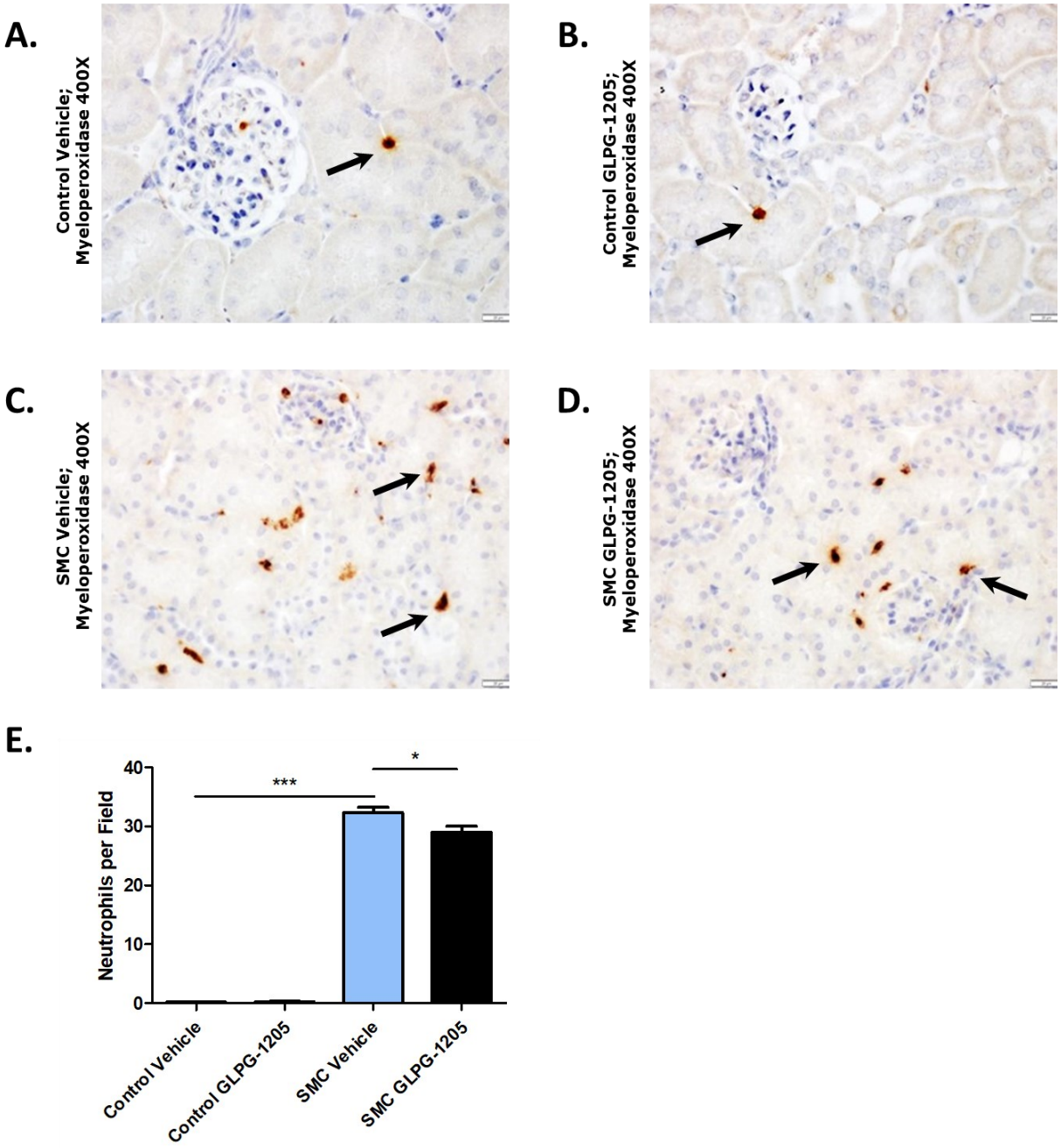

Figure 36. **SMC + GLPG-1205 (prophylaxis treatment, 400 cps methylcellulose) renal neutrophil infiltration.** Representative immunohistochemistry images of myeloperoxidase expression (arrows, →) in control vehicle (**A.**), control GLPG-1205 (**B.**), SMC vehicle (**C.**), and SMC GLPG-1205 (**D.**) in kidneys at AKI (24 hours post-LPS). Mayer's Hematoxylin counterstain, 400X magnification. **E.** Quantification of neutrophils (Myeloperoxidase positive events) per field. Five to ten fields were averaged per biological replicate. Control vehicle: n=3; Control GLPG-1205: n=2; SMC vehicle: n=3; SMC GLGP-1205: n=2. Outlying values were removed from the analysis. Data presented as mean ± standard error of the mean (SEM). One-way analysis of variance (ANOVA) with a Dunnett post-test comparing SMC vehicle to control vehicle and SMC GLPG-1205 was performed (*p≤ 0.05; ***p≤ 0.001). AKI: Acute kidney injury.

3.3. Assessment of GPR84 role in the new surrogate mouse model of coronavirus disease 2019-associated acute kidney injury using GPR84 global knockout mice.

As explained in the previous results section, the second objective of this thesis was to determine the role of GPR84 in the SMC model using the GPR84 antagonist, GLPG-1205, and GPR84 genetic deletion. GPR84 is expressed in various immune cells and is involved in fatty acid metabolism, immunological regulation, cytokine production, reactive oxygen species generation, and calcium influx[80,81,84,85,86]. In COVID-19 patients, GPR84 has been found in bronchoalveolar lavage fluid neutrophils, pointing toward a possible implication of GPR84 in the disease[90]. In CKD models, GPR84 expression was upregulated and linked with increased cytokine production[85]. In preclinical models of renal injury, genetic deletion and GPR84 antagonists showed anti-inflammatory and antifibrotic effects[81,85,89]. It is hypothesised that GPR84 pharmacological antagonism with GLPG-1205 or GPR84 deletion could attenuate indices of renal injury in a SMC model.

In this section, the study was performed with GPR84 KO mice. A study on animals without a functional GPR84 gene was done to verify the results obtained with the GPR84 antagonist, GLPG-1205. The GPR84 KO study followed the same timeline as the one used to assess GLPG-1205 effects. In brief, mice (Ang II + LPS groups) were implanted with an Ang II osmotic minipump (400 ng/kg/min) for eight days. Seven days following minipump implantation, mice were given 10 mg/kg of LPS by i.p. injection. Mice were euthanized 24 hours post-LPS injection. Control groups received a sham surgery and an i.p. injection of saline instead of an Ang II minipump and LPS injection. The key differences in this study are that GPR84 KO mice (male and female; eight to 13 weeks of age) were used instead of ACE2 KO and no GLPG-1205 treatment was administered. ACE2 and GPR84 animals weren't intercrossed due to

time limitations. Therefore, the study using GPR84 KO animals is labelled as “GPR84 Ang II + LPS”. GPR84 mice possess WT ACE2 alleles in this study. Results in GPR84 KO were compared to a combination of GPR84 WT and HET animals that underwent the same procedures. Table 6 of the appendices presents details on animals' age, genotype, and group size as well as treatment type, dose and vehicle used in all studies.

Like in previous studies, animals' general wellness was assessed by body weight (Figure 37.A-B). Baseline body weights in the HET/WT control, KO control, HET/WT Ang II + LPS, KO Ang II + LPS mice were 23.2 g, 21.1 g, 22.4 g, and 22.9 g, respectively. After one week of Ang II (1W Pump), body weights in the HET/WT control and KO control groups were 23.5 g and 21.7 g, while in the HET/WT Ang II + LPS and KO Ang II + LPS groups body weights were 23.7 g and 24.0 g, respectively. At AKI, the body weights were 23.2 g, 21.6 g, 22.0 g, and 22.5 g for the HET/WT control, KO control, HET/WT Ang II + LPS and KO Ang II + LPS groups, respectively. Body weight reported in grams and relative to baseline showed no significant differences between groups at any timepoint. SBP was measured to confirm Ang II minipump function (Figure 37.C-D). 1W Pump SBP in the HET/WT control, KO control, HET/WT Ang II + LPS, KO Ang II + LPS mice were 125 mm Hg, 120 mm Hg, 117 mm Hg, and 124 mm Hg, respectively. 24 hours after LPS (AKI), body weights in the HET/WT control and KO control groups were 122 mm Hg and 116 mm Hg, while in the HET/WT Ang II + LPS and KO Ang II + LPS groups body weights were 121 mm Hg and 129 mm Hg, respectively. SBP reported in mm Hg presented a significant difference between (GPR84) KO control and KO Ang II + LPS at 1W Pump exclusively (*$p \leq 0.05$; Figure 37.C). However, when normalizing groups’ SBP to their respective baseline, no significant differences were observed between groups at baseline and 1W Pump

(Figure 37.D). Additionally, normalized kidney and liver weight was measured to assess the Ang II + LPS and GPR84 deletion effects on tissue size (Figure 37.E-F). Combined (both) normalized kidney weight showed a significant difference between KO control and KO Ang II + LPS exclusively (*p≤ 0.05; Figure 37.E). Individual normalized kidney weight, on the other hand, showed no significant differences between groups. Normalized liver weight showed no significant differences between groups (Figure 37.F).

Kidney function was assessed through ACR (baseline, 1W Pump and AKI) and BUN at AKI (Figure 38). Additionally, plasma electrolytes (chloride, potassium, and sodium), as well as urine sodium, were measured in this study (Figure 38). Baseline ACR in HET/WT control and KO control groups were 13 µg/mg and 11 µg/mg, respectively, while in the HET/WT Ang II + LPS and KO Ang II + LPS groups ACR was 14 µg/mg for both groups (not significant; Figure 38.A). After one week of Ang II (1W Pump), HET/WT control, KO control, HET/WT Ang II + LPS, KO Ang II + LPS mice were 15 µg/mg, 14 µg/mg, 18 µg/mg, and 22 µg/mg, respectively (not significant). At AKI, the ACRs were 12 µg/mg, 16 µg/mg, 480 µg/mg, and 1083 µg/mg for the HET/WT control, KO control, HET/WT Ang II + LPS and KO Ang II + LPS groups, respectively. Significant difference in ACR were solely seen between KO Ang II + LPS and KO control at AKI (***p≤ 0.001) as well as between KO Ang II + LPS and HET/WT Ang II + LPS at AKI (*p≤ 0.05). BUN at AKI significantly increased in HET/WT Ang II + LPS (9.1 mM; *p≤ 0.05) and KO Ang II + LPS (11.5 mM; ***p≤ 0.001) in comparison to HET/WT Control (2.7 mM) and KO control (2.9 mM), respectively (Figure 38.B). No significant differences were found between HET/WT Ang II + LPS and KO Ang II + LPS. As for plasma chloride, potassium, and sodium concentration (Figure 39.A-C), significant increases were seen between KO control and KO Ang II + LPS groups (*p≤

0.05 or **p≤ 0.01). No significant differences were noted between HET/WT Ang II + LPS and KO Ang II + LPS. HET/WT control plasma electrolytes and urine sodium were not measured as no samples were available. In KO control, plasma chloride, potassium and sodium concentrations were 110 mM, 4.0 mM, and 150 mM respectively. Plasma electrolytes concentrations in HET/WT Ang II + LPS were 115 mM for chloride, 6.3 mM for potassium, and 165 mM for sodium. Plasma chloride, potassium, and sodium concentrations in KO Ang II + LPS were 122 mM, 5.4 mM, and 160 mM, respectively. On the other hand, urine sodium concentration was significantly reduced in KO Ang II + LPS compared to KO control (57 mM vs 199 mM, *p≤ 0.05; Figure 39.D). No significant difference in urine sodium was seen between HET/WT Ang II + LPS and KO Ang II + LPS groups.

Various pro-inflammatory, pro-fibrotic, injury and immune cell markers expression were measured to assess renal inflammation, fibrosis, injury, and immune cell infiltration (Figure 40). For all genes evaluated exception for F4-80 (Figure 40.B), expression was significantly upregulated in HET/WT Ang II + LPS and KO Ang II + LPS compared to the HEY/WT control and KO control groups, respectively (*p≤ 0.05, **p≤ 0.01, or ***p≤ 0.001; Figure 40.A, C-J). In HET/WT Ang II + LPS, a 112, 668, 59, 645, 604 and 2473-fold increase (vs HET/WT control) was observed for ARG-1, IL-6, IL-10, KIM-1, MIP-2, and NGAL, respectively (*p≤ 0.05, **p≤ 0.01, or ***p≤ 0.001; Figure 40.A, E-I). In HET/WT Ang II + LPS, IL-1β and TNF-α had a significant 5 and 12-fold increase from HET/WT control (*p≤ 0.05 or ***p≤ 0.001; Figure 40.B, D, J). Similarly, KO Ang II + LPS, IL-1β and TNF-α had a significant 4 and 13-fold-increase from HET/WT control (*p≤ 0.05 or ***p≤ 0.001 vs KO control). ARG-1, IL-6, IL-10, KIM-1, MIP-2, and NGAL were also upregulated by 146, 655, 64, 621, 506, and 2785-fold, respectively, in KO Ang II + LPS mice compared to HET/WT control (**p≤ 0.01, or

***p≤ 0.001 vs KO control; Figure 40.A, E-I). Renal gene expression was not statistically different between KO Ang II + LPS and HET/WT Ang II + LPS mice (Figure 40). As expected, GPR84 expression was undetectable in renal KO control and KO Ang II + LPS groups as the mice from those group have a GPR84 deletion (Figure 40.C). Between HET/WT Ang II + LPS and HET/WT control, a significant upregulation of 74-fold GPR84 was seen (**p≤ 0.01).

Similarly, to the Ang II + LPS pilot and the SMC + GLPG-1205 studies, increased cellularity in the interstitial space was also noted in the GPR84 Ang II + LPS study (data not shown). Myeloperoxidase immunohistochemistry was done to assess neutrophil renal infiltration. The myeloperoxidase staining (Figure 41. A-D) demonstrated little to no neutrophils in the HET/WT control and KO control groups while the HET/WT Ang II + LPS and KO Ang II + LPS groups presented increased neutrophils presence. Quantification of neutrophils per field (Figure 41. E) showed a significant increase of neutrophil in HET/WT Ang II + LPS compared to HET/WT control with respective counts of 16 and 0 neutrophils per filed on average (***p≤ 0.001). Similarly, a significant increase of neutrophil in KO Ang II + LPS compared to KO control was noted (21 vs 0 neutrophils per field ***p≤ 0.001). No significant differences between HET/WT Ang II + LPS and KO Ang II + LPS was observed.

In this study, a combination of male and female mice was utilized. To determine if disease progression with Ang II and LPS differs based on sex, male and female relative body weight, relative SBP, ACR and BUN were compared (Figure 42). The body weight and SBP of each group were normalized to their sex-specific baseline values (Figure 42.A-D). relative body weight and SBP presented no significant differences between groups when males and females were analyzed separately. Moreover, no significant differences were noted when comparing males and females

of the same groups. ACR values at baseline showed no significant differences between males and females within each group nor when males and females were analyzed individually (Figure 42.E-F). At 1W Pump, differences were not significant when males and females were analyzed separately. However, a significant difference between male and female HET/WT control at 1W Pump was seen (*p<0.05). At AKI, a significant increase in both male (**p≤ 0.01) and female (*p≤ 0.05) KO Ang II + LPS ACR was seen when compared to KO control of the same sex. There was no significant difference in ACR between KO Ang II + LPS and HET/WT Ang II + LPS for either sex. Also, no significant sex differences in ACR were seen for any groups at AKI. As for AKI BUN (Figure 42.G-H), a significant increase in KO Ang II + LPS vs KO control was seen in both males (***p≤ 0.001) and females (*p≤ 0.05). Additionally, BUN significantly increased HET/WT Ang II + LPS males compared to HET/WT control males (***p≤ 0.001). Significant sex differences in BUN were observed in HET/WT Ang II + LPS (**p<0.01) and KO Ang II + LPS groups (*p<0.05).

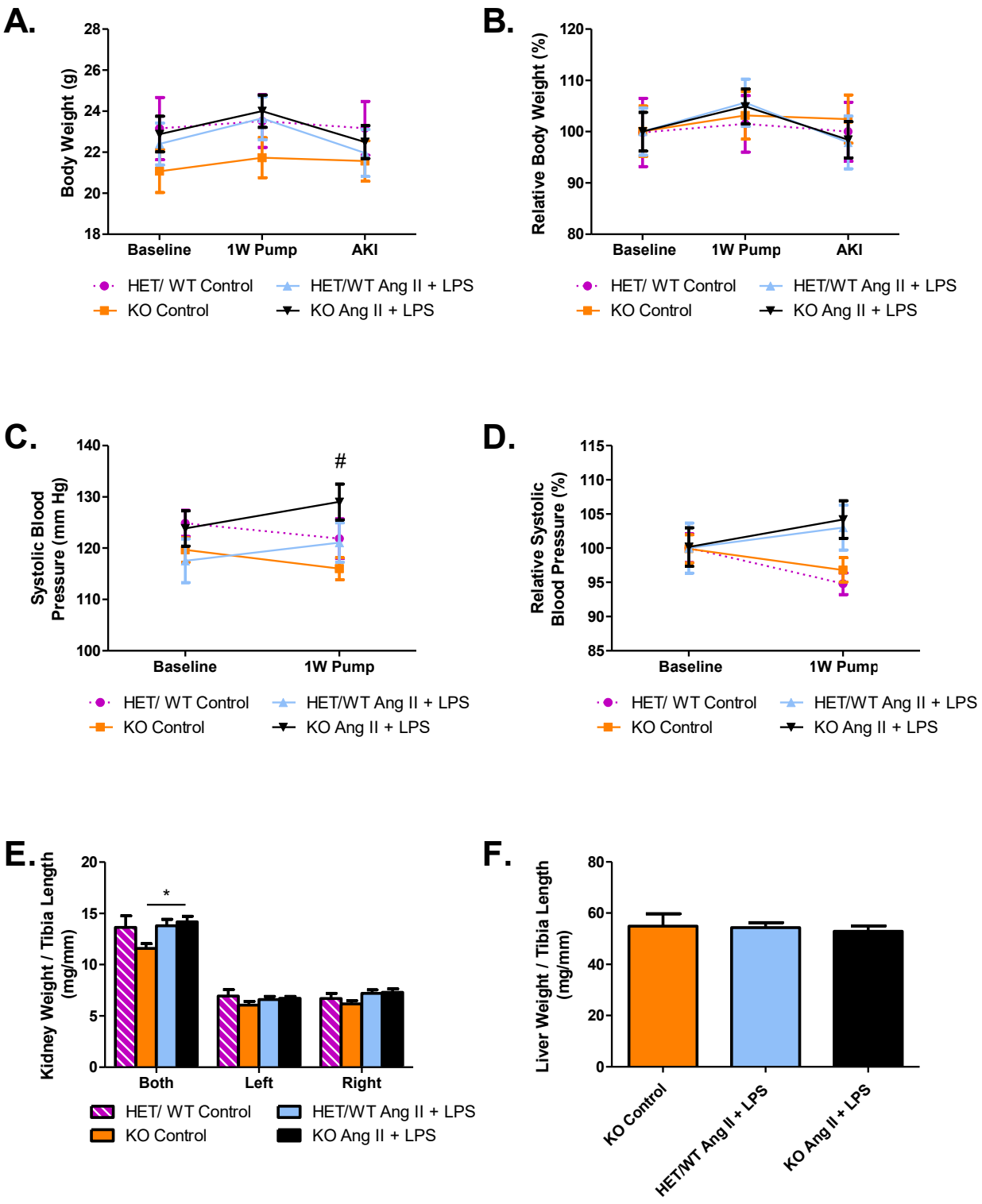

Figure legend on the following page (Figure 37).

Figure 37. **GPR84 Ang II + LPS body weight, systolic blood pressure, normalized kidney weight, and normalized liver weight. A-B.** Body weight reported in grams (**A.**) and relative (**B.**) to baseline (before angiotensin II and lipopolysaccharide; Ang II and LPS), 1W Pump (1 week with Ang II minipump, before LPS), and AKI (24 hours post-LPS injection). 1W Pump body weight (in gram and relative) included the Ang II osmotic minipump weight. **C-D.** Systolic blood pressure (SBP) reported in mm Hg (**C.**) and relative (**D.**) to baseline and 1W Pump. SBP was obtained by tail-cuff photoplethysmography. The last three measurement days of each timepoint were combined. Five preliminary measures and at least seven actual measures were recorded each day. Normalizations (**B.** and **D.**) were obtained by dividing the value of each biological replicate by the mean of their respective group at baseline and multiplying by 100. **E.** Both (combined), left and right kidney weight normalized to tibia length at AKI. **F.** Liver weight normalized to tibia length at AKI. HET/WT Control: n=6; KO Control GLPG-1205: n=11; HET/WT Ang II + LPS: n=11; KO Ang II + LPS: n=12. Outlying values were removed from the analysis. Data presented as mean ± standard error of the mean (SEM). One-way analysis of variance (ANOVA) with a Bonferroni post-test comparing KO control vs KO Ang II + LPS, HET/WT control vs HET/WT Ang II + LPS, and HET/WT Ang II + LPS vs KO Ang II + LPS was performed at each timepoint or category (#: *p≤ 0.05 KO control vs KO Ang II + LPS; *p≤ 0.05). 1W Pump: One-week minipump; AKI: Acute kidney injury; GPR84: G-coupled protein receptor 84; HET: Heterozygous; KO: Knockout; WT: Wild type.

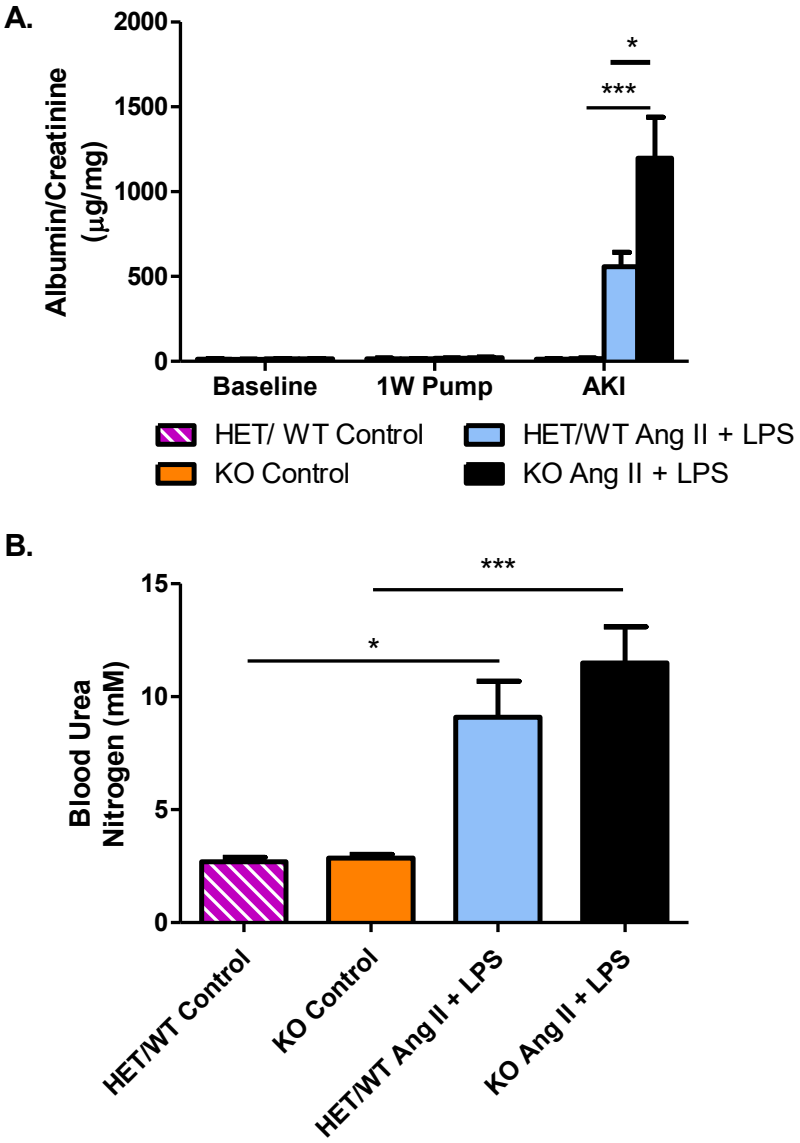

Figure 38. **GPR84 Ang II + LPS albumin to creatinine ratio and blood urea nitrogen. A.** Albumin to creatinine ratio (ACR) at baseline (before angiotensin II and lipopolysaccharide; Ang II and LPS), and AKI (24 hours post-LPS injection). Albuminuria and urine creatinine were obtained by enzyme-linked immunosorbent assay (ELISA) and Jaffe reaction assay, respectively. **B.** Blood urea nitrogen (BUN) at AKI. Analysis blindly performed by IDEXX Bioanalytics. HET/WT Control: n=6; KO Control GLPG-1205: n=11; HET/WT Ang II + LPS: n=11; KO Ang II + LPS: n=12. Outlying values were removed from the analysis. Data presented as mean ± standard error of the mean (SEM). One-way analysis of variance (ANOVA) with a Bonferroni post-test comparing KO control vs KO Ang II + LPS, HET/WT control vs HET/WT Ang II + LPS, and HET/WT Ang II + LPS vs KO Ang II + LPS was performed at each timepoint (*p≤ 0.05; ***p≤ 0.001). 1W Pump: One-week minipump; AKI: Acute kidney injury; GPR84: G-coupled protein receptor 84; HET: Heterozygous; KO: Knockout; WT: Wild type.

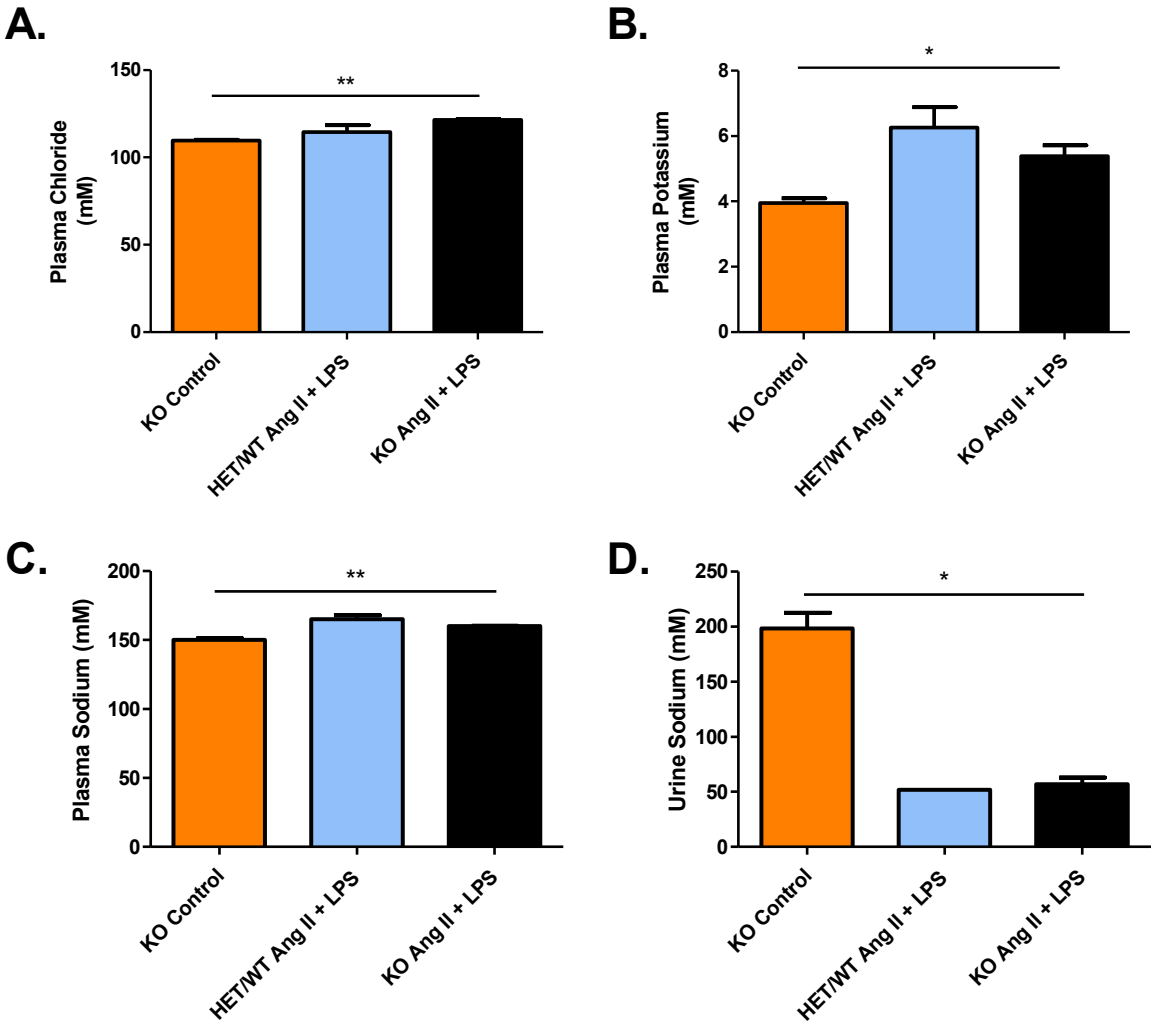

Figure 39. **GPR84 Ang II + LPS plasma chloride, plasma potassium, plasma sodium and urine sodium.** plasma chloride (**A.**), plasma potassium (**B.**), plasma sodium (**C.**), and urine sodium (**D.**) concentrations at AKI (at euthanasia, 24 hours post-lipopolysaccharide). Analysis performed blindly by IDEXX Bioanalytics. HET/WT Control: n=6; KO Control GLPG-1205: n=11; HET/WT Ang II + LPS: n=11; KO Ang II + LPS: n=12. Outlying values were removed from the analysis. Data presented as mean ± standard error of the mean (SEM). One-way analysis of variance (ANOVA) with a Bonferroni post-test comparing KO control vs KO Ang II + LPS, HET/WT control vs HET/WT Ang II + LPS, and HET/WT Ang II + LPS vs KO Ang II + LPS was performed (*p≤ 0.05; **p≤ 0.01). AKI: Acute kidney injury; GPR84: G-coupled protein receptor 84; HET: Heterozygous; KO: Knockout; WT: Wild type.

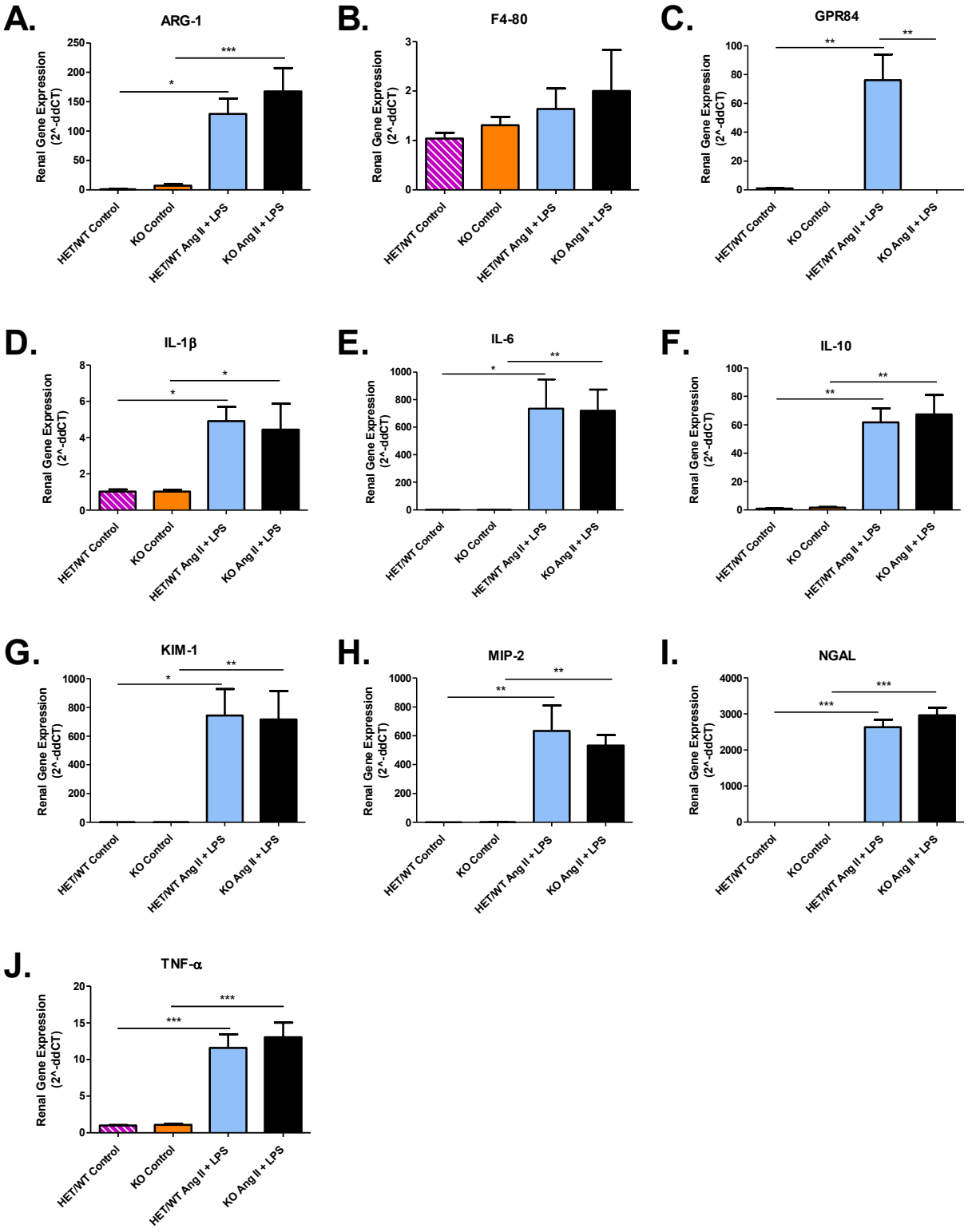

Figure legend on the following page (Figure 40).

Figure 40. **GPR84 Ang II + LPS renal expression of GPR84, and inflammatory, fibrotic, injury, and immune cell markers.** Messenger ribonucleic acid (mRNA) expression of arginase 1 (ARG-1; **A.**), EGF-like module-containing mucin-like hormone receptor-like 1 (F4-80; **B.**), G-coupled protein receptor 84 (GPR84; **C.**), interleukin (IL)-1 beta (**D.**), IL-6 (**E.**), IL-10 (**F.**), kidney injury molecule 1 (KIM-1; **G.**), macrophage inflammatory protein 2 (MIP-2; **H.**), neutrophil gelatinase-associated lipocalin (NGAL; **I.**), and tumour necrosis factor-alpha (TNF-α; **J.**) normalized to glyceraldehyde three-phosphate dehydrogenase (GAPDH) at AKI (24 hours post-lipopolysaccharide injection). Gene expression was assessed by quantitative polymerase chain reaction (qPCR). HET/WT Control: n=6; KO Control GLPG-1205: n=11; HET/WT Ang II + LPS: n=11; KO Ang II + LPS: n=12. Outlying values were removed from the analysis. Data presented as mean ± standard error of the mean (SEM). One-way analysis of variance (ANOVA) with a Bonferroni post-test comparing KO control vs KO Ang II + LPS, HET/WT control vs HET/WT Ang II + LPS, and HET/WT Ang II + LPS vs KO Ang II + LPS was performed (*p≤ 0.05; **p≤ 0.01; ***p≤ 0.001). AKI: Acute kidney injury; GPR84: G-coupled protein receptor 84; HET: Heterozygous; KO: Knockout; WT: Wild type.

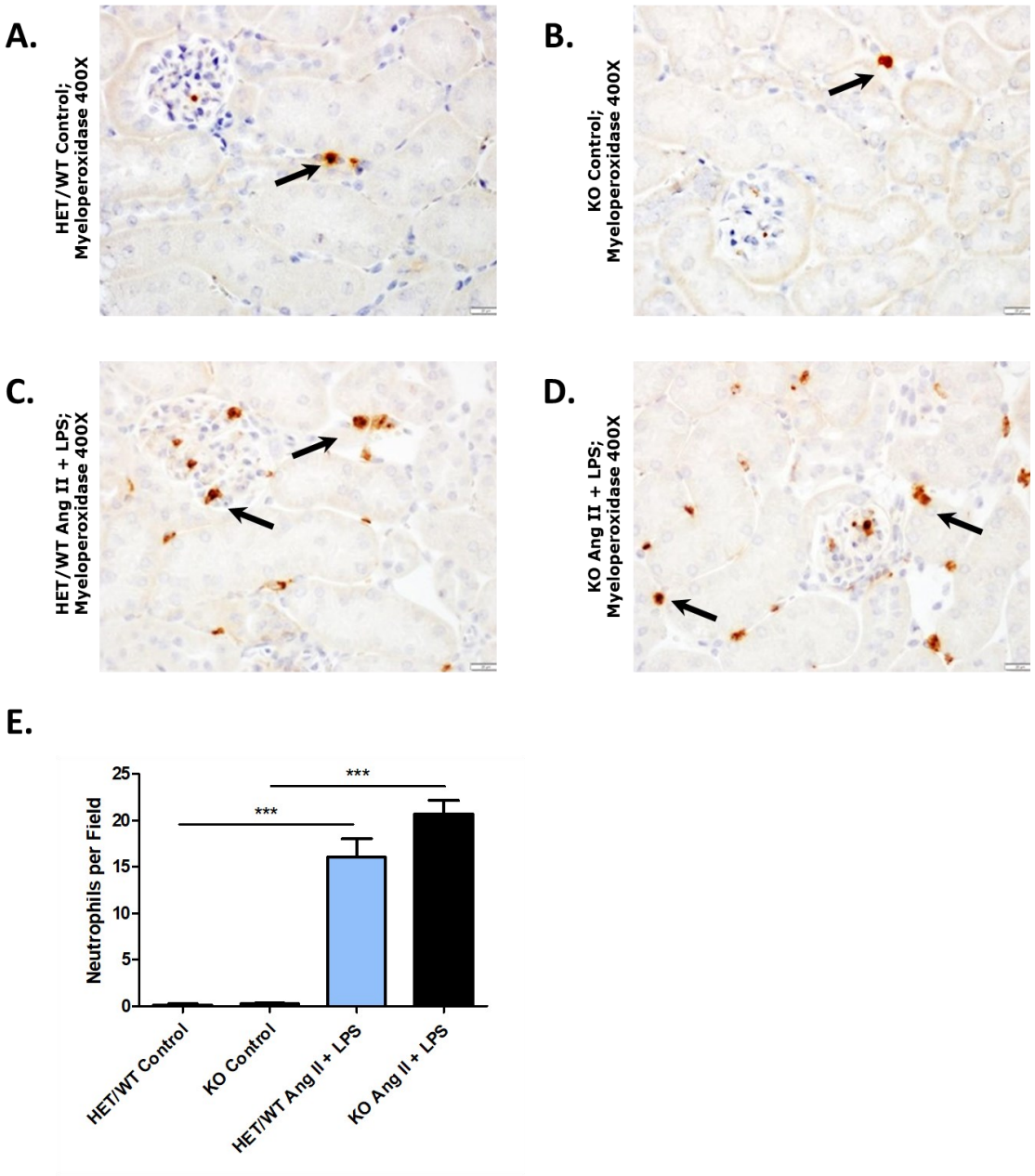

Figure 41. **GPR84 Ang II + LPS renal neutrophil infiltration.** Representative immunohistochemistry images of myeloperoxidase expression (arrows, →) in HET/WT control (**A.**), KO control (**B.**), HET/WT Ang II + LPS (**C.**), and KO Ang II + LPS (**D.**) in kidneys at AKI (24 hours post-LPS). Mayer's Hematoxylin counterstain, 400X magnification. **E.** Quantification of neutrophils (Myeloperoxidase positive events) per field. Five to 20 fields were averaged per biological replicate. HET/WT Control: n=3; KO Control GLPG-1205: n=4; HET/WT Ang II + LPS: n=8; KO Ang II + LPS: n=7. Outlying values were removed from the analysis. Data presented as mean ± standard error of the mean (SEM). One-way analysis of variance (ANOVA) with a Bonferroni post-test comparing KO control vs KO Ang II + LPS, HET/WT control vs HET/WT Ang II + LPS, and HET/WT Ang II + LPS vs KO Ang II + LPS was performed (***p≤ 0.001). AKI: Acute kidney injury. GPR84: G-coupled protein receptor 84; HET: Heterozygous; KO: Knockout; WT: Wild type.

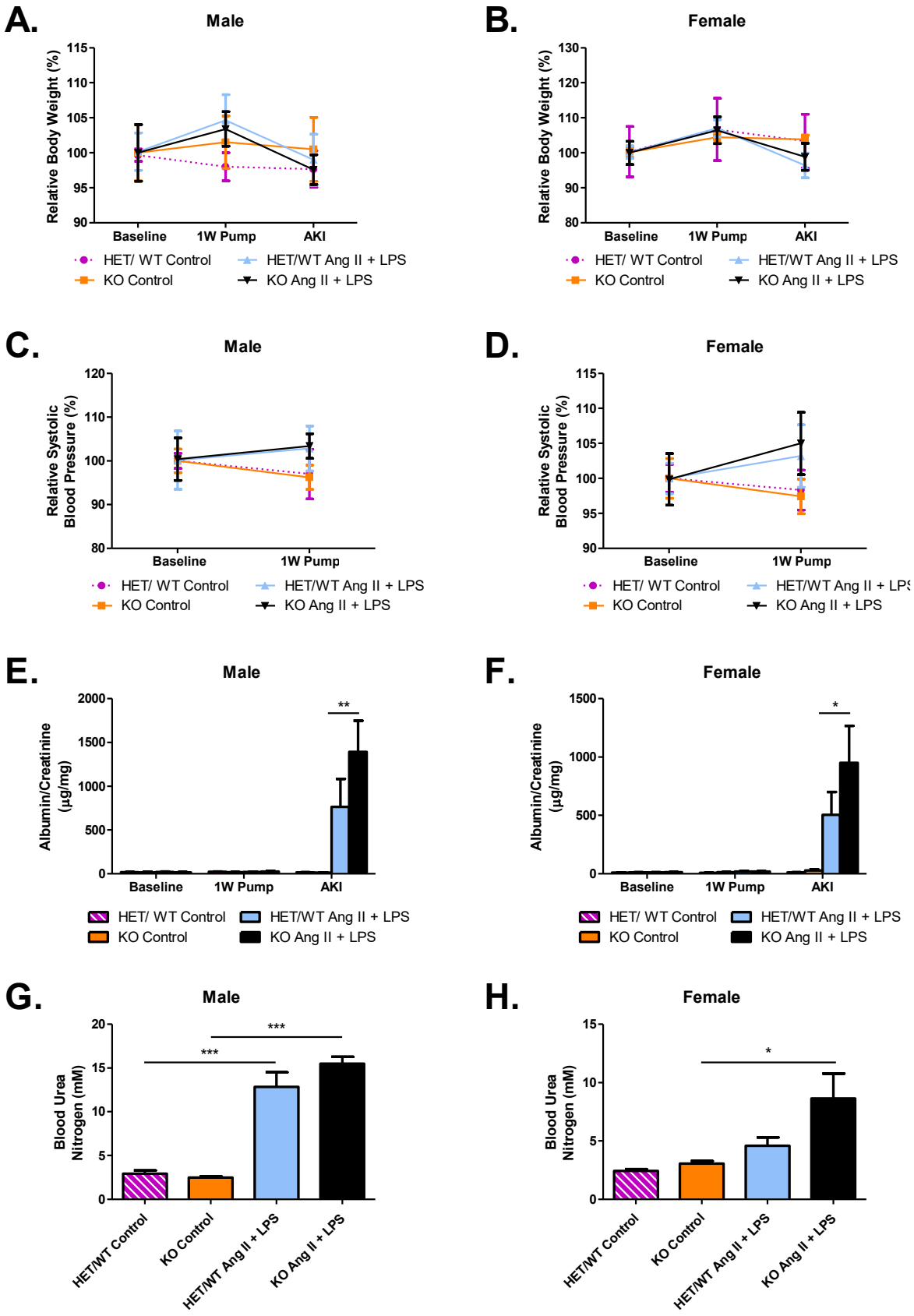

Figure legend on the following page (Figure 42).

Figure 42. **GPR84 Ang II + LPS sex differences in relative body weight, relative systolic blood pressure, albumin to creatinine ratio, and blood urea nitrogen. A-B.** relative body weight in males (**A.**) and females (**B.**) at baseline (before angiotensin II and lipopolysaccharide; Ang II and LPS), 1W Pump (1 week with Ang II minipump, before LPS), and AKI (24 hours post-LPS injection). 1W Pump body weight (in gram and relative) included the Ang II osmotic minipump weight. **C-D.** Relative systolic blood pressure (SBP) reported in males (**C.**) and females (**D.**) at baseline and 1W Pump. SBP was obtained by tail-cuff photoplethysmography. The last three measurement days of each timepoint were combined. Five preliminary measures and at least seven actual measures were recorded each day. Normalizations (**A-D.**) were obtained by dividing the value of each biological replicate by the mean of their respective group at baseline and multiplying by 100. **E-F.** Albumin to creatinine (ACR) in males (**E.**) and females (**F.**) at baseline, 1W Pump, and AKI. Albuminuria and urine creatinine were obtained by enzyme-linked immunosorbent assay (ELISA) and Jaffe reaction assay, respectively. **G-H.** Blood urea nitrogen (BUN) in males (**G.**) and females (**H.**) at AKI. Analysis blindly performed by IDEXX Bioanalytics. HET/WT Control: n=3 males and 3 females; KO Control GLPG-1205: n=5 males and 7 females; HET/WT Ang II + LPS: n=6 males and 5 females; KO Ang II + LPS: n=5 males and 7 females. Outlying values were removed from the analysis. Data presented as mean ± standard error of the mean (SEM). One-way analysis of variance (ANOVA) with a Bonferroni post-test comparing KO control vs KO Ang II + LPS, HET/WT control vs HET/WT Ang II + LPS, and HET/WT Ang II + LPS vs KO Ang II + LPS was performed at each timepoint or category (*p≤ 0.05; **p≤ 0.01; ***p≤ 0.001). 1W Pump: One-week minipump; AKI: Acute kidney injury GPR84: G-coupled protein receptor 84; HET: Heterozygous; KO: Knockout; WT: Wild type.

CHAPTER 4: DISCUSSION

4.1. Development of a new surrogate mouse model of coronavirus disease 2019-associated acute kidney injury

40% of severe SARS-CoV-2 patients admitted to the hospital develop C19-AKI[48]. Current treatment for renal complications limits financial and material resources which applies additional stress on the healthcare system[37]. Indeed, during the pandemic, a surge in COVID-19 patients in addition to regular dialysis patients challenged the management and allocation of RRT to the patients[37,55]. Additionally, supply chain shortages made the acquisition of new RRT instruments difficult and lengthy, thereby adding stress on the healthcare system[37,55]. To explore treatments and accelerate research in case of future coronavirus outbreaks, a mouse model of C19-AKI would represent a critical biomedical research tool. The first objective of this thesis addressed the development of a new surrogate mouse model of C19-AKI disease (abbreviated SMC) that mimics the pro-inflammatory context of this condition.

The SMC consists of ACE2 KO mice receiving a low pressor dose of Ang II (400 ng/kg/min) by osmotic minipump for eight days with a single i.p. injection of LPS (10 mg/kg) on the seventh-day post-minipump implantation. Mice are euthanized 24 hours after the LPS challenge during the AKI window. The control group for the SMC consists of ACE2 WT mice receiving a sham surgery and a saline i.p. injection without osmotic minipump implantation or LPS injection. WT mice were used as controls since the combination of ACE2 KO, Ang II and LPS is considered the model. The ACE2 KO and Ang II combination were chosen as the basis for the SMC since SARS-CoV-2 cell entry through ACE2 causes ACE2 internalization and reduced presence on the cell surface, resulting in RAS imbalance where the inflammatory classical arm is

favoured[4,68]. The deletion of ACE2 along with exogenous administration of Ang II should lead to an exacerbated RAS imbalance. The low pressor dose of Ang II (400 ng/kg/min) was selected based upon the fact that SARS-CoV-2 infection increases Ang II concentration but doesn't affect SBP[4,47,48,58,66,68,137]. Ang II was given for seven days before LPS injection so that an inflammatory climate is established ahead of the LPS insult. Ten days of Ang II administration prior to LPS injection was also evaluated but showed no significant differences in SBP and renal function, injury, and inflammation (data not shown). The SMC model also relies on a single LPS injection as C19-AKI has similar pathophysiology to sepsis-induced AKI[47,138,139]. The LPS dose (10 mg/kg) and time of euthanasia (24 hours post-LPS) were selected as these were shown to cause AKI development by various groups, including ours[140,141,142]. Mice were provided with saline sc. injection (one a few hours after LPS and another one hour before euthanasia) and heat pads after LPS injection to avoid animal loss and dehydration as well as mimic the supportive care provided in the hospital setting[143,144]. Eight to ten-week-old male mice were selected because of their quick availability. However, young mice present no complications or chronic health conditions, which does reflect properly the clinical AKI phenotype[42]. Age and chronic health conditions, such as hypertension, and diabetes, increase the risk of AKI and more severe symptoms of COVID-19[34,36,53]. SMC studies with older age mice could be considered in the future and may better reflect the reality of AKI. Males were preferred over females in this thesis as they often are prone to faster progression of non-diabetic kidney diseases linked with unfavourable outcomes compared to female[145]. Sex effect on renal function, injury, and inflammation under Ang II and LPS was lightly touched during the thesis and will be discussed later (section 4.3.).

Three pilots were performed during model development. Firstly, the Ang II + LPS pilot (section 3.1.1.) had for its objective the assessment of Ang II and LPS combination on renal function, injury, and inflammation. This pilot followed a similar timeline to the SMC explained above. In the second pilot performed (Ang II + LPS long-term pilot; section 3.1.2.), the potential of AKI to CKD transition with Ang II and LPS was assessed. The third and last pilot performed (SMC long-term pilot; section 3.1.3.) during model development allowed the assessment of ACE2 KO, Ang II and LPS combination on kidney function, inflammation, and injury in the short (AKI) and long-term (AKI to CKD transition). The long-term pilots consisted of animals receiving 400 ng/kg/min of Ang II for 28 or 29 days (minipump maximal diffusion time) and injected once with 10 mg/kg of LPS seven or ten days after minipump implantation. Mice were euthanized 19 or 21 days after LPS injection. The first two pilots were performed on a combination of WT male and female mice aged seven to 25 weeks since these pilots were to assess the model (Ang II and LPS) potential and the ACE2 line started its in-house breeding. At that stage, males and females in the model couldn't be compared since the number of males was too low to carry out comparisons.

Body weight was measured in the model since septic models such as LPS cause a reduction in water and food intake, thus leading to dehydration and a decrease in body weight[108,109]. Therefore, body weight was collected to monitor animal wellness and determine that the septic model was working. In literature, administration of LPS leads to an 8% to 12% in body weight reduction after 24 hours while cachexia (over five percent body weight loss) was reported in 29% to 52% of COVID-19 patients[108,142,146,147]. During model development, animals (WT and ACE2 KO mice) on Ang II + LPS had a 7% to 12% body weight loss at AKI (24 hours post-LPS), although the weight loss was not statistically significant (vs control). Data may not have reached

significance due to the low number of biological replicates and the weight variation caused by groups of mixed sex and age[148]. At endpoint (three weeks post-LPS) in the long-term pilots, animals on Ang II + LPS had body weights 9% to 11% over their baseline body weight (not significant vs control). Following AKI, the Ang II + LPS mice slowly gained weight weekly, hinting at a full recovery from the LPS insult. Indeed, in literature, the LPS inflammatory response and AKI occur between six and 48 hours, peaking at the 24 hours mark[149,150]. 48 hours following LPS, renal inflammation declines and recovery ensues[149,150].

SBP was measured to verify successful Ang II delivery by osmotic minipump. Low pressor doses of Ang II are known to lead to a delayed and gradual increase in SBP[110]. SBP response to 400 ng/kg/min of Ang II varies between publications. Indeed, an 8% to 25% increase in SBP was observed for a period of six to 14 days while after a month of Ang II, SBP was reported to increase by approximately 30%[110,151,152]. Similarly, SBP in our model showed mixed responses to Ang II where two pilots showed a 5% to 6% increase in SBP after one week of administration (before LPS, 1W Pump), while the other pilot recorded a 12% increase in SBP. SBP values can be affected by various factors, such as stress, changes in the environment (auditory and olfactory stimuli), handler, cage movement, and activity in the housing room prior to SBP measurement[153]. Additionally, the highest SBP increase coincides with the pilot where the handler had its first experience at measuring SBP in a real study. Following LPS injection, variable progressions in SBP were seen. In one pilot the SBP increased by 5% after LPS, giving an 11% increase at 2W post-LPS (vs baseline). In the other pilot, SBP returned to baseline levels after LPS injection, with a 2 % decrease at endpoint (vs baseline). SBP changes for most timepoints didn't reach significance (vs control) due to the variation between biological replicates. The absence or low

increase in SBP after weeks of Ang II administration could be due to LPS effects on heart contractility[154]. LPS was shown to reduce heart contractility and lead to hypotension during sepsis[154]. Here SBP maintenance (or slight increase) could be due to Ang II administration that counteracts LPS cardiovascular effects. In future studies, assessing pump function through plasma Ang II quantification should be considered as it would provide a more precise answer with less variable results while also giving insight on Ang II half-life in absence of ACE2.

In kidney disease, reductions in either renal blood flow or the number of nephrons can occur and lead to kidney atrophy[111]. Therefore, renal atrophy was assessed through the normalization of kidney weight to tibia length at euthanasia. Limited information is available on kidney weight in the LPS model. In one study, where 10 mg/kg of LPS was given 24 hours before euthanasia, the kidney index (kidney weight normalized to body weight) showed a significant increase (vs control) [155]. LPS usually leads to a reduction in body weight, which is why in this thesis kidney weight was normalized to tibia length, a parameter that is not affected by LPS administration[108,109]. Here, kidney weight normalized to tibia length was unchanged in animals on Ang + LPS (vs control) at both times of euthanasia (AKI - 24 hours post-LPS, and endpoint - three weeks post-LPS). Only in the SMC long-term pilot was normalized kidney weight significantly different between groups. This difference could be due to animals' size. SMC mice's body weight and tibia length (data not shown) were smaller than those of the control group. The ACE2 genotype might also be a cause. Because of the parameter to which kidney weight is normalized, results obtained in the thesis can't be compared to those found in the literature. In COVID-19, kidney atrophy was not evaluated based on the literature available.

In this thesis, overall kidney injury and function were assessed through ACR and BUN. An increase in ACR is suggestive of renal damage (at the glomerular filtration barrier) and early kidney disease[25,27]. A healthy ACR is below 30 µg/mg, while microalbuminuria and macroalbuminuria are described as an ACR between 30 µg/mg and 300 µg/mg, and an ACR over 300 µg/mg, respectively[25]. A significant albuminuria 24 to 48 hours following LPS injection was reported in the litterature[140,156,157]. Similarly, at AKI, albuminuria was statistically significant in the pilots performed, with an average ACR of 460 µg/mg. At endpoint, the average ACR was 16 µg/mg (not significant vs control). As mentioned earlier, 48 hours following LPS recovery is engaged[149,150]. Therefore, it is not surprising to see that one week following LPS injection, ACR had already returned to baseline levels and was maintained until endpoint. At some timepoints in the pilots, high variability in ACR is observed as some biological replicates presented an abnormally high ACR compared to the rest of the group. These values weren't qualified as outliers due to the small number of biological replicates. In COVID-19 patients, mild to moderate proteinuria is a common observation with a frequency of 7% to 63%[158]. Kidney function was also evaluated through BUN, a product of dietary protein breakdown filtered and excreted by the kidneys[29]. In healthy kidneys, BUN is between 2.5 mM and 7.1 mM[29]. An increase in BUN suggests renal malfunction and GFR reduction[29]. In sepsis studies, where a similar dose of LPS and time of euthanasia were selected, BUN increased between 16.2 mM and 50.0 mM[141,142,159,160]. During model development, BUN was measured at euthanasia. When euthanized 24 hours post-LPS (AKI), BUN was significantly increased at 22 mM in Ang II + LPS mice, which falls within the range seen in the litterature[141,142,159,160]. On the other hand, euthanasia at three weeks post-LPS (endpoint) Ang II + LPS BUN was in the healthy range (7.3 mM), which can be expected based on endpoint ACR.

Interestingly, BUN is significantly increased and is a predictor of in-hospital COVID-19 mortality[161].

A gold-standard measure of renal function is GFR (creatinine clearance), the rate at which the blood is filtered by the glomerulus[14,23,24]. GFR requires both plasma and urine creatinine concentration[23,24]. A reduction in GFR or an elevation in plasma creatinine is commonly indicative of abnormal renal function[23,24]. The instrument our group routinely used to measure creatinine (High-performance liquid chromatography; HPLC) was out of service. As serum (plasma) creatinine is a critical value for assessing renal function, other quantification methods were attempted. Serum creatinine analyses by IDEXX Laboratories and IDEXX Bioanalytics were inconclusive as the creatinine concentrations were below IDEXX's detection levels. Additionally, IDEXX measurement through the Jaffe reaction is not ideal for serum creatinine since hemolysis and pseudo-chromogens (e.g. acetone, bilirubin and glucose) cause interference that overestimates creatinine concentration[162,163]. Efforts continue to gain access to an HPLC for serum creatinine measurement. Based on the literature on LPS-induced AKI, a significant increase in serum creatinine between 45 μM and 250 μM (average of 115 μM) could be expected 24 hours after LPS injection[140,141,142,157,159,160].

Renal inflammation, injury, fibrosis, and immune cell infiltration were evaluated through qPCR. The genes assessed are described in Table 7 of the appendices. In LPS-induced AKI and C19-AKI, inflammation is an important theme as shown by the significant upregulation (or production) of pro-inflammatory markers[55,141,142,160,164]. Similar to what has been reported in the literature, a significant upregulation of inflammatory markers (IL-1β, IL-6, and TNF-α) was seen with Ang II + LPS mice at AKI. The level of gene expression can vary depending on euthanasia time. For

example, TNF-α has been shown to quickly increase within an hour of LPS injection and then subsides[165]. By 24 hours, TNF-α is barely detectable, which would explain the low fold increase of TNF-α measured in our model[165]. NGAL and KIM-1 are two renal injury markers whose production are significantly upregulated during LPS-induced AKI[166,167,168]. NGAL and KIM-1 were significantly upregulated (vs control) in the Ang II + LPS pilot at the AKI timepoint. In COVID-19 disease, NGAL and KIM-1 were said to be linked with AKI development and could predict mortality and renal replacement therapy needs[55]. Note that NGAL is also a neutrophil marker as it is expressed by neutrophils[169]. Immune cell infiltration was mainly assessed through Arg-1, F4-80, and MIP-2 expression. LPS leads to innate immune system activation through Toll-like receptor four signalling[64]. The immune cell activation, cytokine production and tissue infiltration process happens within a few hours of LPS injection[169,170,171]. Therefore, it is not surprising to see significant upregulation of Arg-1 and MIP-2, markers of lymphocytes and monocytes, in the kidneys of Ang II + LPS mice during the AKI phase. Expression of F4-80, a macrophage marker, on the other hand, was unchanged by Ang II and LPS at AKI. The macrophage maturation (activation) process goes through multiple steps where bone marrow precursor differentiates into monocytes, which then travel to target tissues (through the bloodstream) where they differentiate into macrophages[64]. The length of the process might delay the increase of F4-80 expression. Imaging mass cytometry showed an increase in lymphocytes, macrophages, and interstitial infiltrates in COVID-19 patients' kidneys, suggesting an innate and adaptive immune tissue response[138]. Whether fibrosis induced by LPS is a common feature of kidney injury is less understood. A few studies have shown that acute fibrosis can occur several hours after LPS injection[166,172]. At AKI, the fibrotic marker CTFG was significantly upregulated,

although the fold increase was low (2-fold vs control). Perhaps, renal expression of additional fibrosis markers (e.g. Transforming growth factor beta and Vascular endothelial growth factor) and histological staining specifically aiming at fibrosis (e.g. Periodic acid-Schiff) should be considered to better evaluate fibrosis in the model[173,174]. In vitro studies showed that SARS-CoV-2 viral infection in renal cells causes induction of fibrotic pathways and tubule-interstitial kidney fibrosis[175]. The anti-inflammatory marker IL-10 was also measured and showed no significant difference in expression (vs control), which is consistent with the literature where IL-10 renal production is low after LPS insult[164]. In COVID-19, systemic levels of IL-10 are significantly increased in severe cases of COVID-19[176]. This feature is unique to the COVID-19 cytokine storm as it was not seen in SARS-CoV infection[176].

In addition to the various markers evaluated, GPR84, a receptor of interest for the second objective of this thesis, was also measured by qPCR. At AKI, a significant upregulation of GPR84 was seen with Ang II and LPS (53-fold vs control). In various CKD mouse models, including 5/6 nephrectomy, doxorubicin-induced nephropathy, and adenine-induced CKD, GPR84 showed an increased expression in macrophages, podocytes, and proximal tubule cells[85]. GPR84 expression was also upregulated by LPS in an acute lung injury model[177]. LPS is said to upregulate GPR84 expression in leukocytes[178]. Additionally, in COVID-19 patients, GPR84 has been found in bronchoalveolar lavage fluid neutrophils[90]. The expression of GPR84 and the genes stated above was also measured in long-term pilots. Three weeks after LPS (endpoint), the expression of all the genes, including GPR84, was no different from the control group. This response is not surprising based on the recovery of body weight, healthy ACR and BUN concentration at that timepoint. As mentioned earlier, with the LPS dose administered the inflammatory response and AKI occur between

six and 48 hours, peaking around 24 hours[149,150]. 48 hours following LPS, renal inflammation declines and recovery is engaged[149,150].

In the thesis, the kidney morphology was assessed by H&E staining. The evaluation of a tissue's general structure can provide further insight into the extent of injury and damage seen by other methods (e.g., ACR and BUN). During model development, histology was assessed for the Ang II + LPS pilot exclusively since the long-term pilots showed no sign of renal injury or damage according to ACR, BUN and qPCR. At AKI, H&E staining showed that Ang II and LPS combination led to proximal tubule lesions characterized by nuclear loss, vacuolization of cytoplasm and protein cast. Increased cellularity in the interstitial space was also noted. Additionally, glomerulopathy was seen, as shown by the focal disappearance of endothelial and mesangial cells. In LPS models, various observations were made depending on the authors, LPS dose and euthanasia time. Edema, mild mesangial expansion, cell swelling, vacuoles, necrosis, tubular cell shrinkage and degeneration, as well as loss of tubular brush border were reported[157,159,160,168]. Similarly to what was seen in our present work, tubular injury and interstitial cell infiltration were also reported in the literature[,159,160,168]. On the other hand, some publications stated that renal morphology can be minimally changed by LPS[165]. In post-mortem analyses of COVID-19 patients' kidneys, acute tubular injury was often seen[47,48,58]. Reports on glomerular disease or injury varied between studies[47,48,58]. In a study where most subjects were males of African descent, collapsing glomerulopathy was seen in 30% of the biopsies but could be related to apolipoprotein L-one polymorphisms[58].

In the H&E general renal structure assessment in the Ang II + LPS study, increased cellularity in the interstitial space was observed. To identify the infiltrating immunohistochemistry targeting of different leukocytes was performed. The first

staining performed was for neutrophils (with myeloperoxidase) since the neutrophils are the most common leukocyte in the blood and therefore a quick increase in this cell type could be expected[64,130,]. The myeloperoxidase staining showed a significant increase in infiltration of neutrophils with Ang II + LPS compared to control with respective values of 27 and 0 neutrophils per field. Similarly, in sepsis, AKI important neutrophil infiltration was stated in the kidneys[179,180]. In COVID-19, neutrophil infiltration is seen in the blood and various tissue including the nasopharyngeal epithelium and the lung[181]. In addition to neutrophil staining, a preliminary analysis of macrophage marker immunostaining (F4-80 and cluster of differentiation 68; CD68) was done and showed no apparent differences between control groups and groups on Ang II + LPS or SMC (data not shown). In post-mortem sepsis patients, macrophage infiltration was seen in the kidney[180]. However, the result obtained here is not surprising since macrophage maturation is a lengthy process, meaning that the increase of renal macrophages may be delayed[64]. The results from macrophage marker staining and other immune markers, such as the cluster of differentiation three (CD3), are currently being finalized or quantified[182].

The last element evaluated during model development was urinary EVs, non-invasive biomarkers of renal injury and disease[131,132]. Podocyte-derived EVs were shown to be early biomarkers of podocyte and glomerular injury as podocyte EVs are significantly increased in diabetic kidney disease, lupus nephritis, and adenine-induced CKD[132]. In adenine-induced CKD, PBI-4050, a GPR84 antagonist, reduced tubular microparticles caused by the insult while also improving tubular injury[132]. On the other hand, a reduction in urinary EV production can also be a sign of reduced renal function[132]. A reduction in urinary EVs is seen with renal function decline caused by age and glomerulosclerosis[132]. It is hypothesized that cell death and nephron loss

could also be a cause of EV reduction[132]. An increase in exosomes was noted in immunoglobulin A nephropathy, CKD patients and inflammatory conditions *in vitro* while other publications reported no difference in exosome numbers during kidney disease[132]. To date, there have been no studies of urinary EVs in LPS sepsis-induced AKI in mice and in COVID-19 patients. In the thesis, EV results are reported as particles since nanoparticle tracking analysis quantifies all particles within a fluid, including EVs. At both AKI (24 hours post-LPS) and endpoint (three weeks post-LPS), particle concentration was not significantly different between animals on Ang II and LPS and controls. Additionally, particle median size and the relative frequency of exosome and microparticle-sized particles were unchanged, suggesting that Ang II and LPS did not affect the type of EVs produced. Perhaps, Ang II and LPS may not change EV concentration or size but rather might influence the cellular origin of EV. The nanoparticle tracking analysis doesn't provide insight into the cellular origin of particles. Besides, urine particles quantified by Zetaview might also originate from cells of the ureter or the bladder as urine travels in those tissues before excretion. Evaluation of EVs with a more refined technique such as flow cytometry would allow testing of this hypothesis. Flow cytometry allows the quantification of EVs specifically and can differentiate EV cellular origin with antibodies while also providing data on EVs concentration and size.

Certainly, the SMC doesn't replicate all the features and complex interactions seen during C19-AKI nor does it fully replicate severe symptoms and complications seen in COVID-19. Important differences between severe cases of COVID-19 and the SMC include the presence of viral particles as well as the age and comorbidities of the subjects. Indeed, the SMC model does not use viral particles, meaning that the response caused SARS-CoV-2 entry in the host cells cannot be fully replicated in the

SMC. The animals used in the SMC model were considered young healthy adults (8–10-week-old mice) that presented no comorbidities while increasing age and comorbidities (e.g., hypertension and diabetes) are risk factors of severe COVID-19[45]. As it was mentioned earlier, in severe cases, COVID-19 is described as a pulmonary illness accompanied by multiple organ failure[48,55]. The pulmonary system is the first system in contact with SARS-CoV-2 as viral entry in the organism occurs through this system[183]. In the lungs, SARS-CoV-2 infection starts by the viral entry of SARS-CoV-2 in the pneumocytes, leading to the activation of the innate immune response, inflammatory cells recruitment and cytokine production[183]. As the viral replication continues, the immune response is exacerbated and leads to the pneumocytes and other pulmonary cell apoptosis[183]. Cytokines produced increase the capillaries' permeability, thereby allowing neutrophil infiltration (into the lung), and viral particle entry in the bloodstream[183]. Neutrophil degranulation (neutrophil extracellular traps) promotes thrombosis and leads to the rupture of the alveolar capillary barrier, causing the entry of blood in the alveolar[183]. Capillary rupture is followed by a hyaline membrane formation, matrix deposition, parenchymal remodelling, and fibrosis[183]. Altogether, this process is described as diffuse alveolar damage and is commonly seen in hospitalized COVID-19 patients[183]. Diffuse alveolar damage is closely related to the acute respiratory distress syndrome, an acute lung injury characterized by respiratory distress, dyspnea, pneumonitis, decrease oxygen saturation (hypoxemia), inflammatory damage at the alveolar capillary barrier, and bilateral infiltrate (ground-glass opacities)[183]. Once SARS-CoV-2 exits the alveolar and reaches the bloodstream where it can affect the cardiovascular system, particularly the endothelial cells composing the vessels[184]. Endotheliitis, endothelial dysfunction and thrombosis are the main cardiovascular features of severe COVID-19[184]. Endothelitis and endothelial

dysfunction are caused by the viral infection of epicardial cells, capillaries' endothelial cells, and perivascular cells, leading to RAS imbalance, which impairs vasoconstriction and vessel permeability, reduces nitric oxide production (vasodilator), and increases reactive oxygen species production (oxidative stress)[184]. Indirect inflammation is another potential factor for endothelitis and endothelial dysfunction[184]. Increased cytokines, endothelial dysfunction, and neutrophil extracellular traps production lead to the activation of endothelial cells' pro-coagulant functions[184]. In COVID-19, high levels of fibrinogen, von Willebrand factor and d-dimer were detected, suggesting hypercoagulation and thrombosis[184]. Endotheliitis and endothelial dysfunction can lead to hypoxia, injury, and cardiomyocytes necrosis[184]. The endothelial dysfunction, oxidative stress, inflammation, and cytokine storm seen during COVID-19 can lead to several other cardiac complications including, myocarditis, myocardial infarction, and arrythmia[184]. In addition to pulmonary and cardiovascular complications, neurological complications can appear in severe cases of SARS-CoV-2 infection, although they are not as well understood[185]. The two main causes of neurological complications in COVID-19 are direct viral infection of neuronal cells and cardiovascular complications[185]. ACE2 and TMPRSS2, the two receptors necessary for SARS-CoV-2 cell entry, are expressed on various cell of the neuronal system, such as ciliated epithelial cells and oligodendrocytes[185]. ACE2 is also expressed in the motor cortex, the ventricles, the olfactory system, the hippocampi, the substantia nigra, the brainstem, and the endothelial cells lining the blood vessels[185]. The cardiovascular complications that can increase the risk of neurological complications include endothelial dysfunction, hypercoagulation, thrombosis, arrythmia, and cytokine storm[185]. Common neurological symptoms in mild COVID-19 are anosmia, ageusia, and headache[185]. In COVID-19 hospitalized patients, encephalopathy is a common

neurological feature[185]. Other neurological complications seen at a lower frequency during COVID-19 are cerebrovascular disease (e.g., stroke), deep vein thrombosis, seizure, meningoencephalitis, intracerebral hemorrhage, and Guillain-Barre syndrome[185]. As for renal complications, the SMC does not fully replicate what was reported in the literature, particularly the histological features of C19-AKI. As mentioned previously, the SMC does not present acute tubular necrosis, myoglobin cast, membranous glomerulopathy global or segmental glomerulosclerosis and collapsing glomerulopathy seen in C19-AKI[47,48,58]. Moreover, coagulopathy, thrombotic microangiopathy and vasculitis noted in certain cases of COVID-19 were not seen in general structure nor were they further assessed in this thesis[47,48,58]. It's important to note that the histological features reported in C19-AKI varied between authors and may also be dependent on various factors, such as apolipoprotein L-one polymorphisms (in people of African descent) [47,48,58].

Whether or not COVID-19 pulmonary, cardiovascular, and neurological complications were replicated in the SMC can't be stated as these features were not assessed in this thesis. The first objective of this thesis was to develop a new surrogate mouse model of C19-AKI disease that mimics the pro-inflammatory context of this condition. LPS given by intraperitoneal (i.p.) injection is expected to enter the bloodstream and therefore could impact the systems mentioned above[186]. Various reports stated that LPS can induce myocardial injury, cardiac dysfunction, reduce heart contractibility and has pro-thrombotic effects[154,187,188]. However, it is unknown if the dose of LPS given in the SMC would lead to complications similar and of the same intensity as in severe COVID-19 cases. In models of LPS-induced acute lung injury, LPS is commonly given intranasal or intratracheally[189]. To refine the SMC model and potentially promote pulmonary complications, giving the full or half (other half i.p.) of

the LPS dose intranasal or intratracheally would be an option. Coagulation seems to be an important feature in cardiovascular and neurological complications[184,185]. Coagulation in the SMC should be verified through the quantification of coagulation factors such as von Willebrand factor, d-dimer, fibrin, thrombin, or tissue factors[184]. To exacerbate coagulopathy (if any) in the SMC, administration of pro-coagulation agents could be added. To refine the model ACE2 KO mice could be crossed with apolipoprotein L-one risk alleles mice to assess glomerulopathies and further study apolipoprotein L-one implication in C19-AKI[58]. The use of the SARS-CoV-2 S protein or inactive viral capsid could also be considered to better mimic the effects of cellular viral entry in COVID-19 pathology.

Overall, the model generated in this thesis, the SMC model, presents multiple similarities with C19-AKI. Similar to C19-AKI, our novel SMC model exhibited significant albuminuria, elevated BUN, important neutrophil infiltration as well a significant upregulation of pro-inflammatory markers as well as inflammatory cell infiltration (based on immune markers expression and histology). Body weight in the SMC is not significantly changed. In C19-AKI, some but not all patients present important body weight loss (cachexia). Administration of Ang II via osmotic minipump had minimal impact upon SBP, consistent with a minor elevation in systemic Ang II concentration, similarly to COVID-19, where Ang II concentration is moderately increased by the reduction of cell surface ACE2 expression. Histological analysis of SMC revealed similarities with C19-AKI, although the literature reports mixed responses. All in all, the SMC shares several important features with C19-AKI. As explained earlier, the SMC doesn't replicate all the features and complex interactions seen during C19-AKI or COVID-19. Nevertheless, the SMC model could represent a novel research tool for therapeutic development against infections associated with

renal injury, including SARS-CoV-2. The simplicity of the SMC developed in this project, which does not rely upon the use of a live virus, makes it an alternative for studying inflammation-associated aspects of AKI-associated C19. Additionally, this model could also be very useful for research and drug testing in the event of other coronavirus outbreaks. By modifying the doses of Ang II and LPS, the SMC model could be repurposed. As shown by the body weight, ACR, BUN and gene expression at endpoint, the original SMC does not lead to an AKI to CKD progression. As this was not an objective of this thesis, the AKI to CKD aspect of the model was not pursued. However, by modifying the dose and number of injections of LPS, the model could potentially evolve into a model of AKI to CKD transition. *Chen et al.* have previously published on CKD development following multiple consecutive injections of LPS at low doses[190]. As AKI is often presented with comorbidities such as hypertension, the SMC model would also be an interesting option to study sepsis AKI in a hypertensive environment by increasing the concentration of Ang II supplemented by osmotic minipump.

The SMC model showed an important upregulation in GPR84, a receptor of interest for our group. This increase in GPR84 further encouraged the second objective of this thesis, which was the assessment of GPR84 in the SMC model.

4.2. Assessment of GPR84 role in the new surrogate mouse model of coronavirus disease 2019-associated acute kidney injury using a GPR84 antagonist (GLPG-1205)

During model development, a significant increase in renal GPR84 expression was noted. The GPR84 is a receptor highly expressed in various immune cells, including monocytes, macrophages, neutrophils and peripheral leukocytes[80,84,85]. GPR84 is involved in fatty acid metabolism, immunological regulation, cytokine

production, and signals intracellularly via reactive oxygen species generation, and calcium influx[80,81,86]. Interestingly, GPR84 was found in bronchoalveolar lavage fluid neutrophils of COVID-19 patients, suggesting a possible involvement of GPR84[90]. In various CKD models, GPR84 is upregulated in macrophages, podocytes, and proximal tubule cells along with increased cytokine production, suggesting that GPR84 contributes to inflammation-associated injuries[85]. In preclinical models of renal injury, global genetic deletion and pharmaceutical antagonists of GPR84 (e.g. PBI-4050 and GLPG-1205) yielded anti-inflammatory and antifibrotic effects[81,85,89]. In a mouse dextran sodium sulphate-induced chronic inflammatory bowel disease model, GLPG-1205 reduced disease activity index score and neutrophil infiltration[82,99]. In lung fibrosis models, GLPG-1205 improved lung function and decreased collagen deposit in bronchial epithelial cells and parenchymal macrophages[98,100]. Additionally, GLPG-1205 demonstrated its safety in phase II clinical trials in idiopathic pulmonary fibrosis and inflammatory bowel disease patients (ulcerative colitis)[178,191]. Therefore, GPR84 deletion or pharmacological antagonism with GLPG-1205 could attenuate indices of renal injury in a surrogate C19-AKI mouse model (SMC). The second objective of this thesis was to determine the role of GPR84 in conditions that involve renal inflammation, such as our SMC model, using the GPR84 antagonist, GLPG-1205, and global GPR84 genetic deletion. In this section, the three studies performed with GLPG-1205 will be discussed.

The GPR84 antagonist, GLGP-1205 was evaluated in the SMC at two different doses (30 mg/kg and 90 mg/kg) on two timelines (co-administration with LPS and prophylaxis treatment prior to LPS). The 30 mg/kg dose was selected for initial analysis based on a preclinical study published by Galapagos[100]. After the first study with GLPG-1205, the dose was increased to 90 mg/kg upon discussions with

collaborators that tested the dose in mice and showed its safety (data not shown). GLPG-1205 was also given as a prophylaxis treatment in an attempt to increase its potency and bioavailability prior to the LPS insult. Methylcellulose of two different viscosities (4000 cps and 400 cps) was also evaluated as vehicles. It was reported that mucosal drug absorption is reduced with increasing viscosity[133,134]. Therefore, using a lower viscosity vehicle such as 400 cps methylcellulose could increase drug absorption and thereby potentially increase its effects.

In all studies performed, regardless of dose, time of administration and vehicle viscosity, GLPG-1205 had no beneficial effects on renal function, injury, and inflammation in the SMC model, as suggested by no significant differences in ACR, plasma and urine electrolytes, and renal gene expression between SMC animals treated with vehicle and GLPG-1205. Interestingly, in the studies with prophylaxis GLPG-1205 treatment, the SMC groups given vehicle and GLPG-1205 both showed an increased, although not significant, ACR at 1W Pump, suggesting an irritable effect of the vehicle on the kidneys. In the prophylaxis GLPG-1205 studies, electrolytes were also analyzed as they can provide insight into tubule function and injury. The tubules are responsible to maintain electrolyte balance[2]. In sepsis AKI patients, disturbance in electrolytes was reported[192]. In severe cases of COVID-19, electrolyte imbalance was characterized by hypernatremia, potassium deficiency and increased chloride concentrations[193]. Similarly, the SMC caused tubular injury, as suggested by the significant changes in plasma and urine electrolytes in SMC vehicle-treated mice. In the SMC studies, it was noted that gene upregulation was more pronounced than what was seen during model development. This difference in expression may be due to the ACE2 deletion and Ang II combination that created a stronger pro-inflammatory environment. Some genes (Arg-1, CTGF, F4-80, and TNF-α), on the other hand,

showed an expression not so different from what was seen during model development. Since the timeline is the same as the Ang II + LPS pilot, genes with time-dependent expressions, such as TNF-α and F4-80, will keep a similar expression pattern[64,165]. Other processes, such as fibrosis (measured through CTGF) may not be significantly activated in this model specifically and therefore expression will remain similar. Some genes (CTGF and F4-80) were not evaluated in all studies as their expression was consistently low and not significant. GLPG-1205 neither had negative effects as parameters measured in control GLPG-1205-treated mice were not significantly different from control vehicle-treated mice. Body weight, SBP and normalized kidney weight were not significantly changed by the SMC model nor by GLPG-1205 treatment. Normalized liver weight was also not affected by the SMC or GLPG-1205 treatment, suggesting that GLPG-1205 doesn't cause liver damage or hepatic cell death[135,136]. BUN, on the other hand, remained at healthy levels with the SMC regardless of vehicle or GLPG-1205 treatment. During model development, AKI BUN was increased above healthy levels. The difference in BUN response may be due to the ACE2 genotype, sex, and age of the mice. It's also important to note that BUN levels may be in the normal range immediately after an insult[45]. Interesting results emerged from renal neutrophil quantification by myeloperoxidase immunohistochemistry. All studies consistently showed a significantly increased neutrophil count (vs control) with the SMC (vehicle-treated) while GLPG-1205 significantly attenuated neutrophil infiltration in the SMC, regardless of the GLGP-1205 regime. When the data of all SMC +GLPG-1205 studies are combined (Figure 44 of the appendices), neutrophil count per field goes from 0 (control groups) to 30 with the SMC (***p≤ 0.001). With GLGP-1205, the number of neutrophils per field was significantly reduced to 21 (***p≤ 0.001 vs SMC vehicle). Indeed, the effect of GLPG-

1205 on neutrophil infiltration but not on any other of the parameters measured is intriguing. This raises questions on the GPR84 role and GLPG-1205 effect on neutrophil function and inflammatory cell infiltration. More studies will be required to clarify those question and better understand the result obtained in this thesis.

Following the analysis of the result, a few hypotheses came out regarding the GLPG-1205 response in the SMC. The first hypothesis is that the GLPG-1205 binding site on GPR84 does lead to the inhibition of GPR84 pathways involved in sepsis models, like the SMC. GLGP-1205 was tested in other mouse models such as dextran sodium sulphate-induced chronic inflammatory bowel disease, and idiopathic pulmonary fibrosis, where it showed promising results[82,100]. GLGP-1205 also went through phase II clinical trials in patients with inflammatory bowel disease (ulcerative colitis)[178]. Although the drug was well tolerated in this clinical study, the Mayo score and biomarkers of the disease were not significantly different between GLPG-1205 and placebo[178]. This thesis is the first published work evaluating GLPG-1205 in a sepsis model and assessing its effects on renal function, injury, and inflammation. It was stated that GPR84 present three distinct ligand binding site and is coupled to the $G_{i/o}$ and $G_{q/i}$ pathways[82,178,]. Perhaps the binding site targeted by GLPG-1205 only partially inactivates GPR84 and doesn't inhibit the G-protein pathways related to acute sepsis and inflammation caused by LPS. Maybe the pathways inhibited by GLPG-1205 binding are more active in chronic inflammation and fibrotic disease than sepsis inflammation, explaining the difference in GLPG-1205 response. More studies with GLPG-1205 in other kidney disease models would provide a better overview and understanding of GLPG-1205 in kidney disease. In the past, another GPR84 antagonist, PBI-4050, showed interesting results in preclinical models of kidney diseases[85,95,97]. The difference in GLPG-1205 and PBI-4050 response may reside in

the binding site of the two molecules on GPR84, thereby inhibiting different GPR84 G-protein pathways. PBI-4050 was said to inhibit $G_{\alpha/i}$ pathways of GPR84[178]. Additionally, PBI-4050 is also a GPR40 agonist, which showed a protective effect in some kidney disease models[178]. PBI-4050 beneficial effects on renal disease may be due to its dual target. GPR40 expression was not assessed in the SMC. It's important to also keep in mind that GPR84 is mostly expressed on immune cells[80,84,85]. Therefore, studying those cells could provide further insight into pathways inhibited by GLPG-1205. Moreover, GLPG-1205 has a hydrophobic nature which makes its dissolution for animal administration more challenging[82]. During the thesis, GLPG-1205 was suspended in 0.5% methylcellulose (4000 cps or 400 cps). The administration period and vehicle selected can greatly impact the potency and pharmacokinetic properties of a drug[194]. It is possible that methylcellulose doesn't allow optimal absorption of GLP-1205, thereby muting its effects. In the dextran sodium sulphate-induced chronic inflammatory bowel disease mouse study, GLPG-1205 was orally administered in 60% polyethylene glycol 200 and showed beneficial effects[82]. In the same study, pharmacokinetic evaluation of GLPG-1205 was carried out in mice given 5 mg/kg of GLPG-1205 in 60% polyethylene glycol 200 by per os (oral administration)[82]. With those parameters, GLPG-1205 had a maximal serum concentration of 4593 ng/mL 30 minutes after administration and a half-life of 1.9 hours[82]. It may be worth testing polyethylene glycol vehicles with GLPG-1205 in kidney disease models. Cremophor, an emulsifier derived from caster oil, could also be considered as a vehicle for GLPG-1205, although it was shown to cause anaphylactic reactions in some cases[195]. Additionally, the absence of response following GLGP-1205 treatment may also be attributed to the lower affinity of the antagonist to the mouse receptor (vs human receptor), although both versions of the receptor share

85% similarity[82,196]. *Jenkins et al*, showed that GLPG-1205 affinity to human GPR84 and mouse GPR84 in which extracellular regions and transmembrane domains were replaced by the human sequences was approximately 25 times higher compared to the mouse GPR84[196]. Other antagonist derived from GLPG-1205 also showed a lower affinity to the mouse GPR84 receptor compared to the human GPR84[197,198]. Perhaps, other animal model or method should be considered to properly evaluate GLPG-1205.

To further assess GPR84 role in the model developed, the Ang II and LPS combination effects on renal function, injury and inflammation were evaluated in GPR84 KO mice.

4.3. Assessment of GPR84 role in the new surrogate mouse model of coronavirus disease 2019-associated acute kidney injury using GPR84 global knockout mice.

In addition to assessing the GPR84 role in the SMC through the GPR84 antagonist, GLPG-1205, the GPR84 role was also evaluated in mice with global GPR84 deletion. For this study, ACE2 and GPR84 animals couldn't be intercrossed due to time limitations. Therefore, all GPR84 mice used had an ACE2 WT genotype. A combination of male and female mice of eight to 13 weeks of age was used as animal inventory was limited. GPR84 HET and WT mice were combined to form the control groups after confirming that GPR84 expression was not different between genotypes (Figure 45 of the appendices).

Conclusions from the GPR84 Ang II + LPS study are similar to those with GLGP-1205. Ang II + LPS leads to a reduction in renal function, and important renal injury and inflammation, as suggested by significant increases in ACR, BUN, neutrophil infiltration and inflammatory, injury and immune markers messenger ribonucleic acid (mRNA) expression in Ang II + LPS mice compared to control mice of

the same genotype. Additionally, Ang II + LPS also had a significant effect on electrolyte concentration compared to control (in KO). Here, normalized liver weight and electrolytes were not measured in HET/WT control as the pilot in which those parameters were collected did not have a HET/WT control group due to low animal availability. The GPR84 Ang II + LPS study is a combination of two pilots. Like GLPG-1205, GPR84 deletion did not improve renal function nor reduce renal injury or inflammation, as no significant differences in ACR, BUN, electrolytes and genes expression were noted between HET/WT Ang II + LPS mice and KO Ang II + LPS mice. Unlike in SMC + GLPG-1205 studies, where pharmaceutical antagonism of GPR84 significantly attenuated renal neutrophil infiltration, GPR84 deletion in Ang II + LPS had no significant effect on neutrophil infiltration when compared with GPR84 HET/WT on Ang II + LPS. Relative body weight, relative SBP as well as normalized kidney and liver weight were not significantly affected by Ang II + LPS nor by GPR84 genotype. Throughout the study, no significant differences were noted between HET/WT control and KO control, demonstrating that GPR84 deletion in healthy conditions doesn't cause renal injury or inflammation. For the most part, males and females presented no significant difference in response to Ang II + LPS apart from BUN, which was significantly higher in males than females. This makes the Ang II + LPS combination interesting for drug testing, as it would allow testing treatments on both males and females.

In preclinical models of renal injury, genetic deletion of GPR84 showed anti-inflammatory and antifibrotic effects[81,85,89]. The GPR84 KO mice utilized in this study had a constitutive (non-inducible) global deletion of the GPR84 gene. The lack of GPR84 expression over multiple generations may have led to adaptation and compensation processes, where other pathways similar to GPR84 compensate for

GPR84 loss, thereby overshadowing the effects of GPR84 deletion in inflammatory models, such as SMC. Redundancy, repetition of genes and pathways of similar function, is particularly crucial in the event of null mutations or system pertubations[199]. Redundancy was obtained by retaining gene duplicates over time[199]. For pathways related to important processes, such as inflammation, redundancy would be essential as inappropriate control of inflammation could put the organism survival at risk[199]. Using inducible GPR84 KO mice may be more appropriate as an adaptation to GPR84 deletion would not occur over generations, and therefore the response generated by GPR84 deletion may be more accurate.

Throughout the thesis, a significant upregulation of GPR84 in the kidneys was measured, although the kidney endogenously expresses GPR84 at low levels[200]. GPR84 is highly expressed in the bone marrow and various immune cells, including monocytes, macrophages, neutrophils and peripheral leukocytes[80,84,85,200]. The increase of immune cell markers detected in renal qPCR and the observation of increased cellularity in the interstitial space suggest that GPR84 renal upregulation could originate from the infiltrating cells. Single-cell ribonucleic acid (RNA) sequencing (or qPCR) on renal and infiltrating cells would be useful to determine the cellular origin of the increased GPR84 renal expression in the SMC. RNA sequencing would also provide insight into the pathways regulated by GPR84. Moreover, RNA sequencing on renal and infiltrating cells treated with GLGP-1205 could help assess the pathways inhibited by GLPG-1205. The same idea goes for GPR84 KO and the potential compensation processes occurring. We hypothesized that the increase of GPR84 may originate from neutrophil since the there's an important neutrophils infiltration in the SMC and NGAL expression, a marker of neutrophils, is significantly upregulated in the SMC[64]. Future studies focusing on locating the cellular origin of GPR84 expression

within kidneys in the SMC along with RNA sequencing should provide a better understanding of GPR84 purpose in the model and help identify pathways modulated by GPR84. This information could also be important to better understand the GLPG-1205 mechanism of action.

CHAPTER 5: SUMMARY

In this thesis a new surrogate mouse model mimicking the pro-inflammatory context of C19-AKI, abbreviated SMC, was developed. Similarly, to C19-AKI, our SMC model exhibited significant albuminuria, elevated BUN, electrolyte imbalance, neutrophil infiltration as well as a significant upregulation of pro-inflammatory and injury markers in the kidneys. Relative body weight and SBP, normalized kidney weight, and urinary EV features were not significantly affected in the SMC model. Results from long-term pilots with the model suggested that the SMC model as presented does not lead to CKD development. GPR84, a pro-inflammatory receptor highly expressed in leukocytes, was significantly upregulated in the SMC. In the second objective of this thesis, GPR84 role in the SMC was assessed via GPR84 antagonist, GLPG-1205, and GPR84 global deletion. In all studies performed, regardless of dose, time of administration and vehicle viscosity, GLPG-1205 had no beneficial effects on renal function, injury, and inflammation in the SMC model, as suggested by no significant differences in ACR, electrolytes, and pro-inflammatory, injury, and inflammatory cell marker expression. The same response was obtained in GPR84 KO mice (on Ang II + LPS). Interestingly, GLPG-1205 significantly attenuated neutrophil infiltration while GPR84 deletion had no effect on this parameter. Males and females presented no significant difference in response to Ang II + LPS apart from BUN being higher in males than females. Future studies focusing on cellular location of GPR84 expression in the SMC along with single-cell RNA sequencing could clarify GPR84 role in the inflammatory models (e.g., SMC) and leukocyte function and infiltration. Single-cell RNA sequencing could also help identify pathways modulated by GPR84 and inhibited by GLPG-1205.

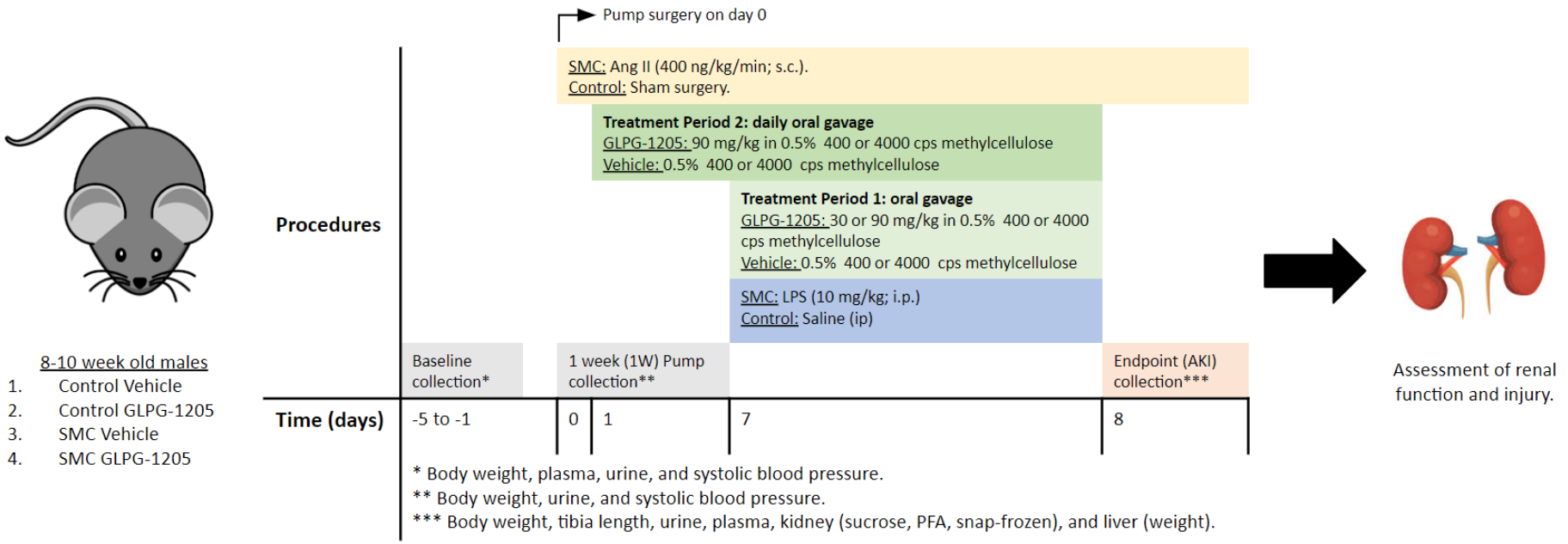

Figure 43. **Surrogate model of coronavirus disease 2019-associated acute kidney injury (C19-AKI) timeline.** The surrogate model of C19-AKI consisted of angiotensin-converting enzyme 2 (ACE2) knockout (KO) mice receiving a low suppressor dose of angiotensin II (Ang II) with a single lipopolysaccharide (LPS) intraperitoneal (i.p.) administration. Mice were euthanized 24 hours after the LPS challenge. G-coupled protein receptor (GPR) 84 role was assessed with GPR84 KO mice and GPR84 antagonists (GLPG-1205). Wild type (WT) littermates were used as controls.

Table 6. **In vivo studies details.** Group, age, sex, genotype, treatment, and timeline of animals from each study performed. Co-administered treatment consists of one GLP-1205 gavage at time of LPS injection. Prophylaxis treatment is referred to as daily gavage from the day following Ang II osmotic minipump implantation until LPS injection, making seven days of treatment. Acronyms in table are defined below.

Study Name	Groups	Biological Replicates (n)	Starting Age (Weeks)	Sex	Genotype	GLPG-1205			LPS (Days post-pump surgery)	Endpoint (Days Post-LPS)
						Treatment Type	Dose (mg/kg)	Vehicle		
Ang II + LPS Pilot	Control	6	8-9 (n=2); 21-25(n=2)	5F; 1M	WT	-	-	-	7-10	1
	Ang II + LPS	12	7 (n=2); 21-25(n=10)	F	WT					
Ang II + LPS Long-Term Pilot	Control	5	6-8	3F; 2M	WT	-	-	-	10	19
	Ang II + LPS	5	8	2F; 3M	WT					
SMC Long-Term Pilot	Control	5	8	M	WT (ACE2)	-	-	-	7	21
	SMC	4	9	M	KO (ACE2)					
SMC + GLPG-1205 (Co-administered with LPS)	Control Vehicle	10	8-10	M	WT (ACE2)	Co-administered with LPS	30	0.5% 4000 cps methylcellulose	7	1
	Control GLPG-1205	10	8-10	M	WT (ACE2)					
	SMC Vehicle	11	8-9	M	KO (ACE2)					
	SMC GLPG-1205	12	8-9	M	KO (ACE2)					
SMC + GLPG-1205 (Prophylaxis, 4000 cps)	Control Vehicle	4	9-10	M	WT (ACE2)	Prophylaxis	90	0.5% 4000 cps methylcellulose	7	1
	Control GLPG-1205	5	9-10	M	WT (ACE2)					
	SMC Vehicle	6	6-9	M	KO (ACE2)					
	SMC GLPG-1205	5	7	M	KO (ACE2)					
SMC + GLPG-1205 (Prophylaxis, 400 cps)	Control Vehicle	5	9	M	WT (ACE2)	Prophylaxis	90	0.5% 400 cps methylcellulose	7	1
	Control GLPG-1205	5	9	M	WT (ACE2)					
	SMC Vehicle	9	9	M	KO (ACE2)					
	SMC GLPG-1205	9	9	M	KO (ACE2)					
GPR84 Ang II + LPS	HET/WT Control	6	9-10	3F; 3M	4 HET; 2 WT (GPR84)	-	-	-	7	1
	KO Control	11	8-13	7F; 5M	KO (GPR84)					
	HET/WT Ang II + LPS	11	8-13	5F; 6M	7 HET; 4 WT (GPR84)					
	KO Ang II + LPS	12	8-13	7F; 5M	KO (GPR84)					

ACE2: Angiotensin converting enzyme 2; Ang II: Angiotensin II; cps: centipoise; F: Female; GPR84: G-coupled protein receptor 84; HET: Heterozygous; KO: Knockout; LPS: Lipopolysaccharide; M: Male; SMC: Surrogate model of coronavirus disease 2019-associated acute kidney injury; WT: Wild-type

Table 7. **Gene assessed by renal qPCR and their role in inflammation, fibrosis, or as immune cell markers.**

Gene	Role in Inflammation, Fibrosis or as an Immune Cell Marker	References
Arginase-1 (ARG-1)	Enzyme expressed in lymphocytes, tissue resident and macrophages (M2 phenotype transition). Involve in anti-inflammatory and reparative response (Th2 activation).	112, 113, 114
Connective tissue growth factor (CTGF)	Extracellular matrix protein upregulated during fibrosis. Modulates growth factors production, inflammatory mediators (e.g., TNF-α and IL-6) and promotes renal fibrosis.	115
EGF-like module-containing mucin-like hormone receptor-like 1 (F4-80)	Glycoprotein expressed on macrophages and various tissue resident macrophages including the kidney. Well-known macrophage marker.	116
Glyceraldehyde 3-phosphate dehydrogenase (GAPDH)	Gene used as an internal control (housekeeping gene). Not involved in inflammation or fibrosis.	117
G-coupled protein receptor 84 (GPR84)	Receptor expressed on monocytes, macrophages, neutrophils, and peripheral leukocytes. Involved in fatty acid metabolism, immunological regulation, cytokine production, ROS generation, and calcium influx.	80, 81, 84, 85, 86
Interleukin (IL)-1β	Pro-inflammatory cytokine produced by dendritic cells, natural killer cells, B lymphocytes, neutrophils, monocytes, and macrophages. Production promoted during early injury or infection by complement or other cytokines. Attract leukocytes to the infection site and promote cytokines production.	118, 119
IL-6	Pleiotropic cytokine produced by macrophages during early infection. Promote inflammatory molecules production (c-reactive protein and complement proteins) by the liver. Shift cell production in the bone marrow to promote neutrophils, eosinophil, and basophil production. Anti-inflammatory and reparative effects on epithelial cells through STAT3 signalling.	118, 120, 121
IL-10	Anti-inflammatory cytokine produced by B and T lymphocytes, natural killer cells, monocytes, and dendritic cells. Supresses T lymphocyte proliferation and pro-inflammatory cytokine production. Inhibits MIP-2 and TNF-α production.	118, 122, 123
Kidney injury molecule 1 (KIM-1)	Biomarker of renal injury. Expressed by PT cells during injury. Linked with tubulointerstitial inflammation and fibrosis. KIM-1 expressing PT cell can acts as residential phagocyte and remove apoptotic cells, thereby easing tubule regeneration.	124
Macrophage inflammatory protein 2 (MIP-2)	Chemokine produced by macrophages, monocytes, and epithelial cells during infection or injury. Involved in neutrophil recruitment, infiltration (chemotactic factor) and activation.	125
Neutrophil gelatinase-associated lipocalin (NGAL)	Protein expressed by neutrophils and tubule cell during injury or infection. Marker of organ injury, more specifically, AKI and renal dysfunction. Released during tubular damage.	118, 126, 127, 128
Tumor necrosis factor alpha (TNF-α)	Pro-inflammatory cytokine produced by T lymphocytes, macrophages endothelial cells, tubular cells and mesangial cells during early injury or infection. TNF-α attract leukocytes to the infection site. Involved in inflammation, apoptosis, lymphoid development and tissue repair and regeneration.	118, 129

PT: Proximal tubule; qPCR: Quantitative polymerase chain reaction; ROS: Reactive oxygen species

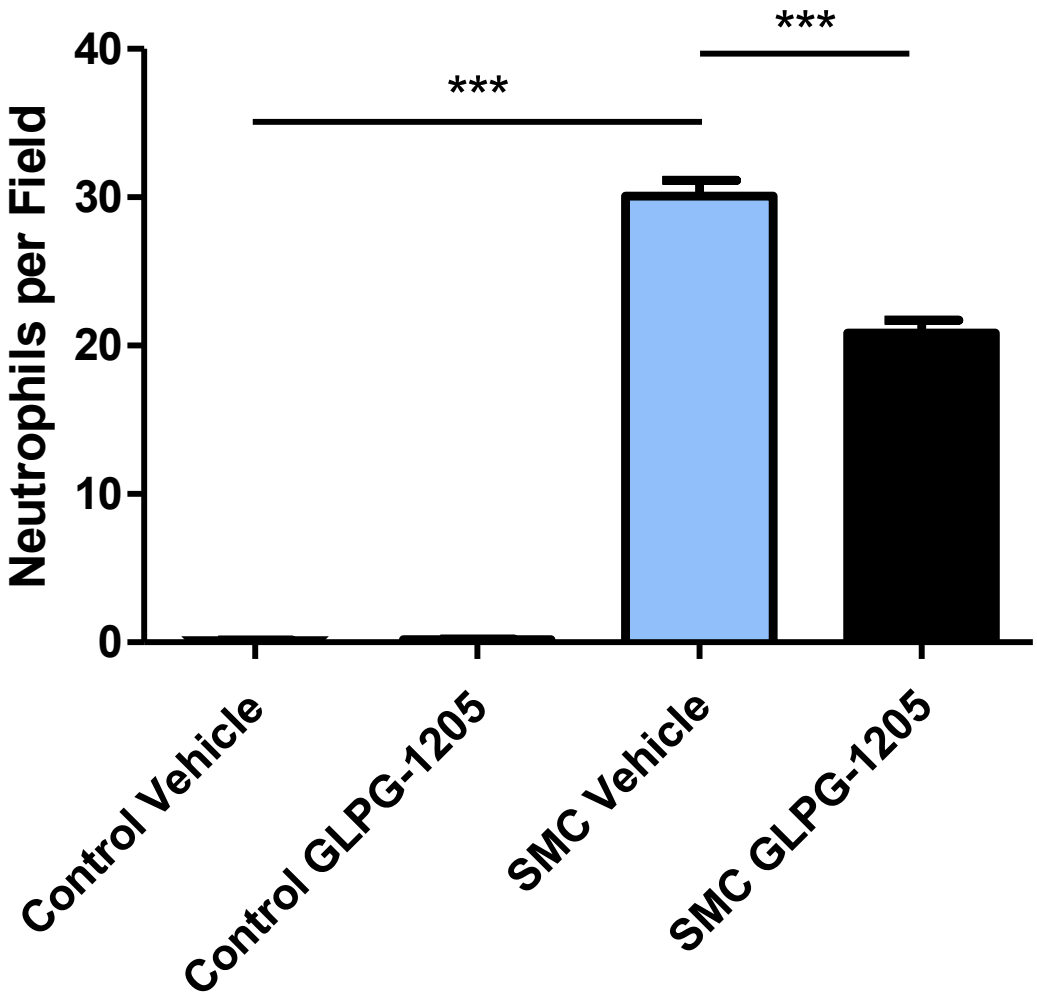

Figure 44. **SMC + GLPG-1205 (all studies combined) renal neutrophil infiltration.** Quantification of neutrophils (Myeloperoxidase positive events) per field from myeloperoxidase immunohistochemistry on AKI (24 hours post-LPS) kidneys. Four to 12 fields were averaged per biological replicate. Control vehicle: n=10; Control GLPG-1205: n=9; SMC vehicle: n=13; SMC GLGP-1205: n=13. Outlying values were removed from the analysis. Data presented as mean ± standard error of the mean (SEM). One-way analysis of variance (ANOVA) with a Dunnett post-test comparing SMC vehicle to control vehicle and SMC GLPG-1205 was performed. (***p≤ 0.001). AKI: Acute kidney injury.

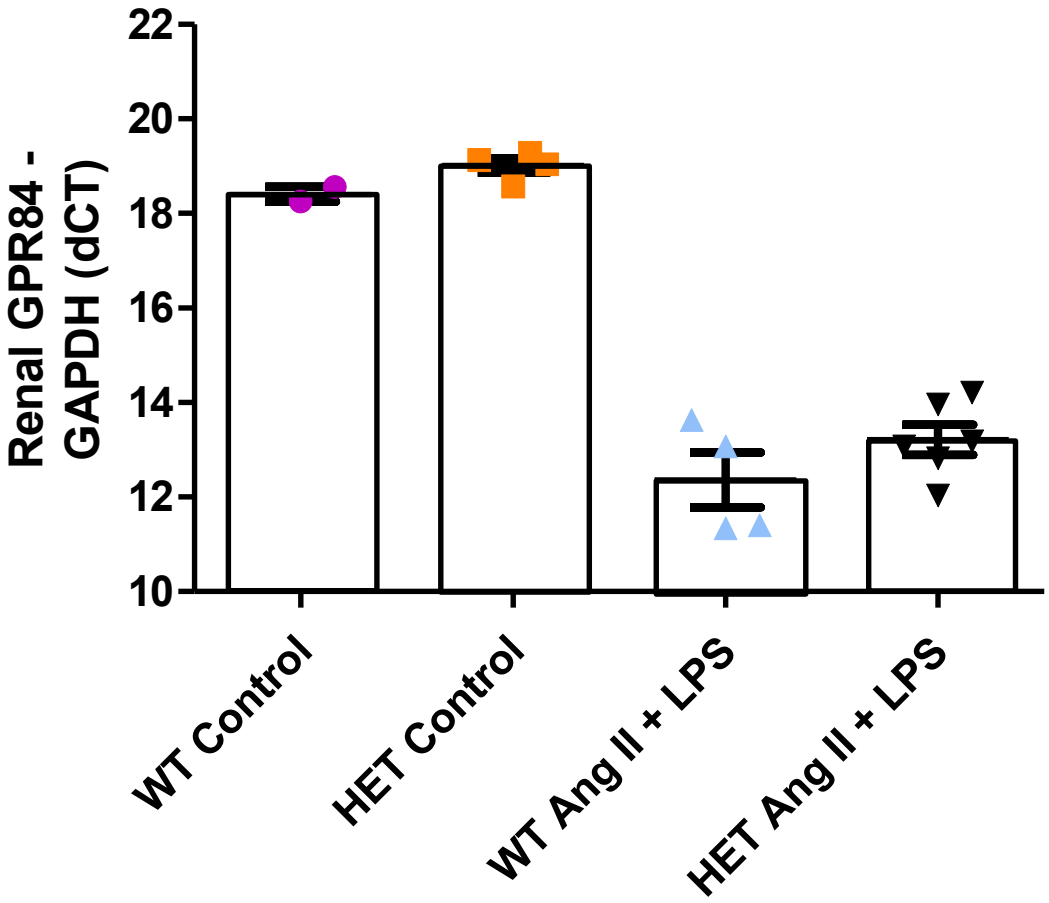

Figure 45. **Renal expression of GPR84 in GPR84 WT and HET mice.** Different in cycle threshold between G-coupled protein receptor 84 (GPR84) and glyceraldehyde three-phosphate dehydrogenase (GAPDH) presented as delta cycle threshold (dCT). Gene expression measured at AKI (24 hours post-lipopolysaccharide injection) and assessed by quantitative polymerase chain reaction (qPCR). WT Control: n=2; HET Control: n=4; WT Ang II + LPS: n=4; HET Ang II + LPS: n=6. Outlying values were removed from the analysis. Data presented as mean ± standard error of the mean (SEM). One-way analysis of variance (ANOVA) with a Bonferroni post-test comparing WT control with HET control and WT Ang II + LPS with HET Ang II + LPS was performed (not significant). AKI: Acute kidney injury; HET: Heterozygous; WT: Wild type.

CHAPTER 7: REFERENCES

1. The Urinary Tract & How It Works. *National Institute of Diabetes and Digestive and Kidney Diseases* https://www.niddk.nih.gov/health-information/urologic-diseases/urinary-tract-how-it-works (2022).

2. Your Kidneys & How They Work. *National Institute of Diabetes and Digestive and Kidney Diseases* https://www.niddk.nih.gov/health-information/kidney-disease/kidneys-how-they-work (2022).

3. How Your Kidneys Work. *National Kidney Foundation* https://www.kidney.org/atoz/content/howkidneyswork (2015).

4. Sarzani, R., Giulietti, F., Di Pentima, C., Giordano, P. & Spannella, F. Disequilibrium between the classic renin-angiotensin system and its opposing arm in SARS-CoV-2-related lung injury. *Am. J. Physiol. Lung Cell. Mol. Physiol.* **319**, L325–L336 (2020).

5. Vitamin D: The Kidney Vitamin? *National Kidney Foundation* https://www.kidney.org/news/kidneyCare/spring10/VitaminD (2014).

6. McMahon, A. P. Development of the Mammalian Kidney. *Curr. Top. Dev. Biol.* **117**, 31 (2016).

7. Daehn, I. S. & Duffield, J. S. The glomerular filtration barrier: a structural target for novel kidney therapies. *Nat. Rev. Drug Discov.* **20**, 770–788 (2021).

8. Scott, R. P. & Quaggin, S. E. Formation and Maintenance of a Functional Glomerulus. *Kidney Development, Disease, Repair and Regeneration* 103–119 (2016) doi:10.1016/b978-0-12-800102-8.00010-2.

9. Bartlett, C. S., Jeansson, M. & Quaggin, S. E. Vascular Growth Factors and Glomerular Disease. Annu. Rev. Physiol. 78, 437 (2016).

10. Satchell, S. C. et al. Conditionally immortalized human glomerular endothelial cells expressing fenestrations in response to VEGF. Kidney Int. 69, 1633–1640 (2006).

11. Fu, J., Lee, K., Chuang, P. Y., Liu, Z. & He, J. C. Glomerular endothelial cell injury and cross talk in diabetic kidney disease. American Journal of Physiology - Renal Physiology 308, F287 (2015).

12. Daehn, I. S. & Duffield, J. S. The glomerular filtration barrier: a structural target for novel kidney therapies. Nat. Rev. Drug Discov. 20, 770 (2021).

13. Jennifer Weil, E. et al. Podocyte detachment and reduced glomerular capillary endothelial fenestration promote kidney disease in type 2 diabetic nephropathy. Kidney Int. 82, 1010 (2012).w

14. Sison, K. et al. Glomerular structure and function require paracrine, not autocrine, VEGF-VEGFR-2 signaling. J. Am. Soc. Nephrol. 21, (2010).

15. Jeansson, M. et al. Angiopoietin-1 is essential in mouse vasculature during development and in response to injury. J. Clin. Invest. 121, (2011).

16. McMahon, A. P. Development of the Mammalian Kidney. Curr. Top. Dev. Biol. 117, 31 (2016).

17. Subramanya, A. R. & Ellison, D. H. Distal Convoluted Tubule. *Clin. J. Am. Soc. Nephrol.* **9**, 2147 (2014).

18. Feher, J. Regulation of Fluid and Electrolyte Balance. *Quantitative Human Physiology* 665–673 (2012) doi:10.1016/b978-0-12-382163-8.00074-8.

19. Floege, J., Johnson, R. J. & Feehally, J. *Comprehensive Clinical Nephrology E-Book*. (Elsevier Health Sciences, 2010).

20. Nielsen, S. *et al.* Vasopressin increases water permeability of kidney collecting duct by inducing translocation of aquaporin-CD water channels to plasma membrane. *Proc. Natl. Acad. Sci. U. S. A.* **92**, 1013 (1995).

21. Korrapati, M. C. & Mehendale, H. M. Urea. *Encyclopedia of Toxicology* 885–888 (2014) doi:10.1016/b978-0-12-386454-3.00357-2.

22. Top 5 Most Important Kidney Health Numbers. *National Kidney Foundation* https://www.kidney.org/news/ekidney/october11/top5 (2014).

23. Estimated Glomerular Filtration Rate (eGFR). *National Kidney Foundation* https://www.kidney.org/atoz/content/gfr (2015).

24. Shahbaz, H. & Gupta, M. Creatinine Clearance. in *StatPearls [Internet]* (StatPearls Publishing, 2021).

25. ACR. *National Kidney Foundation* https://www.kidney.org/kidneydisease/siemens_hcp_acr (2014).

26. Moman, R. N., Gupta, N. & Varacallo, M. Physiology, Albumin. in *StatPearls [Internet]* (StatPearls Publishing, 2022).

27. Know Your Kidney Numbers: Two Simple Tests. *National Kidney Foundation* https://www.kidney.org/atoz/content/know-your-kidney-numbers-two-simple-tests (2017).

28. Kidney Failure Risk Factor: Urine Albumin-Creatinine Ratio (uACR). *National Kidney Foundation* https://www.kidney.org/content/kidney-failure-risk-factor-urine-albumin-to-creatinine-ration-uacr (2020).

29. What is the Difference Between sCr, eGFR, ACR, and BUN? *National Kidney Foundation* https://www.kidney.org/newsletter/what-difference-between-scr-egfr-acr-and-bun (2018).

30. GBD Chronic Kidney Disease Collaboration. Global, regional, and national burden of chronic kidney disease, 1990–2017: a systematic analysis for the Global Burden of Disease Study 2017. *Lancet* **395**, 709 (2020).

31. Kidney Failure Continues To Rise In Canada. https://kidney.ca/News-Media/News/ALL/Kidney-Failure-Continues-To-Rise-In-Canada.

32. Couser, W. G., Remuzzi, G., Mendis, S. & Tonelli, M. The contribution of chronic kidney disease to the global burden of major noncommunicable diseases. *Kidney International* vol. 80 1258–1270 (2011).

33. Global Facts: About Kidney Disease. *National Kidney Foundation* https://www.kidney.org/kidneydisease/global-facts-about-kidney-disease (2015).

34. Chronic kidney disease (CKD) - Symptoms, causes, treatment. *National Kidney Foundation* https://www.kidney.org/atoz/content/about-chronic-kidney-disease (2020).

35. 10 Signs You May Have Kidney Disease. *National Kidney Foundation* https://www.kidney.org/news/ekidney/august14/10_Signs_You_May_Have_Kidney_Disease (2020).

36. Bao, Y.-W., Yuan, Y., Chen, J.-H. & Lin, W.-Q. Kidney disease models: tools to identify mechanisms and potential therapeutic targets. *Zoological Research* **39**, 72 (2018).

37. Acute Kidney Injury (AKI). https://www.kidney.org/atoz/content/AcuteKidneyInjury (2015).

38. Makris, K. & Spanou, L. Acute Kidney Injury: Definition, Pathophysiology and Clinical Phenotypes. *Clin. Biochem. Rev.* **37**, 85–98 (2016).

39. Susantitaphong, P. *et al.* World Incidence of AKI: A Meta-Analysis. *Clin. J. Am. Soc. Nephrol.* **8**, 1482 (2013).

40. Schlondorff, D. O. Overview of factors contributing to the pathophysiology of progressive renal disease. *Kidney Int.* **74**, 860–866 (2008).

41. Vaidya, S. R. & Aeddula, N. R. Chronic Renal Failure. in *StatPearls [Internet]* (StatPearls Publishing, 2020).

42. Sato, Y. & Yanagita, M. Immune cells and inflammation in AKI to CKD progression. *Am. J. Physiol. Renal Physiol.* **315**, F1501–F1512 (2018).

43. Patidar, K. R. *et al.* Acute kidney disease is common and associated with poor outcomes in patients with cirrhosis and acute kidney injury. *J. Hepatol.* **77**, 108–115 (2022).

44. What is Kidney Failure? *National Kidney Foundation* https://www.kidney.org/atoz/content/KidneyFailure (2016).

45. Goyal, A., Daneshpajouhnejad, P., Hashmi, M. F. & Bashir, K. Acute Kidney Injury. in *StatPearls [Internet]* (StatPearls Publishing, 2022).

46. Hoste, E. A. J. *et al.* Global epidemiology and outcomes of acute kidney injury. *Nat. Rev. Nephrol.* **14**, 607–625 (2018).

47. Golmai, P. *et al.* Histopathologic and Ultrastructural Findings in Postmortem Kidney Biopsy Material in 12 Patients with AKI and COVID-19. *J. Am. Soc. Nephrol.* **31**, 1944–1947 (2020).

48. Santoriello, D. *et al.* Postmortem Kidney Pathology Findings in Patients with COVID-19. *J. Am. Soc. Nephrol.* **31**, 2158–2167 (2020).

49. Coronavirus disease (COVID-19) – World Health Organization. https://www.who.int/emergencies/diseases/novel-coronavirus-2019.

50. Perico, L., Benigni, A. & Remuzzi, G. Should COVID-19 Concern Nephrologists? Why and to What Extent? The Emerging Impasse of Angiotensin Blockade. *Nephron* vol. 144 213–221 (2020).

51. Walls, A. C. et al. Structure, Function, and Antigenicity of the SARS-CoV-2 Spike Glycoprotein. Cell 181, 281–292.e6 (2020).

52. Ishfaq, R. *et al.* Why Severity Rate of COVID-19 is High in Patients with Diabetes Mellitus: A Brief Insight. *BioMedica* vol. 36 137–141 (2020).

53. Public Health Agency of Canada. Coronavirus disease (COVID-19): For health professionals. https://www.canada.ca/en/public-health/services/diseases/2019-novel-coronavirus-infection/health-professionals.html (2020).

54. Vaira, L. A., Salzano, G., Deiana, G. & De Riu, G. Anosmia and Ageusia: Common Findings in COVID-19 Patients. *Laryngoscope* doi:10.1002/lary.28692.

55. Hilton, J., Boyer, N., Nadim, M. K., Forni, L. G. & Kellum, J. A. COVID-19 and Acute Kidney Injury. *Crit. Care Clin.* **38**, 473 (2022).

56. Farkash, E. A., Wilson, A. M. & Jentzen, J. M. Ultrastructural Evidence for Direct Renal Infection with SARS-CoV-2. *J. Am. Soc. Nephrol.* **31**, 1683–1687 (2020).

57. Fisher, M. *et al.* AKI in Hospitalized Patients with and without COVID-19: A Comparison Study. *J. Am. Soc. Nephrol.* **31**, 2145–2157 (2020).

58. Kudose, S. *et al.* Kidney Biopsy Findings in Patients with COVID-19. *J. Am. Soc. Nephrol.* **31**, 1959–1968 (2020).

59. Sharma, P. *et al.* COVID-19–Associated Kidney Injury: A Case Series of Kidney Biopsy Findings. *Journal of the American Society of Nephrology* vol. 31 1948–1958 (2020).

60. Yusuf, A. A., Govender, M. A., Brandenburg, J.-T. & Winkler, C. A. Kidney disease and APOL1. *Hum. Mol. Genet.* **30**, R129 (2021).

61. Friedman, D. J. COVID-19 and APOL1: Understanding Disease Mechanisms through Clinical Observation. *J. Am. Soc. Nephrol.* **32**, 1 (2021).

62. Nichols, B. *et al.* Innate immunity pathways regulate the nephropathy gene Apolipoprotein L1. *Kidney Int.* **87**, 332 (2015).

63. Lei, X. *et al.* Activation and evasion of type I interferon responses by SARS-CoV-2. *Nat. Commun.* **11**, (2020).

64. Abbas, A. K., Lichtman, A. & Pillai, S. *Les bases de l'immunologie fondamentale et clinique*. (2020).

65. Batlle, D. et al. Acute Kidney Injury in COVID-19: Emerging Evidence of a Distinct Pathophysiology. J. Am. Soc. Nephrol. 31, 1380–1383 (2020).

66. Bayati, A., Kumar, R., Francis, V. & McPherson, P. S. SARS-CoV-2 uses clathrin-mediated endocytosis to gain access into cells. *Cold Spring Harbor Laboratory* 2020.07.13.201509 (2020) doi:10.1101/2020.07.13.201509.

67. Fountain, J. H. & Lappin, S. L. Physiology, Renin Angiotensin System. in *StatPearls [Internet]* (StatPearls Publishing, 2020).

68. Lanza, K. *et al.* Covid-19: the renin–angiotensin system imbalance hypothesis. *Clinical Science* vol. 134 1259–1264 (2020).

69. Chiranjib Dasgupta, L. Z. Angiotensin II receptors and drug discovery in cardiovascular disease. *Drug Discov. Today* **16**, 22 (2011).

70. GeneCards Human Gene Database. ACE2 Gene - GeneCards. https://www.genecards.org/cgi-bin/carddisp.pl?gene=ACE2#localization.

71. What is a mouse model? *The Jackson Laboratory* https://www.jax.org/why-the-mouse/model.

72. Advantages of using the Mouse as a Model Organism. *Oxford Instruments* https://andor.oxinst.com/learning/view/article/advantages-of-using-the-mouse-as-a-model-organism.

73. Soldatov, V. O., Kubekina, M. V., Silaeva, Y. Y., Bruter, A. V. & Deykin, A. V. On the way from SARS-CoV-sensitive mice to murine COVID-19 model. *On the way from SARS-CoV-sensitive mice to murine COVID-19 model* **6**, 1–7 (2020).

74. Muñoz-Fontela, C. *et al.* Animal models for COVID-19. *Nature* **586**, 509 (2020).

75. Dinnon, K. H., III *et al.* A mouse-adapted model of SARS-CoV-2 to test COVID-19 countermeasures. *Nature* **586**, 560 (2020).

76. Public Health Agency of Canada. Biosafety advisory: SARS-CoV-2 (Severe acute respiratory syndrome coronavirus 2). https://www.canada.ca/en/public-health/services/laboratory-biosafety-biosecurity/biosafety-directives-advisories-notifications/sars-cov-2.html#a4 (2021).

77. Sharfuddin, A. A. & Molitoris, B. A. Pathophysiology of ischemic acute kidney injury. *Nature Reviews Nephrology* vol. 7 189–200 (2011).

78. Huen, S. C. & Cantley, L. G. Macrophage-mediated injury and repair after ischemic kidney injury. *Pediatr. Nephrol.* **30**, 199–209 (2015).

79. Zhang, M.-Z. *et al.* IL-4/IL-13–mediated polarization of renal macrophages/dendritic cells to an M2a phenotype is essential for recovery from acute kidney injury. *Kidney International* vol. 91 375–386 (2017).

80. Wang, J., Wu, X., Simonavicius, N., Tian, H. & Ling, L. Medium-chain fatty acids as ligands for orphan G protein-coupled receptor GPR84. *J. Biol. Chem.* **281**, 34457–34464 (2006).

81. Suzuki, M. *et al.* Medium-chain fatty acid-sensing receptor, GPR84, is a proinflammatory receptor. *J. Biol. Chem.* **288**, 10684–10691 (2013).

82. Labéguère, F. *et al.* Discovery of 9-Cyclopropylethynyl-2-((S)-1-[1,4]dioxan-2-ylmethoxy)-6,7-dihydropyrimido[6,1-a]isoquinolin-4-one (GLPG1205), a Unique GPR84 Negative Allosteric Modulator Undergoing Evaluation in a Phase II Clinical Trial. *Journal of Medicinal Chemistry* (2020) doi:10.1021/acs.jmedchem.0c00272.

83. Marsango, S., Barki, N., Jenkins, L., Tobin, A. B. & Milligan, G. Therapeutic validation of an orphan G protein-coupled receptor: The case of GPR84. *Br. J. Pharmacol.* (2020) doi:10.1111/bph.15248.

84. Simard, J.-C. *et al.* Fatty acid mimetic PBI-4547 restores metabolic homeostasis via GPR84 in mice with non-alcoholic fatty liver disease. *Sci. Rep.* **10**, 1–16 (2020).

85. Gagnon, L. *et al.* A Newly Discovered Antifibrotic Pathway Regulated by Two Fatty Acid Receptors. *The American Journal of Pathology* vol. 188 1132–1148 (2018).

86. Gaidarov, I. *et al.* Embelin and its derivatives unravel the signaling, proinflammatory and antiatherogenic properties of GPR84 receptor. *Pharmacol. Res.* **131**, (2018).

87. Ghosh, M., Xu, Y. & Pearse, D. D. Cyclic AMP is a key regulator of M1 to M2a phenotypic conversion of microglia in the presence of Th2 cytokines. *J. Neuroinflammation* **13**, (2016).

88. Bystrom, J. *et al.* Resolution-phase macrophages possess a unique inflammatory phenotype that is controlled by cAMP. *Blood* **112**, (2008).

89. Berger, A. Science commentary: Th1 and Th2 responses: what are they? *BMJ : British Medical Journal* **321**, 424 (2000).

90. Reusch, N. et al. Neutrophils in COVID-19. Front. Immunol. 12, 652470 (2021).

91. Tavares, L. P. et al. Blame the signaling: Role of cAMP for the resolution of inflammation. Pharmacol. Res. 159, 105030 (2020).

92. Baig, S. *et al.* Treatment with PBI-4050 in patients with Alström syndrome: study protocol for a phase 2, single-Centre, single-arm, open-label trial. *BMC Endocr. Disord.* **18**, 1–10 (2018).

93. Nguyen, Q. T. *et al.* PBI-4050 reduces pulmonary hypertension, lung fibrosis, and right ventricular dysfunction in heart failure. *Cardiovasc. Res.* **116**, 171–182 (2019).

94. Khalil, N. et al. Phase 2 clinical trial of PBI-4050 in patients with idiopathic pulmonary fibrosis. Eur. Respir. J. 53, (2019).

95. Li, Y. *et al.* Fatty acid receptor modulator PBI-4050 inhibits kidney fibrosis and improves glycemic control. *JCI Insight* **3**, (2018).

96. Sundqvist, M. *et al.* Similarities and differences between the responses induced in human phagocytes through activation of the medium chain fatty acid receptor GPR84 and the short chain fatty acid receptor FFA2R. *Biochim. Biophys. Acta Mol. Cell Res.* **1865**, (2018).

97. Thibodeau, J.-F. *et al.* FRI-097-PBI-4050 treatment decreases sepsis-induced liver injury in mice. *Journal of Hepatology* vol. 70 e430 (2019).

98. IPF. https://www.glpg.com/ipf.

99. Vanhoutte, F., O. P612. Human safety, pharmacokinetics and pharmacodynamics of the GPR84 antagonist GLPG1205, a potential new approach to treat IBD. J. Crohns. Colitis 9, S387–S387 (2015).

100. Saniere, L. *et al.* Characterization of GLPG1205 in Mouse Fibrosis Models: A Potent and Selective Antagonist of GPR84 for Treatment of Idiopathic Pulmonary Fibrosis. *A19. LESS IDIOPATHIC: STRUCTURAL AND FUNCTIONAL ABNORMALITIES IN IPF* (2019) doi:10.1164/ajrccm-conference.2019.199.1_meetingabstracts.a1046.

101. A Clinical Study to Test How Effective and Safe GLPG1205 is for Patients With Idiopathic Pulmonary Fibrosis (IPF) - Full Text View - ClinicalTrials.gov. https://clinicaltrials.gov/ct2/show/NCT03725852.

102. Efficacy and Safety of GLPG1205 in Subjects With Active Ulcerative Colitis - Full Text View - ClinicalTrials.gov. https://clinicaltrials.gov/ct2/show/NCT02337608.

103. Biosciences, T. Ace2. https://www.taconic.com/knockout-mouse/ace2-targeted.

104. Gene: Ace2 (ENSMUSG00000015405) - Summary - Mus_musculus - Ensembl genome browser 106. https://useast.ensembl.org/Mus_musculus/Gene/Summary?db=core;g=ENSMUSG00000015405;r=X:162922328-162971416;t=ENSMUST00000131543.

105. Crackower, M. A. *et al.* Angiotensin-converting enzyme 2 is an essential regulator of heart function. *Nature* **417**, 822–828 (2002).

106. Nicol, L. S. *et al.* The role of G-protein receptor 84 in experimental neuropathic pain. *J. Neurosci.* **35**, (2015).

107. Livak, K. J. & Schmittgen, T. D. Analysis of Relative Gene Expression Data Using Real-Time Quantitative PCR and the 2−ΔΔCT Method. *Methods* vol. 25 402–408 (2001).

108. Kim, K. K., Jin, S. H. & Lee, B. J. Herpes virus entry mediator signaling in the brain is imperative in acute inflammation-induced anorexia and body weight loss. *Endocrinol Metab (Seoul)* **28**, 214–220 (2013).

109. Cross-Mellor, S. K., Kent, W. D., Kavaliers, M. & Ossenkopp, K. P. Examining the effects of lipopolysaccharide and cholecystokinin on water ingestion: comparing intake and palatability. *Brain Res.* **861**, 220–232 (2000).

110. Kawada, N. A Mouse Model of Angiotensin II Slow Pressor Response: Role of Oxidative Stress. *Journal of the American Society of Nephrology* vol. 13 2860–2868 (2002).

111. What Is Kidney Atrophy? *National Kidney Foundation* https://www.kidney.org/atoz/content/what-kidney-atrophy (2018).

112. Shin, N. S. *et al.* Arginase-1 Is Required for Macrophage-Mediated Renal Tubule Regeneration. *J. Am. Soc. Nephrol.* **33**, (2022).

113. Tarrant, J. Emerging Translatable Safety Biomarkers. *Comprehensive Medicinal Chemistry III* 255–284 (2017) doi:10.1016/b978-0-12-409547-2.12387-x.

114. T Helper 2 Cell Overview. *ThermoFisher Scientific* https://www.thermofisher.com/ca/en/home/life-science/cell-analysis/cell-analysis-learning-center/immunology-at-work/t-helper-2-cell-overview.html

115. Toda, N., Mukoyama, M., Yanagita, M. & Yokoi, H. CTGF in kidney fibrosis and glomerulonephritis. *Inflamm. Regen.* **38**, (2018).

116. Bio-Rad. F4/80 Antibody - Mouse Macrophage & Microglial marker. *Bio-Rad* https://www.bio-rad-antibodies.com/f480-antibody-cla3-1.html.

117. Eisenberg, E. & Levanon, E. Y. Human housekeeping genes, revisited. *Trends Genet.* **29**, 569–574 (2013).

118. Faix, J. D. Biomarkers of sepsis. *Crit. Rev. Clin. Lab. Sci.* **50**, (2013).

119. Garlanda, C. & Jaillon, S. The Interleukin-1 Family. *Encyclopedia of Immunobiology* 438–446 (2016) doi:10.1016/b978-0-12-374279-7.10001-3.

120. NCI Dictionary of Cancer Terms. *National Cancer Institute* https://www.cancer.gov/publications/dictionaries/cancer-terms (2011).

121. Scheller, J., Chalaris, A., Schmidt-Arras, D. & Rose-John, S. The pro- and anti-inflammatory properties of the cytokine interleukin-6. *Biochimica et Biophysica Acta (BBA) - Molecular Cell Research* vol. 1813 878–888 (2011).

122. Henry, H. L. & Norman, A. W. Encyclopedia of Hormones. 453-462 (Academic Press, 2003)

123. O'Hehir, R. E., Holgate S. T., & Sheikh, A. Introduction to Mechanisms of Allergic Diseases. in *Middleton's Allergy Essentials* 1–27 (Elsevier, 2017).

124. Lim, A. I., Tang, S. C. W., Lai, K. N. & Leung, J. C. K. Kidney injury molecule-1: More than just an injury marker of tubular epithelial cells? *Journal of Cellular Physiology* vol. 228 917–924 (2013).

125. Qin, C.-C., Liu, Y.-N., Hu, Y., Yang, Y. & Chen, Z. Macrophage inflammatory protein-2 as mediator of inflammation in acute liver injury. *World J. Gastroenterol.* **23**, 3043 (2017).

126. Buonafine, M., Martinez-Martinez, E. & Jaisser, F. More than a simple biomarker: the role of NGAL in cardiovascular and renal diseases. *Clin. Sci.* **132**, 909–923 (2018).

127. Edelstein, C. L. Biomarkers of Cardiovascular Risk in Chronic Kidney Disease. in *Biomarkers of Kidney Disease* 485–511 (Academic Press, 2017).

128. Edelstein, C. L. Biomarkers in Acute Kidney Injury. in *Biomarkers of Kidney Disease* 241–315 (Academic Press, 2017).

129. Mehaffey, E. & Majid, D. S. A. Inflammation and Inflammatory Mediators in Kidney Disease: Tumor necrosis factor-α, kidney function, and hypertension. *American Journal of Physiology - Renal Physiology* **313**, F1005 (2017).

130. Kupczyk, M., Bocheńska-Marciniak, M., Górski, P. & Kuna, P. [Myeloperoxidase (MPO) as a marker of neutrophil influx into nasal mucosa after recombinant IL-8 challenge]. *Pneumonol. Alergol. Pol.* **70**, (2002).

131. Kim, D.-K. *et al.* EVpedia: a community web portal for extracellular vesicles research. *Bioinformatics* **31**, 933–939 (2015).

132. Medeiros, T., Myette, R. L., Almeida, J. R., Silva, A. A. & Burger, D. Extracellular Vesicles: Cell-Derived Biomarkers of Glomerular and Tubular Injury. *Cell. Physiol. Biochem.* **54**, 88–109 (2020).

133. Levy, G. & Jusko, W. J. EFFECT OF VISCOSITY ON DRUG ABSORPTION. *J. Pharm. Sci*. 54, 219–224 (1965).

134. Abuhelwa, A. Y., Williams, D. B., Upton, R. N. & Foster, D. J. R. Food, gastrointestinal pH, and models of oral drug absorption. Eur. J. Pharm. Biopharm. 112, 234–248 (2017).

135. Susa, S. T. & Preuss, C. V. Drug Metabolism. in *StatPearls [Internet]* (StatPearls Publishing, 2022).

136. Medications and the Liver. *American College of Gastroenterology* https://gi.org/topics/medications-and-the-liver/ (2011).

137. Viegas, K. A. S. *et al.* EFFECT OF SUBPRESSOR DOSE OF ANGIOTENSIN II ON MODULATION OF THE VASCULAR EXTRACELLULAR MATRIX COMPOSITION: PP.24.488. *Journal of Hypertension* vol. 28 e392 (2010).

138. Alexander, M. P. *et al.* Acute Kidney Injury in Severe COVID-19 Has Similarities to Sepsis-Associated Kidney Injury: A Multi-Omics Study. *Mayo Clin. Proc.* **96**, 2561 (2021).

139. Kellum, J. A., Nadim, M. K. & Forni, L. G. Sepsis-associated acute kidney injury: is COVID-19 different? *Kidney Int.* **98**, 1370 (2020).

140. Gagnon, L. *et al.* FP266PBI-4050 REDUCES SYSTEMIC INFLAMMATION, ELECTROLYTE DISTURBANCES, AND RENAL INJURY IN MICE WITH SEPSIS-INDUCED ACUTE KIDNEY INJURY; ROLE OF GPR84. *Nephrology Dialysis Transplantation* vol. 34 (2019).

141. Yun, Y. *et al.* Tofacitinib Ameliorates Lipopolysaccharide-Induced Acute Kidney Injury by Blocking the JAK-STAT1/STAT3 Signaling Pathway. *Biomed Res. Int.* **2021**, (2021).

142. Liu, X. *et al.* Dihydroartemisinin attenuates lipopolysaccharide-induced acute kidney injury by inhibiting inflammation and oxidative stress. *Biomed. Pharmacother.* **117**, (2019).

143. Brown, R. M. & Semler, M. W. Fluid Management in Sepsis. *J. Intensive Care Med.* **34**, (2019).

144. Perner, A. *et al.* Sepsis: frontiers in supportive care, organisation and research. *Intensive Care Med.* **43**, 496–508 (2017).

145. Neugarten, J., Acharya, A. & Silbiger, S. R. Effect of gender on the progression of nondiabetic renal disease: a meta-analysis. *J. Am. Soc. Nephrol.* **11**, 319–329 (2000).

146. Piirsalu, M. et al. Treatment With Lipopolysaccharide Induces Distinct Changes in Metabolite Profile and Body Weight in 129Sv and Bl6 Mouse Strains. Front. Pharmacol. 11, 371 (2020).

147. Anker, M. S. *et al.* Weight loss, malnutrition, and cachexia in COVID-19: facts and numbers. *J. Cachexia Sarcopenia Muscle* **12**, 9–13 (2021).

148. Cai, K. C. et al. Age and sex differences in immune response following LPS treatment in mice. Brain Behav. Immun. 58, 327–337 (2016)

149. Tod, P. *et al.* Time-Dependent miRNA Profile during Septic Acute Kidney Injury in Mice. *Int. J. Mol. Sci.* **21**, (2020).

150. Róka, B. *et al.* The Acute Phase Response Is a Prominent Renal Proteome Change in Sepsis in Mice. *Int. J. Mol. Sci.* **21**, (2019).

151. Wang, Y. *et al.* A pressor dose of angiotensin II has no influence on the angiotensin-converting enzyme 2 and other molecules associated with SARS-CoV-2 infection in mice. *FASEB J.* **35**, e21419 (2021).

152. Gomolak, J. R. & Didion, S. P. Angiotensin II-induced endothelial dysfunction is temporally linked with increases in interleukin-6 and vascular macrophage accumulation. *Front. Physiol.* **0**, (2014).

153. Wilde, E. *et al.* Tail-Cuff Technique and Its Influence on Central Blood Pressure in the Mouse. *J. Am. Heart Assoc.* (2017) doi:10.1161/JAHA.116.005204.

154. Yasuda, S. & Lew, W. Y. W. Lipopolysaccharide Depresses Cardiac Contractility and β-Adrenergic Contractile Response by Decreasing Myofilament Response to Ca2+ in Cardiac Myocytes. *Circ. Res.* (1997) doi:10.1161/01.RES.81.6.1011.

155. Yu, Y.-Y. et al. Self-developed NF-κB inhibitor 270 protects against LPS-induced acute kidney injury and lung injury through improving inflammation. Biomed. Pharmacother. 147, 112615 (2022).

156. Kato, T., Mizuno, S. & Kamimoto, M. The decreases of nephrin and nuclear WT1 in podocytes may cause albuminuria during the experimental sepsis in mice. *Biomed. Res.* **31**, 363–369 (2010).

157. Song, H. *et al.* Generation and Characterization of Mouse Models of C3 Glomerulonephritis With CFI D288G and P467S Mutations. *Front. Physiol.* **0**, (2021).

158. Yildirim, C. *et al.* Early predictors of acute kidney injury in COVID-19 patients. *Nephrology* **26**, 513–521 (2021).

159. Mei, S. *et al.* Autophagy is activated to protect against endotoxic acute kidney injury. *Sci. Rep.* **6**, 22171 (2016).

160. Li, T. *et al.* Protective effect of HS on LPS-induced AKI by promoting autophagy. *Mol. Med. Rep.* **25**, (2022).

161. Küçükceran, K., Ayrancı, M. K., Girişgin, A. S., Koçak, S. & Dündar, Z. D. The role of the BUN/albumin ratio in predicting mortality in COVID-19 patients in the emergency department. *Am. J. Emerg. Med.* **48**, 33–37 (2021).

162. Syal, K., Banerjee, D. & Srinivasan, A. Creatinine estimation and interference. *Indian J. Clin. Biochem.* **28**, 210–211 (2013).

163. Samra, M. & Abcar, A. C. False estimates of elevated creatinine. *Perm. J.* **16**, 51–52 (2012).

164. Patel, S., Dhande, I., Gray, E. A., Ali, Q. & Hussain, T. Prevention of lipopolysaccharide-induced CD11b immune cell infiltration in the kidney: role of AT receptors. *Biosci. Rep.* **39**, (2019).

165. Pabla, N., Scindia, Y., Gigliotti, J. & Bajwa, A. Mouse models of acute Kidney Injury. in *Preclinical Animal Modeling in Medicine* (IntechOpen, 2022).

166. Castellano, G. *et al.* Endothelial dysfunction and renal fibrosis in endotoxemia-induced oliguric kidney injury: possible role of LPS-binding protein. *Crit. Care* **18**, 1–18 (2014).

167. Plotnikov, E. Y. *et al.* Mechanisms of LPS-Induced Acute Kidney Injury in Neonatal and Adult Rats. *Antioxidants (Basel)* **7**, (2018).

168. Cheng, S., Wu, T., Li, Y., Huang, J. & Cai, T. Romidepsin (FK228) in a mouse model of lipopolysaccharide-induced acute kidney injury is associated with down-regulation of the CYP2E1 gene. *Med. Sci. Monit.* **26**, e918528 (2020).

169. Peerapornratana, S., Manrique-Caballero, C. L., Gómez, H. & Kellum, J. A. Acute kidney injury from sepsis: current concepts, epidemiology, pathophysiology, prevention and treatment. *Kidney Int.* **96**, 1083–1099 (2019).

170. Zhang, W. *et al.* Negative Regulation of Tec Kinase Alleviates LPS-Induced Acute Kidney Injury in Mice via theTLR4/NF-B Signaling Pathway. *Biomed Res. Int.* **2020**, 3152043 (2020).

171. Bhargava, R. *et al.* Acute lung injury and acute kidney injury are established by four hours in experimental sepsis and are improved with pre, but not post, sepsis administration of TNF-α antibodies. *PLoS One* **8**, (2013).

172. Castellano, G. *et al.* LPS-Binding Protein Modulates Acute Renal Fibrosis by Inducing Pericyte-to-Myofibroblast Trans-Differentiation through TLR-4 Signaling. *Int. J. Mol. Sci.* **20**, 3682 (2019).

173. Lopes, T. G. *et al.* Markers of renal fibrosis: How do they correlate with podocyte damage in glomerular diseases? *PLoS One* **14**, (2019).

174. Burt, A. D., Ferrell, L. D., & Hübscher, S. G. Cellular and Molecular Techniques. in *Macsween's Pathology of the Liver* 88–110 (Elsevier, 2018).

175. Jansen, J. *et al.* SARS-CoV-2 infects the human kidney and drives fibrosis in kidney organoids. *Cell Stem Cell* **29**, (2022).

176. Lu, L., Zhang, H., Dauphars, D. J. & He, Y.-W. A Potential Role of Interleukin 10 in COVID-19 Pathogenesis. *Trends Immunol.* **42**, 3 (2021).

177. Yin, C. *et al.* Regulatory role of Gpr84 in the switch of alveolar macrophages from CD11blo to CD11bhi status during lung injury process. *Mucosal Immunol.* **13**, 892–907 (2020).

178. Chen, L.-H., Zhang, Q., Xie, X. & Nan, F.-J. Modulation of the G-Protein-Coupled Receptor 84 (GPR84) by Agonists and Antagonists. *J. Med. Chem.* **63**, 15399–15409 (2020).

179. Yoo, J.-Y. *et al.* LPS-Induced Acute Kidney Injury Is Mediated by Nox4-SH3YL1. *Cell Rep.* **33**, 108245 (2020).

180. Lerolle, N. *et al.* Histopathology of septic shock induced acute kidney injury: apoptosis and leukocytic infiltration. *Intensive Care Med.* **36**, 471–478 (2010).

181. Reusch, N. *et al.* Neutrophils in COVID-19. *Front. Immunol.* **12**, (2021).

182. Immune cell markers poster. https://www.abcam.com/primary-antibodies/immune-cell-markers-poster (2022).

183. Batah, S. S. & Fabro, A. T. Pulmonary pathology of ARDS in COVID-19: A pathological review for clinicians. Respir. Med. 176, 106239 (2021).

184. Aleksova, A. et al. Long-term effect of SARS-CoV-2 infection on cardiovascular outcomes and all-cause mortality. Life Sci. 310, 121018 (2022).

185. Hingorani, K. S., Bhadola, S. & Cervantes-Arslanian, A. M. COVID-19 and the brain. Trends Cardiovasc. Med. 32, 323 (2022).

186. Al Shoyaib, A., Archie, S. R. & Karamyan, V. T. Intraperitoneal Route of Drug Administration: Should it Be Used in Experimental Animal Studies? Pharm. Res. 37, 12 (2019).

187. Kong, W. et al. GTS-21 Protected Against LPS-Induced Sepsis Myocardial Injury in Mice Through α7nAChR. Inflammation 41, 1073–1083 (2018).

188. Berkowitz, S. et al. LPS-Induced Coagulation and Neuronal Damage in a Mice Model Is Attenuated by Enoxaparin. Int. J. Mol. Sci. 23, (2022).

189. Animal Models of Acute Lung Injury. https://www.thoracic.org/professionals/clinical-resources/critical-care/critical-care-research/animal-models-of-acute-lung-injury.php.

190. Chen, H. *et al.* Lipopolysaccharide Induces Chronic Kidney Injury and Fibrosis through Activation of mTOR Signaling in Macrophages. *AJNR Am. J. Neuroradiol.* **42**, 305–317 (2015).

191. A Clinical Study to Test How Effective and Safe GLPG1205 is for Participants With Idiopathic Pulmonary Fibrosis (IPF) - Study Results - ClinicalTrials.gov. https://clinicaltrials.gov/ct2/show/results/NCT03725852.

192. Jung, S.-Y. *et al.* Electrolyte and mineral disturbances in septic acute kidney injury patients undergoing continuous renal replacement therapy. *Medicine* **95**, (2016).

193. Sjöström, A., Rysz, S., Sjöström, H. & Höybye, C. Electrolyte and acid-base imbalance in severe COVID-19. *Endocrine Connections* **10**, 805 (2021).

194. Marty, M. S. *et al.* The Effect of Route, Vehicle, and Divided Doses on the Pharmacokinetics of Chlorpyrifos and Its Metabolite Trichloropyridinol in Neonatal Sprague-Dawley Rats. *Toxicol. Sci.* **100**, 360–373 (2007).

195. Cremophor. 763 (2016).

196. Jenkins, L. *et al.* Discovery and Characterization of Novel Antagonists of the Proinflammatory Orphan Receptor GPR84. *ACS Pharmacol Transl Sci* **4**, 1598–1613 (2021).

197. Mancini, S. J. *et al.* On-target and off-target effects of novel orthosteric and allosteric activators of GPR84. *Sci. Rep.* **9**, 1861 (2019).

198. Al Mahmud, Z. *Defining Ligand Binding Modes of the Orphan G Protein-coupled Receptor GPR84*. (2019).

199. Sambamoorthy, G. & Raman, K. Understanding the evolution of functional redundancy in metabolic networks. *Bioinformatics* **34**, i981–i987 (2018).

200. GPR84 G protein-coupled receptor 84 [Homo sapiens (human)] - Gene - NCBI. https://www.ncbi.nlm.nih.gov/gene/53831.